FDOT

Work Program Number: 0510738

FINAL REPORT

STRENGTH AND DURABILITY OF BACKFILL GEOGRIDS FOR RETAINING WALLS

Contractor:

Florida Atlantic University
Department of Ocean Engineering
777 Glades Road
Boca Raton, FL 33431

Principal Investigator:
Dr. D.V. Reddy
Professor and Director
Center for Marine Structures and Geotechnique
(561) 297-3443

Contract Monitor:
Mr. Peter Lai
Assistant State Geotechnical Engineer
Florida Department of Transportation
Tallahassee, FL

April 2000

1. Title and Subtitle Strength and Durability of Backfill Geogrids for Retaining Walls	**1. Work Program No.** 0510738
	2. Job State No. 99700-3321-119
9. Performing Organization Name and Address Florida Atlantic University Dept. of Ocean Engineering 777 Glades Road Boca Raton, FL 33431	**3. Contract or Grant No.** B-9907
	5. Report Date May 2000
	6. Author Dr. D. V. Reddy
12. Sponsoring Agency Name and Address Florida Department of Transportation Structures Division 605 Suwannee Street, M.S. 33 Tallahassee, FL 32399-0450	**13. Type of Report and Period Covered** Final Report 8/22/95 -- 8/31/99

15. Abstract

The report presents an experimental and analytical investigation of two types of geogrids: Tensar High Density Polyethylene (HDPE) and Matrex Polyester Terephthalate (PET). The tasks comprised: i) long term pullout resistance, ii) creep and creep rupture, iii) durability and degradation.

i) For pullout, sand and limerock were used for the backfill material, which meet the FDOT (Florida Department of Transportation) Material Specifications, with simulation of unsaturated and saturated conditions. Eight pullout test boxes were designed and constructed. The measured strain-time relations for unsaturated and saturated soils for various levels of the pullout force until the peak value (up to 10,000 hours of exposure), and varying distances from the loading end were plotted. The normal and principal stresses in the soil, and the strains along the geogrid were determined from the finite element analysis for the unsaturated soil condition for various pullout force levels. The results were analyzed and a generalized method proposed for practical design using sliding resistance factors.

ii) For creep, accelerated exposure has been used with super-ambient temperatures for different simulated exposure conditions, and soil water related to the soil conditions in Florida. The temperatures were: 30 °C, 45 °C, 55 °C, and 65 °C; with submergence in the following groundwater-simulating solutions: calcareous (pH 9.0), phosphate (pH 4.5), limerock, seawater, and freshwater (for PET specimens only). The load levels were 30%, 40%, 50% of the ultimate load value. Elongations were measured at 30 seconds, 1, 2, 4, 6, 8, 15, 30, 75 minutes, 3, 7 hours, and every 24 hours until 10,000 hours. The data was plotted and regression analysis applied. The results enabled formulation of the creep equations for reliable geogrid life cycle analysis.

iii) For durability, accelerated exposure was used, with super-ambient temperatures for different simulated exposure conditions, and soil-water related to the soil conditions in Florida. The temperatures were 35 °C, 50 °C, and 65 °C, with submergence in the same groundwater-simulating solutions as for creep and creep rupture testing. The immersion periods were 30 days, 60 days, 90 days, 120 days, 365 days, and 417 days. Long term performance at ambient temperatures was extrapolated, based on the Arrhenius method. The data enabled reliable life cycle analysis of geogrids based on durability.

16. Key Words Geogrids, Pullout, Creep, Durability, MSE Retaining Walls	**17. No. of Pages** 288

FOREWORD

The objectives of this study are to evaluate and resolve, through an experimental and analytical investigation, some of the concerns related to long-term performance of geogrids by determining i) the pullout resistance of HDPE and PET geogrids in sand and limerock, under dry and saturated conditions, and ii) the creep, creep rupture, and durability characteristics of HDPE and PET geogrids exposed to accelerated testing, with super-ambient temperatures for different simulated exposure conditions, and soil water related to the soil conditions in Florida. This will enable cost-effective applications of geogrids, compared to steel reinforcement, which enable the maximum utilization of public funds in Florida's transportation industry. The performance indicators would be changes in design standards.

ACKNOWLEDGEMENT

The Principal Investigator would like to thank the Florida Department of Transportation (State Project: 99700-3321-119, Work Program # 0510738), for its generous financial support. Gratitude is expressed to Mr. P. W. Lai, Assistant State Geotechnical Engineer, Structures Division, FDOT, Tallahassee, FL for his support, continued interaction with outstanding, and invaluable input, guidance, and encouragement.

Thanks are due to the following companies / departments for the participation and support:

Tensar Earth Technologies Inc.*
Reinforced Earth Company*
Department of Mechanical Engineering, FAU
(Dr.L.E.Carlsson)

Appreciation is due to Mr. Fernando Navarrete and Mr. Shangsui Gao, who were the principal contributors, with their Ph.D. dissertation work and Master's thesis, respectively, based on the project. Other Graduate Assistants who participated were Dr. W. Ahn, , Mr. M. Barbosa, Mr. K. Bethune, Mr. B. Butul, Mr. N. Chauvet, Ms. K. Darn, Mr. C. Gonzalez, Mr. C. Hanners, Mr. T. Pierro, and Mr. G. Sitomer. The administrative support of Dr. S. E. Dunn, Professor and Chairman, Department of Ocean Engineering and Dr. J. T. Jurewicz, Dean of Engineering, Florida Atlantic University, is gratefully acknowledged.

* Provided the test specimens Tensar High Density Polyethylene (HDPE) and Matrex Polyester Terephthalate (PET), respectively.

ABSTRACT

The report presents an experimental and analytical investigation of two types of geogrids: Tensar High Density Polyethylene (HDPE) and Matrex Polyester Terephthalate (PET). The tasks comprised: i) long term pullout resistance, ii) creep and creep rupture, iii) durability and degradation.

i) For pullout, sand and limerock were used for the backfill material, which meet the FDOT (Florida Department of Transportation) Material Specifications, with simulation of unsaturated and saturated conditions. Eight pullout test boxes were designed and constructed, each with a specially designed stainless steel clamp. The measured strain-time relations for unsaturated and saturated soils for various levels of the pullout force until the peak value (up to 10,000 hours of exposure), and varying distances from the loading end were plotted. The normal and principal stresses in the soil, and the strains along the geogrid were determined from the finite element analysis for the unsaturated soil condition for various pullout force levels. The results were analyzed and a generalized method proposed for practical design using sliding resistance factors.

Based on the tests and theoretical analysis, the PET geogrid showed better pullout resistance performance than the HDPE geogrid, when used in fine sand (sliding coefficient is 1.12 under unsaturated working condition). Since fine sand can provide more contact surface, a larger friction resistance is mobilized. On the other hand, for the HDPE geogrid, a coarser sand with good gradation is the better choice (sliding coefficient is 1.05 under unsaturated working condition). For a PET geogrid in limerock, the sliding coefficient was 1.08 under the unsaturated testing condition, and 0.669 under the saturated condition. This gives a 38.1% reduction due to the wetting effect. Similarly, the sliding coefficient for test specimen PET in sand was 1.12 in the unsaturated condition, and 0.688 under saturated condition. From the test results, it can be inferred that the wetting condition causes a 38.6% decrease in the resistance. For the test specimen HDPE in limerock, the sliding coefficient was 1.05 in the unsaturated condition and 0.758 under the saturated condition. The decrease is only 27.8%. In sand, the sliding coefficient was 1.02 under the unsaturated condition, and 0.729 under the saturated condition, with a 28.5% reduction. For fine sand with good gradation, a reduction of about 43% was observed by Chua et al. in the pullout tests performed in the University of New Mexico (1993). As for the test in clay, a reduction of about 19% was observed. Chua pointed out that the optimum moisture content for this clay was about 20.4% which might explain the small reduction in resistance. From the test results, it can be inferred that the saturated condition has more impact on fine sand than coarser sand; the reduction in the sliding coefficient is larger for the PET geogrid than the HDPE geogrid. This is because the friction resistance is subjected to a greater loss due to saturation, and the bearing resistance is marginal. The results from the experimental

investigation and the finite element analysis under unsaturated soil test condition are in good agreement.

ii) For creep, accelerated exposure has been used, with super-ambient temperatures for different simulated exposure conditions, and soil water related to the soil conditions in Florida. The temperatures were: 30 °C, 45 °C, 55 °C, and 65 °C, with submergence in the following groundwater-simulating solutions: HDPE specimens - calcareous (pH 9.0), phosphate (pH 4.5), limerock and seawater, and freshwater for PET specimens only. The load levels were 30%, 40%, 50% of the ultimate load value. Elongations were measured at 30 seconds, 1, 2, 4, 6, 8, 15, 30, 75 minutes, 3, 7 hours, and every 24 hours, up to 10,000 hours. It was observed that HDPE geogrids undergo larger creep than PET geogrids. The different exposures do not play an important role in the rate of creep, since there was larger variability from specimen to specimen, than from different solutions. Creep rupture occurred in all the HDPE specimens exposed to 50% of the ultimate load. For the specimens exposed to 40% of the ultimate load, creep rupture occurred for specimens exposed to 55° C and 65° C temperatures. The PET specimens did not experience creep rupture except for two specimens; for these two cases the rupture can be attributed to either defects in the specimens or defective clamping.

iii) For durability, accelerated exposure was used, with super-ambient temperatures for different simulated exposure conditions, and soil-water related to the soil conditions in Florida. The temperatures were 35 °C, 50 °C, and 65 °C, with submergence in the following groundwater-simulating solutions: HDPE specimens - calcareous (pH 9.0), phosphate (pH 4.5), limerock and seawater, and PET specimens - calcareous (pH 9.0), phosphate (pH 4.5), limerock, seawater, and freshwater. The immersion periods were 30 days, 60 days, 90 days, 120 days, 365 days, and 417 days. Long term performance at ambient temperatures was extrapolated, based on the Arrhenius method. The data will enable reliable life cycle analysis of geogrids based on durability.

In the durability curves, it can be seen that the effect of degradation in HDPE geogrids is negligible for up to 10,000 hours for seawater and limerock, For the calcareous (pH 9.0), and phosphate (pH 4.5) exposures, a very small degradation was observed, but it is negligible since for the calcareous solution the maximum degradation is 3% and for the phosphate exposure 1.2% for the 65° C, and 2.1% for 50° C in 10,000 hours. For 35° C, the degradation was less than 1% in any of the exposure. This results indicate excellent performance of HDPE geogrids in the solutions to which they were exposed. The PET geogrids showed a small degradation, mainly for the 65 °C. The variation in degradation between the different solutions was minimal indicating hydrolysis as the main cause. The maximum degradation was 13.3% for the Phosphate solution at 65° C, but the maximum at 35° C for the limerock exposure was only 1.2%. This indicates that hydrolysis is the main cause, since the amounts of degradation do not vary uniformly in the different

exposures, and hydrolysis is accelerated by elevated temperatures. The PET geogrids showed a small degradation, mainly for the 65 °C exposure. The variation in degradation between the different solutions was minimal indicating hydrolysis as its main cause. The maximum degradation was 13.3% for the Phosphate solution at 65° C, but the maximum at 35° C for the limerock exposure was only 1.2%. This indicates that hydrolysis is the main cause since the amounts of degradation do not vary uniformly in the different exposures, and hydrolysis is accelerated by elevated temperatures. The Arrhenius method is not precise for small degradations of the HDPE specimens. For 99% property retained or 1% degradation, the Arrhenius method could be applied only to the calcareous exposure. For the PET specimens, the Arrhenius method for 99% and 97% property retained was applied to all the exposures except seawater. For 95% property retained the Arrhenius method could be applied to all the exposures, except the seawater and calcareous exposures.

TABLE OF CONTENTS

LIST OF TABLES

CHAPTER

Table

Page No.

8. DURABILITY TESTING

9. DURABILITY ANALYSIS

10. DISCUSSION

LIST OF FIGURES

CHAPTER

Figure

Page No.

5. FINITE ELEMENT ANALYSIS OF PULLOUT

6. CREEP AND CREEP RUPTURE TESTING

8. DURABILITY TESTING

9. DURABILITY ANALYSIS

10. DISCUSSION

11. CONCLUSIONS

APPENDIX A

CHAPTER 1

INTRODUCTION

Due to the economic advantages, the use of polymeric reinforcement in soil-reinforced structures has increased considerably. With the rapid development of the geosynthetic industry, there is a wide range of applications for geogrid reinforcement in soil, such as retaining walls, embankments, paved roads, foundations, and slope stabilization (Fig 1.1).

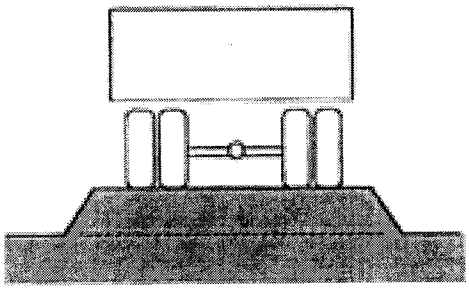

Unpaved Road

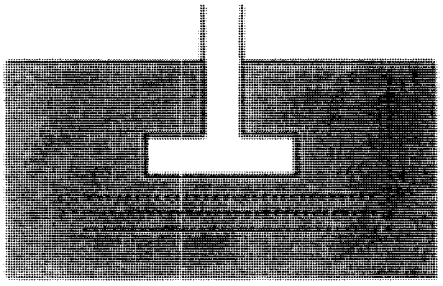

Foundation

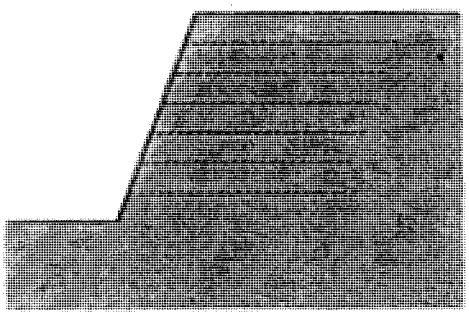

Embankment

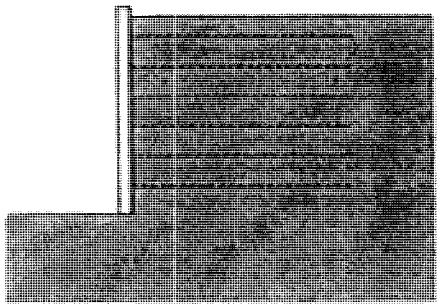

Retaining Wall

Fig 1.1 Typical examples of soil reinforcement application

The main polymers currently used for reinforcement include polypropylene (PP), polyester (PET), and polyethylene (PE). Geogrids are the newest generation of polymeric geosynthetics designed specifically to provide soil reinforcement. Their three-dimensional open structure, which interlocks with the surrounding soil, creates a positive connection between the two components of the mechanically stabilized earth (MSE) structure (Koerner, 1994). This bonding between soil and reinforcement creates a more efficient, cost-effective structure.

However, due to the relatively short experience with these polymeric materials, there are uncertainties regarding their durability, with respect to retainment of the design properties after being subjected to construction stresses and exposed to in-soil environments over the expected design life. Potential degradation of polymeric reinforcement, with time, will depend on the characteristics of a specific polymer, configuration, and the environment to which it is exposed. This dictates the need for more research in this area. If geogrids have to be used as an alternative to steel reinforcement to overcome the corrosion problem, their performance has to be established based on laboratory and field testing for site specific conditions, e.g. high water tables and temperatures ranging between 80° F to 100° F in Florida. Typical soil temperatures are in the range of 50-60 °F (10-15.6 °C); temperatures near the surface of the wall can reach 85-100 °F (29.4 - 37.8 °C). The pH values of various MSE materials used by the Florida Department of Transportation are in the range of 4.5 to 9.

This study addresses the long term pullout resistance, creep and creep rupture, durability and degradation. This investigation is restricted to testing of geogrids (Tensar-HDPE, Matrex-PET) in view of their wider usage and the restrictions imposed by time and funding.

CHAPTER 2

BACKGROUND

2.1 GEOGRIDS

Geogrids are polymeric geosynthetics designed specifically to provide soil reinforcement. A positive connection between the two components of the mechanically stabilized earth (MSE) structure is created by the three-dimensional open structure of geogrids, which interlocks with the surrounding soil. This bonding between soil and the reinforcement creates a more efficient, cost-effective structure. The main polymers currently used for reinforcement include polypropylene (PP), polyester terephthalate (PET), and polyethylene (PE). Geogrids were first introduced into North America in the early 1980's. ASTM D5262 1992 defines a geogrid as "a geosynthetic formed by a rectangular network of integrally connected elements with apertures greater than 6.35mm (1/4 in.) to allow interlocking with the surrounding soil, rock, earth, and other surrounding materials to function primarily as a reinforcement". Geogrids are produced for biaxial and uniaxial load-carrying configurations and have been specifically developed for long-term reinforcement of critical soil structures.

2.1.1 HDPE GEOGRIDS

HDPE is the acronym for High Density Polyethylene, The uniaxial HDPE geogrids used in this research are manufactured by stretching a punched sheet of extruded HDPE in one direction under carefully controlled conditions. This process aligns the polymer's long-chain molecules in the direction of drawing, and results in a product with high one-directional tensile strength and modulus.

2.1.2 PET GEOGRIDS

PET is the acronym for Polyester Terephthalate. PET geogrids are made of polyester multifilament yarns, which are interlocked by weaving to create a stable network, such that the yarns retain their relative position. It is then coated with PVC. Compared to HDPE, PET is more flexible in bending and exhibits a relatively lower junction strength.

2.2 GEOGRIDS IN SOIL REINFORCEMENT

Utilization of geosynthetic reinforced soil technology has grown dramatically in the past ten years due to enhanced durability, simplicity and rapidity of construction, less site preparation, less space requirement for construction operations, reduced right-of-way acquisition, elimination of the need for rigid, unyielding deformations, feasibility for wall heights in excess of 25 m, and cost-effectiveness. A significant advantage of

mechanically stabilized earth (MSE) walls is their flexibility and capability to absorb deformations due to poor subsoil conditions in the foundations. The cost savings are of the order of 25 to 50% in comparison with conventional reinforced concrete retaining structures, especially when supported by deep foundations.

Mechanically stabilized walls with geogrid reinforcement offer cost-effective technical alternatives to conventional reinforced concrete retaining structures for bridge abutments and wing walls, and locations with right-of-way restrictions, such as embankments and excavations necessitating steeper slopes. They are particularly suited to ground subject to slope instability and at locations of poor foundation soils.

Stresses in the reinforcing elements are transferred to the surrounding soil by bonding between the soil and the reinforcement. This bond is formed through 1) friction, 2) passive soil resistance, or 3) a combination of both, and developed along both sides of the section of the reinforcing element in the resisting zone behind the failure plane. To maintain equilibrium, the bond must resist the maximum tensile load carried by the reinforcing element (pull-out resistance).

2.3 HDPE MANUFACTURING, CLASSIFICATION AND PROPERTIES

Polyethylene is possibly the best known member of the polyolefin family, derived from polymerization of olefin gases. PE is a partly crystalline and partly amorphous material. The properties of PE are determined by its molecular structure. PE consists of

backbone of long molecular chain from which short chain branches occasionally project. The length, type, and frequency of distribution of these branches, as well as other parameters such as molecular weight and distribution, determine the degree of crystallinity and network of molecules that anchor the crystal-like regions to one another. These structural characteristics affect the short and long-term mechanical properties. The extent of crystallinity of PE is reflected by density. The higher density materials have more crystalline regions, which results in greater stiffness and tensile strength.

To protect the polymer during processing, storage, and service, PE is blended with small quantities of heat stabilizers, anti-oxidants, and ultra-violet (UV) screens or stabilizers.

2.4 PET MANUFACTURING, CLASSIFICATION AND PROPERTIES

Thermoplastic (TP) polyesters are the fastest growing of the engineering thermoplastics due to its high performance. Crystallization of the TP polyesters is slow and generally reaches no more than 50%. The excellent mechanical properties of TP polyesters are attributed to orientation effects. These orientation effects are specially strong with large and complex polymer repeating units such as those of the TP polyesters. To accomplish this orientation the TP polyester is melted and then cooled quickly so that the polymer chains become non align or amorphous. Then it is heated to a soft stage above the glass transition temperature (T_g) and stretched in the machine direction. The temperature is then raised while maintaining the cross-direction tension. Then, the TP

polyester is cooled below the glass transition temperature to set the shape. The most common of the TP polyesters is PET.

2.5 VISCOELASTICITY

Plastics are viscoelastic materials, with deformation and strength properties varying with temperature and duration of loading, and also affected by certain environmental conditions. As the name implies, viscoelastic materials respond to stress as superposition of elastic and viscous elements. The springs in the highly simplified model of Fig. 2.1 represent the elastic elements of a polymer (e.g. chain rigidity, chemical bonds, and crystallinity), each spring having a different constant that represents a time-independent modulus of elasticity. The dashpots represent the viscous fluid elements (e.g., molecules slipping past each other), each one having a different viscosity or time-dependent response.

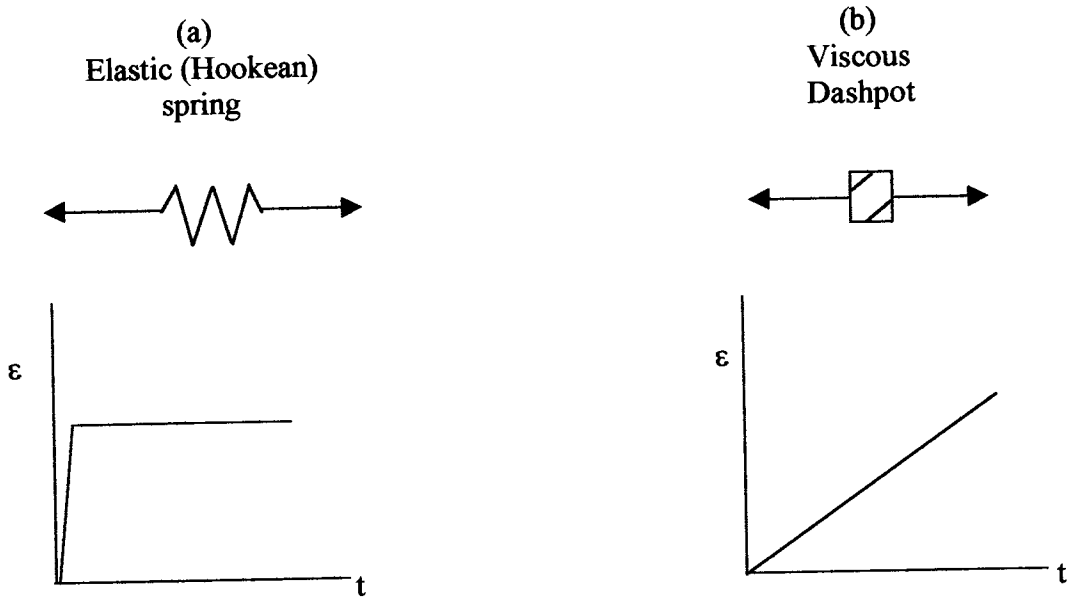

ε = Deformation
t = Time

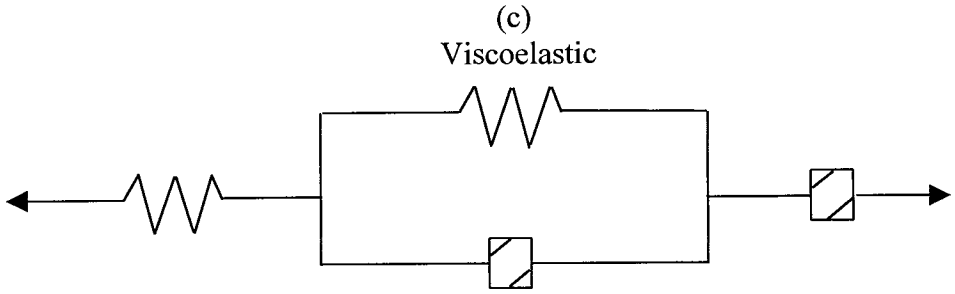

Fig 2.1 Model of viscoelastic behavior

When a constant load is applied and sustained on this model, it results in an initial deformation which continues to increase indefinitely, Fig 2.2. This phenomenon of continuing deformation, which also occurs in concrete, soft metals, wood, and structural metals at very high temperatures, is called creep. If the load is removed after a certain time (say at point t_1 in Fig 2.2), there is a rapid initial strain recovery followed by a continuing recovery that occurs at a steadily decreasing rate; in this model the recovery is never complete. However, if the creep strain does not cause irreversible structural changes and sufficient time is allowed, the strain recovery will be almost completed. The rate and extent of deformation and recovery are sensitive to temperature, and can also be influenced by environmental effects such as by absorption of solvents or other materials with which the plastics may have come in contact with while under stress. An analogous response of viscoelastic materials is stress-relaxation. The initial load required to achieve a certain deformation will tend to gradually relax when that deformation is kept constant, Fig. 2.3. Initially, stress-relaxation occurs rapidly and then steadily decreases with increasing time.

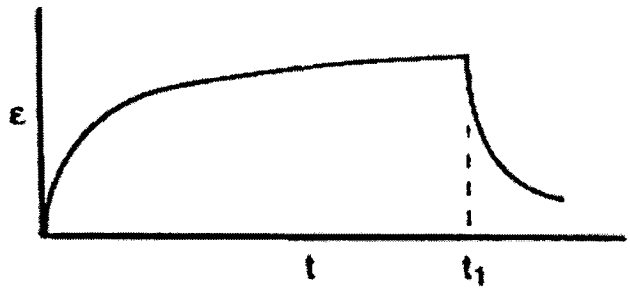

Fig 2.2 Viscoelastic response, creep (constant load)

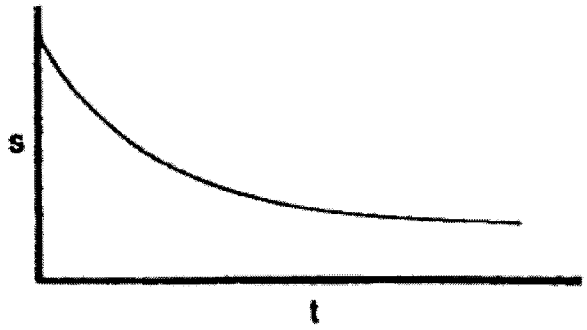

Fig. 2.3 Viscoelastic response, stress relaxation (constant deformation)

CHAPTER 3

LITERATURE REVIEW

3. 1 PULLOUT

Stresses in the reinforcing element are transferred to the surrounding soil by bonding between the soil and the reinforcement. This bond is formed through 1) friction, 2) passive soil resistance, or 3) a combination of both, and developed along both sides of the reinforcing element in the resisting zone behind the failure plane. To maintain equilibrium, the bond must resist the maximum tensile load carried by the reinforcing element (pullout resistance).

Reinforced soil structures have undergone a rapid development as a result of significant advances in analytical techniques and laboratory testing. Pullout resistance of geosynthetics is one aspect of analysis that relates both designs of reinforced soil structures such as walls and slopes, and the configuration of any anchor trench in a geomembrane-lined containment facility. Factors influencing the evaluation of pullout resistance in the laboratory are the type of soil, material properties, including coating, geometry of the geosynthetic, and the test apparatus [Fannin and Raju 1991]. Soil parameters of major interest are the shear strength characteristics, effective stress, and

coefficient of frictional interaction. Since pullout resistance is a function of soil-geosynthetic interaction, the tensile strength, and geometric shape of the geogrid are of major importance. The test setup, depends on the sample dimensions, boundary conditions, and the loading system.

Factors affecting the evaluation of pullout resistance are the type of soil, material properties, geometry of the geosynthetic, and configuration of the test apparatus. The last factor, namely configuration of the test apparatus, relates to the sample dimensions and its preparation, boundary conditions, and the loading system (Fannin *et al.*, 1991).

Fannin and Raju [1991] performed large-scale pullout testing of geogrids and geomembranes embedded in sand. The tests were carried out in a pullout box 1.3 m long, 0.64 m wide, and 0.6 m deep under normal stresses that ranged from 5 to 90 kPa. The sand sample was prepared by pluviation through a hopper. The sand sample was placed in 8 layers to a relative density of about 76%. The principal finding was that the interface bond or shear in pullout, is dependent on relative displacement between the geosynthetic and the soil, the stiffness of the test specimen, and the normal stress acting on it.

The follow up of this work was part of Raju's doctoral dissertation [1995], with tests on five types of geosynthetics: three geogrids, a smooth geomembrane, and a textured geomembrane. The pullout response of these polymeric materials was compared with that of an inextensible fully rough sheet. The mobilization of pullout resistance was described from measurements of pullout force, displacement of the clamped and embedded ends, strain along the embedded length of the specimen, and lateral force on

the interface of soil and the retaining plate. A generalized method was proposed for use with independent measurements of force and strain, based on a combination of available methods, that is applicable to both grids and sheet test specimens. Cyclic loading of the test specimen in most cases revealed that the interaction factor mobilized was equal to or slightly exceeded the value mobilized in a corresponding constant loading test. A conceptual model was proposed that links a load ratio to stable and unstable behavior in cyclic pullout, and identifies a threshold ratio above which unstable behavior results, being >1 for a rigid Geogrid, and =1 for all other test specimens.

Chua *et al.* [1993], performed pullout tests on a HDPE geogrid in both sand and clay samples, under both dry and saturated conditions. The objective of their study was to determine the change in pullout strength of a material in both sand and clay, observe the progression of the failure mechanism, and determine how earth structures respond to flooding due to a failed drainage system in the field. The pullout box they utilized for their laboratory testing was 0.75 m long, 0.70 m wide, and 0.60 m deep. The sand sample (dry) was compacted to a relative density of about 70% and subjected to a normal stress of 161 kPa. The clay sample (dry) was compacted to about 100% and 88% Standard Proctor, AASHTO T-99, and subjected to a normal pressure of 28.7 kPa. The results of the tests for sand samples showed a decrease in the pullout strengths of the geogrid due to wetting, and to 0.57 times of the strength in dry conditions. However, the results of the tests for clay samples showed a relatively lesser decrease in the pullout strengths of the geogrid under saturated conditions, i.e. 0.81 times the strength in dry conditions.

Farrag et al. [1993], conducted a pullout testing program to develop reliable testing procedures and interpretation schemes for evaluation of the short-term and long-term pullout performance of geosynthetic reinforcements. The inner dimensions of the pullout box used was 1.52m long, 0.9m wide, and 0.76m high. Pullout tests were performed on both HDPE and PET geogrids in sand of varying thickness (0.6m on an average) with an average displacement rate of 6mm/min. The important conclusions drawn were as follows: 1) Increased thickness of soil cushioning the geosynthetic decreases the effects of top and bottom boundaries; a thickness of at least 0.3m above and below the geogrid is recommended to eliminate the influence of these boundaries, 2) The displacement rate effects are minimized if rates of the order of less than 6mm/min are used.

Farrag *et al.* [1995] evaluated the functional relationship between soil water content and the interface frictional parameters depending on soil type, density, and the confining pressure. Pullout tests were performed on HDPE geogrid specimens in two different types of cohesive soils at optimum moisture content and higher levels of moisture content for the Modified Proctor test, AASHTO T180. The inner dimensions of the pullout box used were 1.22 m long, 0.8 m wide, and 0.6 m high. Pullout tests were performed immediately after applying the confining pressure, and the results represented essentially unconsolidated-undrained test conditions. The pullout rate was 2 mm/min and the confining pressure was 48.2 kPa. The porewater at the interface of the geogrid and the soil was measured during pullout by making use of a vibrating wire piezometer. The results indicated that an increase in the soil water content causes a decrease in the pullout resistance.

Finite element analysis, using two-dimensional plane strain formulation, has been used to predict the performance of geogrid reinforced backfills by Karpurapu and Bathurst [1992] using a program GEOFEM. A finite element analysis, SSTIN, was developed by Desai [1991] to compare with field test data on a geogrid reinforced earth retaining precast concrete wall obtained by Fishman and Desai [1991].

The computed geogrid strains were smaller than the measured values. However, it was concluded that the finite element analysis should be further refined to obtain more reliable results (Chan *et al.*, 1993). The authors also outlined the areas in which the refinement is needed, i.e. simultaneous construction sequence and nonlinear soil behavior, and interfaces between the soil used for the wall fill and geogrids.

Chua, Aspar, and De La Rocha [1993] used the program GEO 2D, developed at the University of New Mexico, which is an updated Lagrangian code that allows large deformations in the soil-fabric system, for predicting the deformation pattern due to pullout forces. Both unsaturated and saturated sand/clay media were addressed, but only with continuum (not poroelastic) elements.

3.2 CREEP AND CREEP RUPTURE

3.2.1 DEFINITION

Creep is the physical phenomenon occurring in most material, and particularly in plastics, termed creep is the deformation of the material over a prolonged period of time under constant pressure (Environmental Protection Agency, 1990). Creep is a material, load, temperature, and time-dependent phenomenon. It is associated with all the mechanical deformations: tensile, compression, torsion, and flexure (ASTM D 2990-93a, 1993). However, tensile creep is the only deformation that matters for geogrid, since it is a flexible material. It is of primary importance in the design of polymeric reinforced structures. (Allen 1991).

The tensile creep test is carried out by applying in-plane stress while the compressive creep test is realized by applying normal loading. Creep and creep-rupture data must be taken into consideration for the determination of the creep modulus and strength of the material for long-term behavior (Cazzuffi et al, 1997).

The creep test measures the dimensional changes of a specimen subjected to a constant load during a certain period of time, while the creep rupture test measures the time taken for rupture to occur under constant load (ASTM D 2990-93a, 1993). Creep behavior is commonly assessed at constant times and temperatures, and is shown Fig 3.1: either strain versus time (or log time) or strain rate versus time.

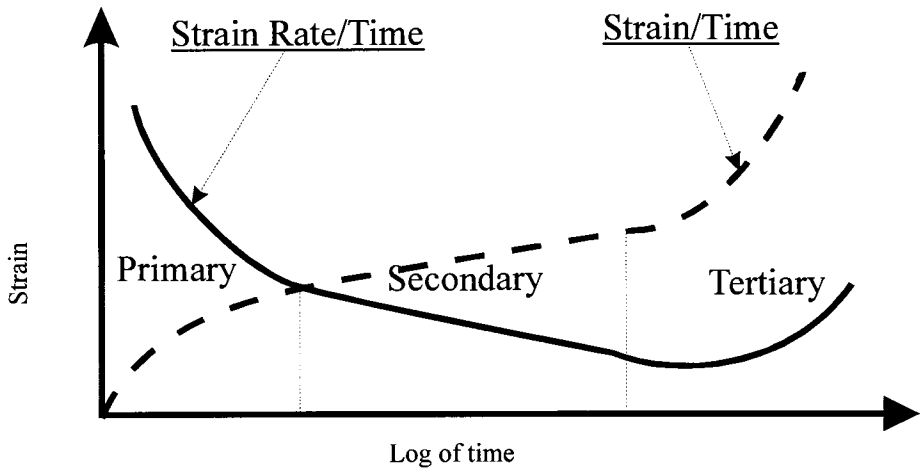

Figure 3.1. Typical creep curves Cazzuffi [1997].

HDPE and PET are viscoelastic materials for which the history of deformation has an effect on the response. For example, if a load is continuously applied, it causes an instantaneous initial deformation, and then increases at a decreasing rate. The stress and strain are related by a modulus that depends on the duration and is independent of the magnitude of the applied stress and strain for a given temperature, Fig. 3.2. Viscoelastic behavior becomes nonlinear at high stress or strain or elevated temperatures, Figs. 3.2 and 3.3.

Creep, expressed in terms of the decreasing modulus contributing to increasing deformation, (i.e. loss of stiffness), and creep-rupture, expressed in terms of decreasing life with increasing stress and temperature, are important parameters for life prediction. The transition from ductile to brittle behavior enables the realistic estimation of life from the creep-rupture plot. The creep and creep-rupture schematics for life prediction are shown in Figs. 3.2, 3.3, and 3.4.

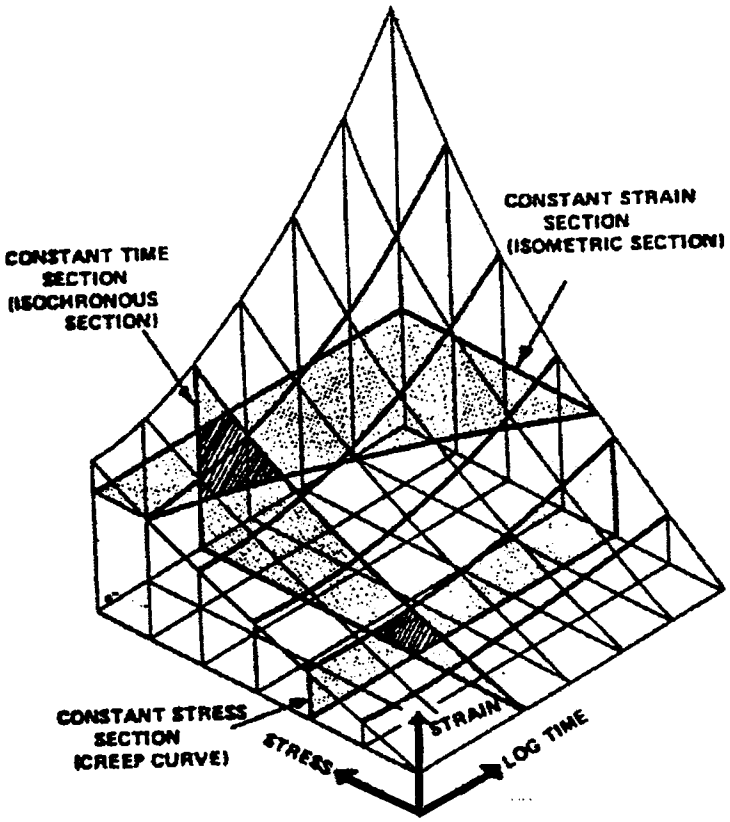

Fig. 3.2 Constant stress-strain time coordinates

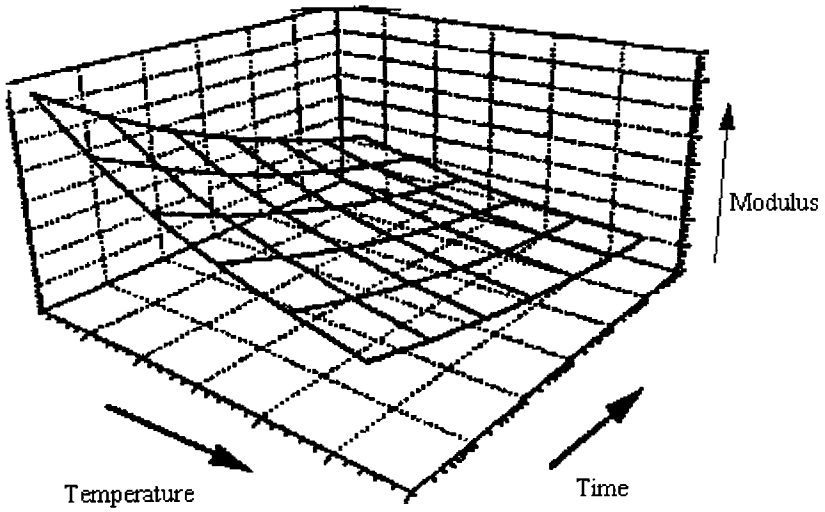

Fig. 3.3 Schematic of the viscoelastic behavior of polymers

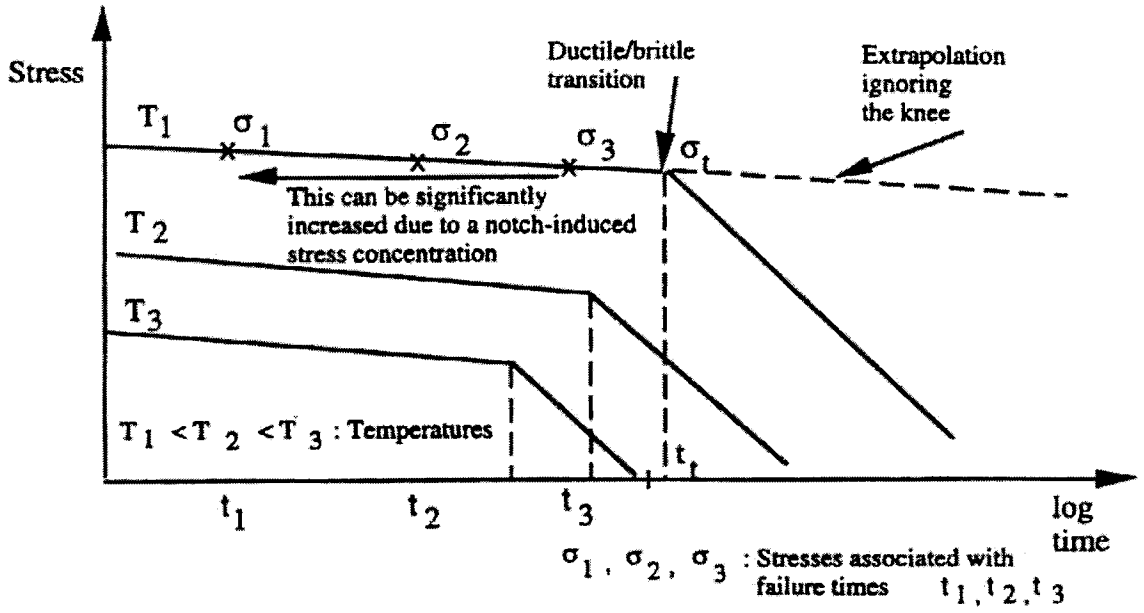

Fig. 3.4 Creep-rupture behavior for semi-crystalline polymers

3.2.2 DIFFERENT PHASES OF CREEP RESPONSE

The creep behavior of a constant polymeric material can be divided into three phases called primary, secondary, and tertiary creep. During the primary phase the strain increases but the strain rate decreases, in the secondary phase (also called steady state) both the strain and strain rate are constant, and the tertiary phase is characterized by a rapid increase of strain and strain rate leading to the specimen's rupture.

Geosynthetic structure tends to dominate primary creep, whereas the polymer material normally dominates the secondary and tertiary creep. (Allen, 1991). For polymeric materials, tertiary creep is the dominating phase for polyethylene and

polypropylene, while in geosynthetics made of polyester, primary creep is the dominating phase, thus some materials do not show strain and strain rate increases before rupture.

Long-term performance is a function of polymer type, grade, manufacturing techniques (since they influence the orientation and length of molecules), and the percent of crystallinity. These will control the degree of molecular orientation and entanglement between molecules, the percent of crystallinity, the molecular length, and hence the long-term strain response (den Hoedt, 1986). The polymer creep response is also affected by load level and temperature (Allen 1983). Since the polymer material dominates secondary and tertiary creep, these polymer characteristics will generally control when and at what load level a given geosynthetic will rupture. Macrostructure affects creep behavior, since debonded fibers can straighten and thus increase creep strains, postponing the creep-rupture limit. Even though several studies show that temperature has little influence on creep behavior, time-temperature superposition principles are used to estimate the long-term properties of polymeric materials. Moreover, for HDPE, increasing the molecular weight can reduce the temperature influence (Bush, 1992). However, the effect of load is many times greater than the effect of temperature (Cazzuffi et al, 1997). D. I. Bush, 1989, tested three oriented polyethylene grids at 10° C ,20° C , and 40° C. under a range of sustained loads to provide long-tem strain-time data. These test showed that the effect of load was many times greater than the effect of temperature. Thus, these polyethylene grids are relatively insensitive to temperature changes.

3.2.3 TENSILE CREEP BEHAVIOR

Cazzuffi et al. (3) evaluated the tensile creep behavior of high-strength geosynthetics, using the CEN European Method in order to compare the European and American methods. Twelve specimens were placed in a load frame, and tested at a constant temperature and humidity (controlled air-conditioned room). HDPE extruded geogrids, PET woven geogrids, and PP/PET woven/nonwoven composite geotextile were trimmed to conform to the CEN Standard (European Standard), and tensile creep tests were performed. Comparing the CEN and ASTM methods, no major differences in the procedures were observed, although parameters such as specimen sizes and loading time differed slightly. The test temperature was 20°C and the humidity 65%; three different loads were applied, 20%, 30%, and 50% of the wide-width tensile strength. Strain versus time and strain rate versus time graphs were plotted for each load and material. The testing time extended to 10000 min. Only one specimen posed a problem: the HDPE extruded geogrid approached failure for a load equal to 50% of the wide-width tensile strength; other specimens remained acceptable for this small period of time.

3.2.4 CREEP RUPTURE ENVELOPE

While characterizing the creep behavior of a material, it is interesting to evaluate the creep rupture envelope (ASTM D 2990-93a, 1993), which is the curve connecting the rupture points of several tensile creep-rupture test curves, Fig. 3.5 The creep-rupture tests are carried out for different temperatures and loads. The envelope curves are of primary importance for designing with geomembranes.

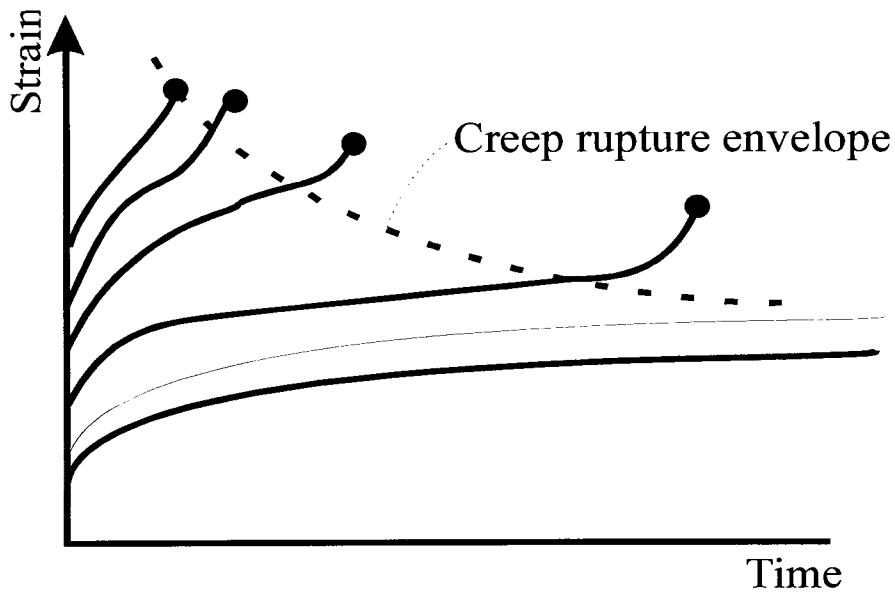

Figure 3.5. Creep rupture envelope (ASTM D 2990-93a, 1993).

3.3 DURABILITY AND DEGRADATION

3.3.1 INTRODUCTION

The principal types of degradation in geosynthetic materials are ultraviolet light degradation, chemical aging, biological degradation and geosynthetic macrostructure. Since geosynthetics will typically be buried in soil or covered, strength loss cause by UV degradation will occur only at and before the geosynthetic is installed. Chemical aging and biological degradation can occur throughout the life of the structure.

3.3.2 ULTRAVIOLET LIGHT DEGRADATION

There is some evidence to suggest that extended exposure to UV light before soil burial may accelerate the geosynthetic degradation process in soil (Jailloux and Segrestin, 1998). UV degradation is a photo-oxidative process which attacks only the surface of the polymer fibers (Wrigley, 1987). Chain scissions within the polymer occur, resulting in material embrittlement and eventual failure (Schneider and Groh, 1987).

Polyolefins are specially susceptible to UV degradation and must be protected either chemically or physically. Carbon black effectively shades the oxidation prone molecules and is the most common method of protecting polyolefins. Polyesters are not affected as much by photo-oxidation but may suffer moderate strength loss, depending of the choice of pigments used in the polymer (ICI, 1986). Strength losses due to UV

degradation for extruded high density polyethylene (HDPE) geogrids have been found to be much less for geotextiles due to their great filament thickness (Wrigley, 1987).

3.3.3 CHEMICAL AGING

Chemical degradation of geosynthetics is a result of both environmental factors and polymer compositional factors. For a given polymer type, the greatest amount of chemical degradation will normally occur in polymers that have low molecular weights, low percent crystallinity, low density, and low draw ratios (Elias, 1990). One can expect the greatest amount of degradation to occur, in general, at relatively high temperatures, in moderate to high moisture conditions, in soils that are actively chemically, mostly in terms of pH. (Elias, 1990). Thickness of the polymer fibers may also have a strong influence on the degradation rate, since degradation mechanisms are dependent on diffusion processes or exposure and removal of surface material (Wrigley, 1987). The main chemical degradation mechanisms in typical soil environments are oxidation, hydrolysis, and environmental stress cracking (ESC).

3.3.3.1 Oxidation

The oxidation reaction can either be initiated by ultraviolet radiation or thermal energy. Since geogrids will be normally buried in reinforcement applications, thermally activated oxidation is of most interest. Of the polymers used in geosynthetics, relatively speaking, PP is potentially the most susceptible to oxidation, followed by HDPE and PET

which have a relatively low susceptibility. Oxidation is the reaction of free radicals within the polymer with oxygen, resulting in breakdown and/or crosslinking of the molecular chains and embrittlement of the polymer. (Allen and Elias, 1995).

Antioxidants are typically added to prevent oxidation during processing and use. As the antioxidants are used up, resistance of the polymer to oxidation will decrease. The rate of polymer oxidation depends on how much and what type of antioxidant is present initially, at what rate it is used up, how well it is distributed within the polymer, and how fast it can be leached out by the flow of fluids, such as water, into and around the polymer (Van Zanten, 1986). Environmental factors which affect the rate of oxidation include temperature, oxygen concentration which in soil can vary from 21 percent in gravels at shallow depth to approximate 1 percent in fine-grained soils at deeper depths (Yanful, 1993; Yanful, et. al., 1993), and the presence of transition metal ions such as iron (most common) or copper which act as a catalyst and accelerate the oxidation reaction. Thermal oxidation at typical in-soil temperatures appears to be quite slow.

3.3.3.2 Hydrolysis

Hydrolysis occurs when water molecules react with the polymer molecules, resulting in chain scission, reduced molecular weight, and strength loss. Of the polymers typically used for geosynthetics, only PET is potentially susceptible to hydrolysis, since hydrolysis is simply the very slow inverse reaction of the synthesis of PET when water is present. Water does not cause significant hydrolysis without other environmental factors, such as

the presence of specific catalytic ions or elevated temperatures. The presence of specific catalytic ions, as well as pH, can influence the rate of hydrolysis. High pH (alkaline) hydrolysis can result in relatively rapid rate of hydrolysis, whereas neutral or low pH conditions can result in a slow hydrolysis rate.

The chemical environment is an important aging factor, especially considering the aggressive environment that can be formed in the soil. The principal mechanisms of chemical degradation have been defined as follows (Van Zanten, 1986):

Metathesis - breaking of carbon - carbon bonds.

Solvolysis - breaking of carbon - noncarbon bonds in the amorphous (liquid).

Oxidation - liquid reaction with molecular oxygen.

Dissolution- separation into component molecules by solution.

Each of these mechanisms leads to bond breakage at the molecular level, which is called bondcism. If these mechanisms occur under stress, environmental stress cracking (ESC) will occur. The rate of hydrolysis is also highly temperature dependent and can become relatively rapid at high temperature in the vicinity of the glass transition temperature or above for the polymer, which is on the order of 70° C to 80° C (158° F to 176° F). Temperature may affect the hydrolysis reaction in two different ways: a) the rate of diffusion of water is a function of temperature, and b) the hydrolysis reaction follows the Arrhenius Law, i.e., the reaction rate increases and decreases exponentially with

temperature variations. Typical soil temperatures are in the range of 50-60 °F (10-15.6 °C); temperatures near the surface of the wall can reach 85-100 °F (29.4 - 37.8 °C). The polymer does not need to be submerged for hydrolysis to occur, as hydrolysis can occur in moderate to high humidity conditions, though the reaction rate becomes slower as the humidity decreases (McMahon, et. al., 1959).

Hydrolysis appears to be the result of both a surface erosional phenomenon as well as a diffusional process of water to the polymer fiber core. These two phenomena have given rise to the terms "outer" and "inner" hydrolysis. Outer, or superficial, hydrolysis is dominant in high pH conditions and is characterized by loss in fiber cross-sectional area with minimal reduction in the molecular weight of the polymer which remains (Anderson, et. al., 1992). Inner, or diffusional controlled hydrolysis is dominant in neutral and acidic conditions and characterized by significant loses in molecular weight of the polymer with minimal surface erosion or damage (Anderson, et. al., 1992).

3.3.3.3 Environmental Stress Cracking (ESC)

Rupture of a polymer when under stress is either ductile or brittle in nature. The ductile failure mode occurs when stresses are high enough to cause tie molecules to stretch out, lamellae to separate and start unfolding, resulting in fracture of the spherulites and plastics flow of the molecular structure (Lustiger, 1983). When failure occurs in a brittle manner, stress levels are usually lower, allowing sufficient time for tie molecules

to slowly disentangle themselves from adjacent spherulities, initiation crack formation followed by slow crack growth (Bright, 1993).

3.4 LIFE PREDICTION

There is an identified need to investigate the long-term behavior in relatively short laboratory time scale, by evaluating the effect of soil degradation mechanisms at field-related temperatures and stresses, compounded by synergistic effects, with accelerated testing, high stress, elevated temperatures, and/or aggressive liquids.

Because of the strong time and temperature dependence of polyethylene and other thermoplastic materials, it is both possible and necessary to accelerate the failure mechanism. The key is the use of time-temperature shifting functions that can reliably connect high temperature/high pressure performance to actual service conditions.

The long-term properties can be predicted based on viscoelastic behavior: i) the time-temperature (WLF) superposition (Aklonis and Macknight, 1983), which describes the equivalence of time and temperature, ii) the Arrhenius equation (Koerner, 1998), which describes the temperature dependency of the degradation reaction on time and temperature, and iii) the rate process method, describing which curve fits time-to-failure test data at elevated temperatures to enable predictions of time-to-failure at lower temperatures, (Popler, 1993).

3.4.1 WLF METHOD

Based on the time-temperature (WLF) superposition principle, for each of the three load levels, creep curves are plotted for different temperatures, and superposed by horizontal shifts along a logarithmic time scale to give a single curve covering a large range of times, termed a master curve. The shift factor, $a_{T'}$, is function of temperature and described as follows:

$$\log a_{T'} = [-C_1 \times (T-T_r)] / [C_2 + (T-T_r)] \quad \text{----------} (3.1)$$

where,

$a_{T'}$ = shift factor

C_1 and C_2 = universal constants, which vary from polymer to polymer

T_r = reference temperature

T = Test temperature

The large time-scale master curve enables the determination of the long-term mechanical properties and service life, Fig. 3.6 (Aklonis and Macknight, 1983). Fig. 3.7 shows the three master curves (modulus-time curves at three different stress levels) obtained by time shifting. The extrapolation equation for any other loading condition will be determined, similar to the procedure used for the Hydrostatic Design Basis (HDB) test described in the ASTM Standard D2837.

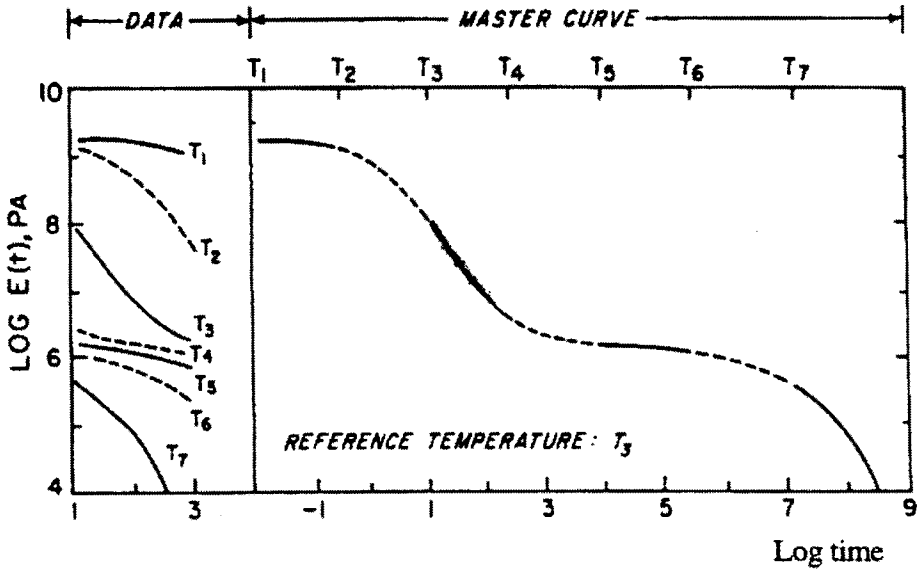

Fig. 3.6 Master curve from experimentally measured modulus-time curves at various temperature [Aklonis and MacKnight, 1983]

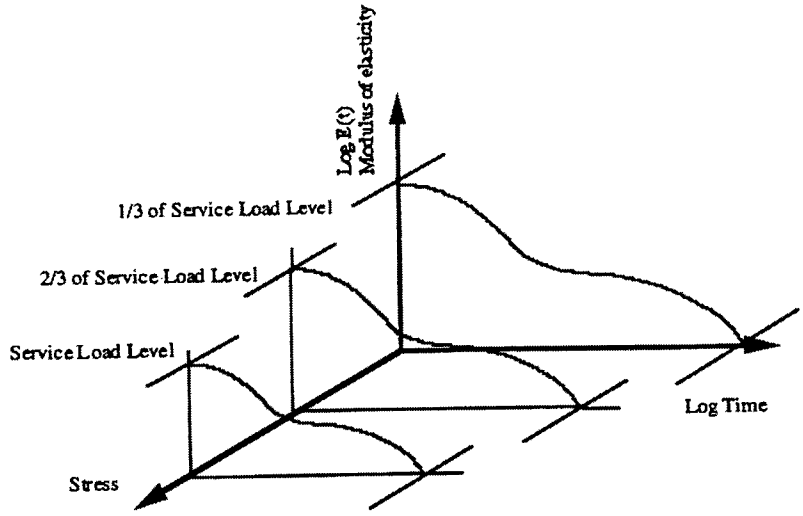

Fig. 3.7 Master curves at different load levels

3.4.2 ARRHENIUS METHOD

In 1886, Arrhenius formulated an expression for the relationship between temperature and the rate of degradation. Equation 3.2 gives the Arrhenius equation [Koerner, 1998]:

$$\frac{r_{T\text{-test}}}{r_{T\text{-site}}} = e^{-Eact/R[1/T\text{-test} - 1/T\text{-site}]} \qquad (3.2)$$

where: Eact/R = slope of Arrhenius plot,

T-test = incubated (high) temperature, in °K,

T-site = site-specific (lower) temperature, in °K,

r = reaction time,

Eact = effective activation energy, J/mole, and

R= universal gas constant, 8.314 J/mole

Eqn. 3.2 can also be written as follows:

$$\ln(r_{T\text{-test}}/ r_{T\text{-site}}) = (Eact/R)(1/T\text{-test}-1/Tsite) \qquad (3.3)$$

or

$$\frac{Eact}{R} = \frac{\ln(1/t1) - \ln(1/t2)}{(1/T1) - (1/T2)} \qquad (3.4)$$

where: t = time, hour, and, T = temperature, °K

In the Arrhenius plot, degradation is plotted as the logarithm of the reciprocal of time versus the reciprocal of temperature. From this the slope of the Arrhenius plot can be obtained using equation (3.4). A schematic of the Arrhenius plot is given in Figure. 3.8.

It is noted that the temperature has an exponential effect on the time required for a specified level of degradation based on this model, and the data used in Equation 3.1 is obtained at a constant level of degradation (indicated by the modulus decay) in the material. The extrapolation for failure time is similar to that used in the W-L-F Method. The WLF and Arrhenius equations are accurate for linear amorphous polymers, but catastrophic failure that occurs at ductile-brittle transition make the prediction difficult for semi-crystalline polymers. In this model the temperature has an exponential effect on the time required for a specific level of degradation.

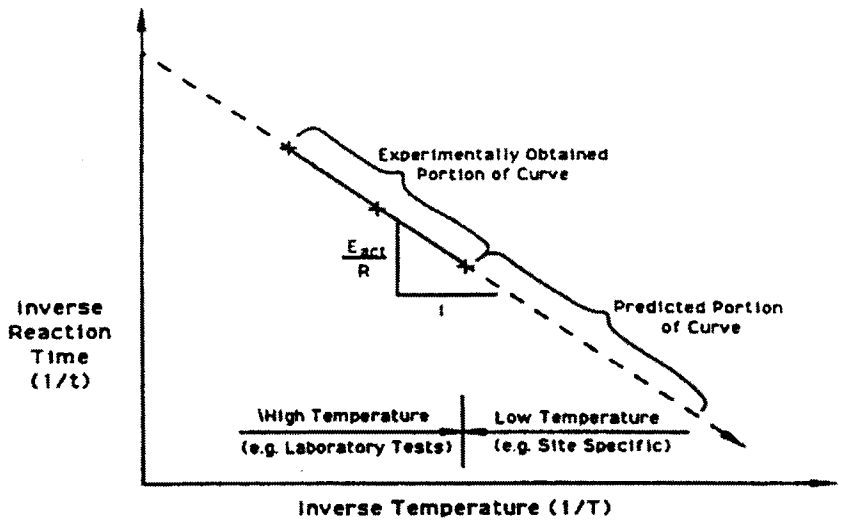

Fig. 3.8. Generalized Arrhenius plot, for a specified stress level, used for life prediction from super-ambient temperature experimental data

3.4.3 RATE PROCESS METHOD (RPM)

The conventional time-temperature shifting procedure for pressurized pipe is the rate process method (RPM) which, in essence, curve fits time-to-failure test data at two elevated temperatures to enable predictions of times-to-failure at lower temperatures. The time to failure for thermoplastic pipe depends upon the operating temperature and the induced stress. The RPM has been used by the gas industry to extrapolate design parameters at the operating temperature from elevated temperature, sustained hydrostatic pressure tests of pipes, [Poplelar, 1993], and [Koerner, 1998]. RPM, that has evolved from analyzing numerous test data, assumes that the time to failure is governed by an Arrhenius relation wherein the activation energy varies linearly with the logarithm of stress [Poplelar, 1993], and [Koerner, 1998]. The RPM Method can be applied to geomembranes, the difference is in the stressing of the material [Koerner 1994].

The RPM equation is expressed by one of the following two equations in the case of geomembranes:

$$\log t_f = A_0 + A_1 T^{-1} + A_2 \log P \qquad (3.5)$$

$$\log t_f = A_0 + A_1 T^{-1} + A_2 T^{-1} \log P \qquad (3.6)$$

where,

t_f = time to failure

T = temperature

A_0, A_1 and A_2 = constants

P = stress in geomembrane

For the use of the RPM, a minimum of two experimental failure curves at different elevated temperatures is required, and the Equation i.e. 3.5 or 3.6, that gives the best correlation is used.

CHAPTER 4

PULLOUT TESTING

4.1 MATERIAL PROPERTIES

4.1.1 GEOSYNTHETIC TEST SPECIMENS

4.1.1.1 Geogrid HDPE Properties

The HDPE geogrid is manufactured by stretching a punched sheet of extruded high-density polyethylene in one direction under carefully controlled conditions. This process aligns the polymer's long-chain molecules in the direction of drawing, and results in a product with high one-directional tensile strength and modulus. The properties of Geogrid UX-1600 SB are presented in Table 4.1. Based on the information provided by the manufacturer, the long term load capacity was measured by tensile creep testing to 10,000 hours as described in the Geosynthetic Research Institute test method GG3-87 "Creep Behavior and Long Term Design Load of Geogrids".

Table 4.1 Properties of UX-1600 SB (HDPE) Geogrids

PROPERTIES	TEST METHOD	UNITS	VALUE
INTERLOCK			
Apertures	Calipered		
--MD		mm	137 (nom.)
--CMD		mm	16.7 (nom.)
Open area	COE Method	%	60 (nom.)
Thickness	ASTM D1777-64		
--ribs		mm	1.8 (nom.)
--junctions		mm	5.8 (nom.)
REINFORCEMENT			
Creep Limited Strength	GRI GG3-87	kN/m	43.8 (min.)
Flexural Rigidity	ASTM D1388-64	mg-cm	6600000 (min.)
Tensile Modulus --MD	GRI GG1-87	kN/m	1896 (min.)
Junctions	GRI GG2-87		
--strength		kN/m	102 (min.)
--efficiency		%	90 (min.)
MATERIAL			
High Density Polyethylene	ASTM D1248 Type III/Class A/Grade 5	%	97.0 (min.)
Carbon Black	ASTM 4218	%	2.0 (min.)
DIMENSIONS			
Roll Length		m	30
Roll Width		m	1.0 & 1.3
Roll Weight		N	334 & 436

4.1.1.2 Geogrid PET Properties

PET is the acronym for Polyester. The PET geogrid is bidirectional made of polyester multi-filament yarns, which are interlocked by weaving to create a stable network, such that the yarns retain their relative position. Compared to HDPE, PET is more flexible in bending, and exhibits a relatively lower junction strength. The measured dimensions and properties of Geogrid Matrex 60 are shown in Tables 4.2 and 4.3. Based on the information provided by the manufacturer, the life expectancy is 75 years.

4.1.2 SOIL TEST SPECIMENS

Two kinds of soil were used in the present study: sand and limerock. Both of them are very common in Florida, and meet the FDOT Materials Specifications FM1-7027 and FM1-7011. The optimum moisture content is around 11%. The sand has an average grain size of 0.55 mm, and effective grain size of 0.16 mm. The friction angle is about 36°, and the density 1560 kg/m^3. The uniformity coefficient is 5.2 and the coefficient of gradation 0.63.

The limerock is well graded with 0.9 mm average grain size and 0.15 mm effective grain size. Its friction angle is around 34°, and the density 1498 kg/m^3. It has a uniformity coefficient of 9 and coefficient gradation of 1.14. A mechanical sieve analysis was performed on the soils and the results are listed in Table 4.4.

Table 4.2 Dimensional Properties of PET Geogrids.

Properties	Manufacturing Process	Coating Type	Polymer Type	Dimensional Properties			Long Term Design Strength GRI GG4 (in sand) (kN/m)
				Mass/Unit Area ASTM D 5261-92 (g/m^2)	Aperture Size (mm)		
					MD	XD	
Matrex 30	Woven	PVC	PET	332	81.3	12.7	15
Matrex 60	Woven	PVC	PET	593	81.3	12.7	30
Matrex 90	Woven	PVC	PET	661	81.3	12.7	44
Matrex 120	Woven	PVC	PET	748	81.3	7.6	58
Matrex 180	Woven	PVC	PET	1017	81.3	7.6	76
Matrex 240	Woven	PVC	PET	1288	81.3	5.1	109

Table 4.3 Mechanical Properties of PET Geogrids

Properties	Ultimate Tensile Strength (kN/m)	Tensile Strength (kN/m)	Limit State (Creep) Tensile Strength (kN/m)	
Test Method	**ASTM D-4595**	**ASTM D-4595(1) 5% strain**	**GG3(3) 5% strain**	**GG3(3) 10% strain**
Matrex 30	48	39	20	31
Matrex 60	93	52	35	52
Matrex 90	137	65	52	78
Matrex 120	181	78	72	109
Matrex 180	259	104	78	142
Matrex 240	370	146	111	204

* GG: Geogrid Junction Strength Method

* GRI: Geosynthetic Research Institute Test Method

Table 4.4 Gradation of Soils (Backfill specifications)

Sieve size (mm)	Percent Passing (%)		
	FDOT	**Sand**	**Limerock**
90	100	100	100
20	70-100	100	100
4.75 (No.4)	30-100	100	100
0.425 (No.40)	15-100	43.8	27.1
0.150 (No.100)	5-65	8.3	10.6
0.075 (No.200)	0-15	0.2	0.1

4.2 TEST SETUP

4.2.1 INTRODUCTION

Eight pullout boxes were designed at Florida Atlantic University (1996) to evaluate the development of pullout resistance with increasing displacement of the geogrid specimens. Measurements included pullout force, pullout displacement, and strain in the geogrid specimens. The shop drawings are presented in Figs 4.1-4.5.

4.2.2 LARGE PULLOUT APPARATUS

The pullout box contains the soil sample and geogrid test specimen with a clamp assembly for gripping the geogrid test specimen, airbags for imposing confining pressure, a spring assembly for the application of the pullout force, and a watering system for the saturated condition.

4.2.2.1 Pullout Box

In the ASTM draft proposal for pullout testing, the minimum dimensions for the pullout box are proposed as follows: 0.76 m long, 0.46 m wide, and 0.305 m deep. Also, a minimum clearance on the sides is indicated as 7.5 cm. The ASTM draft proposal further recommends the use of a metal sleeve to minimize the influence of the front boundary.

The internal dimensions of the pullout box were based on the following criteria: (1) The box had to be long enough to accommodate a geosynthetic test specimen representative of the material used in field structures, (2) The box had to accommodate test specimens of length to width ratio around 2, and (3) The width and the depth of the pullout box had to be large enough to minimize the boundary effect. A summary of the pullout boxes and testing characteristics is presented in Table 4.5.

The internal dimensions of the pullout box were first chosen to be 1.22 m long, 0.60 m wide, and 0.60 m deep. After the pre-analysis and investigation, all others were reduced to be 1.22 m long, 0.46 m wide, and 0.33 m deep. All dimensions exceed the ASTM requirements greatly. These gave a clearance of 80 cm between the specimen and the side wall of the apparatus.

The steel pullout box was composed of eight main sections, bottom plate, bottom beams, side walls, side columns, front wall, rear wall, steel pad, and top cover (Figs 4.1-4.5). The base plate (#21) was edge stiffened with four steel tubings (#1) (63.5 mm x 63.5 mm x 5 mm) and three steel angles (#12) (50 mm x 50 mm x 3 mm). They supported the pullout box and provided the reaction for the normal stress that applied on the test specimen. The steel base plate was 3 mm in thickness to provide the soil sample with a rigid support condition (Fig 4.1).

The side walls (#23) were made of steel plates edge-stiffened with four mild steel tubings (#2) (50 mm x 50 mm x 5 mm) (Fig 4.2). These four tubings also served as

Table 4.5 Summary of the Pullout Test Boxes and Test Modes

Research Institution or Company	Dimensions (cm) L x W x D	Soil Properties	Test Specimen	Boundary Preparation	Sample Preparation	Test Mode
STS Consultants Ltd., IL, USA (Bergado et al. 1986)	134 x 70 x 38	Fontainbleau sand (SP); dense sample	Tensar SS2 and SR2	A slot introduced to transfer the rigid front boundary into the box	Compacted using vibratory plate	Constant rate of displacement (1 mm/min)
University of Missouri-Rolla (Lentz and Pyatt, 1988)	76.2 x 29.2 x 10	Fine sand and Course sand	Tensar SS1 and SR2	——	Placed using V-shaped hopper and each layer vibrated to densify	Constant rate of displacement (2.5 mm/min)
Kyushu University, Japan (Ochiai, Yasuda et al. 1992)	60 x 40 x 40	Toyoura sand: at 85~90% of max. density	Geogrids Tensar SS-2 and SR-2	——	Compacted to achieve required density	Constant rate of displacement (1 mm/min cyclic loading)
Institute of Soils, Rocks and Foundations Switzerland (Kharchafi and Dysli, 1993)	80 x 55 x 20	Fine-grained sand; moist silt	Nonwoven heat bonded polypropylene	Metal clamp buried in sand to avoid rigid front wall	——	Stopped at regular intervals to enable taking X-ray shots
The Reinforced Earth Co. (Cowell and Sprague, 1993)	152 x 61 x 30.4	Uniform fine sand with silt trace	Geogrids and Geotextiles	Lubricated tapered metal sleeve on front wall	Sand placed at 95% of standard Proctor density	Constant rate of displacement (1 mm/min)

columns to give the lateral support for the side walls, and transmit the confining pressure load from the top beams (#3, #11) to the bottom ones (#1). The sizes of these columns were 13.5 mm smaller than those of the bottom beams. This made a three-edge welding connection (3 mm high) possible between the bottom beams (#1) and side columns (#2). Two pieces of Lucite-ES acrylic sheet are glued to the inside faces of the side walls to minimize the side wall effect by reducing the friction between the soil sample and the side walls.

At the top of the side columns (#2), bolts (#41) (ϕ12) were welded through steel plates (#34) (5 mm thick). These bolts went through the holes located on the top beams (#3, #11) so that the top cover could be bolted tightly (Elevation C-C).

The front wall was mainly made of three parts, two front beams (#4), two small plates (#31), and one big plate (#24), with a rectangular slot in the middle. The two small plates (#31) went through the slot, and were welded to the front beams (#4). They helped to minimize the influence of the front wall boundary. On the two front beams (#4), four bolts (#42) were welded on to connect the clamping assembly support frames (Elevation C-C).

The removable top cover was made of two tubings (#3) (50 mm x 50 mm x 5 mm) and two angles (#11) (50 mm x 50 mm x 3 mm). Holes were made near the ends of the beams to receive the bolts (#41) from the side columns (#2) (Fig 4.4).

The back wall of the pullout box was also made of 3 mm thick steel plate (#25). There was a small hole with 20 mm in diameter in the center of the plate for the wires from the instrumentation on the test specimen (Fig 4.4).

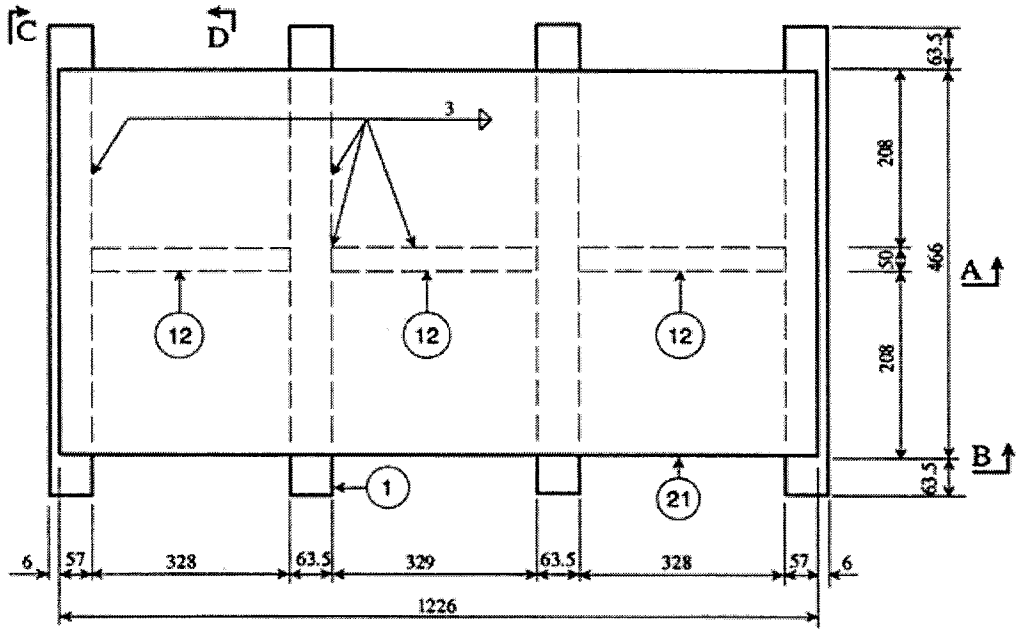

Bottom Plan

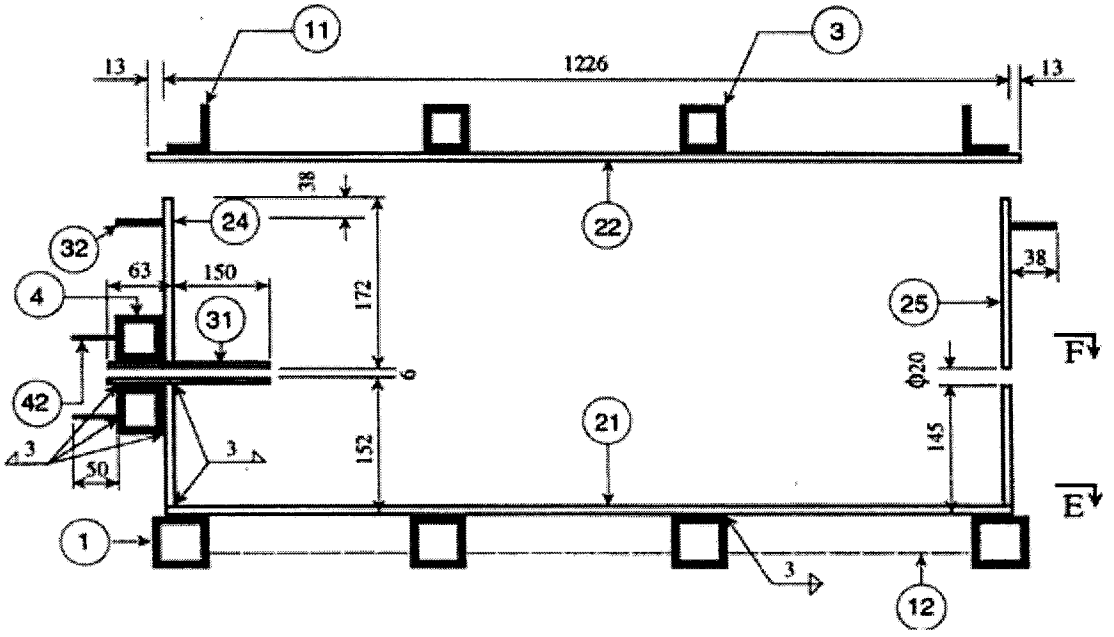

Section A - A

Figure 4.1 Pullout box shop drawing (I) (Units in mm)

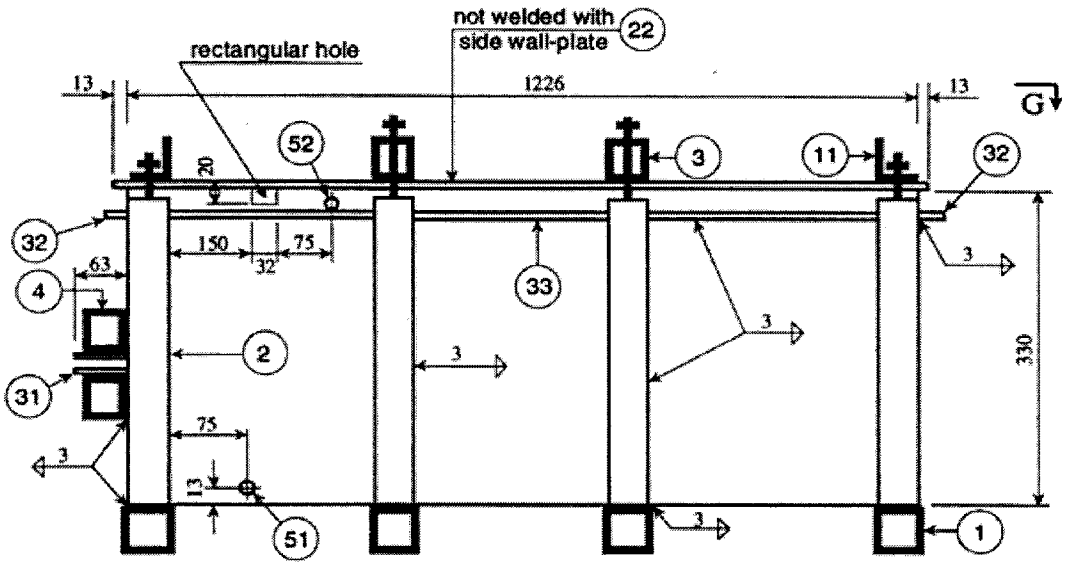

Section B -B

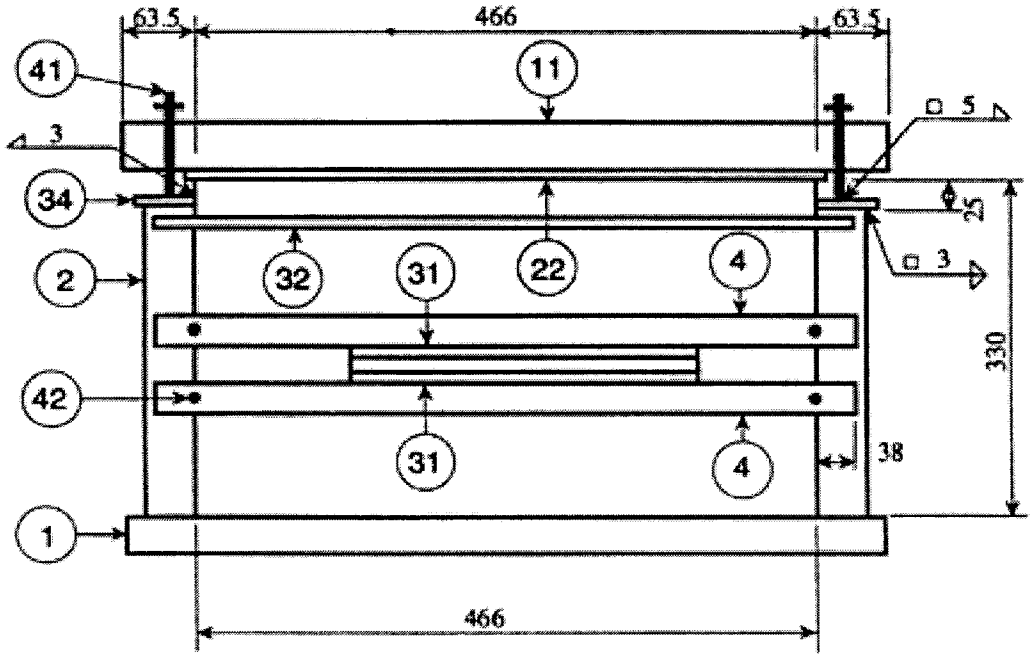

Section C - C

Figure 4.2 Pullout box shop drawing (II) (Units in mm)

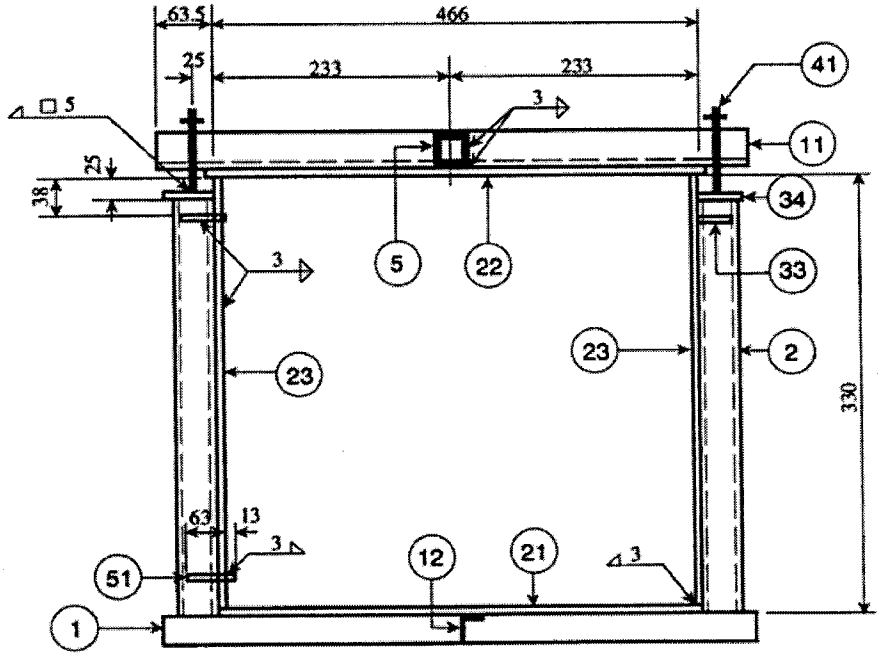

Section D -D

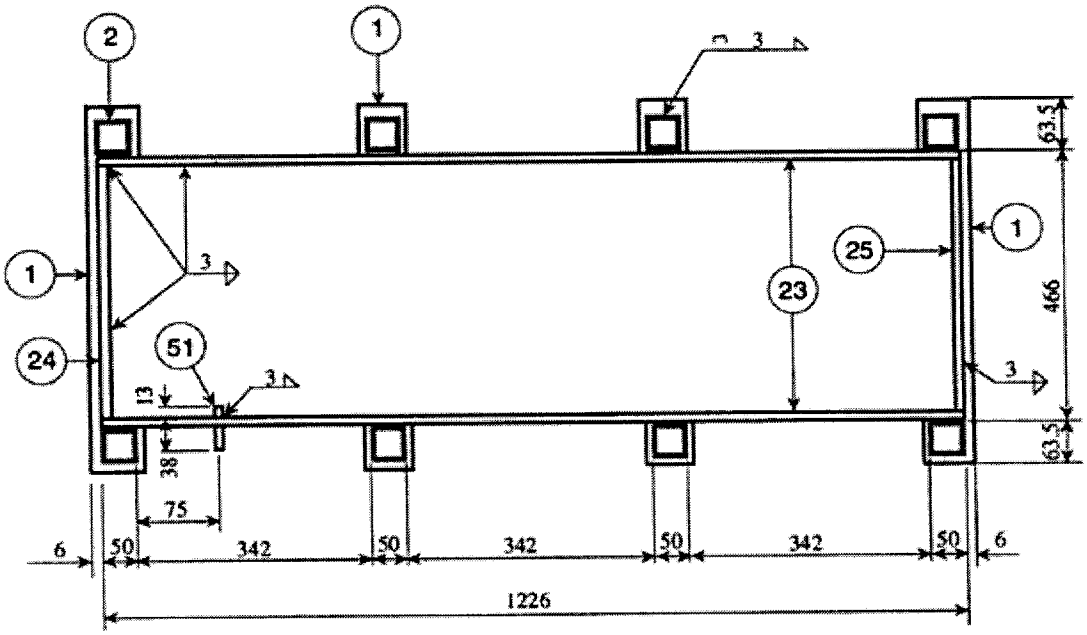

Section E -E

Figure 4.3 Pullout box shop drawing (III) (Units in mm)

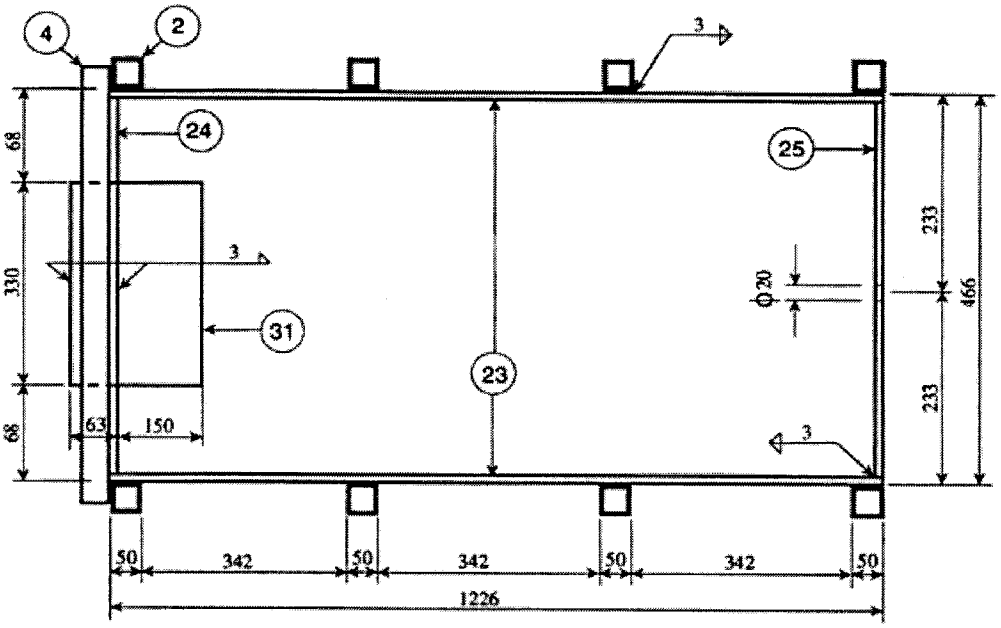

Section F - F

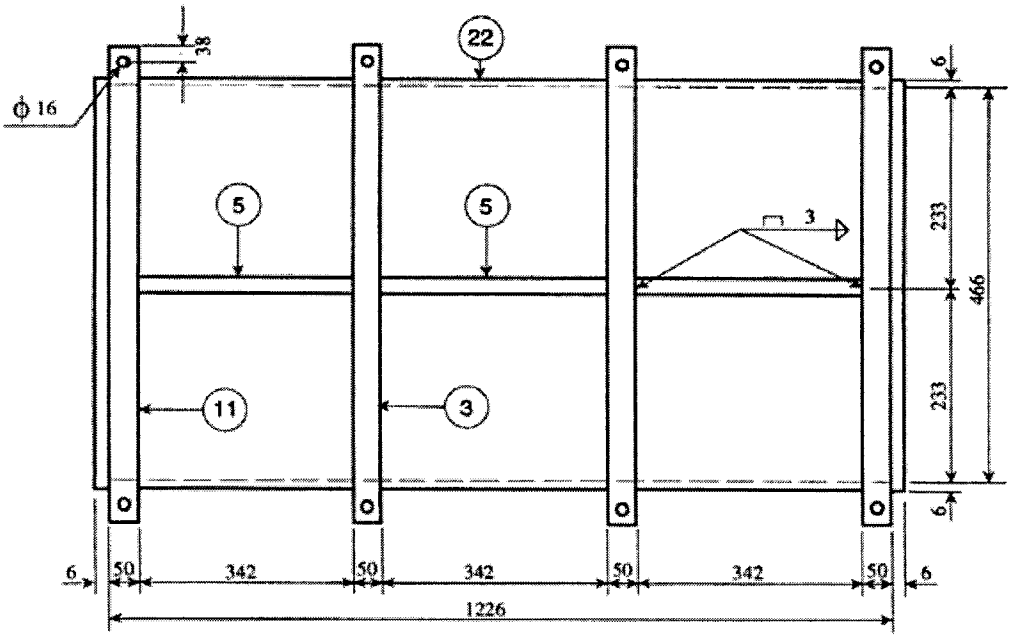

Section G - G

Figure 4.4 Pullout box shop drawing (IV) (Units in mm)

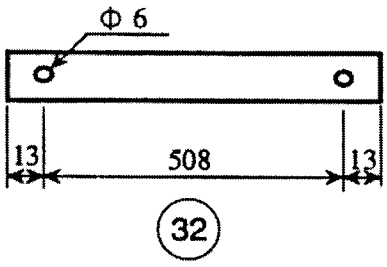

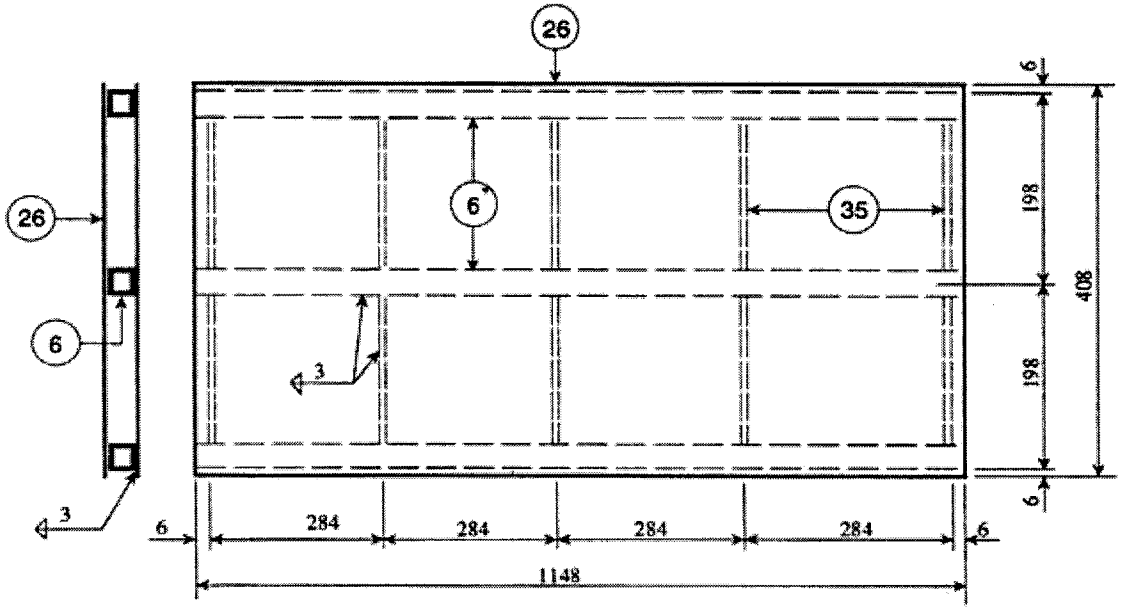

Steel Pad

Figure 4.5 Pullout box shop drawing (v) (Units in mm)

4.2.2.2 Clamps (Model A, B)

Two kinds of clamps were used to fasten the test specimens. All clamps were stiff enough to assure a uniform pullout displacement across the width of the test specimens. Clamp A was used for geogrid HDPE (Fig 4.6). It had two identical jaws with unique contours that fit the specimen very well. The inner corner of the front lip was rounded well to assure that the specimen would not be split. The space between the upper and lower lips was big enough to let the specimen to be pushed in transversely, but small enough to prevent it from sliding out.

Clamp B, used for geogrid PET (Fig 4.7), was comprised of five identical plates. All the surfaces were well frosted to provide good fastening ability. The test specimen was wrapped around the plates. All plate edges were filleted to give a smooth surface.

4.2.2.3 Airbags

Airbags, manufactured by Indianapolis Industrial Products, Inc., were used to apply the confining pressure during the experiment. Each bag had a maximum capacity of 820 kPa.

4.2.3 STRAIN APPARATUS

4.2.3.1 Strain Gages

Four strain gages were fixed on each test specimen to measure tensile strains during the testing. Their location was along the center line of the specimen with 250 mm spacing (Figs 4.8 and 4.9).

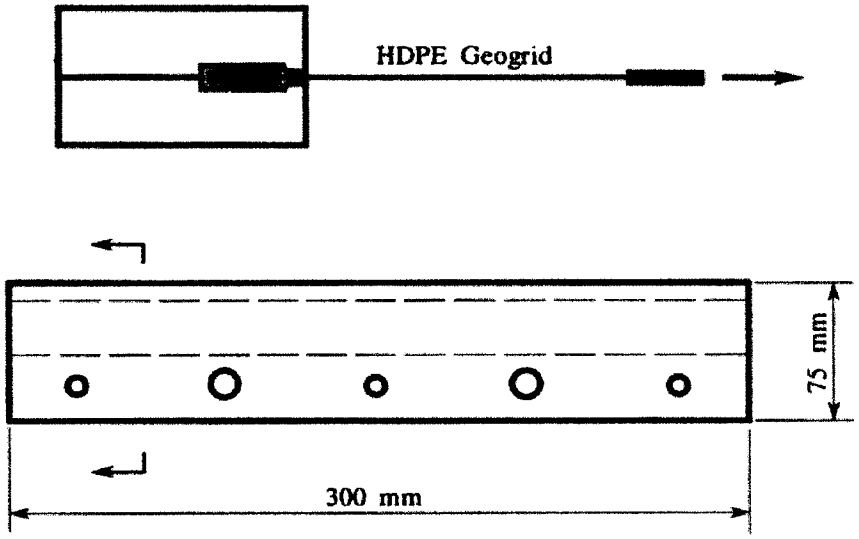

Figure 4.6 Detail of clamp A

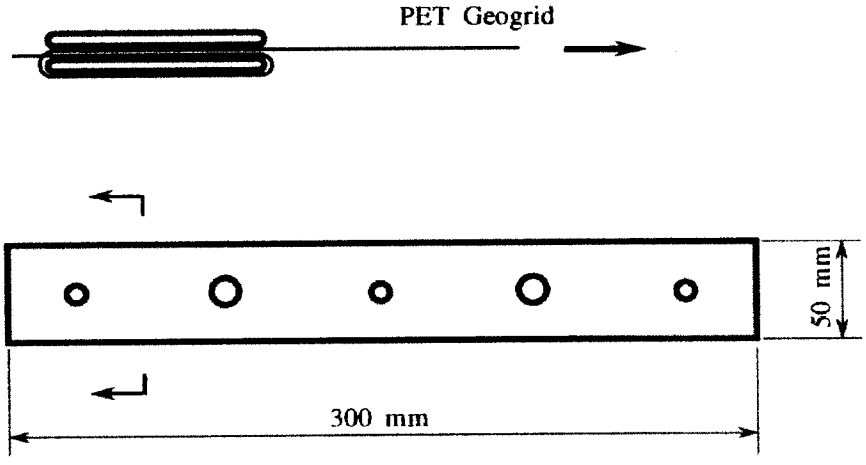

Figure 4.7 Detail of clamp B

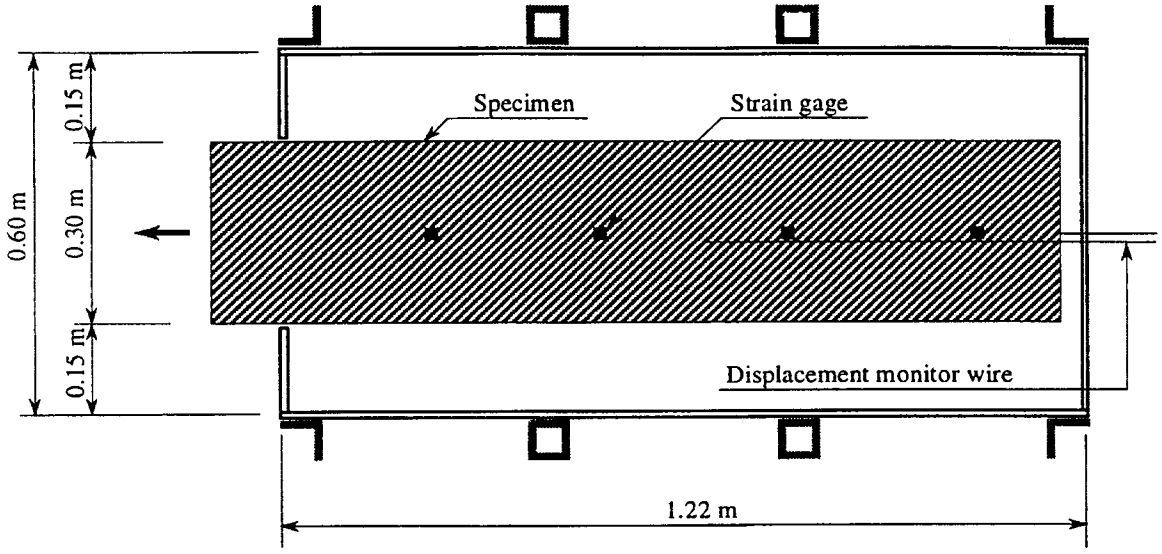

Figure 4.8 Plan of pullout box

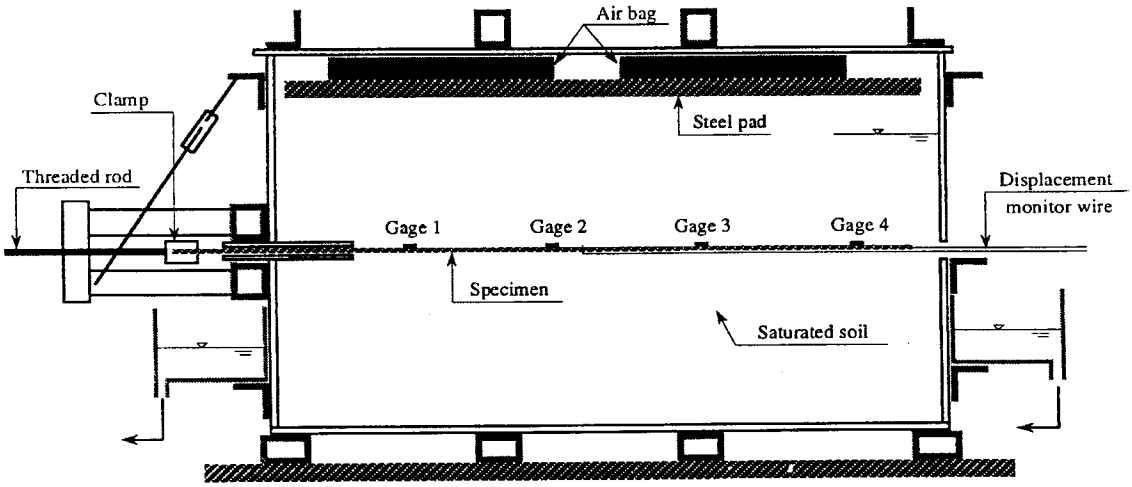

Figure 4.9 Longitudinal section of pullout

The gage utilizes a special plastic carrier base that is able to withstand extremely large elongation without creeping or cracking, and is capable of measuring approximately 10 to 20 % of strain with necessary accuracy.

4.2.3.2 Strain Indicator and Channel Box

The Digital Strain Indicator, Model P-3500, and Switch and Balance Unit, Model SB-10 are products of Micro-Measurements Division of Measures Group, Inc.. The Indicator is a portable, battery-powered instrument using strain gage based transducers. The Switch and Balance Unit has 10 Channels, with an open position to allow the use of additional SB-10's with a single P-3500 Strain Indicator.

4.2.4 MISCELLANEOUS AGENTS

Glue: Adhesive Type CN, Cyanoacrylate Base product of Yokyo Sokki Kenkyijo Co., Ltd.. The operating temperature ranges from –30°C to 100°C under curing pressure 980 kPa. It has a strain limit of 20 % and excellent electrical properties.

Degreaser: Type CSM-1A, a 1-1-1 Trichloro-ethylene solvent used to degrease the surface of the test specimen because of its inertness to polyethylene. The degreaser prevents embedment of contaminants on the surface of the geogrid specimen products of Micro-Measurements Division of Measures Group, Inc..

Neutralizer: Type MN5A-1, a mild ammonia solution that leaves the test specimen with a slightly alkaline pH value-product of Micro-Measurements Division of Measures Group, Inc..

ARON Polyprimer: Used only for geogrid PET, this is a surface preparation agent which allows cyanoacrylate adhesives such as TML type CN to be used for strain gage bonding on polyethylene and polypropylene-product of Yokyo Sokki Kenkyijo Co., Ltd..

Coating Material: A single-component microcrystaline-wax to form a good moisture and water resistant coating.

4.2.5 TEST CONDITIONS

All four tests under saturated conditions were conducted in the air-conditioned laboratory, with almost no change in temperature. The mean temperature was about 22.6°C. The unsaturated tests were performed in a covered shed with good ventilation. The variation in temperature was very limited with an average of 24.3°C. There was no disturbance like shaking or impact. See Fig. 4.10 to 4.13.

Figure 4.10 Layout of pullout boxes 1-4

Figure 4.11 Layout of pullout boxes 5-8

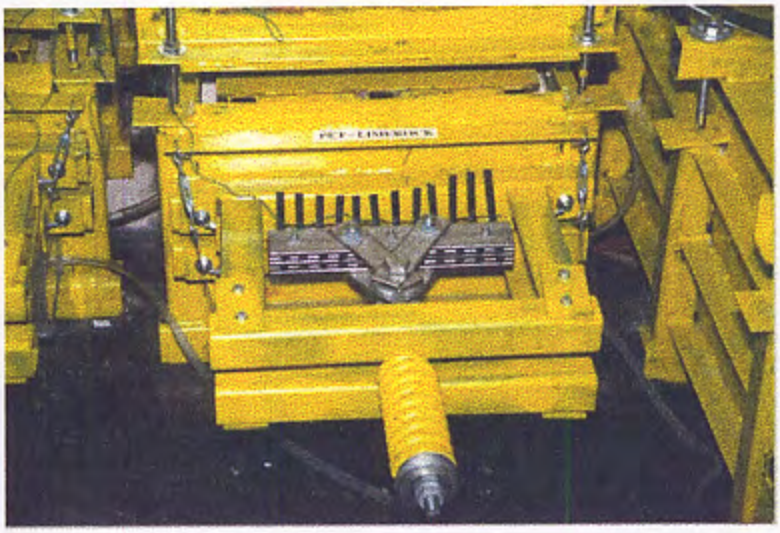

Figure 4.12 Front view of pullout box

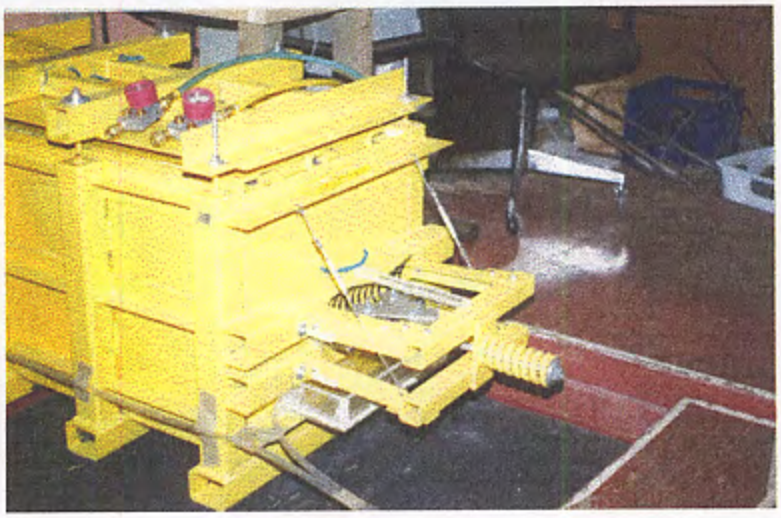

Figure 4.13 Side view of pullout box

4.3 TEST PROCEDURES

4.3.1 INTRODUCTION

Eight pullout boxes were designed, and constructed for the following tests (Figs 4.14 and 4.15).

Test 1: HDPE in limerock under saturated condition

Test 2: PET in limerock under saturated condition

Test 3: HDPE in sand under saturated condition

Test 4: PET in sand under saturated condition

Test 5: HDPE in sand under unsaturated condition

Test 6: PET in sand under unsaturated condition

Test 7: HDPE in limerock under unsaturated condition

Test 8: PET in limerock under unsaturated condition

There were eight steps in the preparation of each test, including compacting the soil (sand or limerock), placing the test specimen, and application of the surcharge pressure on the soil. Procedures followed in the preparation of each test are described in the following sections.

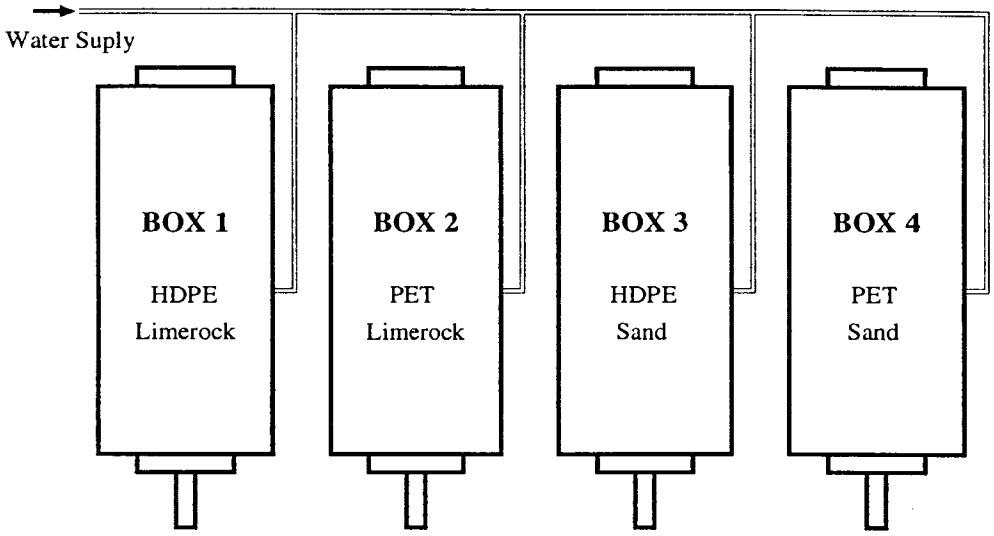

Figure 4.14 Test setup layout 1

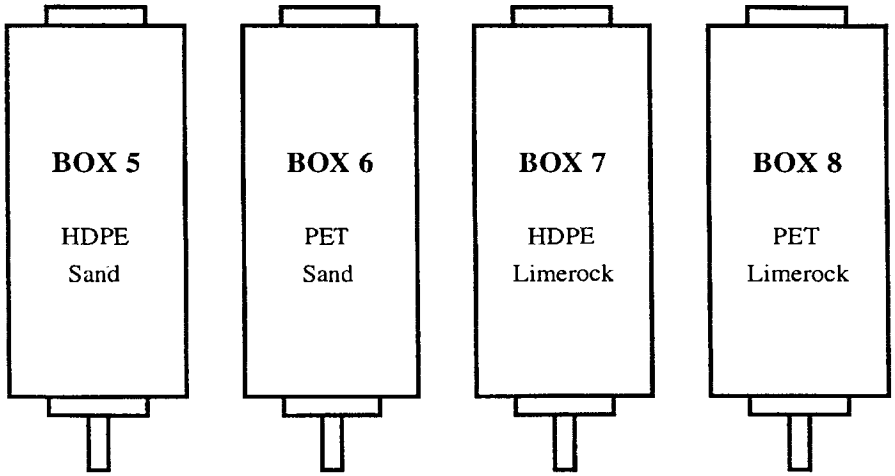

Figure 4.15 Test setup layout 2

4.3.2 TEST PREPARATION

4.3.2.1 Trimming the Geogrid Specimen

The geogrid specimen was cut to a width of 0.30 m. For HDPE, the length is 1.3 m, and for PET 1.5 m. Four gages were mounted on each specimen along the centerline.

4.3.2.2 Specimen Surface Preparation

1) Remove grease, scale, dust, paint, *etc.*, from the bonding area.
2) Spray the gage location with degreaser and wipe clean with a gage sponge.
3) Grind an area somewhat larger than the bonding area uniformly and finely with No. 400 abrasive paper. Sand the surface first at 45° angle to the direction of testing and then at right angles to get a pattern of cross hatches.
4) Clean the gage area with compressed air to remove any particles left by sanding operation.
5) Wipe the ground area with neutralizer. Wiping should be made till the cleaning tissue is kept contamination free.
6) After surface preparation, stick the strain gage before the prepared surface is oxidized or is or contaminated.

4.3.2.3 Bonding Procedures

1) Apply the required amount of the adhesive on the back of the gage base. The amount of adhesive is two drops (increased when needed).
2) Spread the adhesive on the back of the gage thinly and uniformly, using an adhesive nozzle.
3) Use a polyethylene sheet and press down the gage constantly with the thumb. The work has to be done quickly as curing is completed very fast.
4) The curing time is different depending on the test specimen, temperature, humidity and pressing force. In this test, the curing time was set to be 48 hours.

4.3.2.4 Gage Waxing Operation

A coating material, type W-1, produced by Yokyo Sokki Kenkyijo Co., Ltd., is used for moisture and water-proofing of the strain gages bonded on the test specimen surface. The W-1 is light-yellow colored micro-crystalline wax that can be used immediately after heat-melting.

1) Put W-1 wax in an oil bath with temperature adjustment and melt it completely at 100°C ~ 120°C. The melted W-1 becomes a light yellow transparent liquid.
2) Dip the tip of a brush in the melted W-1, for warming.

3) Soak the brush tip in the melted W-1 and apply it at once over the strain gage and extruded adhesive. W-1 hardens as soon as it cools and turns cloudy yellow.

4) As the once-used brush gets cool due to heat absorption of the test specimen, repeat the steps (2) and (4) till complete application.

4.3.2.5 Gage Protection

A plastic tube with a diameter slightly larger than the width of the gage was used to cover the gage. As the gage was embedded in the soil under both the confining pressure and the pullout force, proper coverage was needed to prevent damage of the strain gage. Also, a nylon sleeve was used to permit the extension of the strain gage wire. The sleeve served two purposes: (1) protection of the wire, and (2) provision of unrestrained movement of the wire during the experiment.

4.3.3 PLACEMENT OF THE SOIL SAMPLES AND TEST SPECIMENS

Prior to each test, the pullout box was thoroughly cleaned. Sand (limerock) was placed and rammed in several layers to a targeted relative density in excess of 95% in the Standard Proctor test. Each layer was approximately 75 mm thick. Four rammed layers brought the sand (limerock) to the mid-height of the slot in the front wall of the box. The surface of the soil at this point was leveled with trowel and checked with water-level gage. The surface was ready to receive the test specimen.

The instrumented test specimen was then placed on the surface of the sand (limerock) with the gages facing upward. The four strain gage wires were passed through a 20 mm hole at the rear wall of the box. The front part of the specimen extended out of the box at the front through the slot.

Four more layers of sand (limerock) were then placed following the same procedure described previously.

4.3.4 APPLICATION OF THE SURCHARGE LOAD

The surface of the last layer of sand (limerock) was leveled to receive the built-up steel pad. This pad was made of two steel plates and eight box stiffeners. It was rigid enough to distribute the surcharge load uniformly. The top level of the load plate was at the same level as the rim of the pullout box. The confining pressure was about 41 kPa.

Two airbags were placed at proper locations on the top of the steel plate. The sides of the airbags were oriented 45° to the side of pullout box, so that the outlets located at the corners of the bags were normal to the longitudinal wall, Fig 4.16. This arrangement enabled the outlets to be connected to the air supply hoses. The pullout box cover was then placed in position and bolt-connected to the side columns of the pullout-box. The pressure gages were connected to the airbags, and surcharge pressure applied from the laboratory air supply. A constant surcharge pressure was maintained.

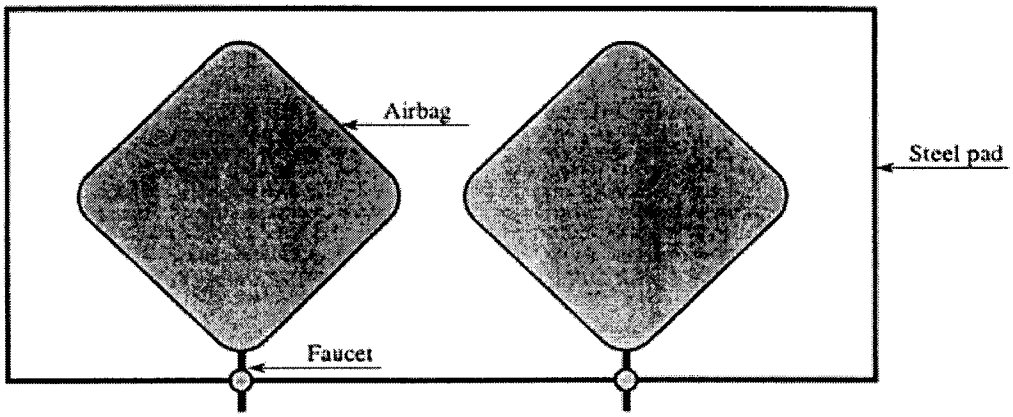

Figure 4.16 Airbags arrangement

4.3.5 CLAMPING THE TEST SPECIMEN

The test specimen was clamped and connected to the pullout assembly following the application of the surcharge loading. The clamping procedures for HDPE and PET were different, Figs 4.6 and 4.7 After clamping and bolting, four brackets were connected between the clamp and pullout assembly, Fig 4.17.

4.3.6 SATURATION OF THE SOIL

For the tests under saturated condition, water was filled in slowly from the inlet on the top of the pullout box. The water level was checked through a plastic hose from the bottom of the box. When the water reached the level at the top of the exit slot, water filling was stopped. Any surplus water was collected by water collectors located at both ends of the pullout box, and drained into the sewer through another set of plastic tubes.

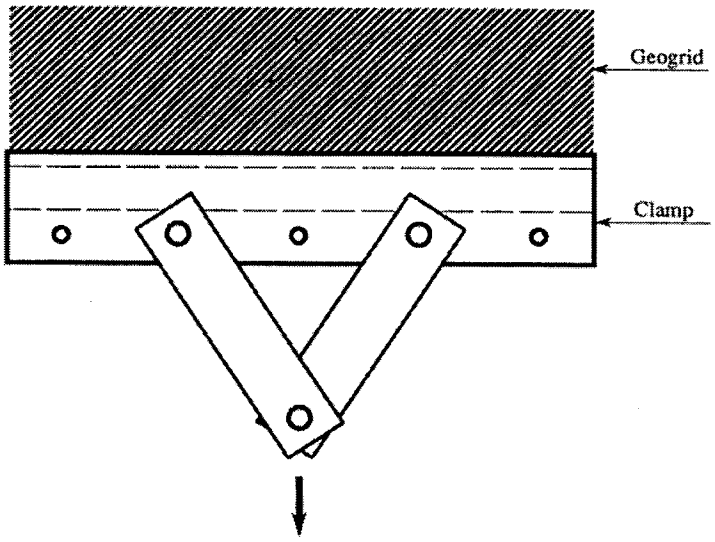

Figure 4.17 Clamping assembly

4.4 TEST RESULTS

4.4.1 INTRODUCTION

The results are presented for pullout tests on both HDPE and PET test specimens. The test conditions addressed saturated and unsaturated soil. The confining pressure was kept at about 41 kPa at the geogrid specimen level. The test mode was in load-control. In each test, a sustained load was applied incrementally until the specimen was pulled out. The first loading stage (Stage-I) was kept for about 9,800 hours under 10% of expected pullout load. In the second loading stage (Stage-II), a sustained load of 10 to 25% of the expected pullout load was applied incrementally. Each increment lasted for approximately 25 hours. The peak pullout resistance occurred when the displacement of the embedded end was first observed. Any larger pullout load would be accompanied with substantial displacement and a quick drop back.

4.4.2 STRAIN-TIME RELATION AT STAGE I

Figs 4.18 and 4.19 show the strain-time relation for the eight pullout tests at the first testing stage (Stage-I) based on gage readings in gage 1. The pullout load was 4.27 kN/m for the tests under the saturated test condition, and 5.693 kN/m for tests under the unsaturated condition. These loads had been maintained for about 9,800 hours. As this was the initial load application stage (Stage-I), the geogrid specimen experienced an unstable stage in which some degree of sliding occurred. It is a natural phenomenon when the geogrid specimens are initially pulled.

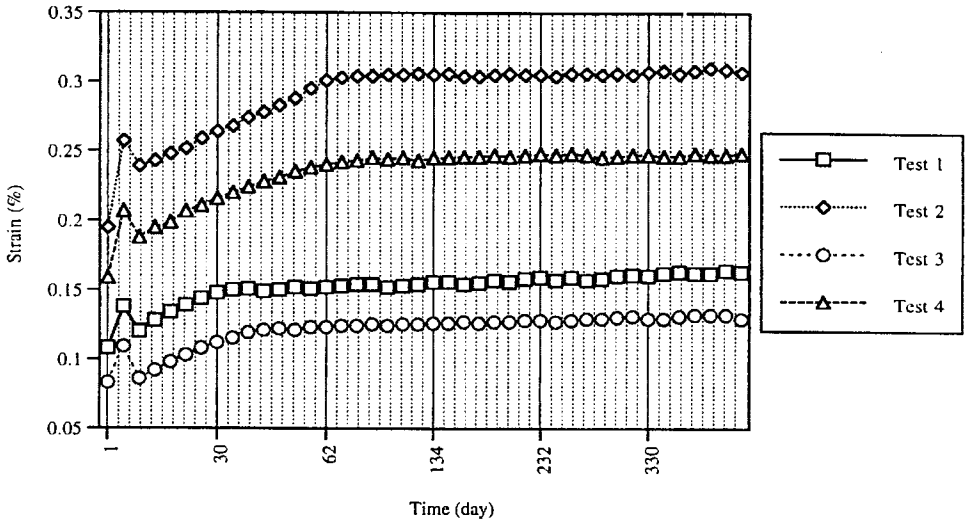

Fig. 4.18. Strain-time relations for HDPE and PET geogrids in sand and limerock under saturated condition at stage-I (strain gage 1)

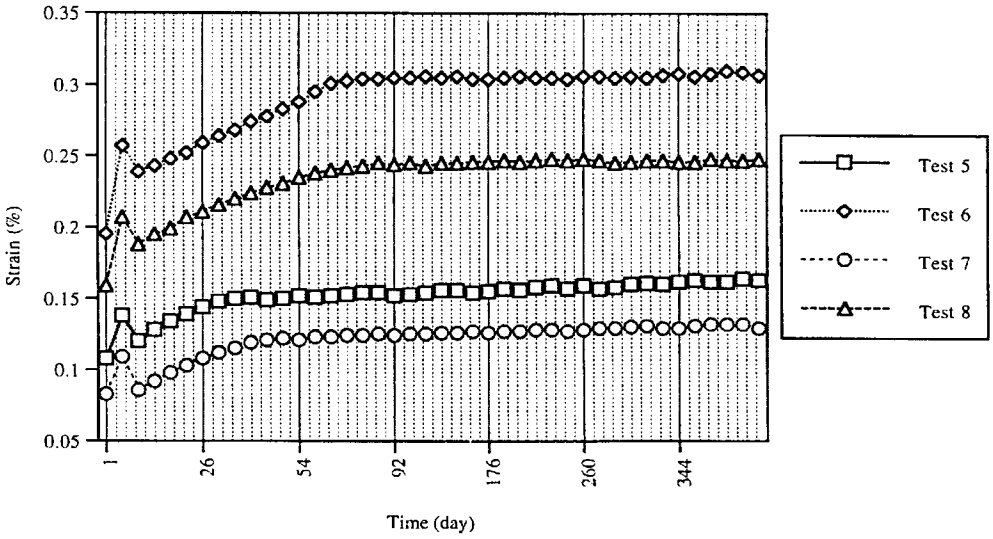

Fig. 4.19. Strain-time relations for HDPE and PET geogrids in sand and limerock under saturated condition at stage-I (strain gage 1)

4.4.3 STRAIN-TIME RELATION AT STAGE II

Figs 4.20 - 4.37 represent the final pullout stage (Stage-II) of the tests. In each test, the pullout load was applied incrementally until the specimen was pulled out. For tests under saturated condition, the first four pullout loading steps were 11.39 kN/m, 21.35 kN/m, 31.31 kN/m, and 35.58 kN/m. For tests under unsaturated condition, the first four pullout loading steps were 15.66 kN/m, 31.31 kN/m, 45.55 kN/m, and 54.09 kN/m. The peak value of the pullout load was different for each test, depending on the calculated peak capacity. Each load increment was maintained constant for about 25 hours. The increment was about 10 to 25% of the expected pullout load. The geogrid anchorage capacity was defined as the pullout load at which the embedded end of the geogrid specimen started to move.

From the test results, it was observed that the characteristic response of the curve can be divided into four zones, an initial strain increasing soon after the application of the pullout force, an unstable zone with some drop in the strain value, a transition zone with gradual strain increment, and a final stable zone.

4.4.4 STRAIN DISTRIBUTION PROFILE

Figs 4.19 and 4.20 show the strain distribution profile along the specimen based on the distance from the front wall. The strain readings are from gages 1, 2, 3, and 4. The load level is at the final pullout loading stage (Stage II).

For the strain distribution pattern along the test specimen, a similar trend and contours can be seen clearly. In each case, the strain decreases with the distance from the clamped end, and the magnitude of the strain at the front end is greater than that at the rear end. Compared to the strain at the front end, the strain at the rear end is about six to nine times smaller. This is because the interface resistance between the soil and geogrid prevents the pullout load very effectively from being transmitted to the rear part of the geogrid specimen.

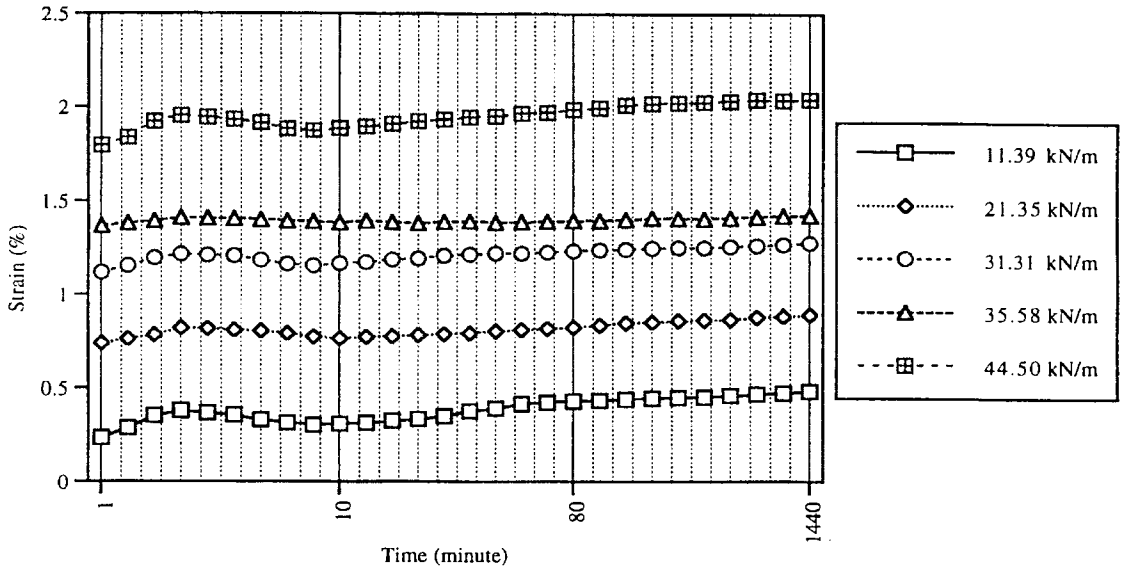

Fig. 4.20. Strain-time relations for HDPE geogrid in limerock under saturated condition at stage-II (strain gage 1)

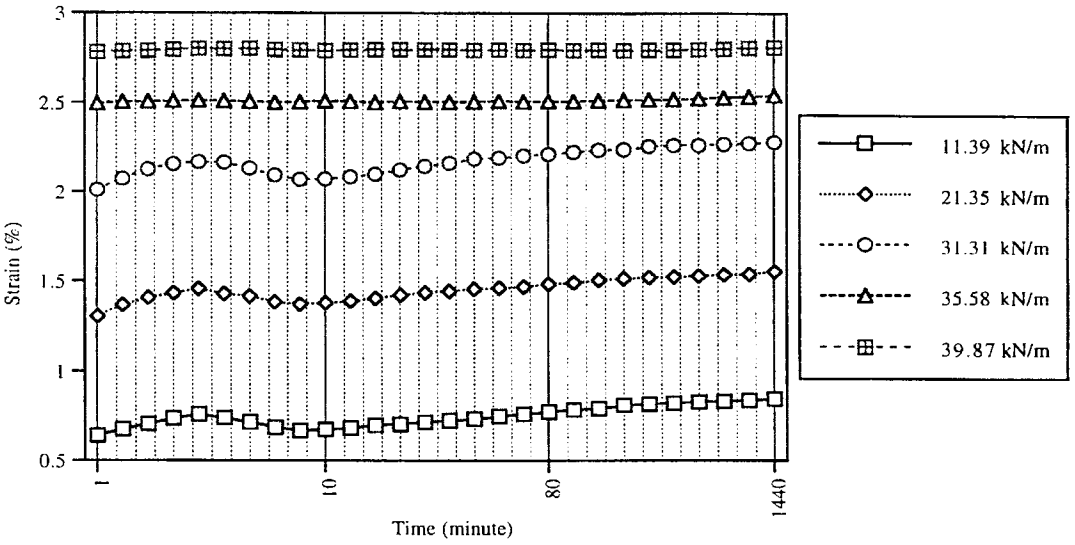

Fig. 4.21 Strain-time relations for PET geogrid in limerock under saturated condition at stage-II (strain gage 1)

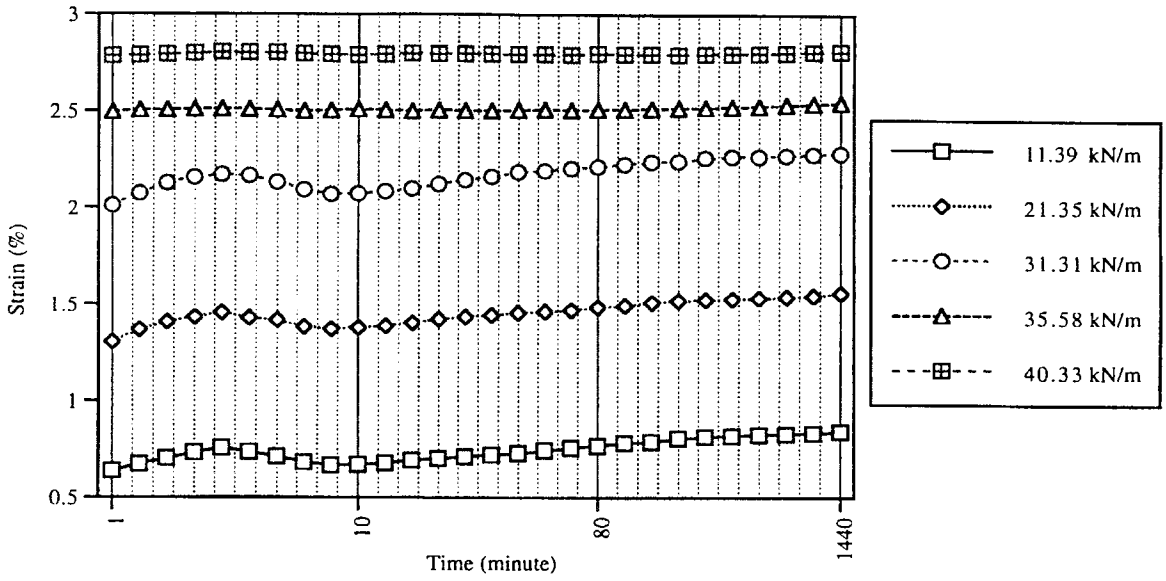

Fig. 4.22 Strain-time relations for HDPE geogrid in sand under saturated condition at stage-II (strain gage 1)

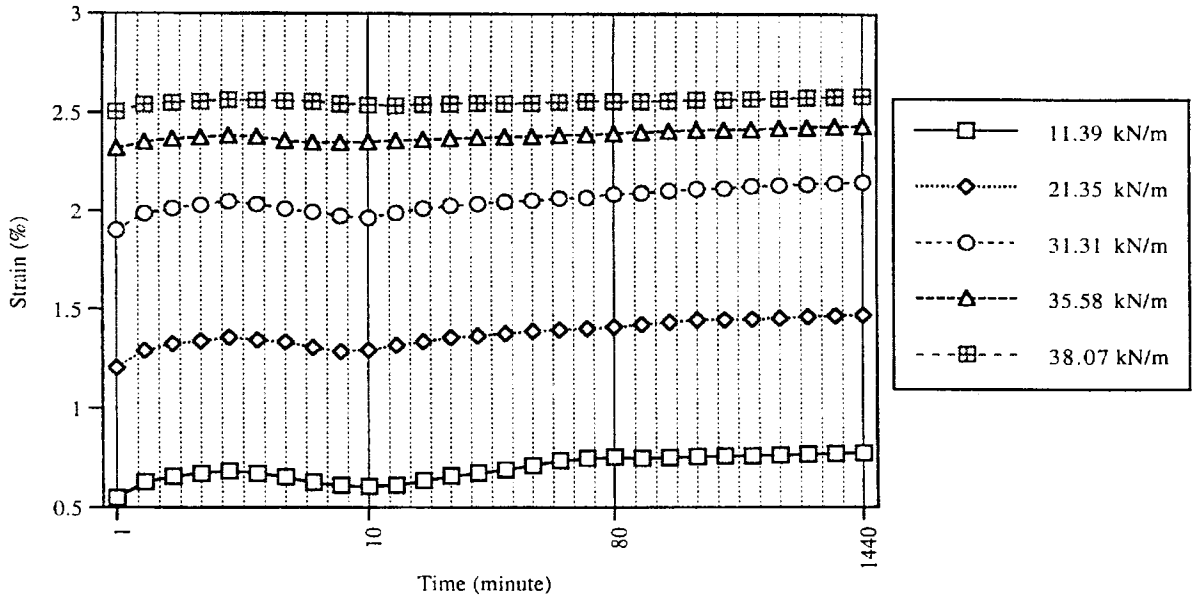

Fig. 4.23 Strain-time relations for PET geogrid in sand under saturated condition at stage-II (strain gage 1)

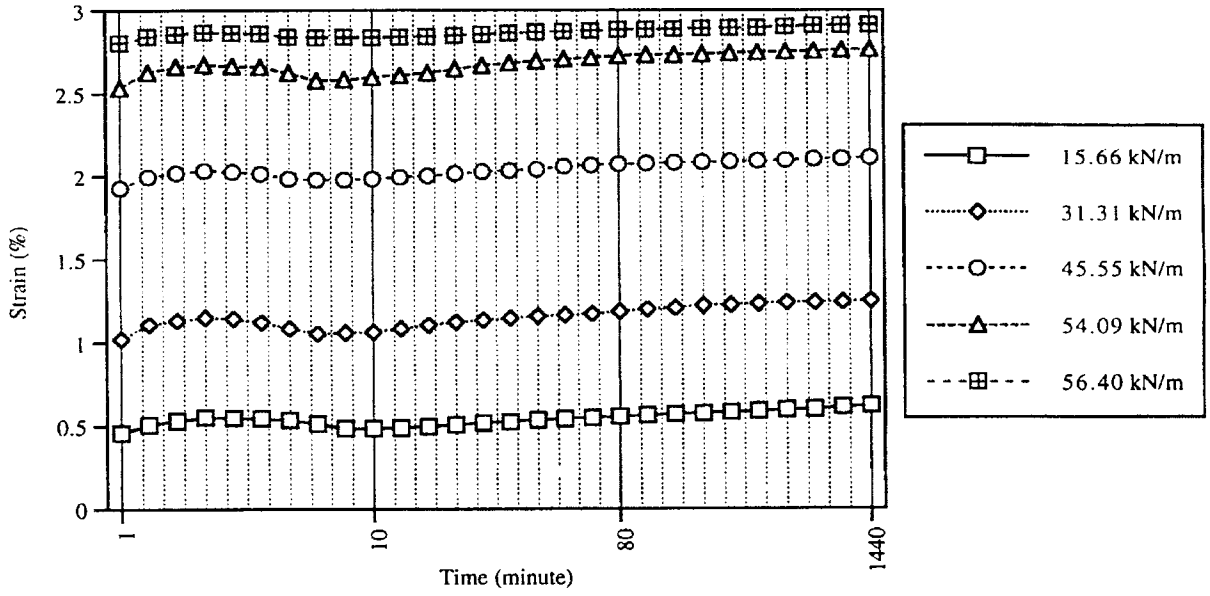

Fig. 4.24 Strain-time relations for HDPE geogrid in sand under unsaturated condition at stage-II (strain gage 1)

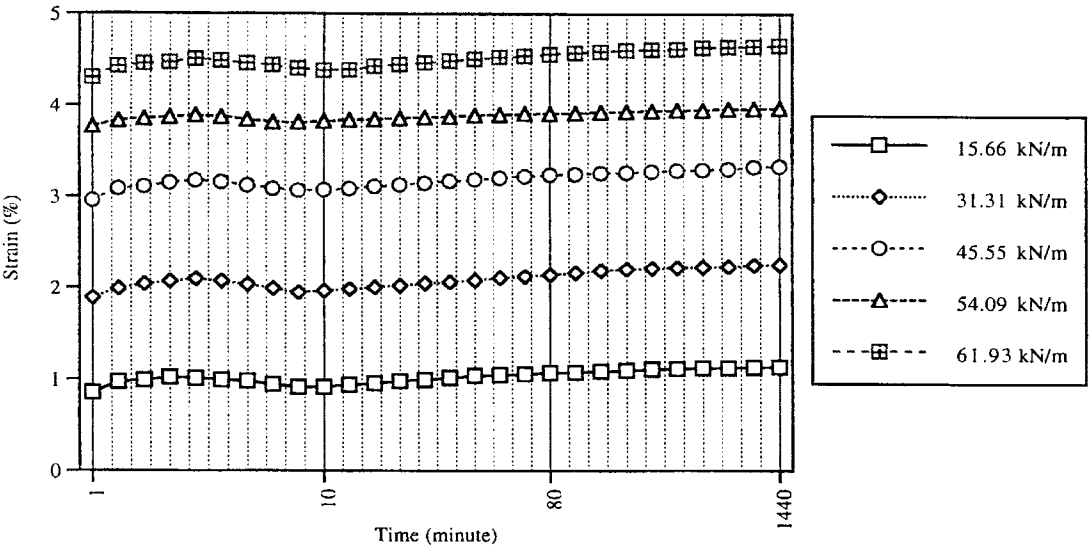

Fig.4.25 Strain-time relation for PET geogrid in sand under unsaturated condition at stage-II (strain gage 1)

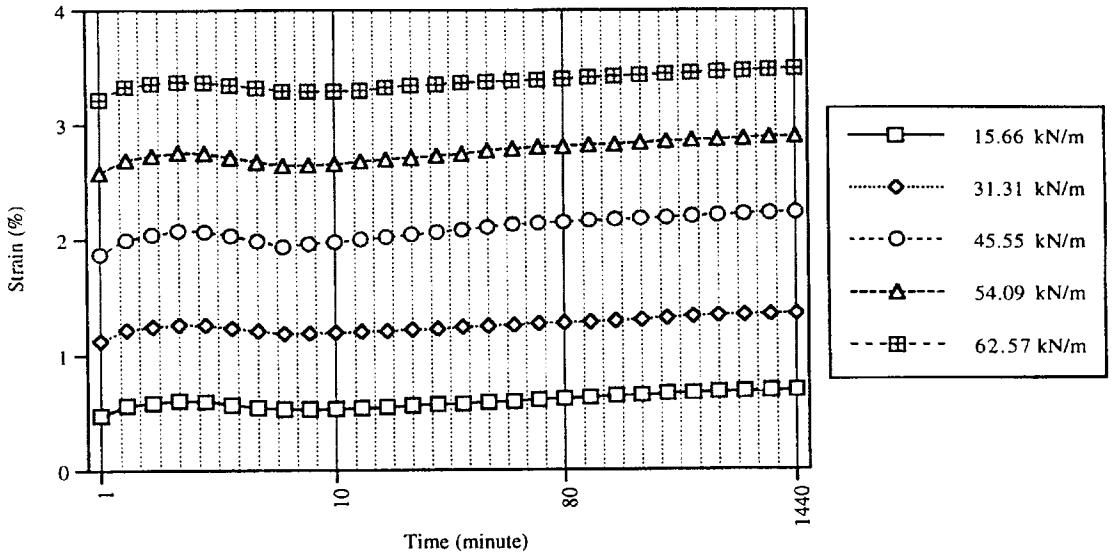

Fig. 4.26 Strain-time relations for HDPE geogrid in limerock under unsaturated condition at stage-II (strain gage 1)

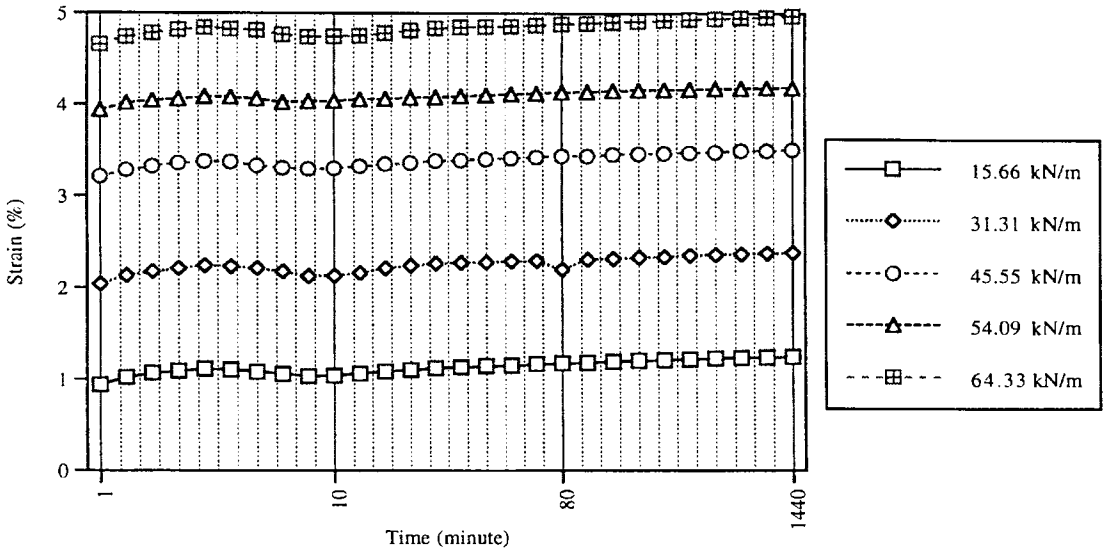

Fig. 4.27 Strain-time relations for PET geogrid in limerock under unsaturated condition at stage-II (strain gage 1)

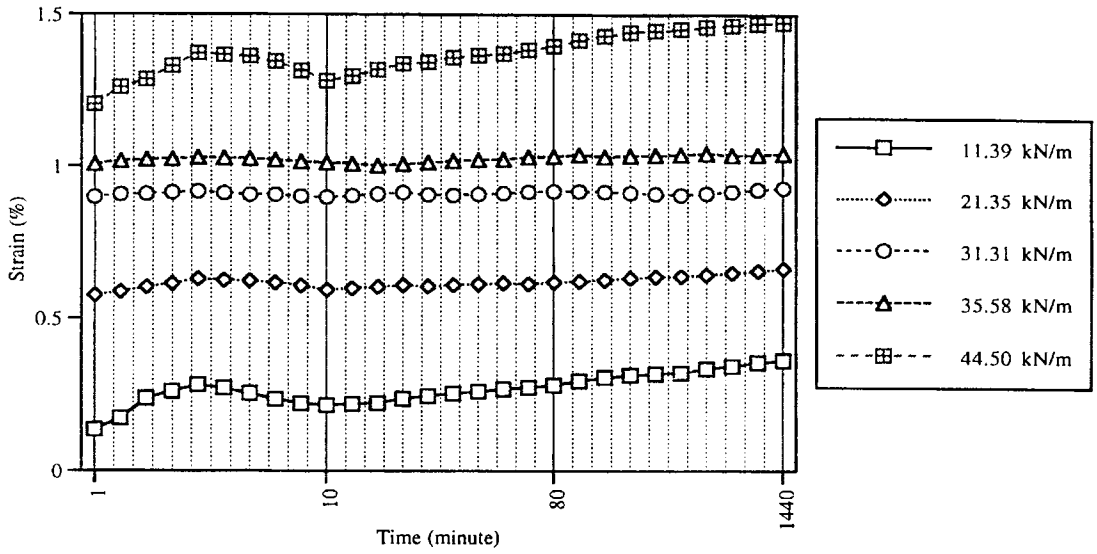

Fig. 4.28 Strain-time relations for HDPE geogrid in limerock under saturated condition at stage-II (strain gage 2)

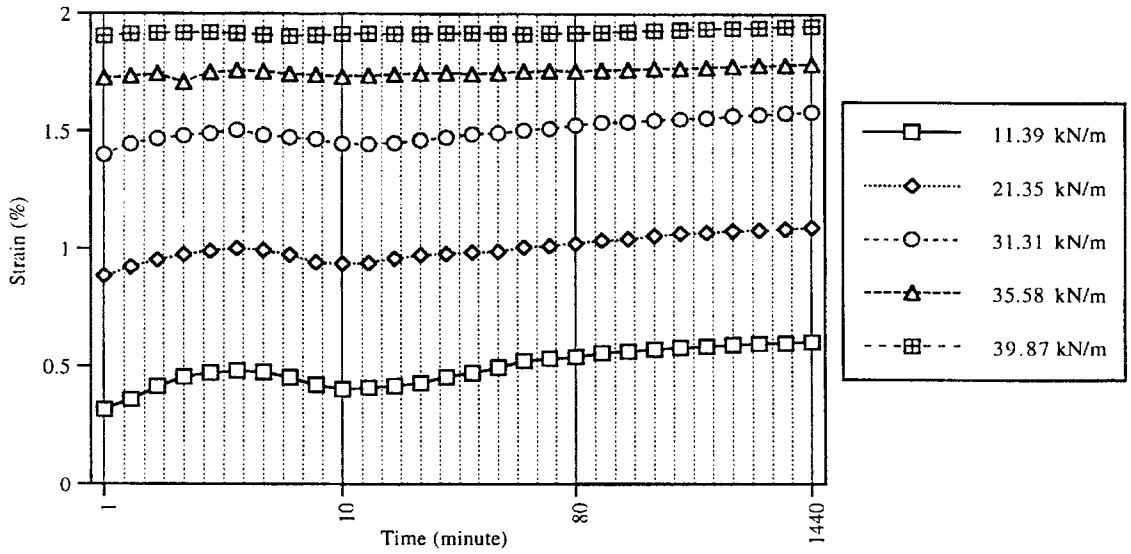

Fig. 4.29 Strain-time relations for PET geogrid in limerock under saturated condition at stage-II (strain gage 2)

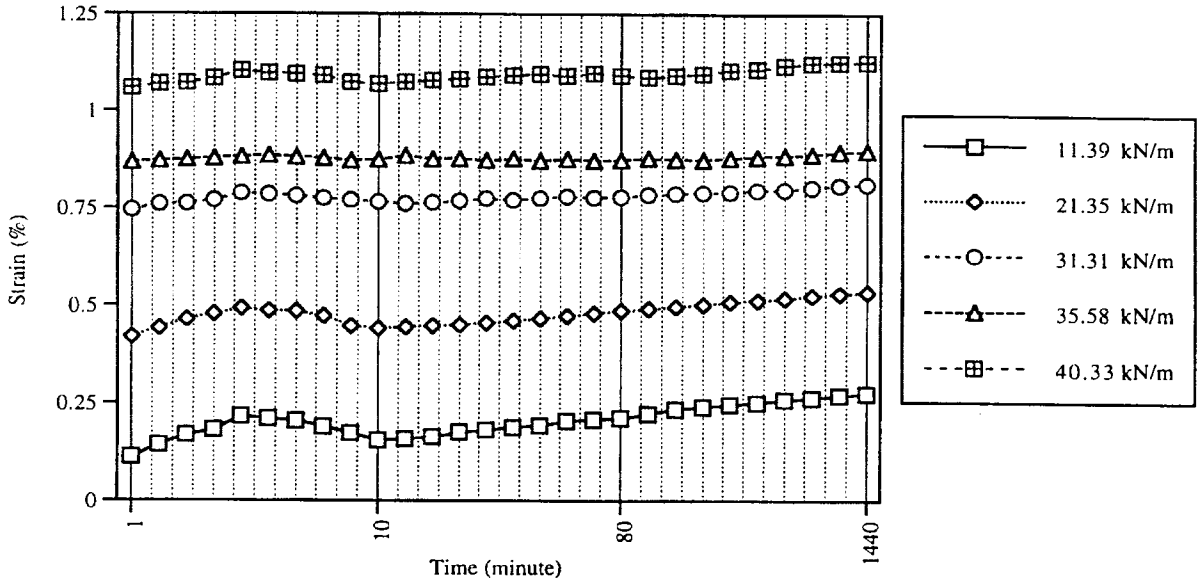

Fig. 4.30 Strain-time relations for HDPE geogrid in sand under saturated condition at stage-II (strain gage 2)

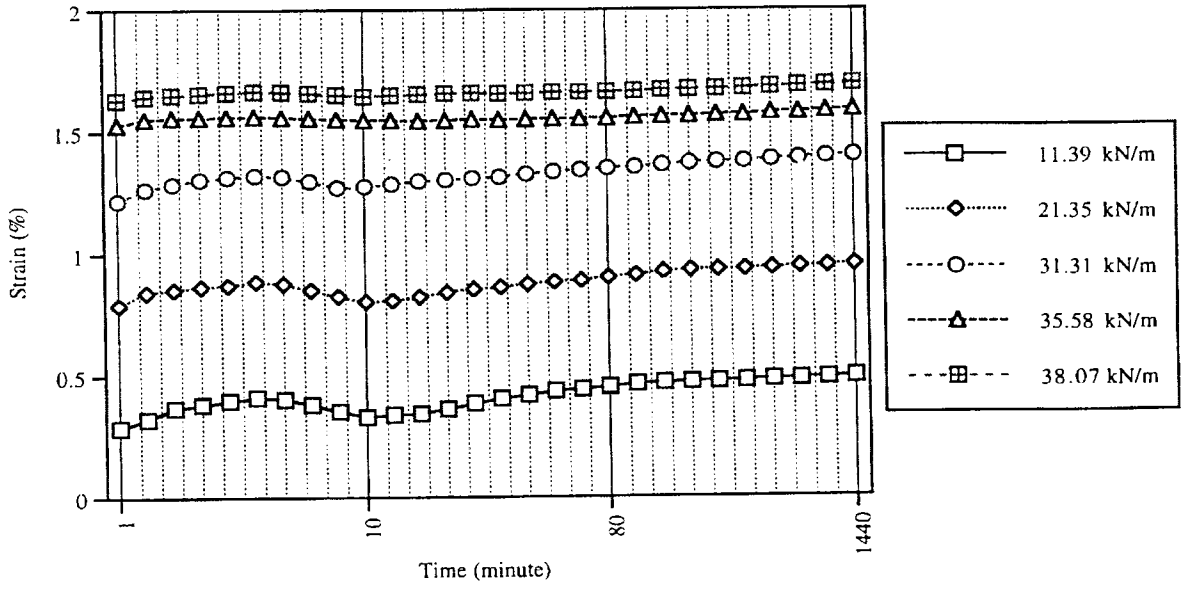

Fig. 4.31 Strain-time relations for PET geogrid in sand under saturated condition at stage-II (strain gage 2)

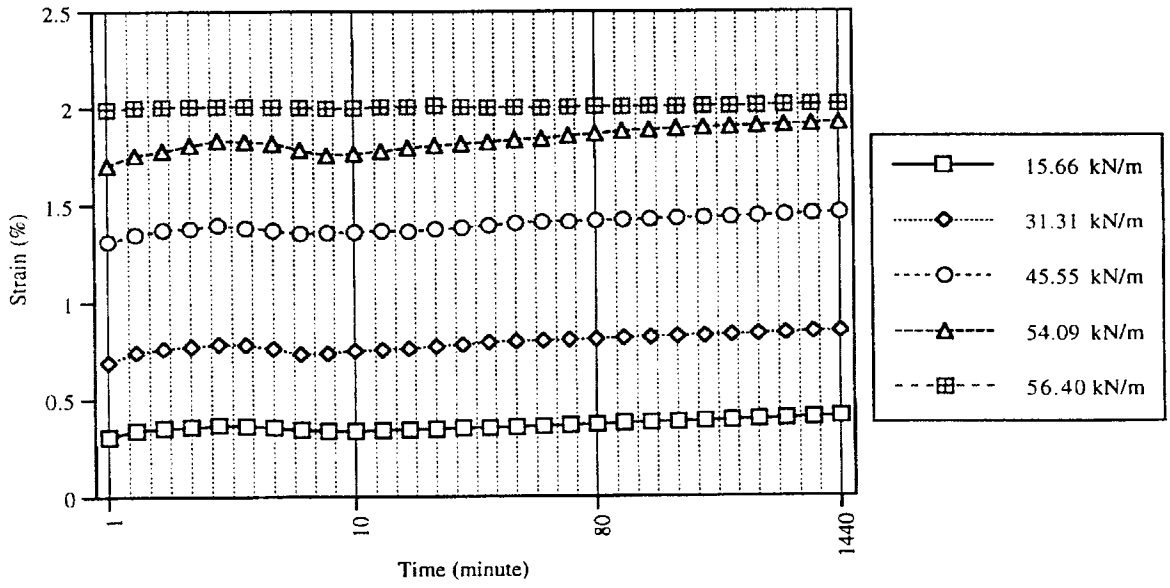

Fig. 4.32 Strain-time relations for HDPE geogrid in sand under unsaturated condition at stage-II (strain gage 2)

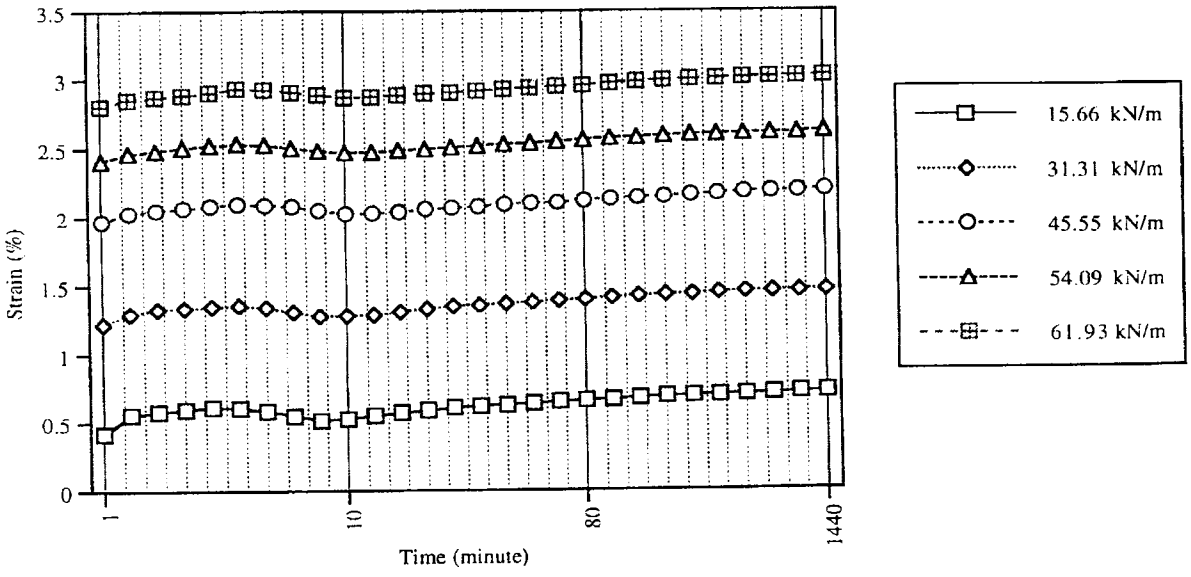

Fig. 4.33 Strain-time relations for PET geogrid in sand under unsaturated condition at stage-II (strain gage 2)

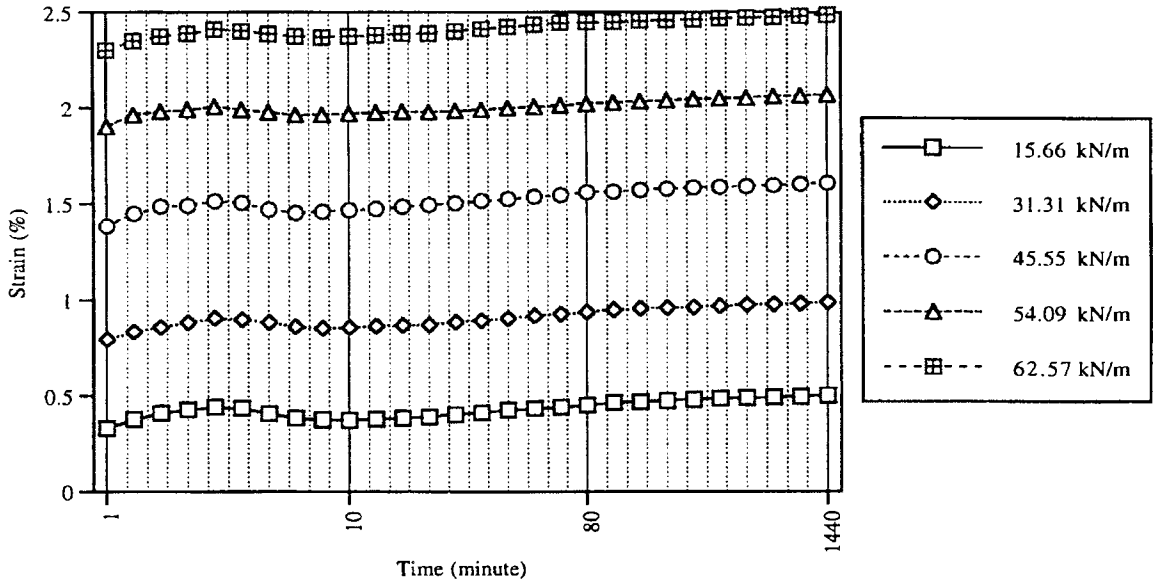

Fig. 4.34 Strain-time relations for HDPE geogrid in limerock under unsaturated condition at stage-II (strain gage 2)

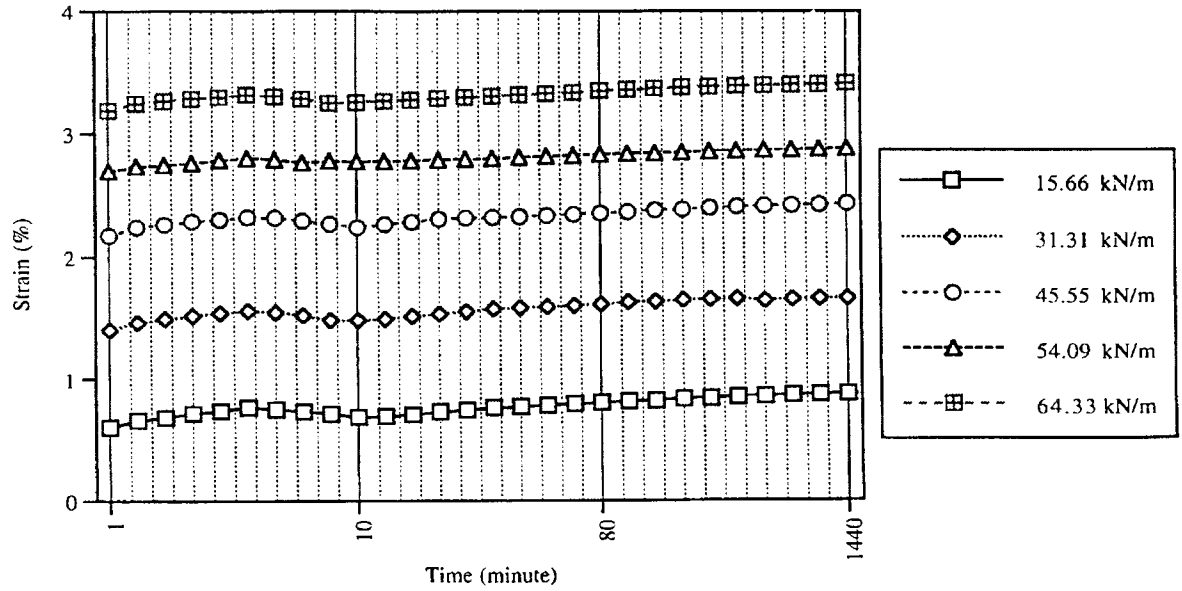

Fig. 4.35 Strain-time relations for PET geogrid in limerock under unsaturated condition at stage-II (strain gage 2)

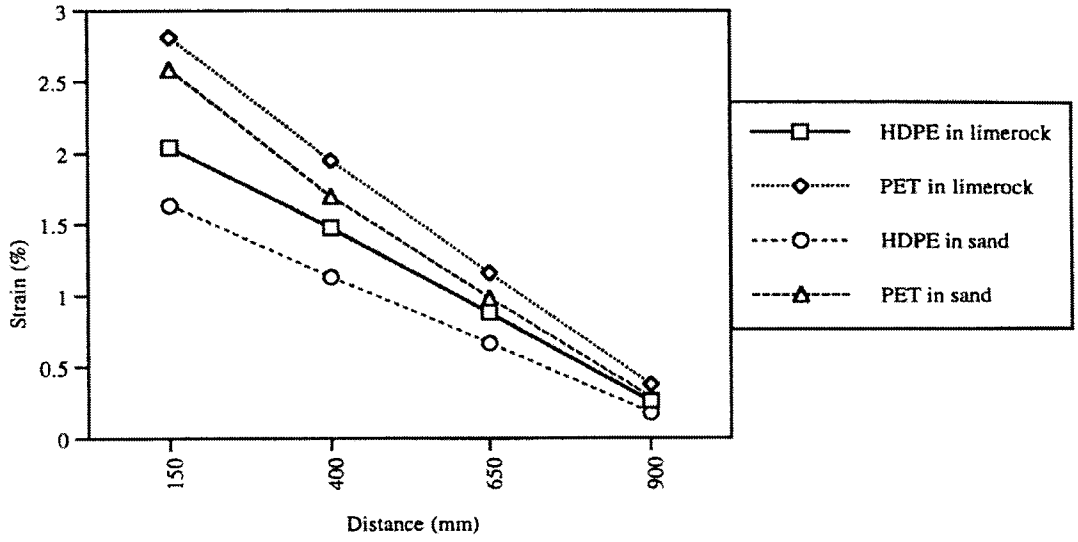

Fig. 4.36 Strain distributions with respect to the distance from the front wall for HDPE and PET geogrids in limerock under saturated condition at P_{ult}

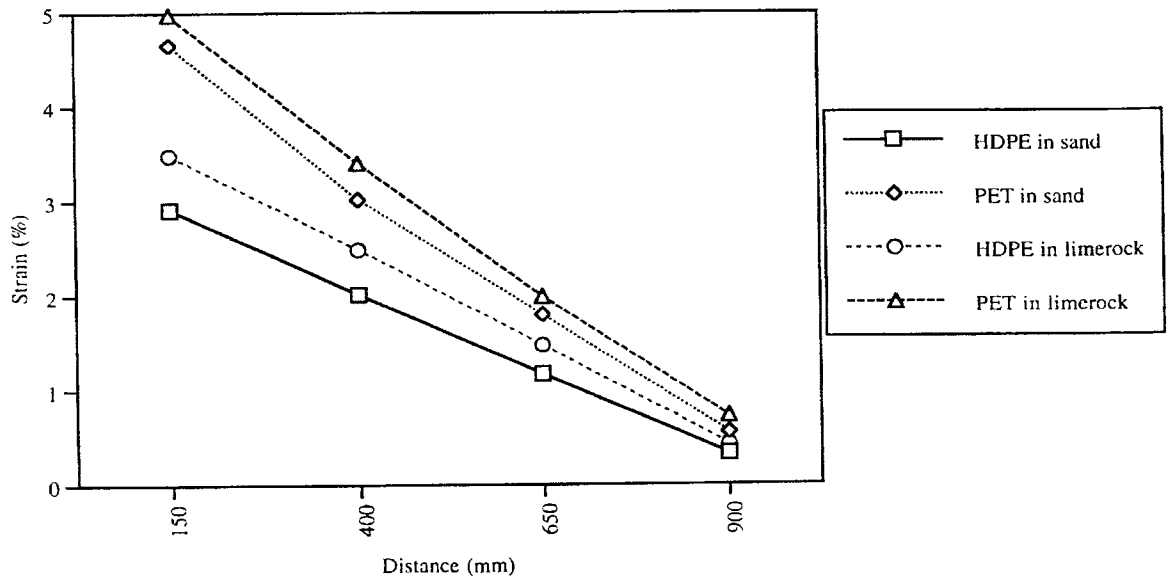

Fig. 4.37. Strain distributions with respect to the distance from the front wall for HDPE and PET geogrids in limerock under unsaturated condition at P_{ult}

CHAPTER 5

FINITE ELEMENT ANALYSIS OF PULLOUT

5.1 MODELING OF THE PULLOUT TEST

5.1.1 BOUNDARY CONDITION SIMULATION

The pullout test for unsaturated soil condition was simulated by the finite element method (Software: ANSYS 5.3) in analyzing the reinforced solid soils. The uniformly distributed load was applied on the top of the soil element to simulate the confining pressure. The boundary conditions of the front and back walls are roller-supported conditions between soil and side walls. The bottom nodes were fully restrained in all three directions. The finite element mesh and idealization of the pullout test are presented in Fig 5.1

5.1.2 SOIL AND REINFORCING ELEMENT MODELING

The soil elements and the reinforcing elements were modeled by using eight-noded isoparametric elements. This element is defined by eight nodes with two degrees of freedom at each node: translations in the nodal x and y directions. It has plasticity, creep, swelling, stress, stress stiffening, large deflection, and large strain capabilities. The geometry, node locations, and the coordinate system for this element are shown in Fig.5.2

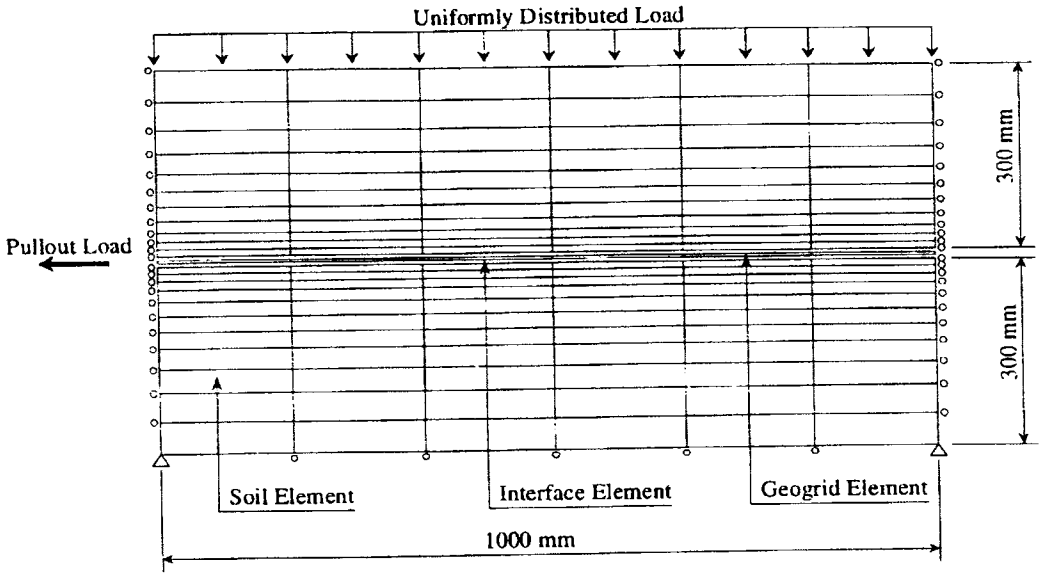

Fig. 5.1 Finite Element Idealization of Pullout Test

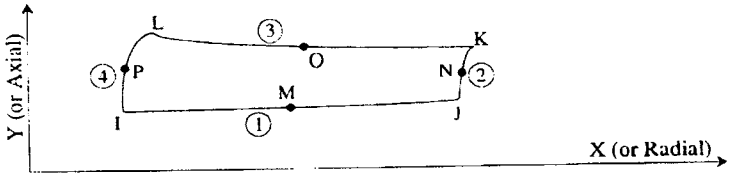

Fig. 5.2 Eight-Node Structural Solid Element

5.1.3 INTERFACE ELEMENT MODELING

The interface element was modeled by contact elements. This element represents two surfaces that may be continuous or break or slide relative to each other. It has the capacity of supporting compression in the direction normal to the surfaces and shear in the tangential direction. The element has two degrees of freedom at each node: translations in the x and y direction. The geometry, node locations, and the coordinate system for this element are shown in Fig 5.3

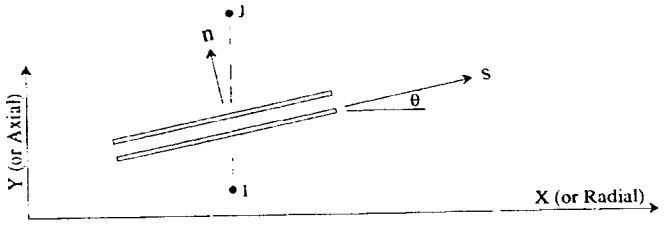

Fig. 5.3 Interface Element

5.2 RESULTS AND ANALYSIS

The confining pressure was applied and kept constant on the top of soil specimen, while the pullout load acting on the reinforcing element was increased step by step, until the peak value was reached. During this process, the pullout force is applied according to some percentage of the total pullout load. These are 10%, 25%, 50%, 75%, and 90%.

This enables the monitoring of stress and strain during the pullout force application. When the pullout force reached 100% of pullout load, failure occurred, no measurements could be made.

5.2.1 NORMAL STRESSES FOR GEOGRID IN SOIL

Fig 5.4 shows the normal stress distribution (MPa) for the HDPE geogrid in sand under the unsaturated test condition, with no pullout load, subjected to confining pressure only. Along the reinforcing element there were some small regions with stress concentrations. They were caused by the reinforcing effect from the bonding force between the reinforcing element and the soil. The stress distribution patterns were almost symmetric along the reinforcing element and along the vertical centerline of the test setup.

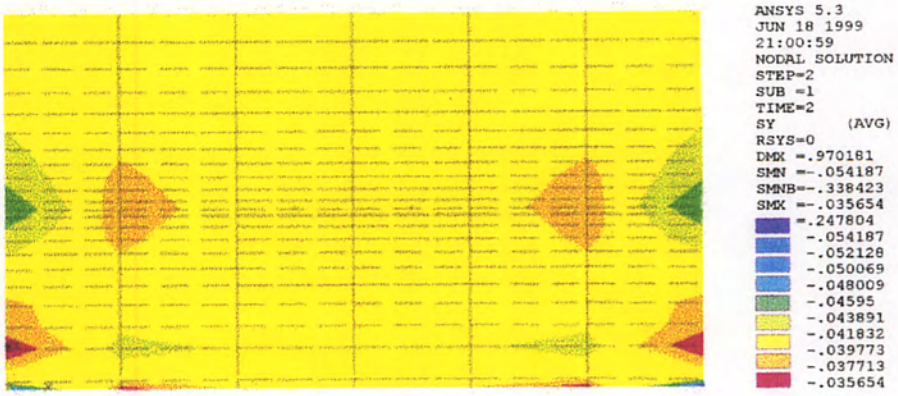

Fig. 5.4 Normal stress distribution from finite element analysis for HDPE geogrid in sand under unsaturated condition (0% Pult)

As the confining pressure and boundary support conditions were kept constant throughout the test, the stress development and variation were dependent on the magnitude of pullout force. From the analysis values, it can be seen that the stress variations were confined to within 150 mm above and below the reinforcing element.

When the pullout force reached 10% of the total pullout load (Fig 5.5), the stress distribution pattern remained the same in the rear section. However, the maximum pullout load made the stress distribution asymmetric near the front wall. As a whole, the stress distribution pattern can be initially divided into five major regions in the horizontal direction. In Region I, there was a stress concentration between the front wall and 80 mm distance from it. This stress concentration was as high as 115%. Under the confining pressure, the friction force between the soil and the reinforcement, and the free movement at the front wall in the vertical direction, led to the Region II, at a distance around 200 mm from the front wall. The region was nearly circular in shape and with a stress decrease.

Region III was located in the central part of the pullout box. As it was sufficiently distant from both front and back walls, there was much less boundary influence on it. The stress was more uniform in distribution. The Region IV was located 200 mm away from the rear wall. Region V was the region at the rear wall that corresponded to Region I at the front wall. Unlike Regions I and II at the front wall, Regions IV and V remained unchanged.

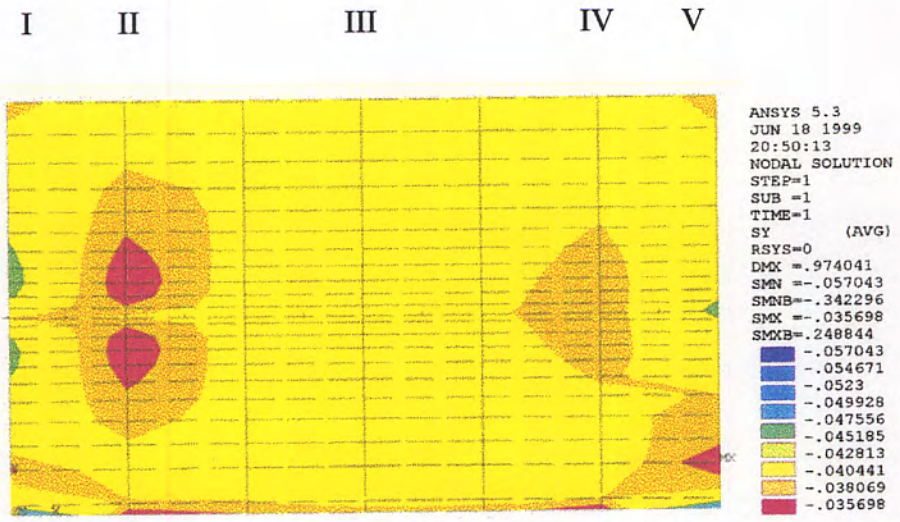

Fig 5.5 Normal stress distribution from finite element analysis for HDPE geogrid in sand under unsaturated condition (10% Pult)

When the pullout force increased to 25% of the total pullout load, Fig 5.6, the stress in Region I increased with the area unchanged. The two separated parts in Region II merged together, extended forward, and reached the front wall. Region IV extended and moved to the center of the test setup. Region V remained undisturbed.

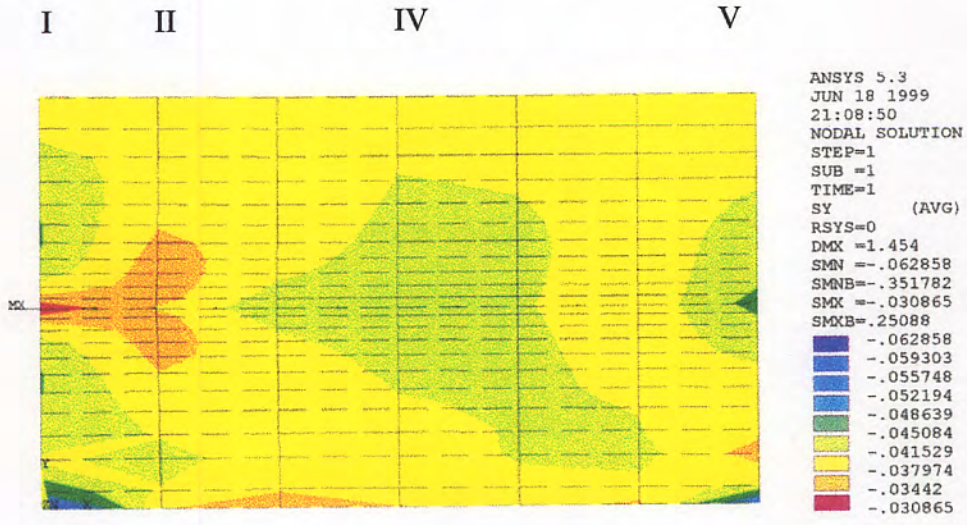

Figure 5.6 Normal stress distribution from finite element analysis for HDPE geogrid in sand under the unsaturated condition (25% P_{ult})

Under the pullout force at 50% of total pullout load, Fig 5.7, the stresses in Regions I and II kept increasing, they merged together into Region VI, concentrated and symmetric along the reinforcement. Regions III and IV merged into Region VII with a decreased well-distributed stress. At the same time, in the right half of Region VII, a new Region VIII emerged; the stress in this region was lower than the values in Regions III and IV.

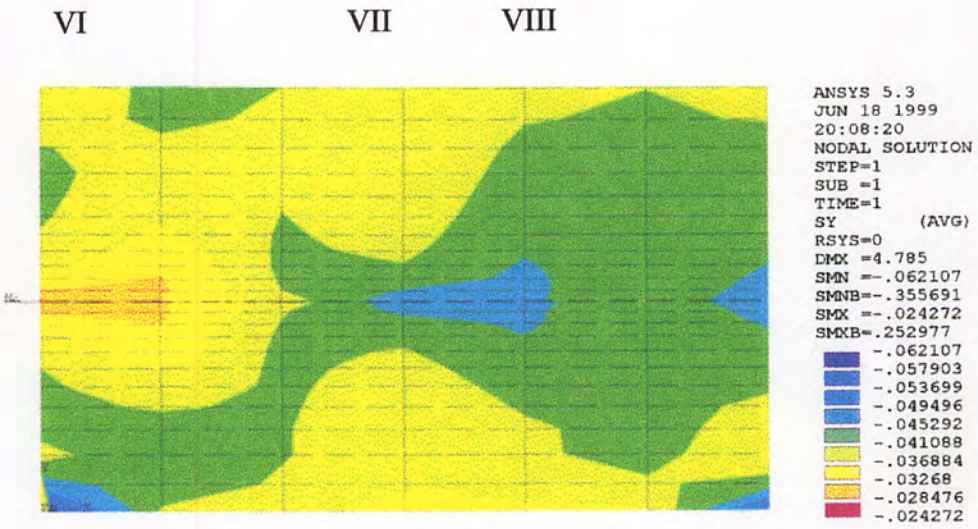

Fig. 5.7 Normal stress distribution from finite element analysis for HDPE geogrid in sand under unsaturated condition (50% Pult)

When the pullout force equaled to 75% of total pullout load, Fig 5.8, Regions VI and VII moved backward, and Region VIII extended all the way to the back wall. In the final stage, when the pullout force reached 90% of total pullout load, Fig 5.9, the stress concentration in Region VI was as high as 130% along the reinforcement just behind the slot. Regions VII and VIII moved backward, with only a small area left. The stress reduction was about 45% near the end of reinforcement .

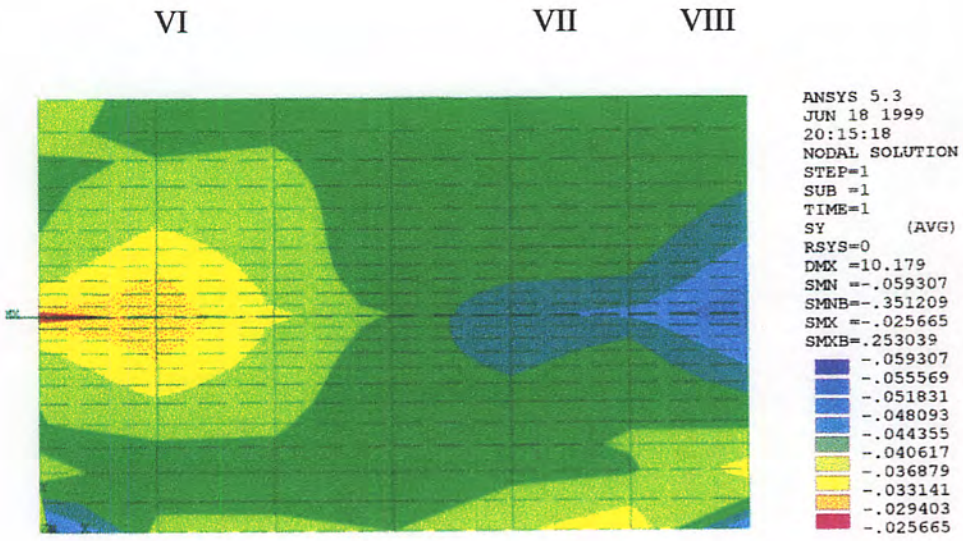

Fig.5.8 Normal stress distribution from finite element analysis for geogrid HDPE in sand under the unsaturated condition (75% Pult)

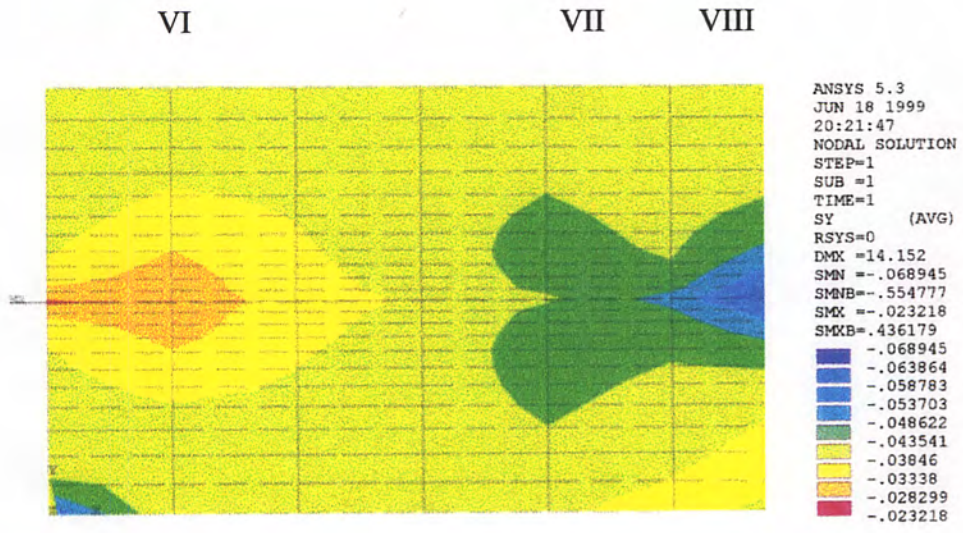

Fig. 5.9 Normal stress distribution from finite element analysis for HDPE geogrid in sand under unsaturated condition (90% Pult)

5.2.2 PRINCIPAL STRESSES FOR GEOGRID IN SOIL

Figs 5.10 - 5.14 show the principal stress distribution (MPa) patterns along the reinforcing element. These enabled the tracking of the pullout load transmission based on the increment of the pullout load applied on the reinforcing element. As the pullout load increased step by step, the affected area extended from the front wall to the back one gradually.

The stress distribution was very uniform throughout the test modeling under the confining pressure only. The application of pullout force interrupted this uniformity. When the pullout force at 10% of total pullout load, Figure 5.10, the stress variation was very little. It extended to only 70 mm from the front wall. The high stress variation area extended further to the back, as far as 200 mm, when the pullout force reached 25% of total pullout load, Fig 5.11 The affected range in the vertical direction was 50 mm above and below the reinforcement. As the pullout force reaches 50% of total pullout load, Fig.5.12, the large variation area kept moving toward the back wall, with the furthest end as far as 550 mm from the front wall, and well beyond the vertical centerline of the test setup. The effective range in the vertical direction was 100 mm.

Under the 75% of total pullout load, Fig 5.13, the high stress variation area kept propagating backward, extending to about 80% of the total length of the reinforcing element. At the sub-final loading stage (90% of total pullout load), Fig 5.14, the stress concentration area extended almost through all the length of the model, finally reaching

the rear wall. This means that almost the whole zone surrounding the reinforcing element was under critical condition, and pullout failure was imminent. At the final loading stage (100% of total pullout load), the last contact element at the very rear end of the model failed. The whole reinforcement element slided out of the pullout setup, the deformation was larger than the software's display-limit .

Fig. 5.10 Principal stress distribution from finite element analysis for HDPE geogrid in sand under unsaturated condition (10% Pult)

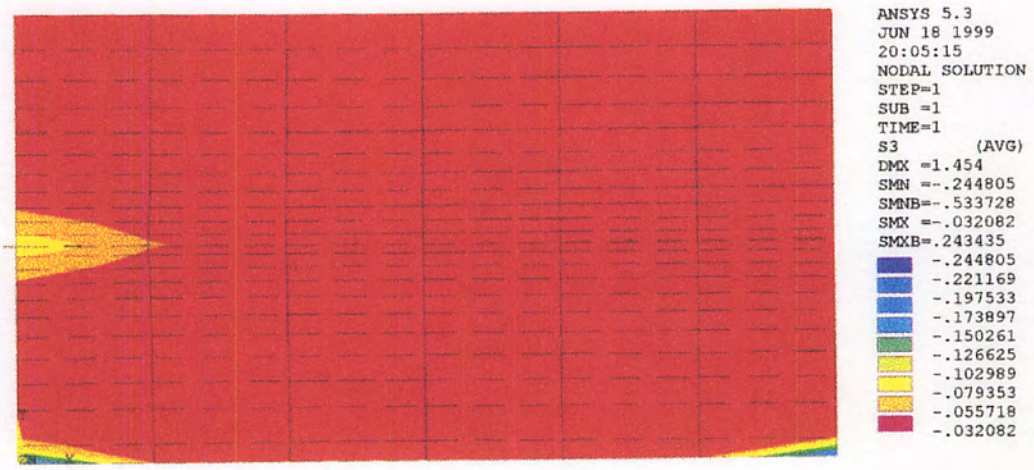

Fig. 5.11 Principal stress distribution from finite element analysis for HDPE geogrid in sand under unsaturated condition (25% Pult)

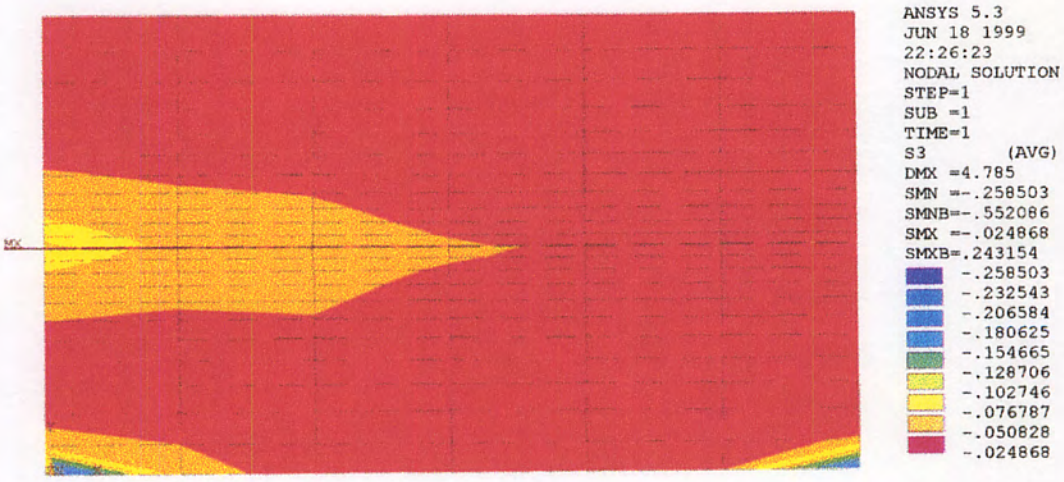

Fig. 5.12. Principal stress distribution from finite element analysis for HDPE geogrid in sand under unsaturated condition (50% Pult)

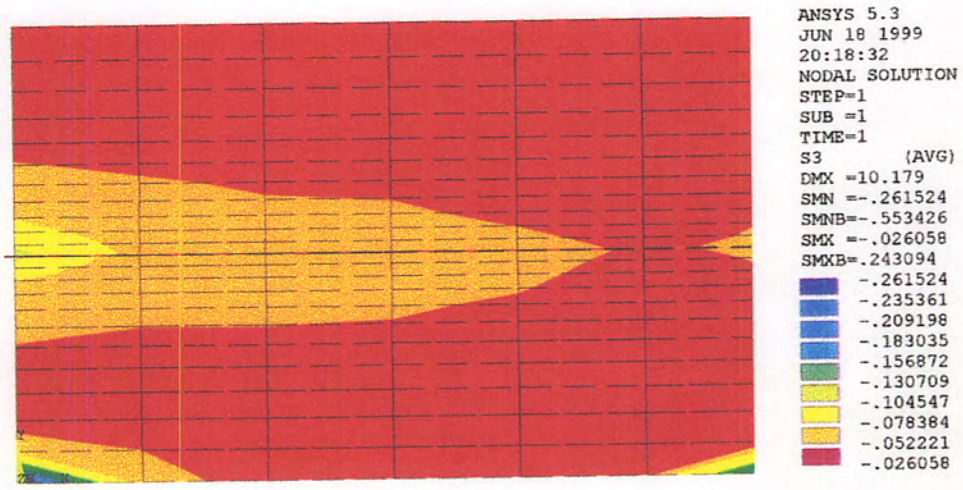

Fig. 5.13 Principal stress distribution from finite element analysis for HDPE geogrid in sand under unsaturated condition (75% Pult)

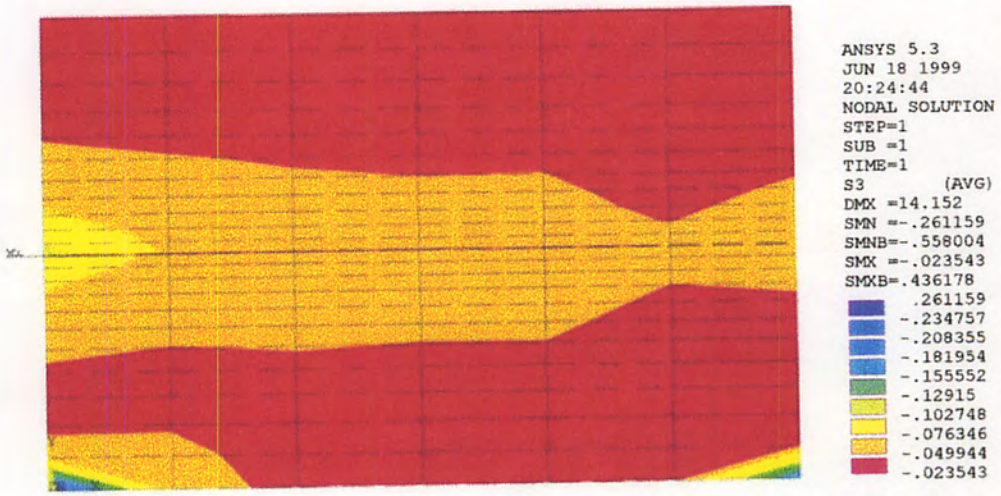

Fig. 5.14 Principal stress distribution from finite element analysis for HDPE geogrid in sand under unsaturated condition (90% Pult)

5.2.3 STRAIN ANALYSIS FOR GEOGRID IN SOIL

Fig 5.15 shows the strain distributions in the reinforcing elements for the HDPE geogrid in sand under the unsaturated condition. From the strain distributions given in this figure, it can be seen that the strain variations occurred mainly in the reinforcing elements. The strain variations in the soil element were very limited and unnoticeable compared to those in the reinforcing element. There are two major reasons for this phenomenon. Firstly, the soil element was restrained within the pullout box; the roller boundary condition did not allow any movement horizontally, especially in the regions near the front and rear ends of the reinforcing elements. Secondly, the pullout load was applied directly on the reinforcing element, not on the soil elements.

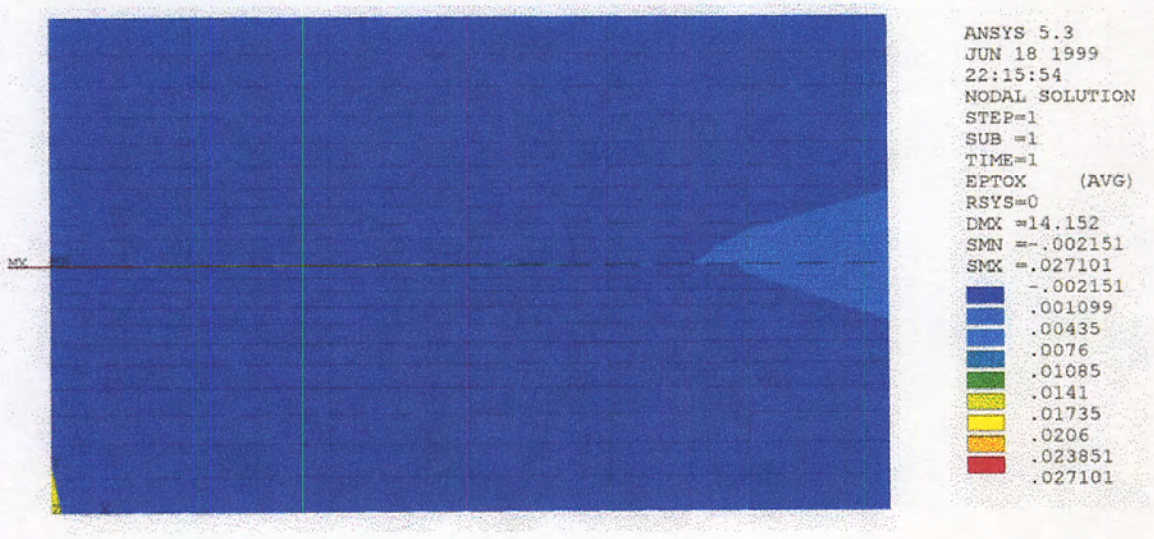

Fig. 5.15 Strain distribution from finite element analysis for HDPE geogrid in sand under unsaturated condition (90% Pult)

CHAPTER 6

CREEP AND CREEP RUPTURE TESTING

6.1 MATERIAL PROPERTIES

6.1.1 GEOSYNTHETIC TEST SPECIMENS

6.1.1.1 HDPE Geogrid Properties

The properties of Geogrids, UX-1400 SB, are presented in Table 6.1. Based on the information provided by the manufacturer, the long term load capacity was measured by tensile creep testing to 10,000 hours as described in the Geosynthetic Research Institute test method, GG3-87 "Creep Behavior and Long Term Design Load of Geogrids".

6.1.1.2 PET Geogrid Properties

The properties have been listed in section 4.1.1.2

6.1.2 ENVIRONMENTAL EXPOSURES

The four different solutions used for the HDPE Geogrids and the five for the PET geogrids and are listed below :

a) Phosphate (pH 4.5)

b) Calcareous (pH 9.0)

c) Sea water

d) Limerock

e) Water (only for PET specimens)

The compositions of the solution were based to simulate the characteristics of soils found in Florida, and are as follows:

A. Phosphate (pH 4.5): The solution is composed of Hydrochloric Acid ACS Agent, Calcium Phosphate Dibasic, and Water.

B. Calcareous (pH 9.0): The solution is composed of Sodium Hydroxide Solution, Calcium Carbonate, and Water.

C. Sea water: Sea water was taken from the ocean at Palmetto Beach, Boca Raton, FL.

D. Limerock: The limerock. used is very common in Florida, and meets the FDOT Materials Specifications FM1-7011. The optimum moisture content is around 11%. The limerock is well graded with 0.9 mm average grain size and 0.15 mm effective grain size. Its friction angle is around 34°, and the density 1498 kg/m^3. It has a uniformity coefficient of 9 and coefficient gradation of 1.14. A mechanical sieve analysis was performed on the soil and the results are listed in Table 4.4.

E. Water: Tap water was used

Table 6.1 Properties of UX-1400 SB (HDPE) Geogrids

PROPERTIES	TEST METHOD	UNITS	VALUE
INTERLOCK			
Apertures	Calipered		
--MD		mm	144.8 (nom.)
--CMD		mm	16.7 (nom.)
Open area	COE Method	%	60 (nom.)
Thickness	ASTM D1777-64		
--ribs		mm	0.76 (nom.)
--junctions		mm	2.8 (nom.)
REINFORCEMENT			
Creep Limited Strength	GRI GG3-87 (or ASTM D5262)	kN/m	20.7 (min.)
Flexural Rigidity	ASTM D1388-64	mg-cm	6600000 (min.)
Tensile Modulus --MD	GRI GG1-87	kN/m	737.7 (min.)
Junctions	GRI GG2-87		
--strength		kN/m	49.1 (min.)
--efficiency		%	90 (min.)
MATERIAL			
High Density Polyethylene	ASTM D1248 Type III/Class A/Grade 5	%	97.0 (min.)
Carbon Black	ASTM 4218	%	2.0 (min.)
DIMENSIONS			
Roll Length		m	30
Roll Width		m	1.3
Roll Weight		N	196

6.2 TEST SETUP

6.2.1 INTRODUCTION

20 tanks were fabricated at Florida Atlantic University (1997) to evaluate the creep and creep rupture of HDPE and PET geogrid specimens. Measurements include the elongation of the specimens and time for the specific elongation. Different exposures and elevated temperatures were used to determine the long-term behavior of the geogrids, and to simulate different exposure conditions, with soil water related to the soil conditions in Florida. The different variables are presented in the test procedures section (6.3).

A mock-up and pilot tank was fabricated, Fig. 6.1. The creep tanks were designed based on the experience obtained. The shop drawings are presented in Figs 6.2 to 6.5. Instead of the 11 tanks originally specified, the number was increased to 20 due to the revisions and addition at test loads and temperatures. This delayed the commencement of the creep experiments. The 20 tanks were fabricated at Florida Atlantic University for the sake of economy.

6.2.2 CREEP AND CREEP RUPTURE APPARATUS

The creep and creep rupture tanks were filled with different solutions and soils, with 6 single rib geogrid test specimens in each tank. The test setup was comprised of clamps for gripping each specimen, heaters and pumps to maintain the temperatures and

compositions of the solutions, clocks for time measurement, dial gages with extensions to record the elongations, loading lever arms (1:5), and weights for the application of constant loads.

6.2.2.1 Creep and Creep Rupture tank

The internal dimensions of the tanks were determined based on the experience gained with the pilot tank (figs 6.2 - 6.5), and on the following criteria: 1) The box had to be long and wide enough to accommodate 6 single rib HDPE or PET geogrid test specimens with enough space for the safe and easy installation of the test specimens. 2) The height of the tanks had to be adequate to accommodate the test specimens plus more than the maximum predicted elongation of the test specimens.

The creep and creep rupture tank was composed of 5 main sections, bottom plate, bottom beams, for square tube columns, plexiglas walls, and top tubing for support of lever arms. Figs 6.2 - 6.5.

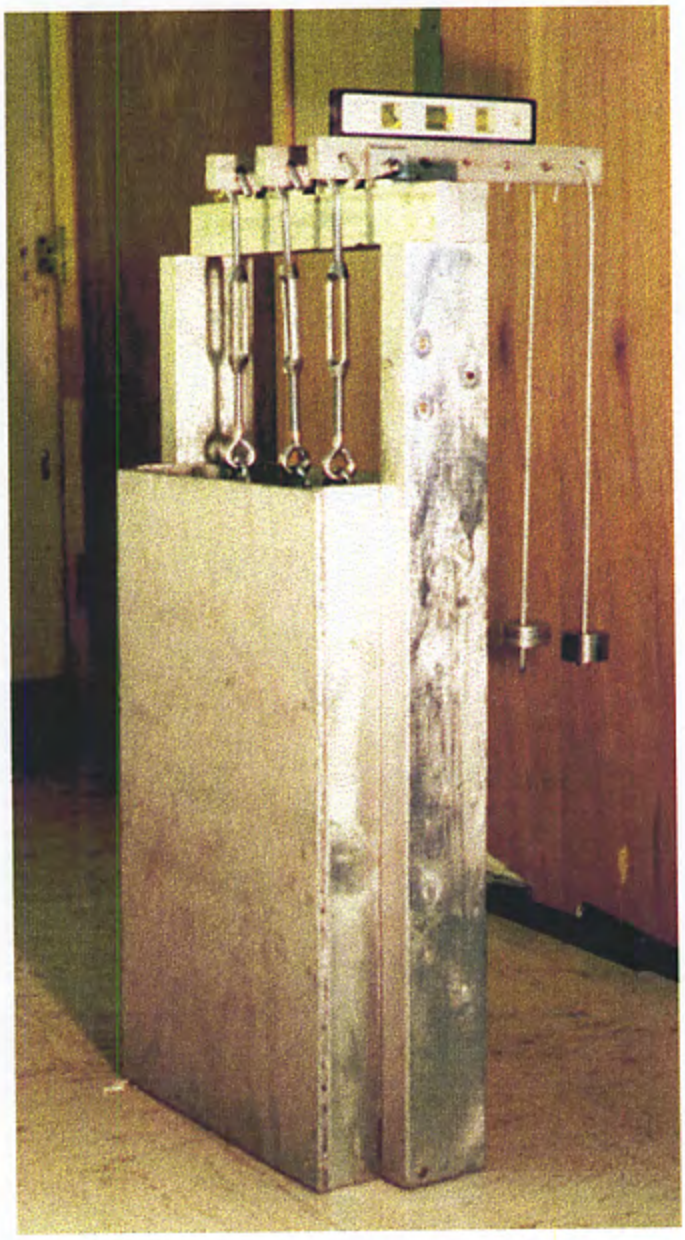

Figure 6.1 Creep tank mock-up

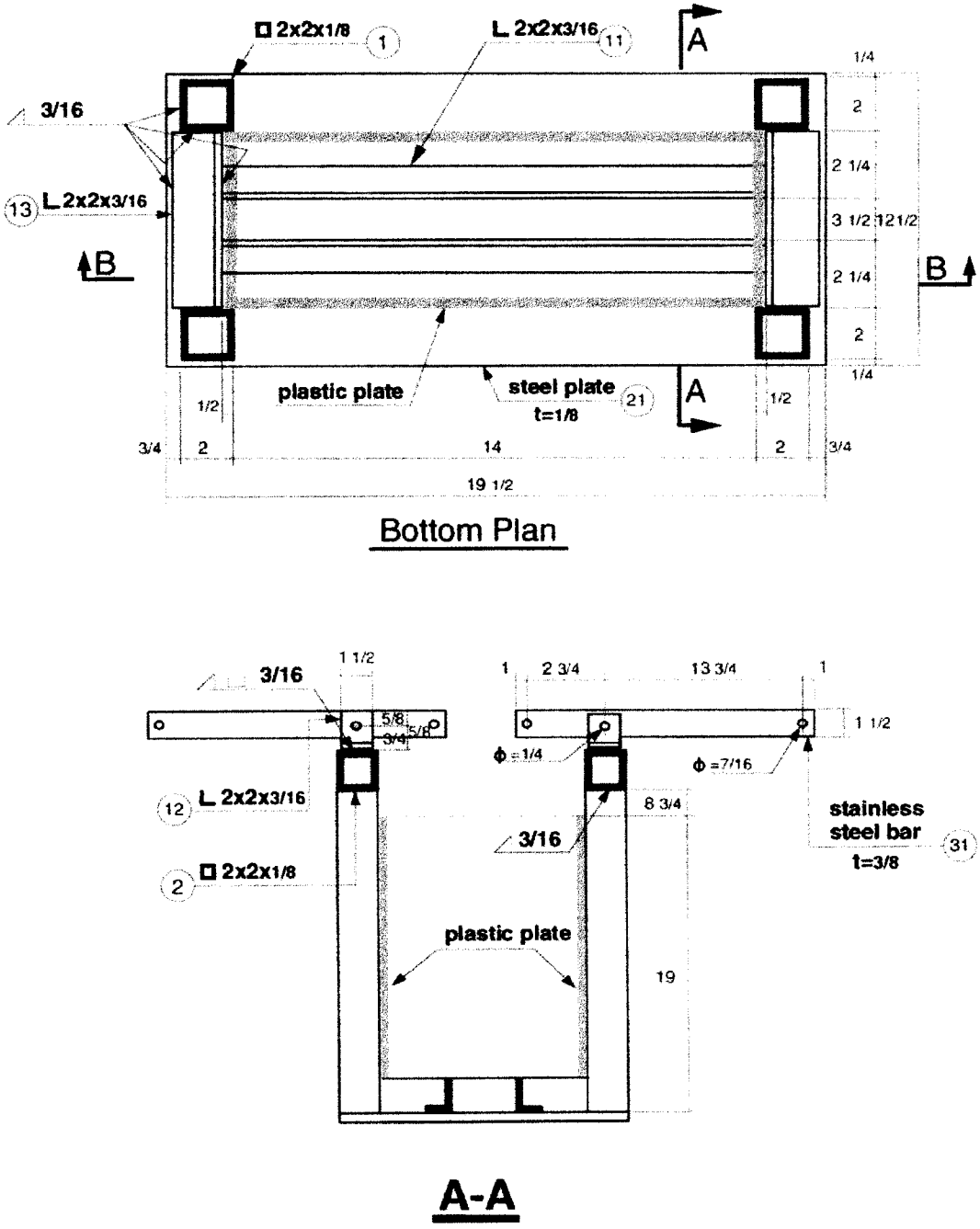

Figure 6.2 HDPE creep tank

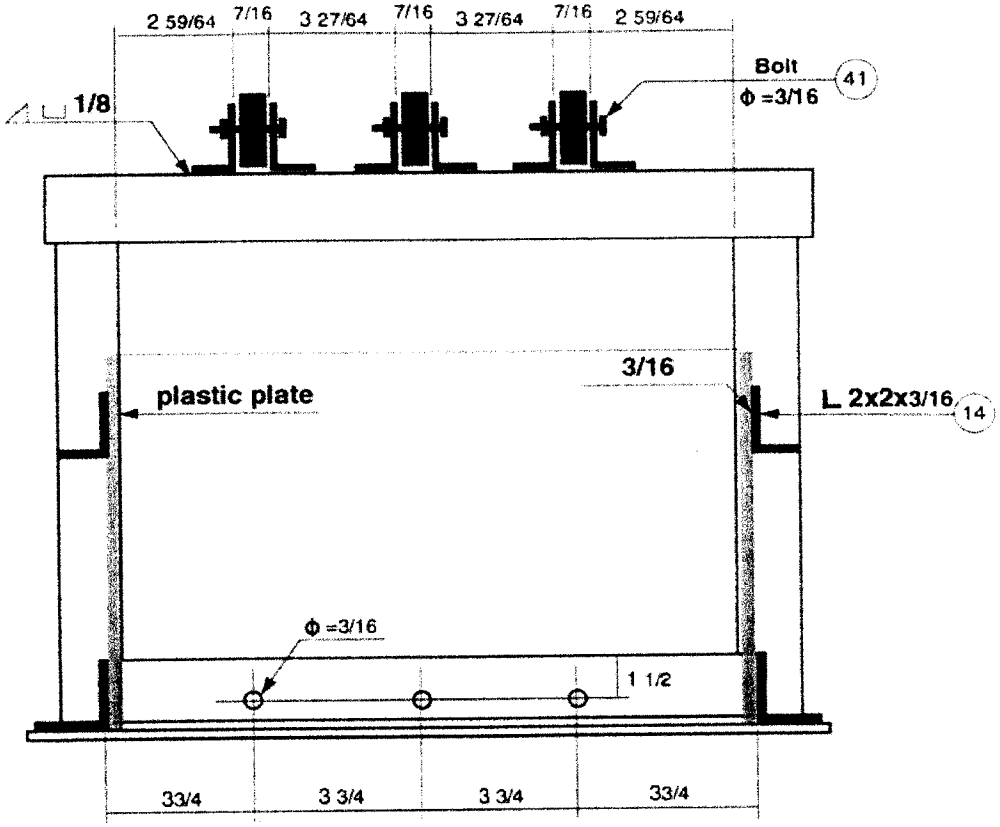

B-B

Note:

I. a. Materials: ASTM A36.
b. Dimension unit: in. (1 in. = 25.4mm)
c. 1 = Tubing 2x2x1/8 (length = 32 3/4). There are four in all
2 = Tubing 2x2 1/8 (length = 19). There are two in all
11 = Angle 2x2 3/16 (length = 15). There are two in all
12 = Angle 2x2 3/16 (length = 1 1/2). There are twelve in all
13 = Angle 2x2 3/16 (length = 8). There are four in all
14 = Angle 2x11/2 x 3/16 (length = 8). There are four in all
21 = Steel plate t= 1/8 (11 x 191/2). There is one in all
41 = Bolt 3/16. There are six in all

II. A Materials: Stainless steel #304
31 = Bar 3/8 x 11/2 x 181/2. There are six in all

Figure 6.3 HDPE creep tank

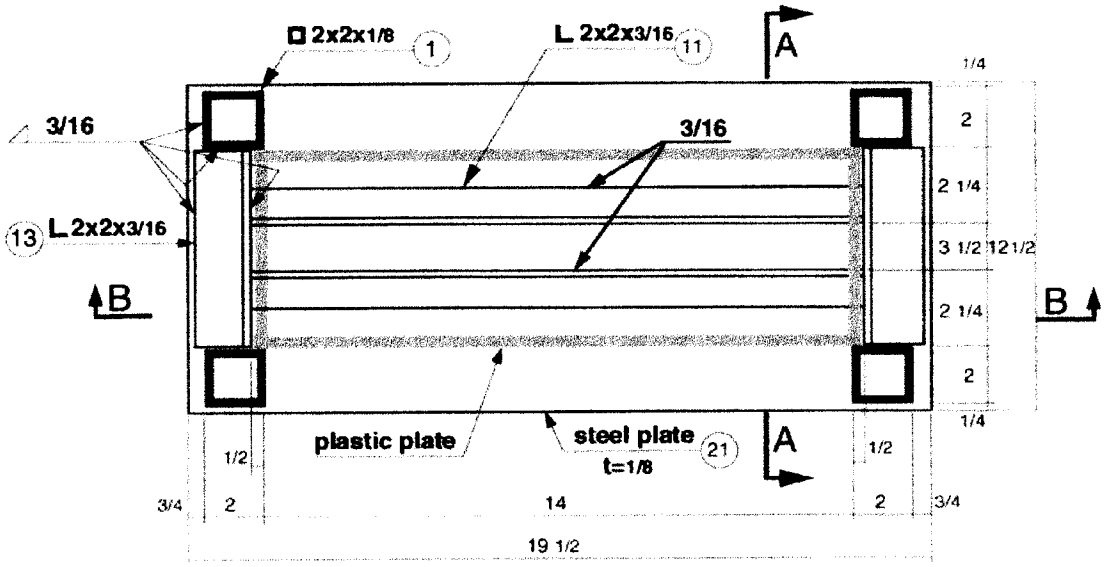

Bottom Plan

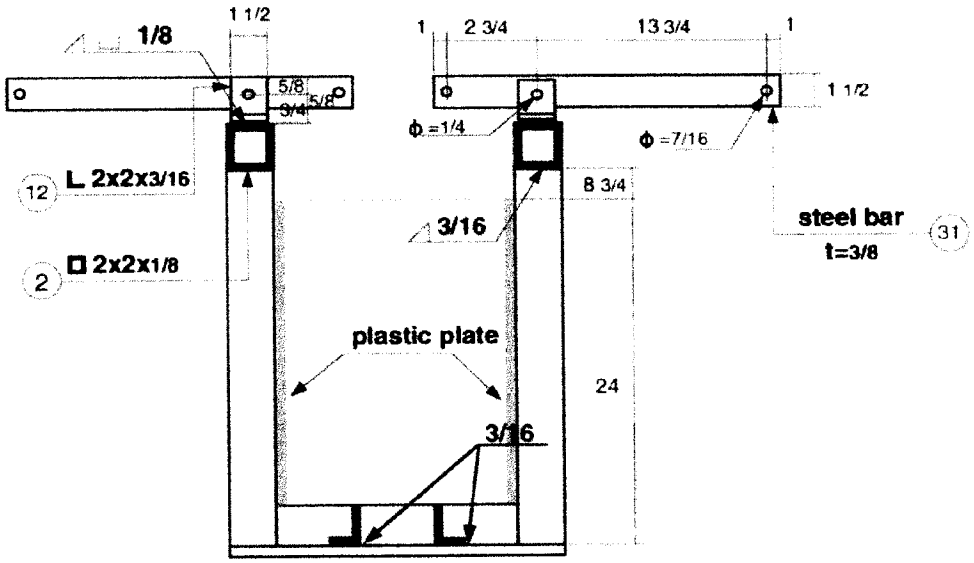

A-A

Figure 6.4 PET creep tank

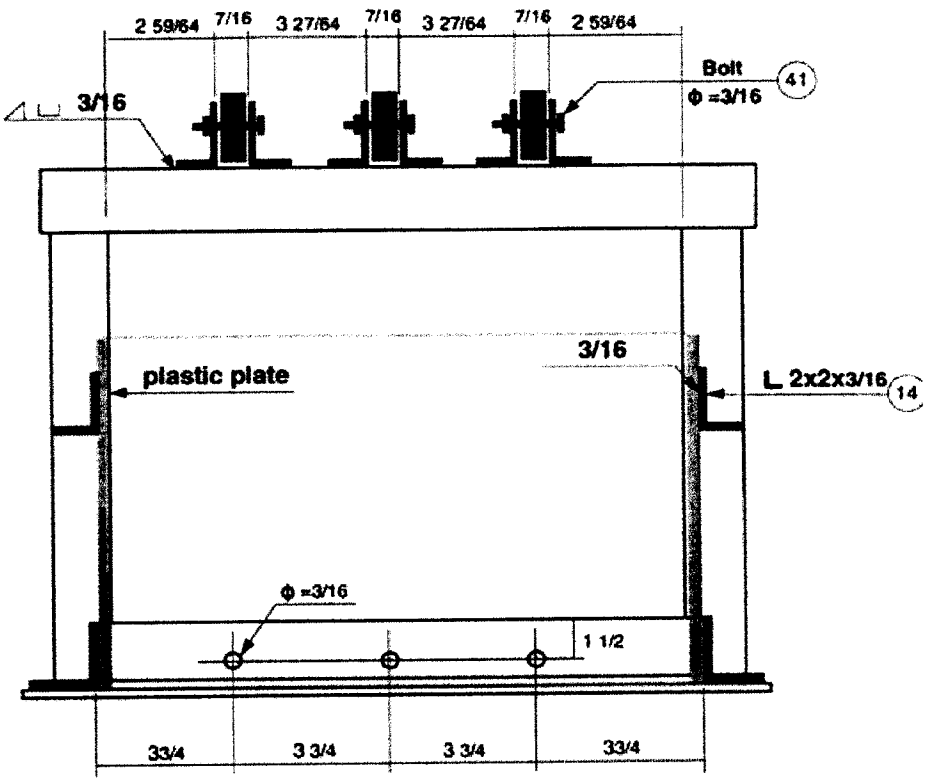

Note:

I. a. ASTM A36.

b. Dimension unit: in. (1 in. = 25.4mm)

c. 1 = Tubing 2x2x1/8 (length = 32 3/4). There are four in all

2 = Tubing 2x2 1/8 (length = 19). There are two in all

11 = Angle 2x2 3/16 (length = 15). There are two in all

12 = Angle 2x1 1/2 x 3/16 (length = 1 1/2). There are twelve in all

13 = Angle 2x2 3/16 (length = 8). There are four in all

14 = Angle 2x1 1/2 x 3/16 (length = 8). There are four in all

21 = Steel plate t= 1/8 (11 x 19 1/2). There is one in all

41 = Bolt 3/16. There are six in all.

II.A Materials: Stainless steel #304

B. 31 = Bar 3/8 x 1 1/2 x 18 1/2. There are six in all

Figure 6.5 PET creep tank

6.2.2.2. Clamps (Models A and B)

Two kinds of clamps were used to fasten the test specimens. All clamps were stiff enough to assure a uniform pullout displacement across the width of the test specimens. Clamp A was used for geogrid HDPE (Fig 6.6). It had two identical jaws with unique contours that fit the specimen very well. The inner corner of the front lip was rounded well to assure that the specimen would not be split. The space between the upper and lower lips was big enough to let the specimen to be pushed in transversely, but small enough to prevent it from sliding out.

Clamp B, used for geogrid PET (Fig 6.7), was comprised of three identical plates. All the surfaces were well frosted to provide good fastening ability. The test specimen was wrapped around the plates. All plate edges were filleted to give a smooth surface. A design change was made from a circular clamp, which was producing stress concentration in the geogrid.

6.2.2.3 Dial Gages

Eighty-two dial gages (MSC 76450071, measuring range 1", least count=0.001") with removable spindles, 30 dial gages (MSC 76450089, measuring range 2", least count=0.001") with removable spindles and one dial gage (Starrett 25-5041, measuring range 4", least count=0.001"), were mounted to measure the elongations of HDPE and PET geogrids, for a maximum total expected deformation of up to 5" for the HDPE

geogrids with a deformation in the order of 2" in the first 48 hours. The dial gages characteristics conformed with Test Method GG3 and will be readjusted by removing the spindle extensions.

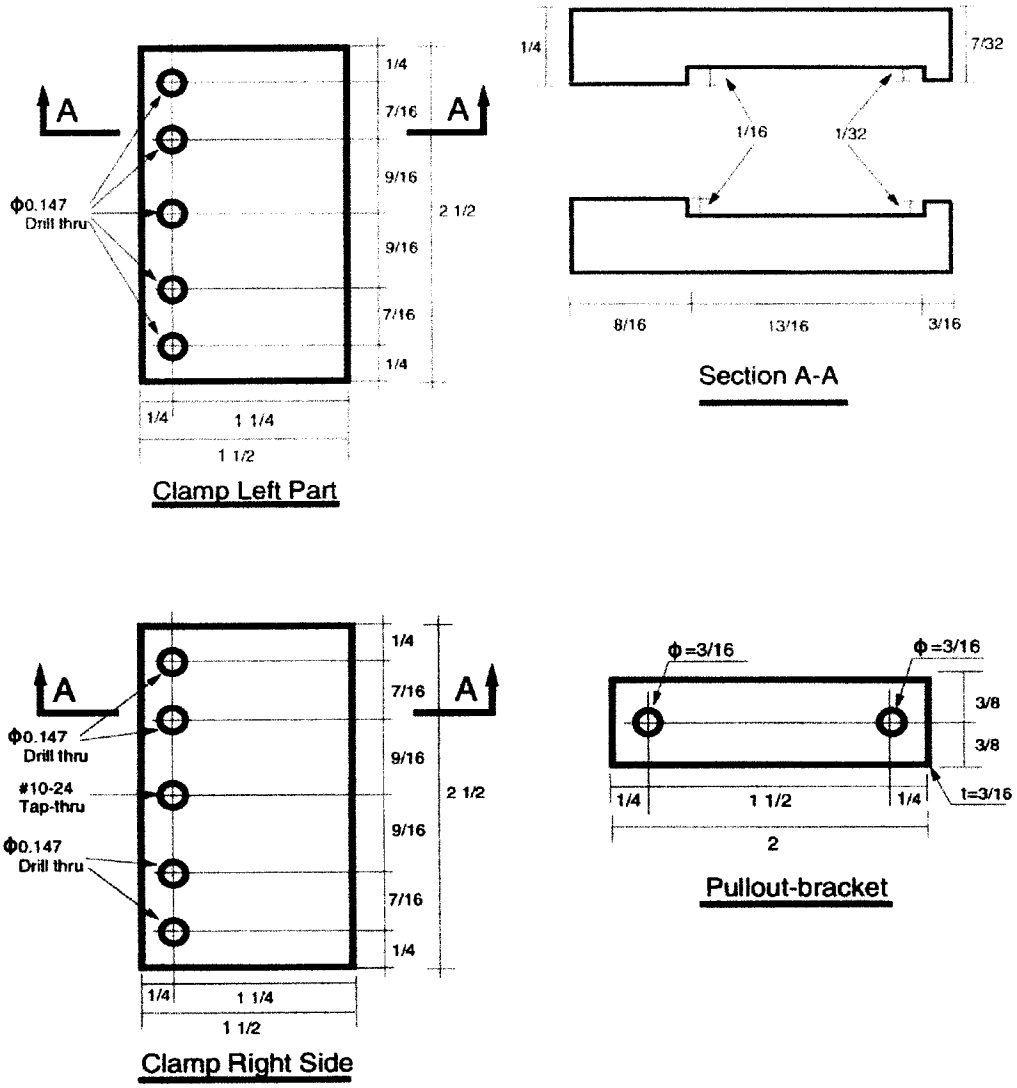

Note:

1. Materials: stainless steel. #304
2. Dimension unit: in. (1in. = 25.4mm)
3. The surface should be smooth but frosted.
4. There are two pullout- brackets in all.

Figure 6. 6 Clamp for HDPE specimens

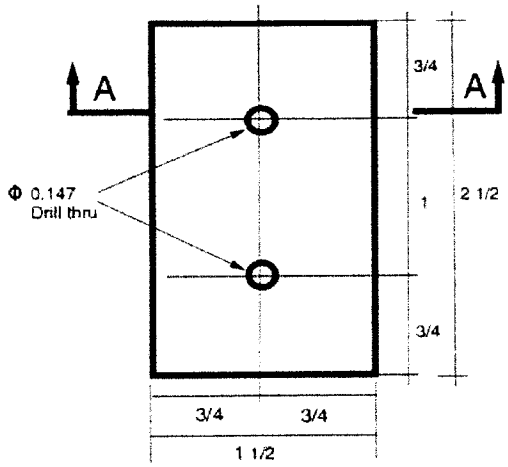

Clamp Left Side

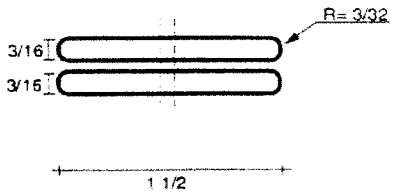

Section A-A

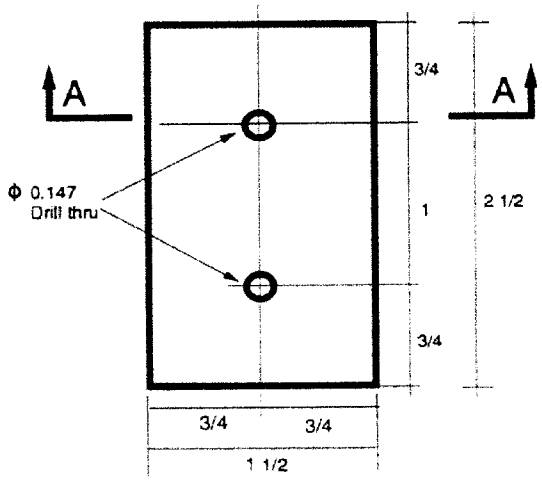

Clamp Right Side

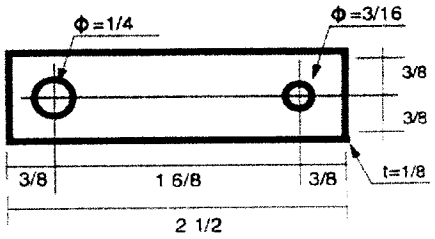

Pullout bracket

Note:

1. Materials: stainless steel. #304
2. Dimension unit: in. (1in. = 25.4mm)
3. The surface should be smooth but frosted.
4. There are four pullout brackets in all.

Figure 6.7 Clamp for PET specimens

6.2.2.4 Time Measurement

Four ENM T50B212P 115v, 50/60hz clocks for measurements up to 10,000 hrs were installed in the 9 tanks for the lower temperatures for HDPE and PET specimens and 6 similar clocks in each of the remaining tanks. The specimens, exposed at the lower temperatures and load levels, were not expected to break. .Hence, only one clock was used for each of the HDPE and PET specimens to record the time.

6.2.2.5 Lever Arm and Turnbuckle

The lever arms were designed to have a 1 to 5 ratio in order to provide large loads with a minimum number of weights, due to the large number of tanks and space and load magnitude limitations. The large deformations, expected mainly in the HDPE specimens, were provided for with turnbuckles installed between the lever arm and the clamps.

6.3. TEST PROCEDURES

6.3.1. INTRODUCTION

To simulate different exposure conditions, 20 tanks were fabricated with soil water related to the soil conditions in Florida, Figs. 6.8 and 6.9.

The variables are as follows:

HDPE: 2 specimens x

4 temperatures x

4 solutions x

3 load levels

Total = 96 HDPE specimens

PET: 2 specimens x

4 temperatures x

5 solutions x

3 load levels

Total = **120 PET specimens**

TOTAL = 216 specimens

Temperatures :

86 °F (30°C)

113 °F (45°C)

131 °F (55°C)

149 °F (65 °C)

Solutions :

Phosphate (pH 4.5)

Calcareous (pH 9.0)

Sea water

water (only for PET specimens)

Limerock

Load levels :

30%

40%

50%

of the ultimate value

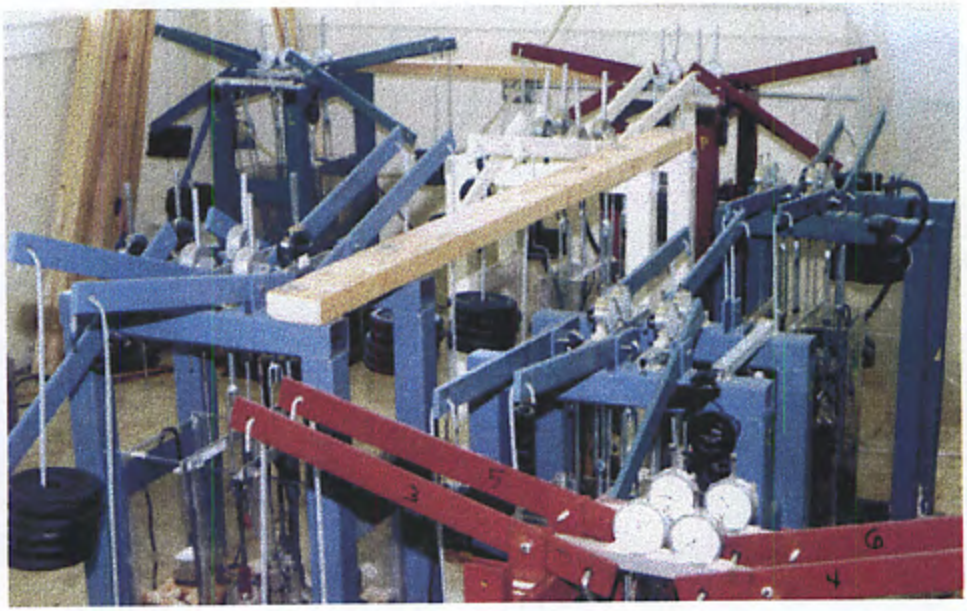

Figure 6.8 Creep tanks for lower temperatures

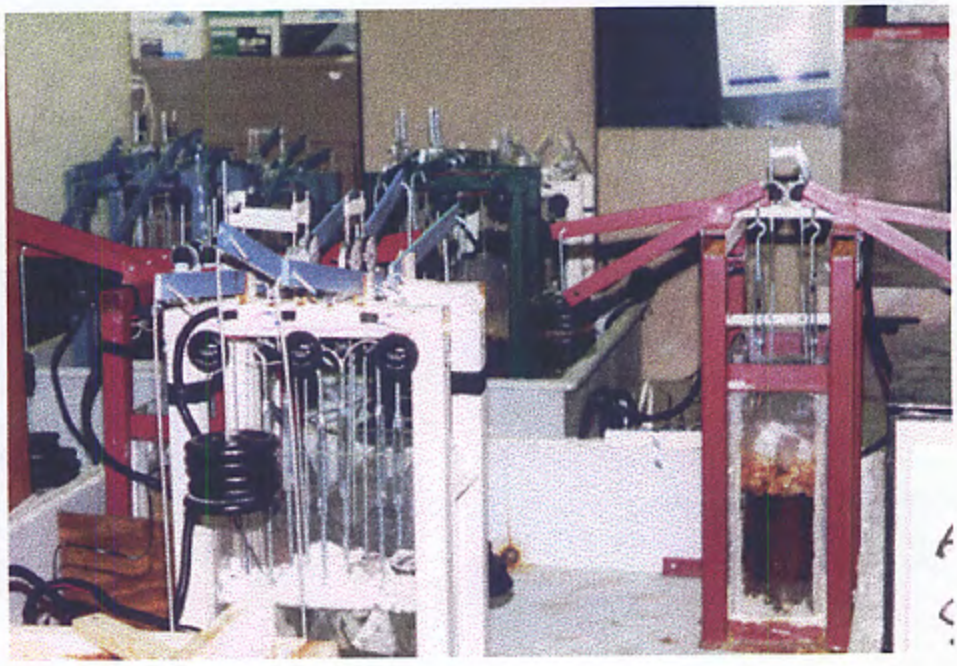

Figure 6.9 Creep tanks for higher temperatures

6.3.2. TEST PREPARATION

6.3.2.1 Trimming the Geogrid Specimen

The geogrid specimen was cut to a width of 0.07 m (three ribs) for HDPE cutting the 2 outside ribs, leaving only the middle one to sustain the loads and 0.03 m (single rib) for PET . For HDPE, the length is 0.34 m, and for PET 0.22 m.

6.3.2.2 Clamping the Test Specimen

The clamping procedures for HDPE and PET were different, Figs 6.10 After clamping and bolting, four brackets were connected.

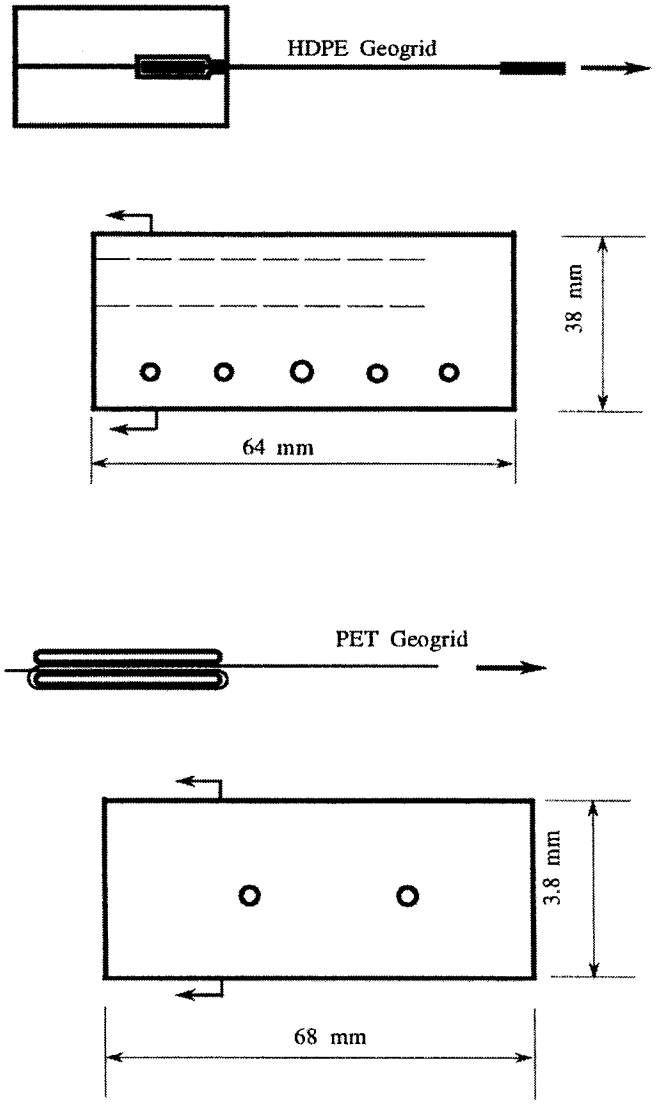

Figure 6.10 HDPE and PET clamping

6.3.3. PLACEMENT OF THE SOIL WATER SAMPLES AND TEST SPECIMEN

Prior to each test, the creep and creep rupture tank was thoroughly cleaned. The test specimens were then placed in the tank one by one and secured to the bottom. The upper ends were then connected to the turnbuckles. Subsequently the turnbuckles were connected to the lever arms with "S" connectors. Once the six specimens were in place, the soil water was put into the tank, the solutions (Phosphate and Calcareous) were stabilized, and the heater(s) and pumps connected. A period of at least 24 hours was provided to stabilize the temperatures to follow ASTM standards D 5262 - 92 and D 4595 -86.

6.3.4. APPLICATION OF THE SURCHARGE LOAD

A pretension force, equal to 1.25% of the expected breaking force, was applied in conformance with ASTM standards D 5262 - 92 and D 4595 -86. After no movement was detected in the dial gages, the loads were carefully applied, ensuring that the loads were not dropped, but applied as rapidly as possible.

6.3.5. TEMPERATURE, PH, WATER LEVEL, AND LENGTH CONTROL

The temperatures were controlled daily to maintain the water soil at a temperature in the range of $T \pm 2°$ C, to follow specifications in the ASTM standards D 5262 - 92 and D 4595 -86; to prevent evaporation and isolate the soil water, polyurethane packing foam

was placed on top of the soil water. The pH values were measured every three days and adjusted when necessary by adding the required material. For water control, water was added every day to tanks at 55 and 65 ° C and every 2 to 3 days for the 45 and 30 ° C tanks. The water was kept above the level of the clamps to assure submergence of the specimens at all times.

When the specimens had creeped to the stage, when the dial gage had covered its entire range, the spindles were removed, and the readings adjusted. The lever arms were kept horizontal (± 10°) by turning the turnbuckles with the clamps held to avoid overloading.

6.4. TEST RESULTS

6.4.1 INTRODUCTION

The results are presented for creep strain and creep rupture tests on both HDPE and PET test specimens. The test parameters are listed in Section 6.3.1. The values of creep strain were plotted for each of the two specimens which are call: "specimen set I" and "specimen set II" each graph corresponds to a geogrids type, specimen set, temperature and load level, including all environmental exposures. Regression analysis carried out for each specimen.

6.4.2 CREEP CURVES

Creep strain curves for the HDPE and PET specimens are presented in Figures 6.11 to 6.58. The graphs show strain in percentage against time in hours plotted in log scale. Regression analysis including the formulas and R values for the curves is presented in the plots and will be explained in chapter 7.

It can be observed, that HDPE geogrids show large deformations, up to 55 % strain under the most extreme conditions (i.e. T= 65°C and Load level = 50% ultimate load, figs. 6.33 and 6.34), while for PET specimens the maximum strain was 14 % for the same conditions. (Figs 6.57 and 6.58)

This shows that PET geogrids resist creep strain better than HDPE at similar temperatures and load levels. Creep rupture occurred in the HDPE specimens for load levels = 40% and 50% ultimate load, while only two of the PET specimens broke but, this was attributed to defective specimen or incorrect clamping.

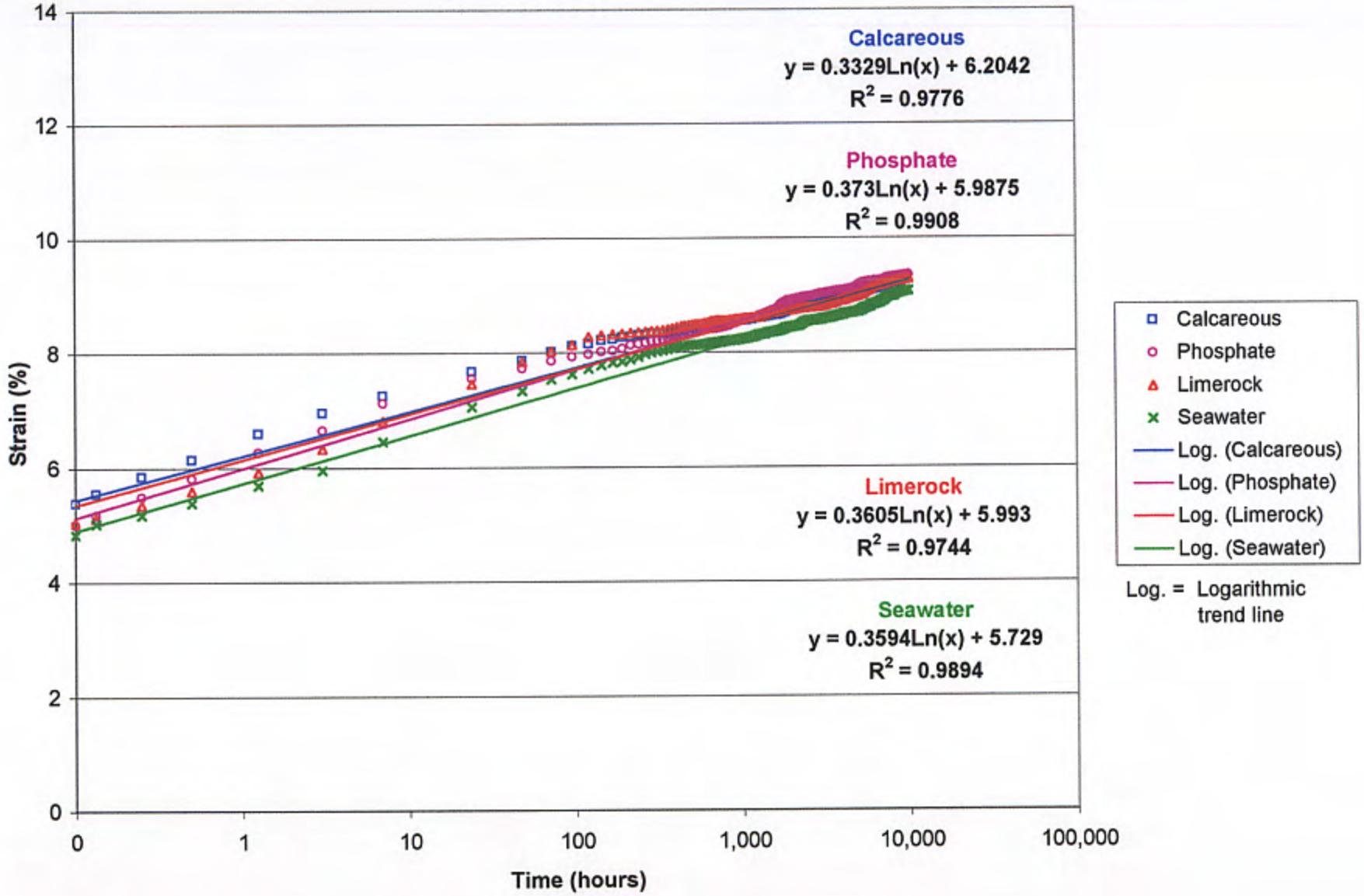

Fig. 6.11. Creep curves for HDPE geogrids, T = 30°C, Load level = 30% ultimate load - Specimen set I

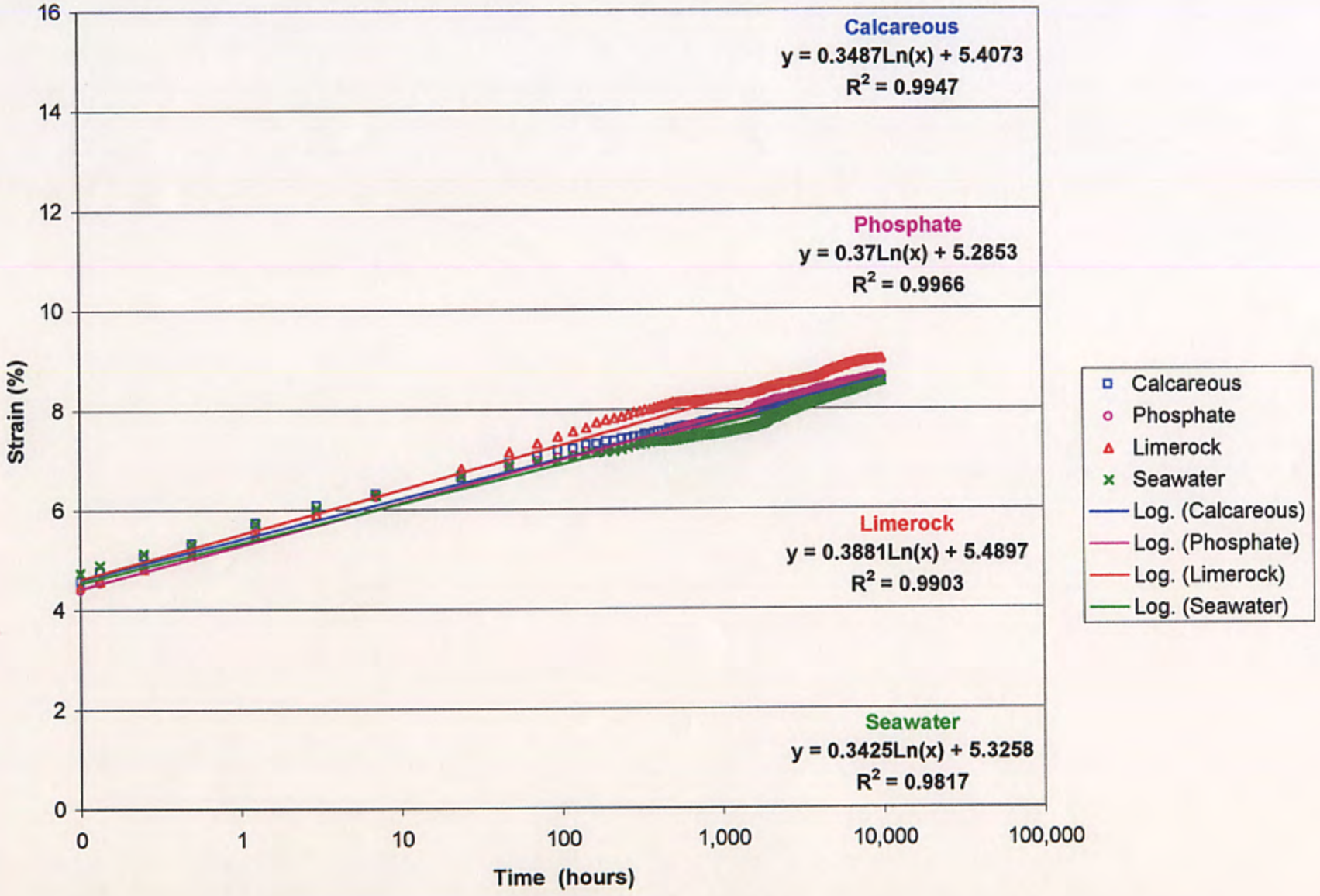

Fig. 6.12. Creep curves for HDPE geogrids, T = 30°C, Load level = 30% ultimate load - Specimen set II

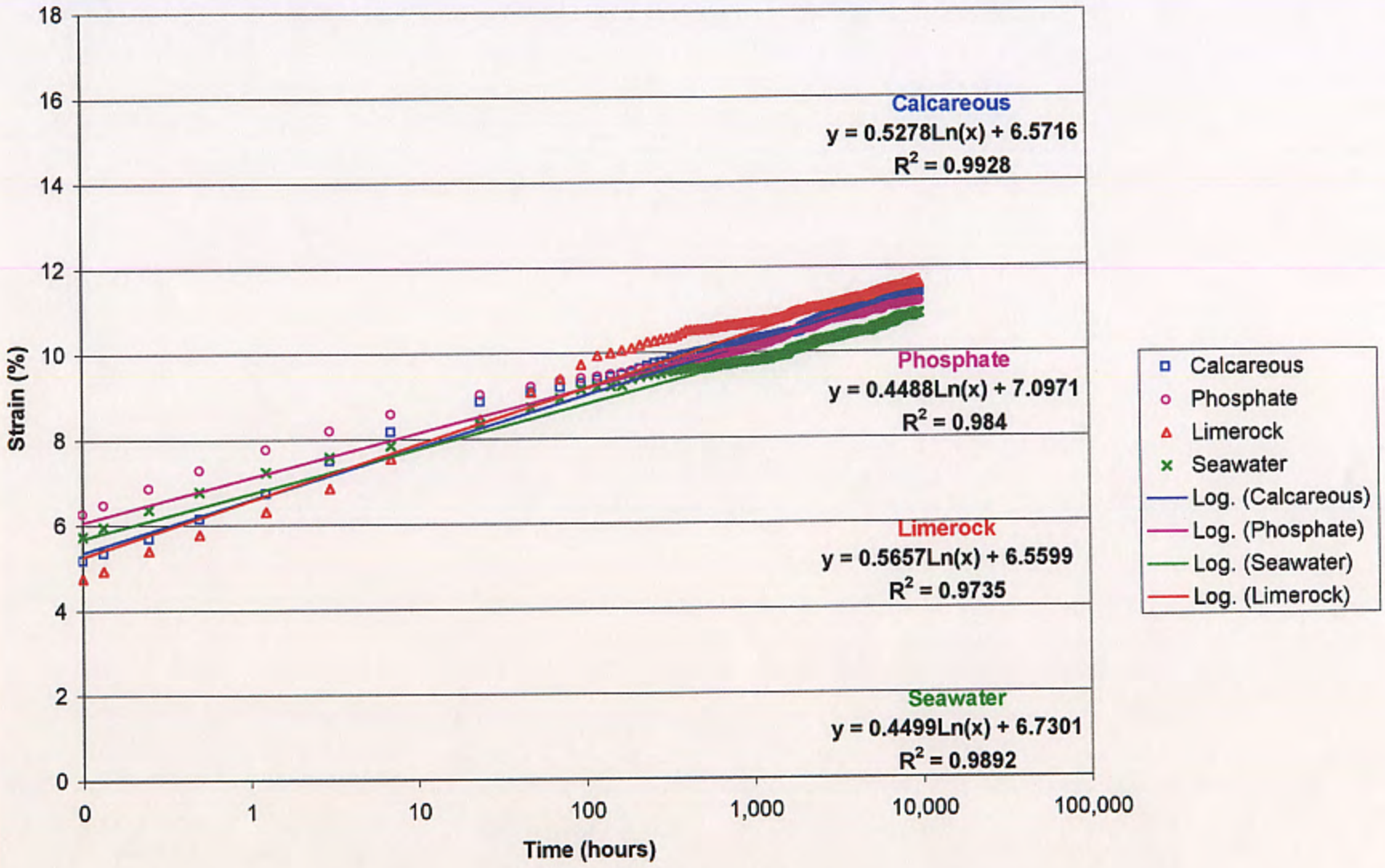

Fig. 6.13. Creep curves for HDPE geogrids, T = 30°C, Load level = 40% ultimate load - Specimen set I.

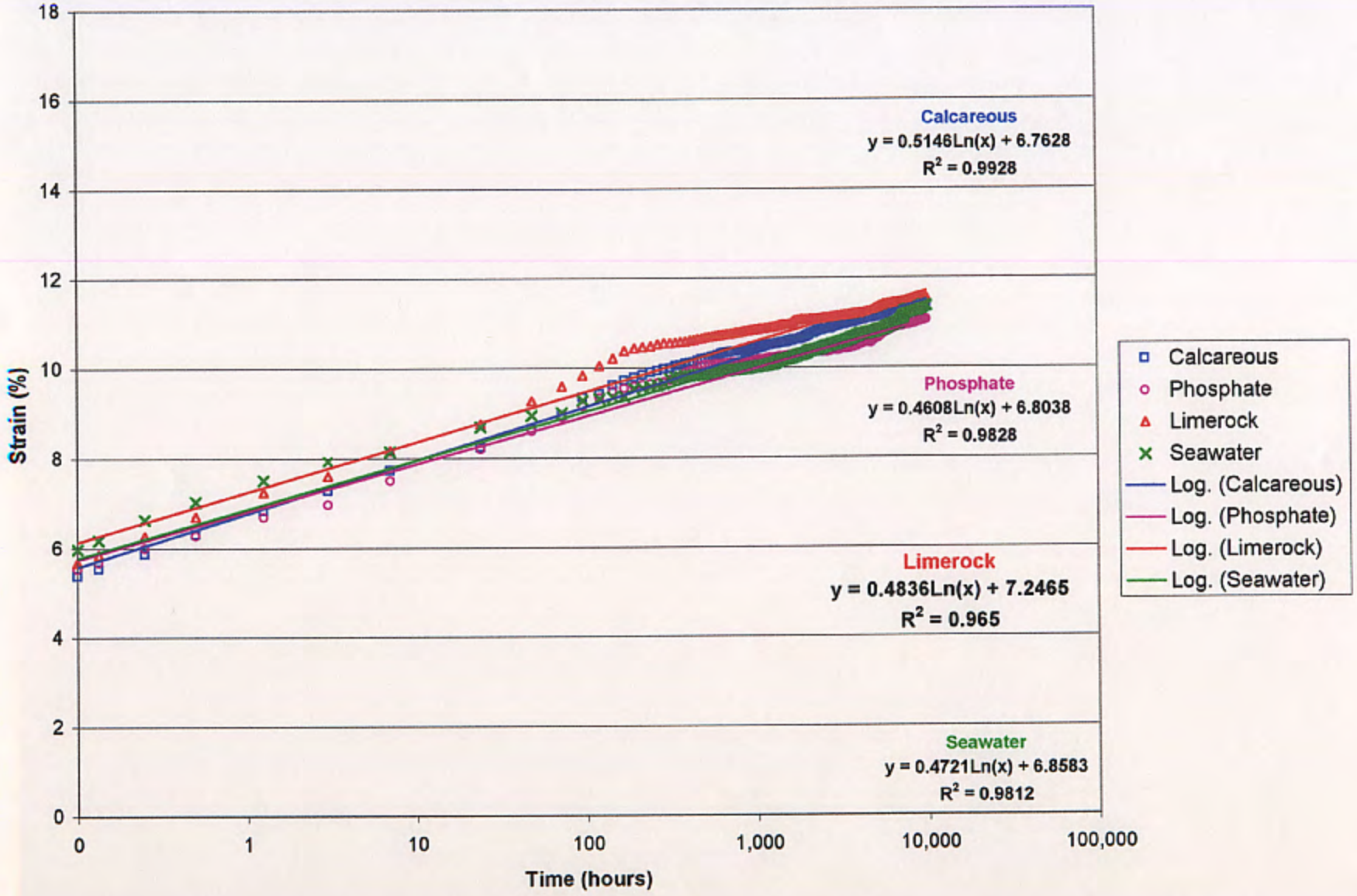

Fig. 6.14. Creep curves for HDPE geogrids, T= 30°C, Load level = 40% ultimate load - Specimen set II

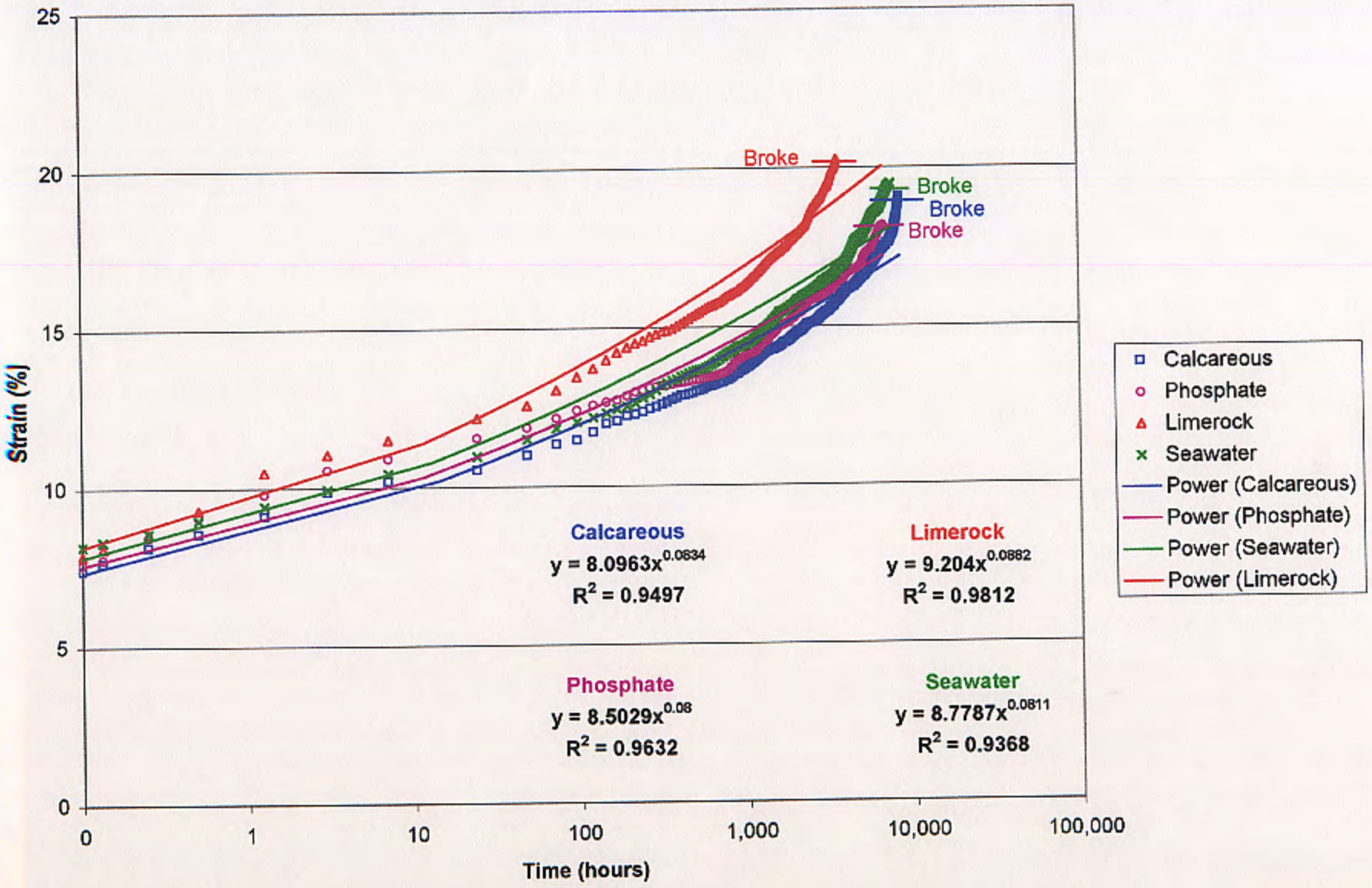

Fig. 6.15. Creep curves for HDPE geogrids, T = 30°C, Load level = 50% ultimate load - Specimen set I

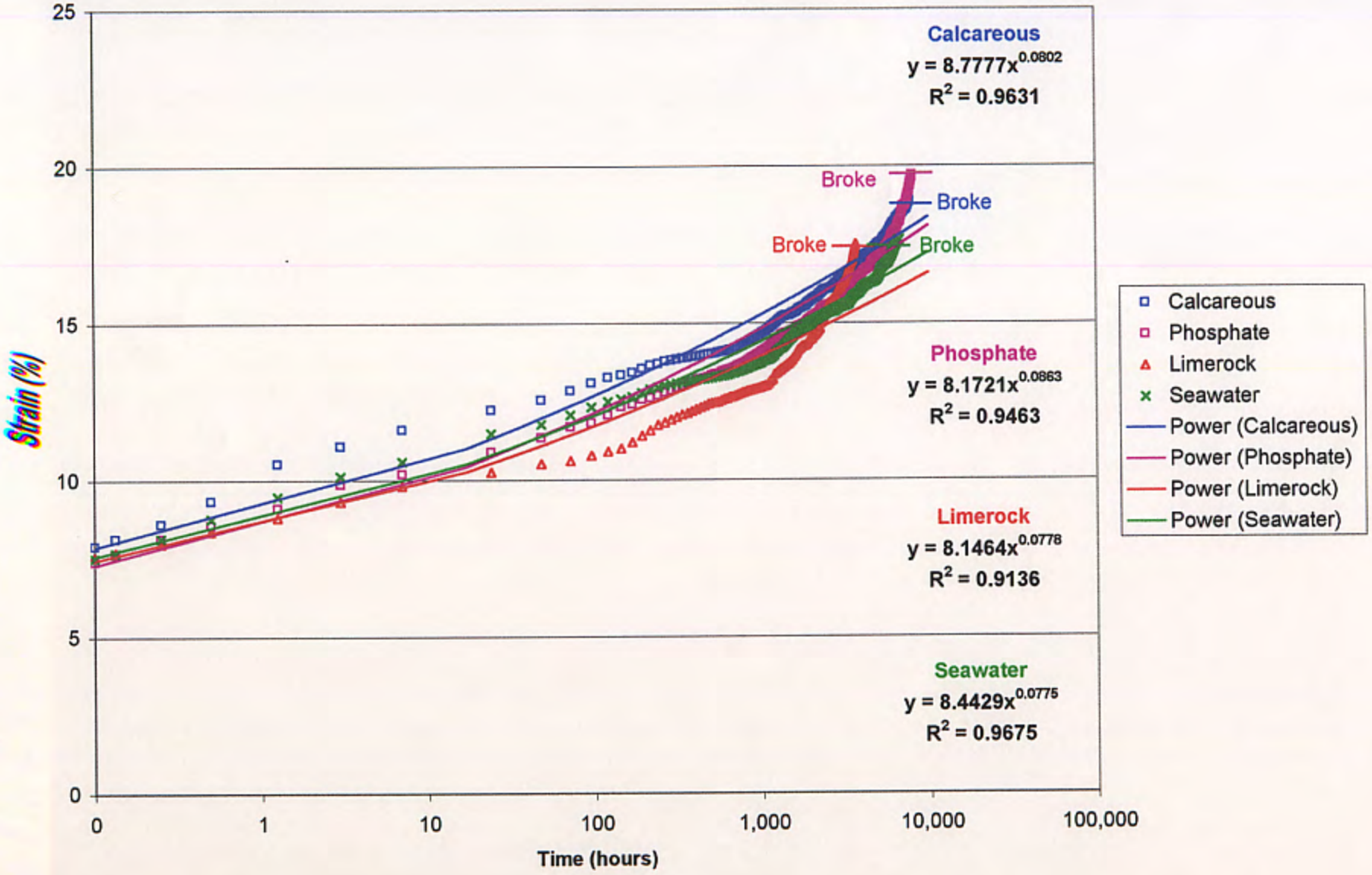

Fig. 6.16. Creep curves for HDPE geogrids, T = 30°C, Load level = 50% ultimate load - Specimen set II

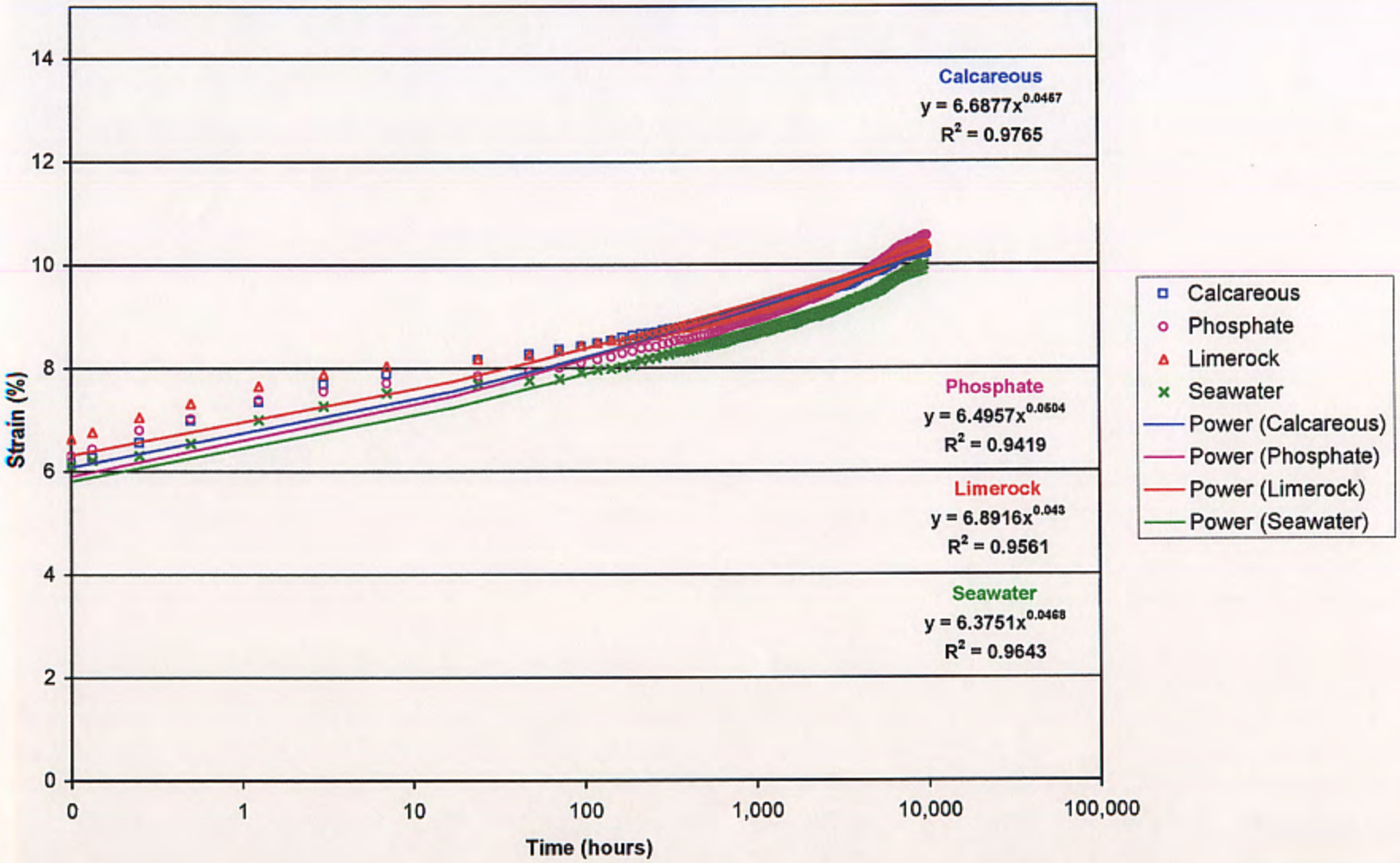

Fig. 6.17. Creep curves for HDPE geogrids, T = 45°C, Load level = 30% ultimate load - Specimen set I

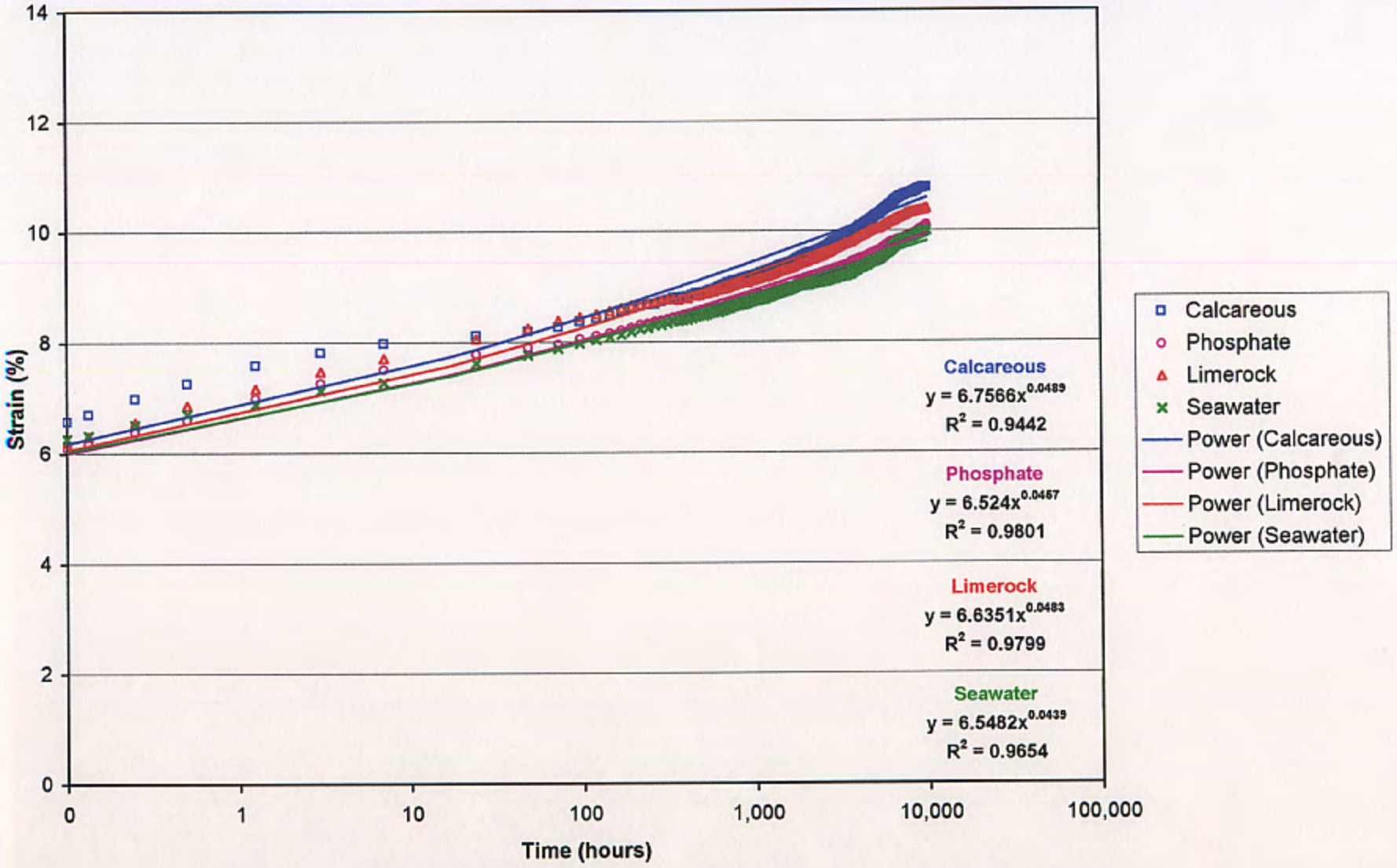

Fig. 6.18. Creep curves for HDPE geogrids, T = 45°C, Load level = 30% ultimate load - Specimen set II

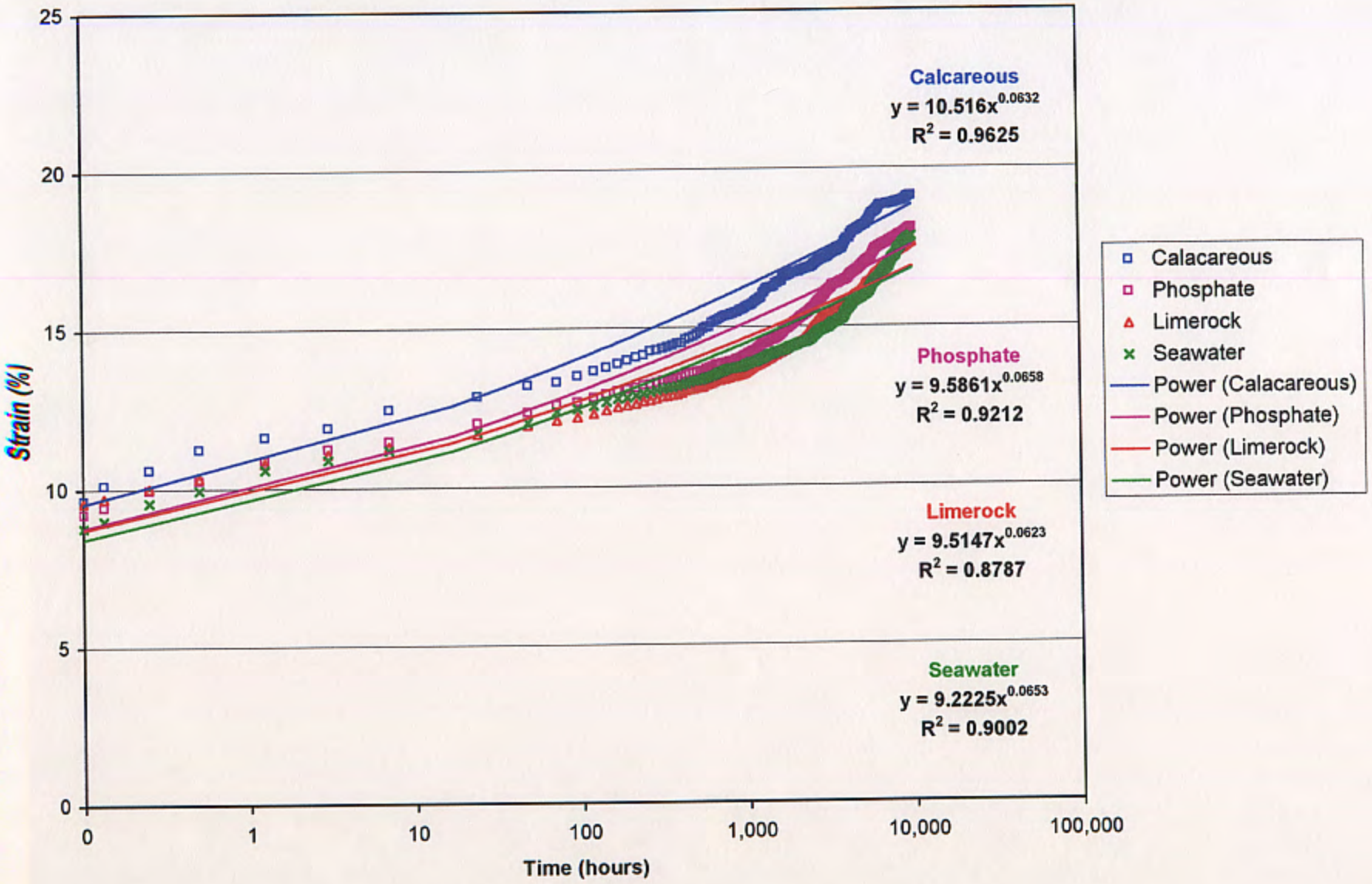

Fig. 6.19. Creep curves for HDPE geogrids, T = 45°C, Load level = 40% ultimate load - Specimen set I

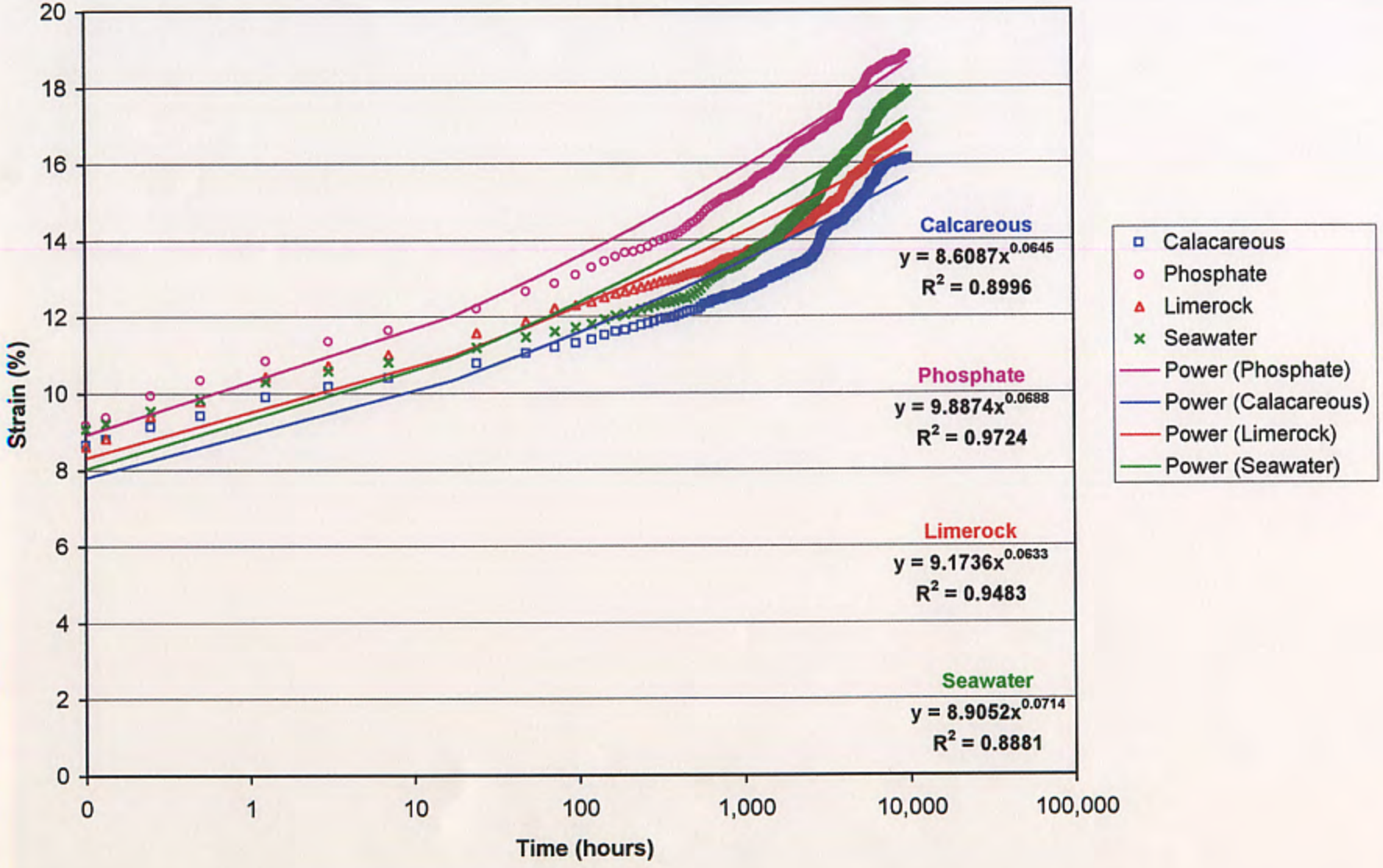

Fig. 6.20. Creep curves for HDPE geogrids, T = 45°C, Load level = 40% ultimate load - Speciment set II

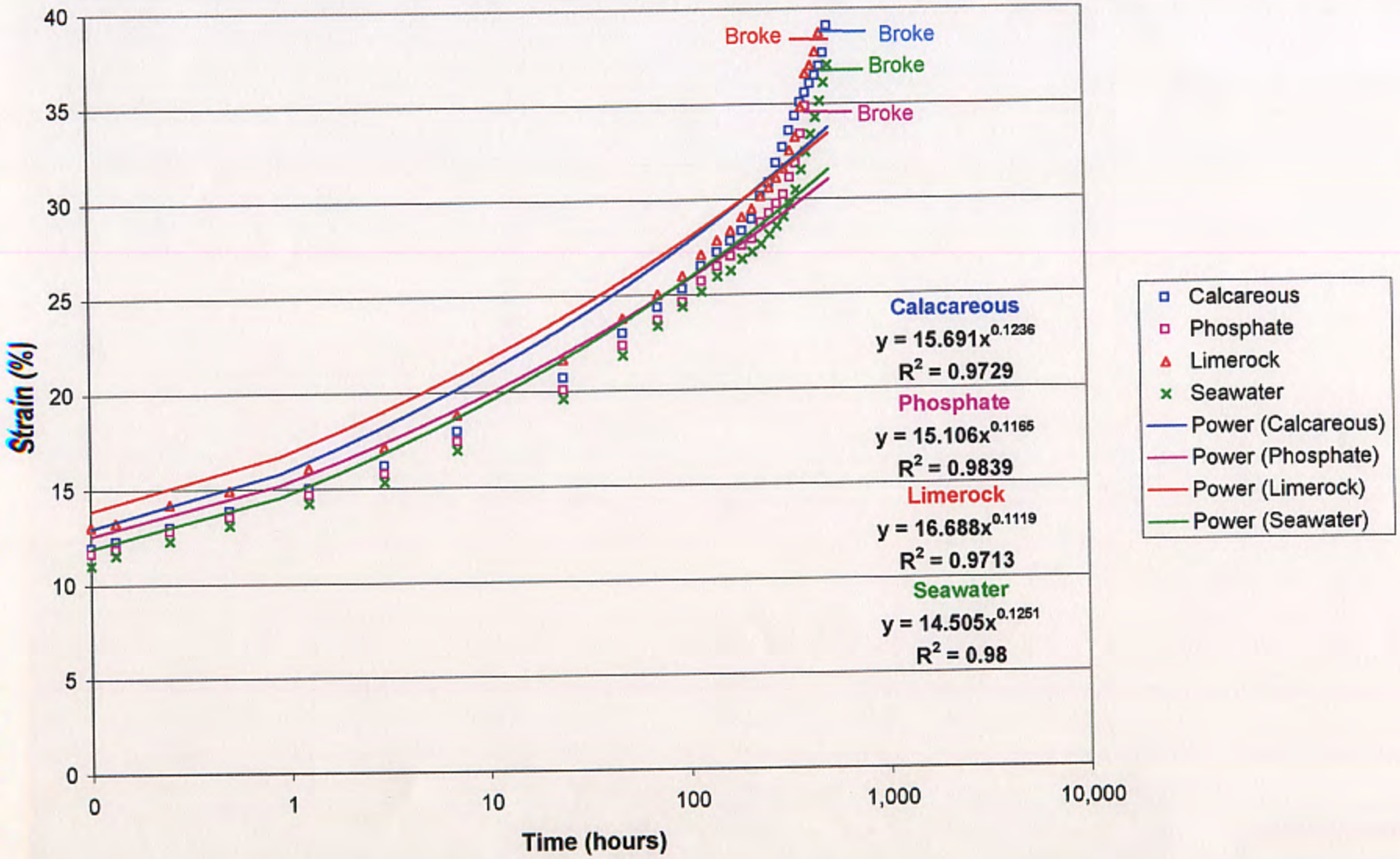

Fig. 6.21. Creep curves for HDPE geogrids, T = 45°C, Load level = 50% ultimate load - Specimen set I

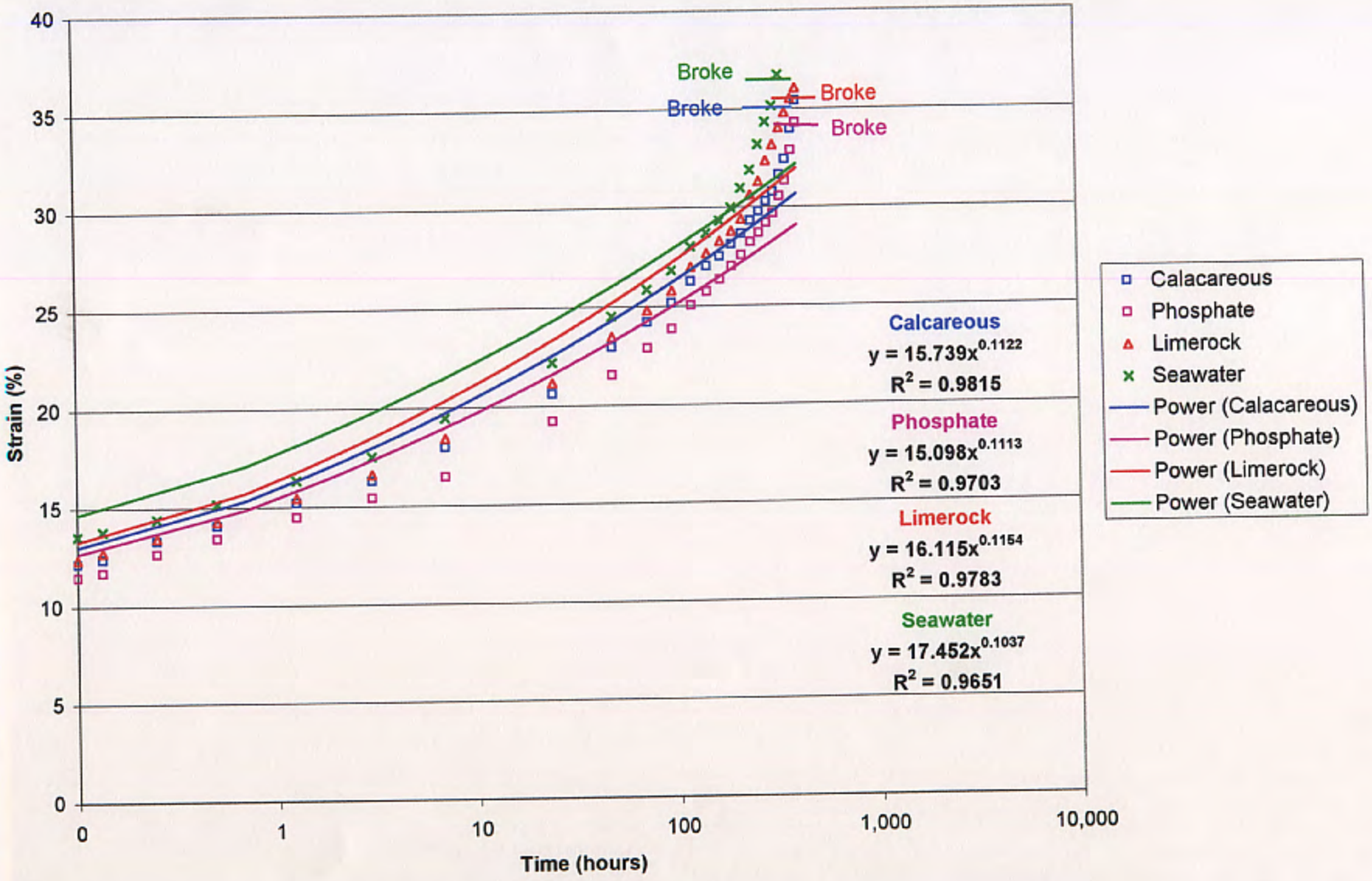

Fig. 6.22. Creep curves for HDPE geogrids, T = 45°C, Load level = 50% ultimate load - Specimen set II

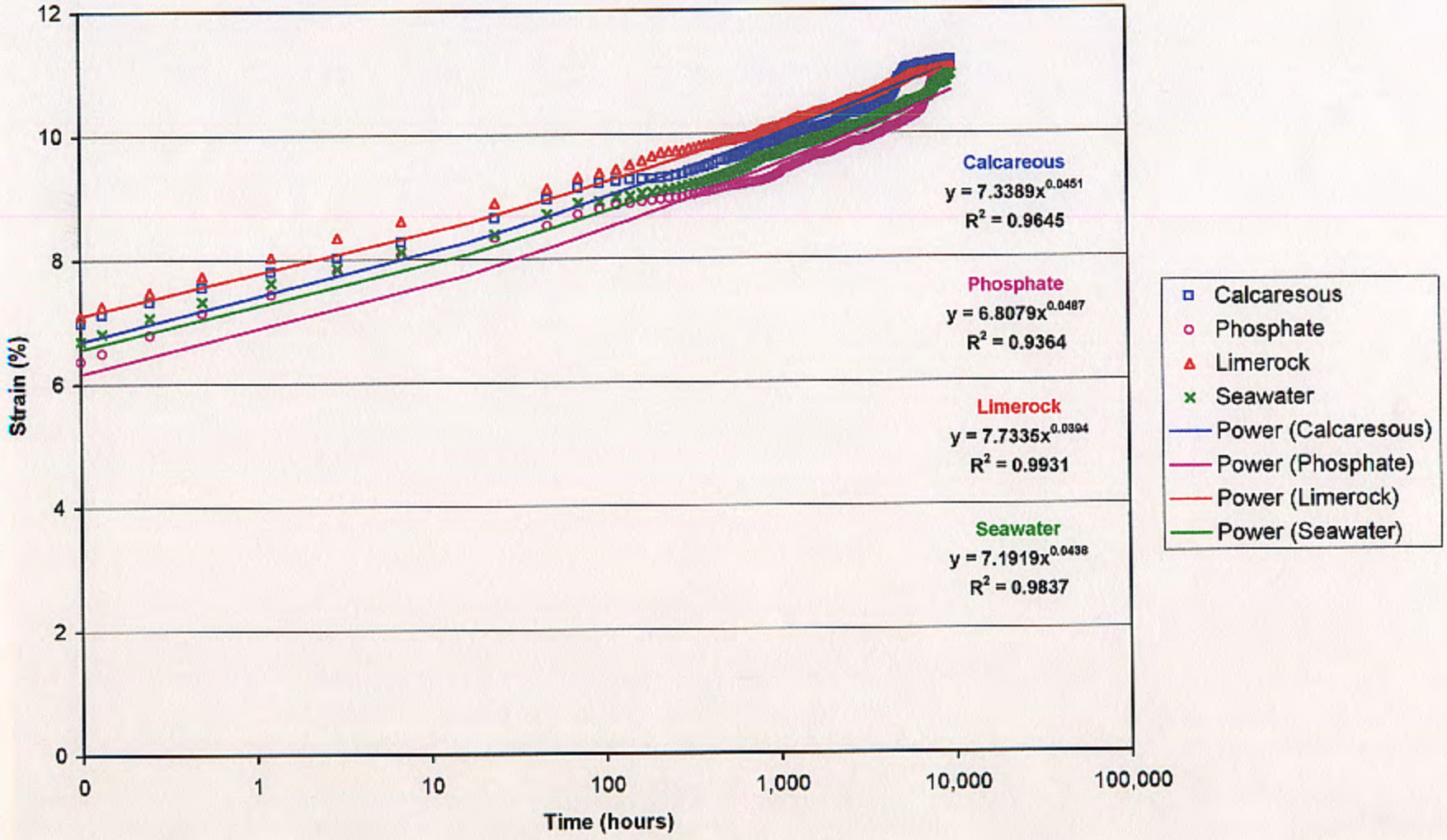

Fig. 6.23. Creep curves for HDPE geogrids, T = 55°C , Load level = 30% ultimate load - Specimen set I

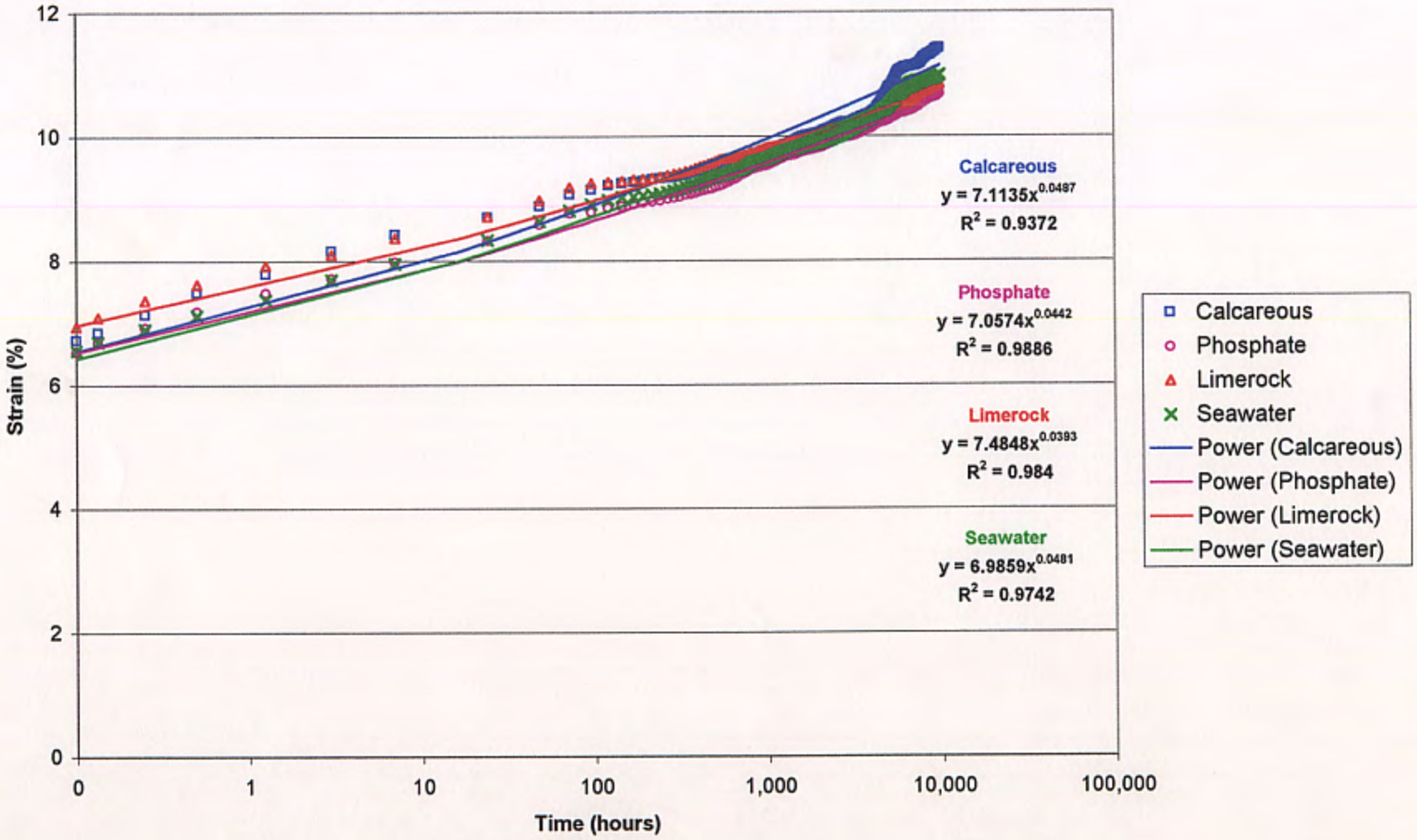

Fig. 6.24. Creep curves for HDPE geogrids, T = 55°C, Load level = 30% ultimate load - Specimen set II

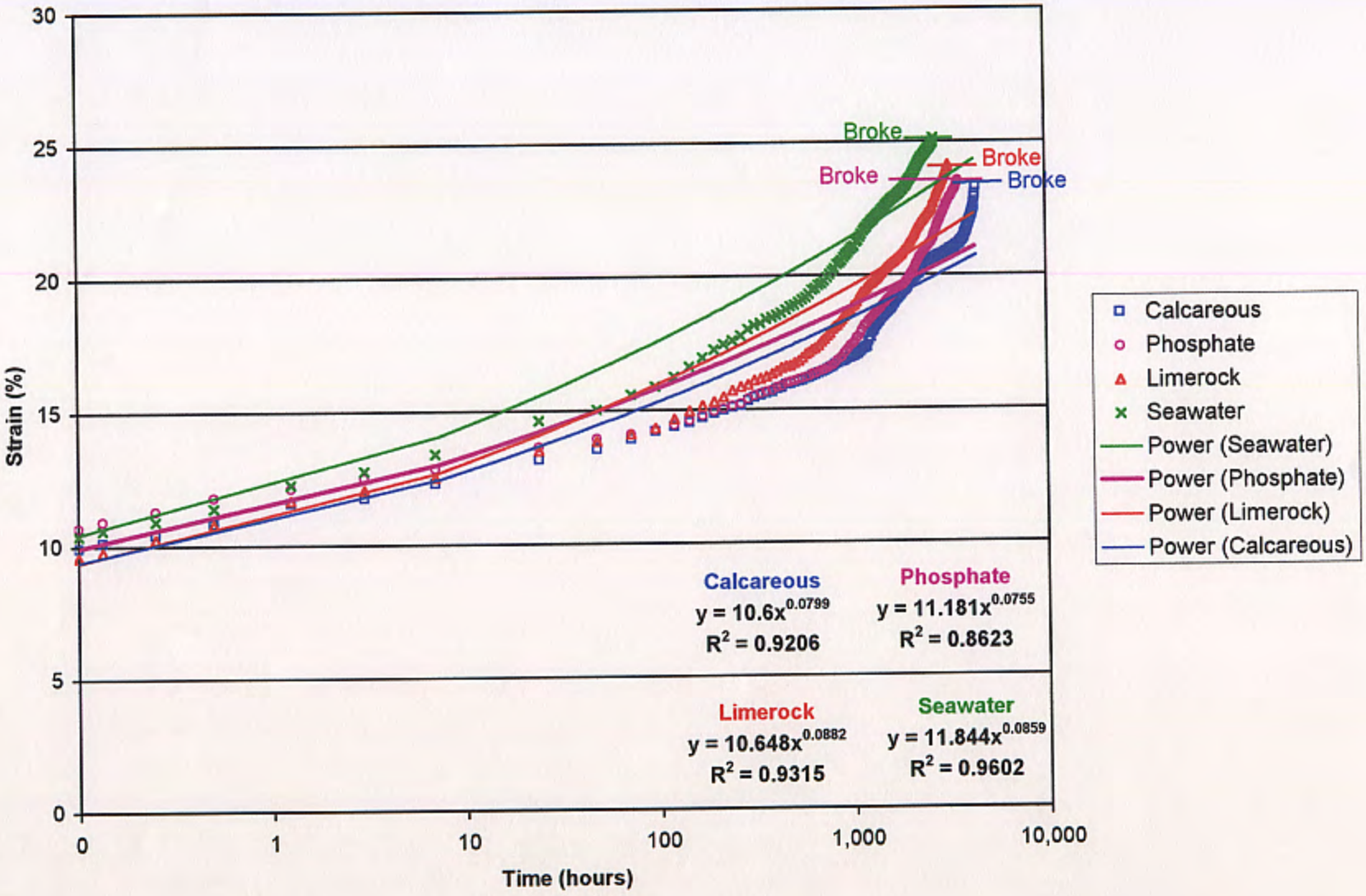

Fig. 6.25. Creep curves for HDPE geogrids, T = 55°C, Load level = 40% ultimate load - Speciment set I

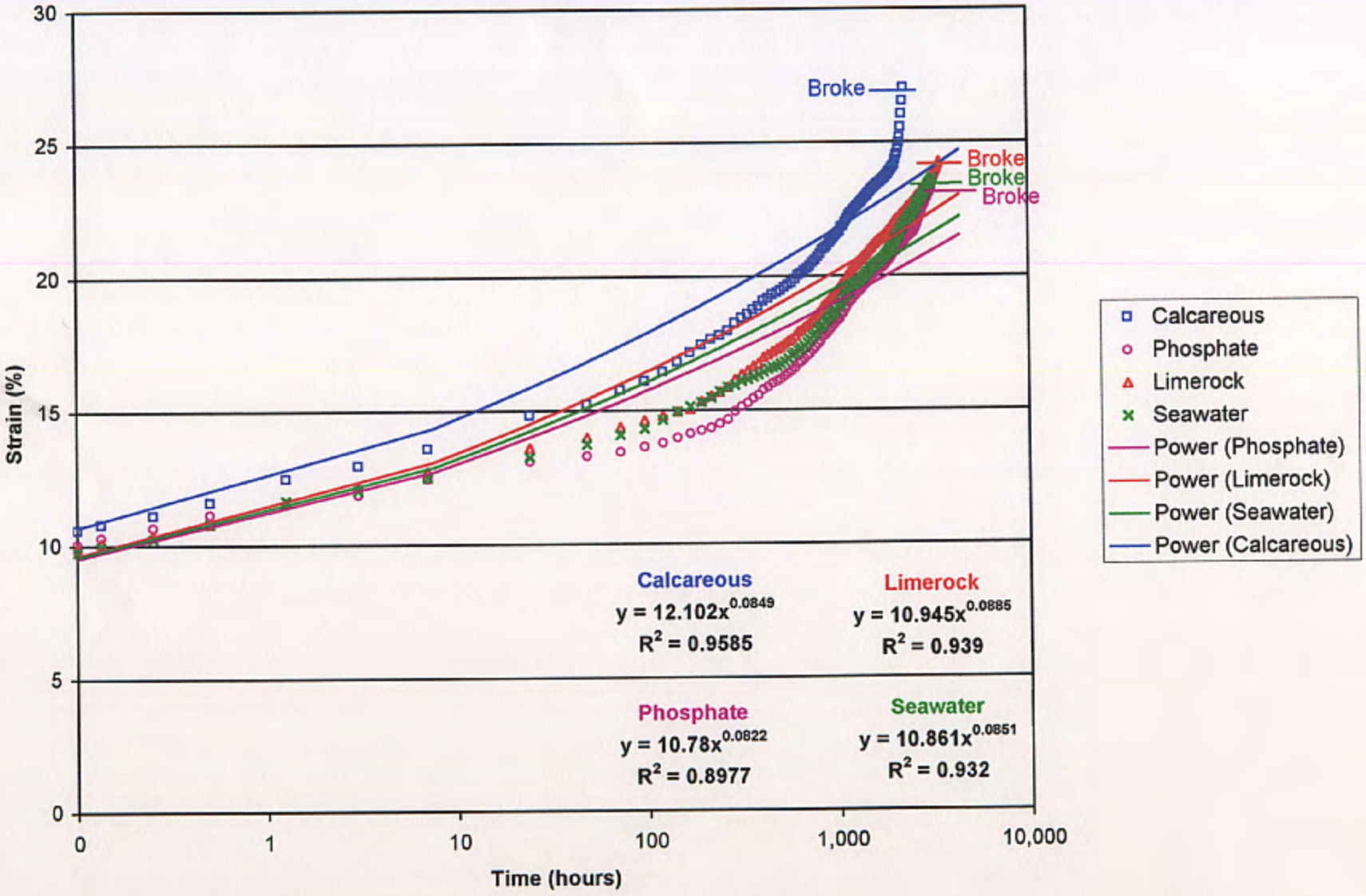

Fig. 6.26. Creep curves for HDPE geogrids, T = 55°C, Load level = 40% ultimate load - Specimen set II

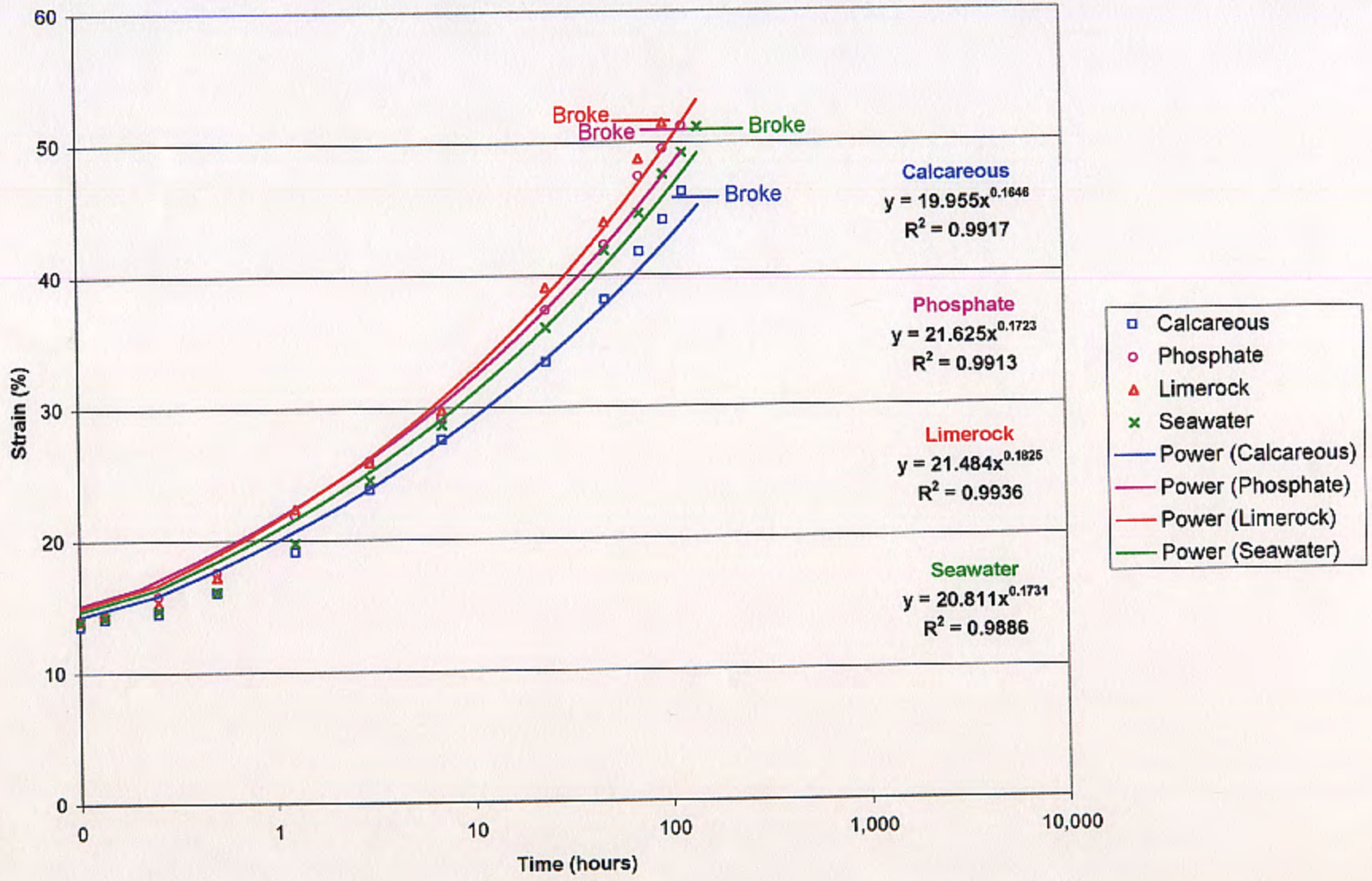

Fig. 6.27. Creep curves for HDPE geogrids, T = 55°C, Load level = 50% ultimate load - Specimen set I

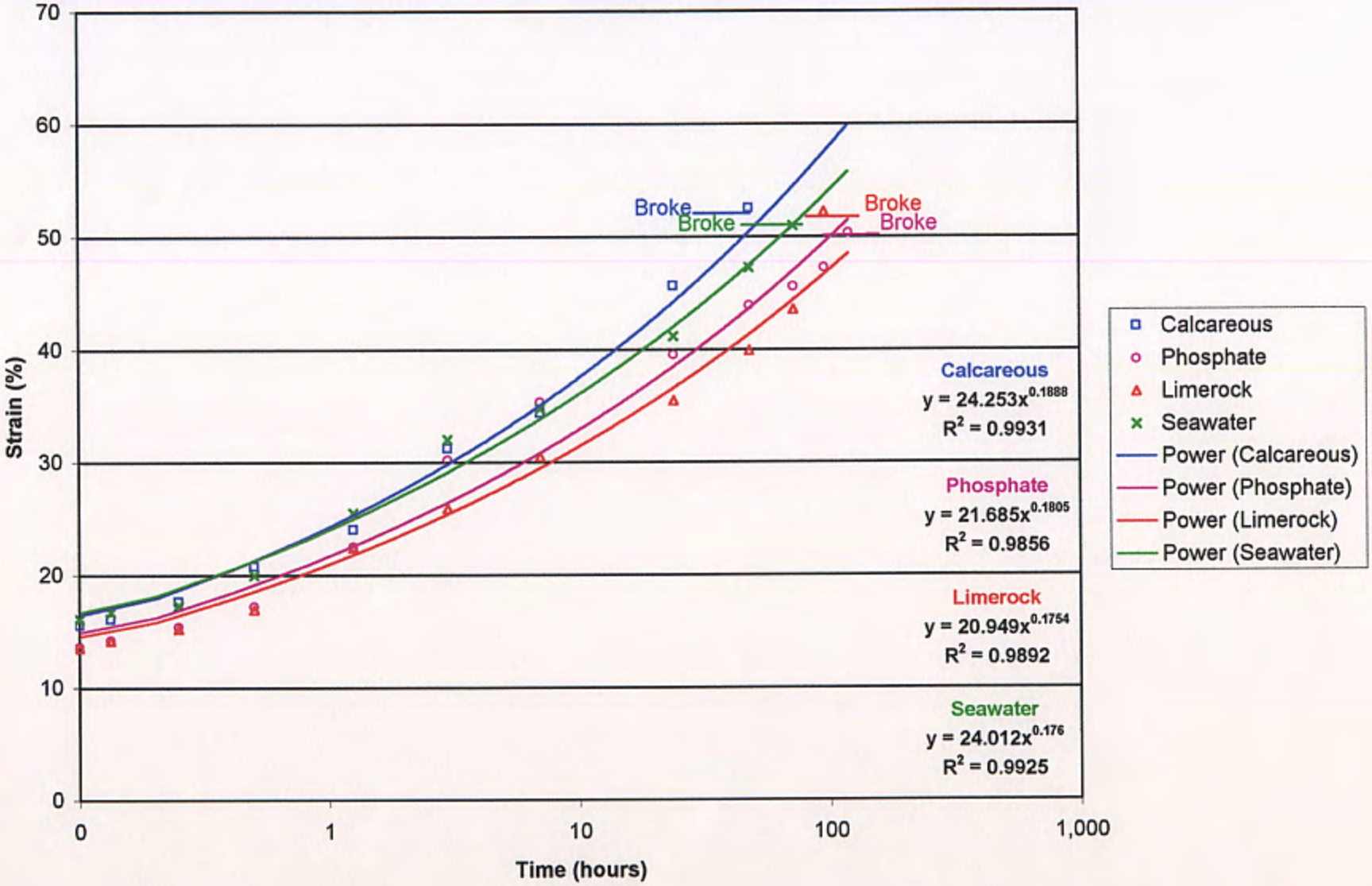

Fig. 6.28. Creep curves for HDPE geogrids, T = 55°C, Load level = 50% ultimate load - Specimen set II

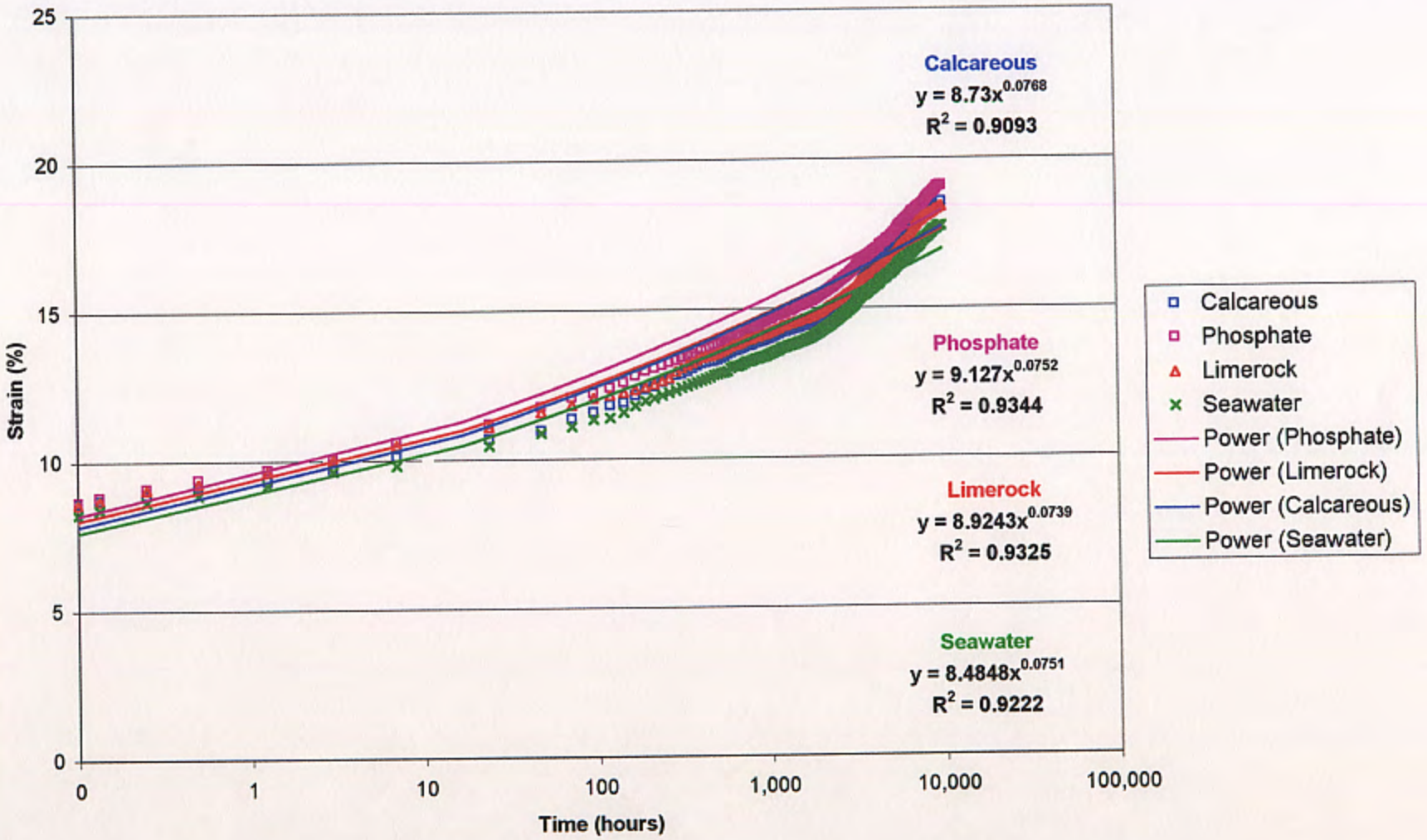

Fig. 6.29. Creep curves for HDPE geogrids, T = 65°C, Load level = 30% ultimate load - Specimen set I

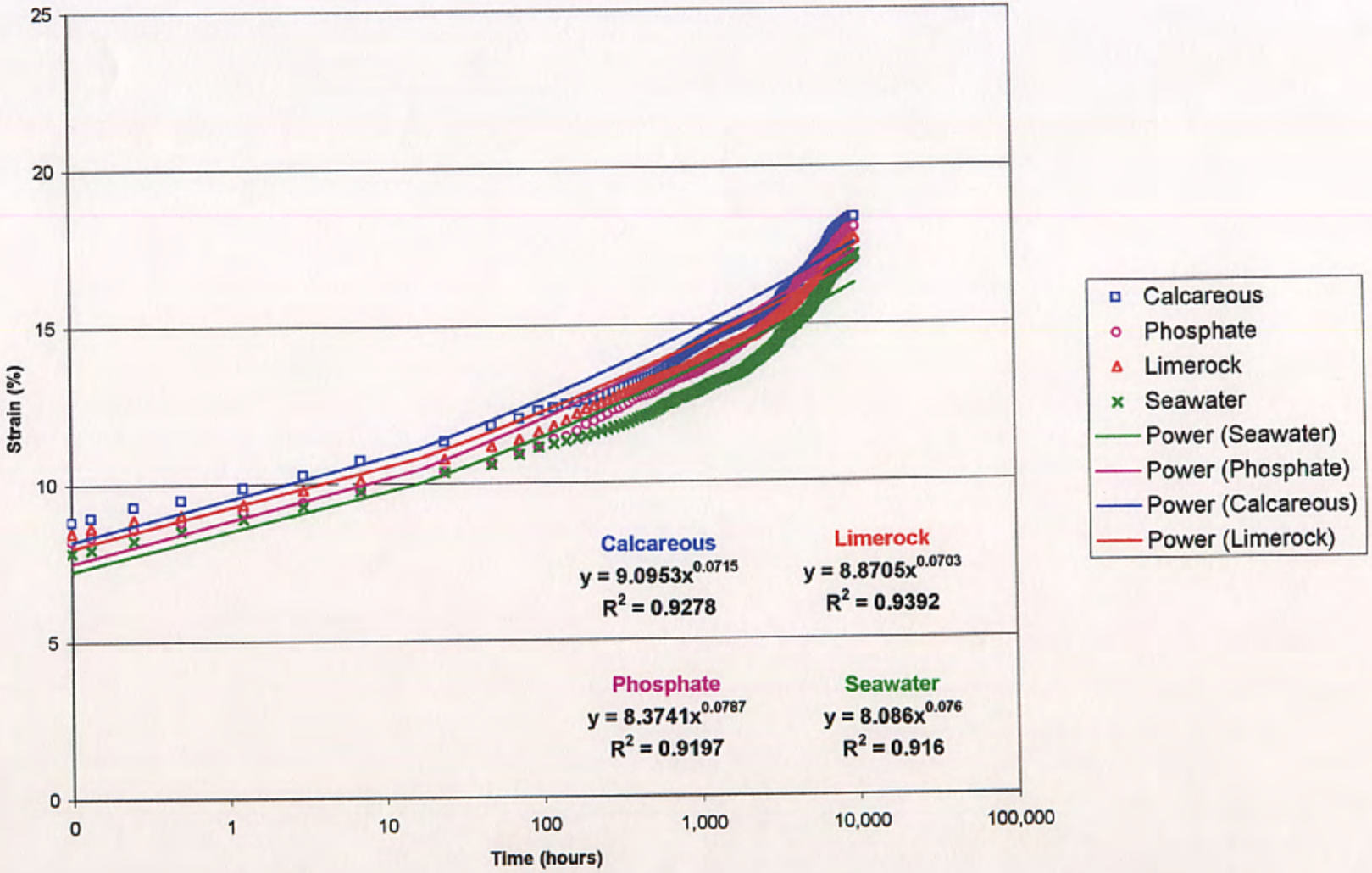

Fig. 6.30. Creep curves for HDPE geogrids, T = 65°C, Load level = 30% ultimate load - Specimen set II

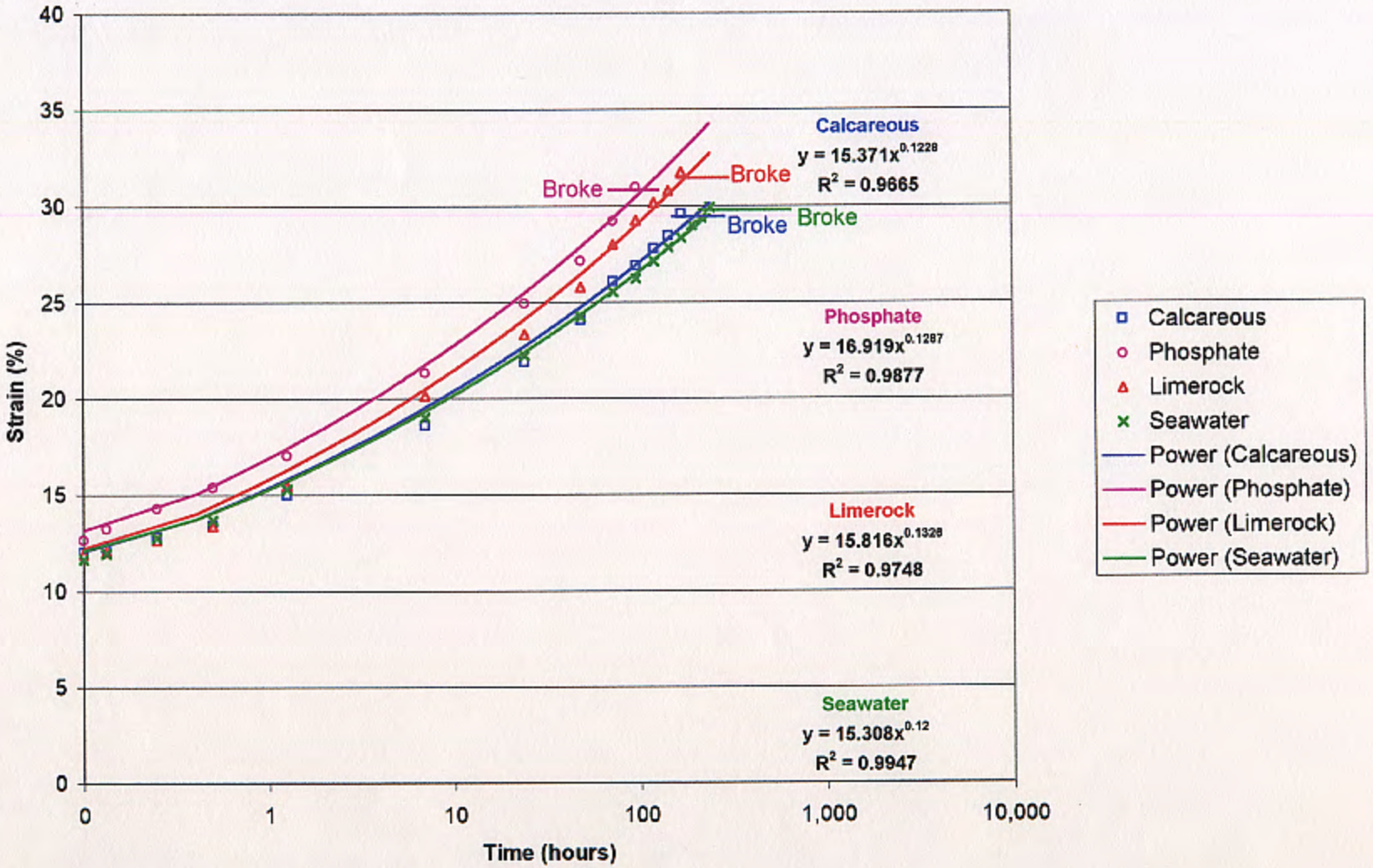

Fig. 6.31. Creep curves for HDPE geogrids, T = 65°C, Load level = 40% ultimate load - Specimen set I

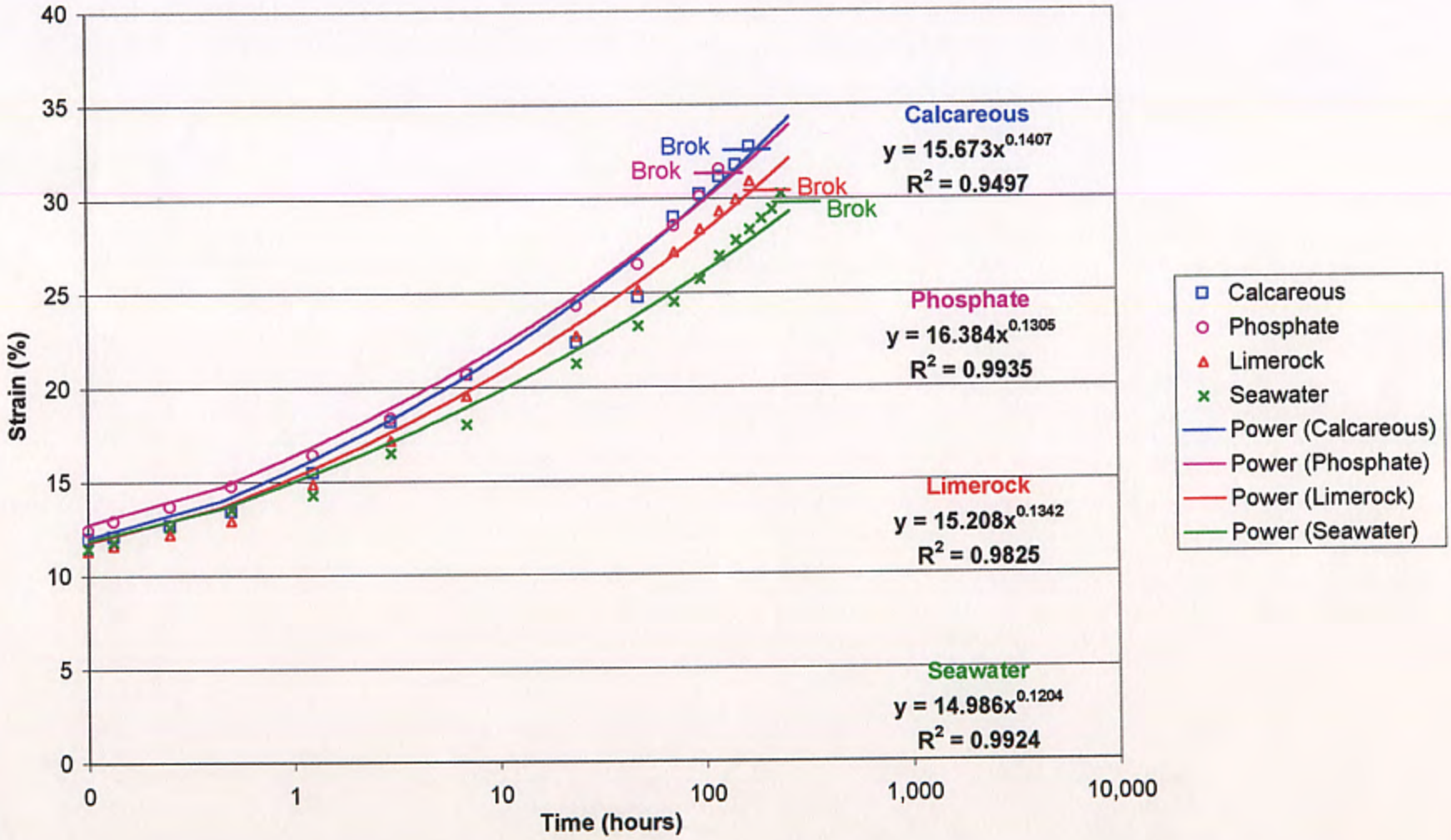

Fig. 6.32. Creep curves for HDPE geogrids, T = 65°C, Load level = 40% ultimate load - Specimen set II

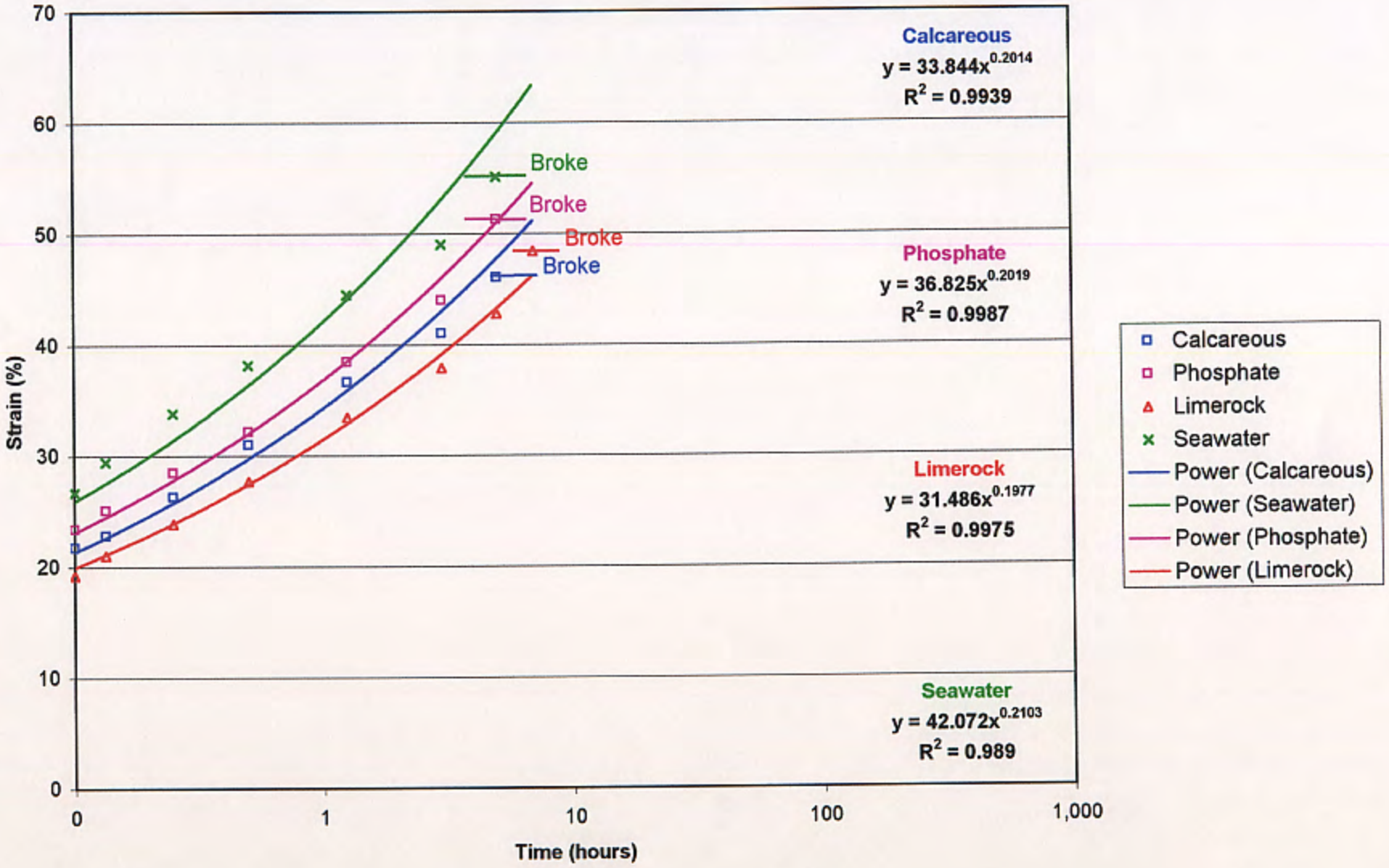

Fig. 6.33. Creep curves for HDPE geogrids, T = 65°C, Load level = 50% ultimate load - Specimen set I

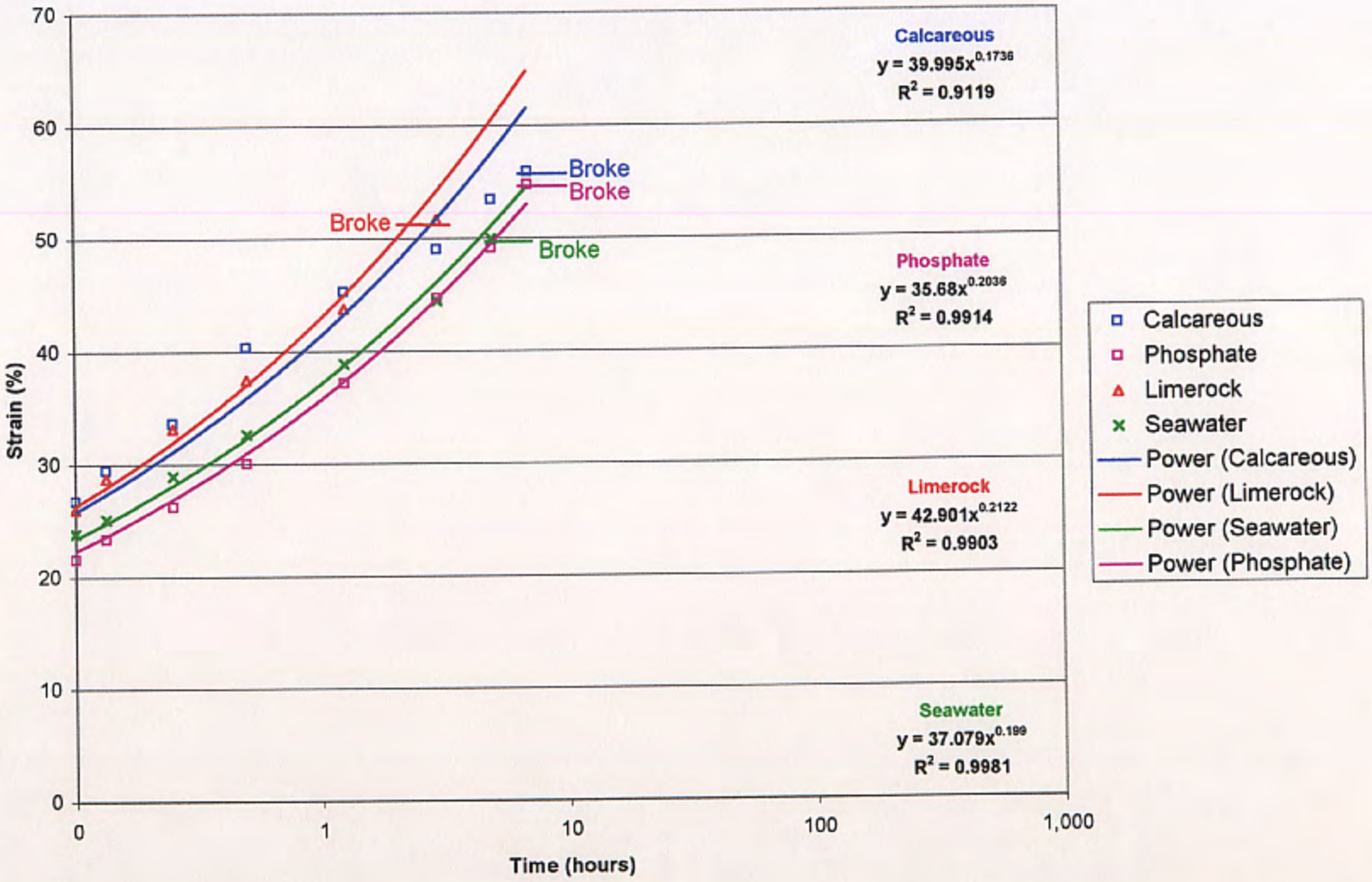

Fig. 6.34. Creep curves for HDPE geogrids, T = 65°C, Load level = 50% ultimate load - Specimen set II

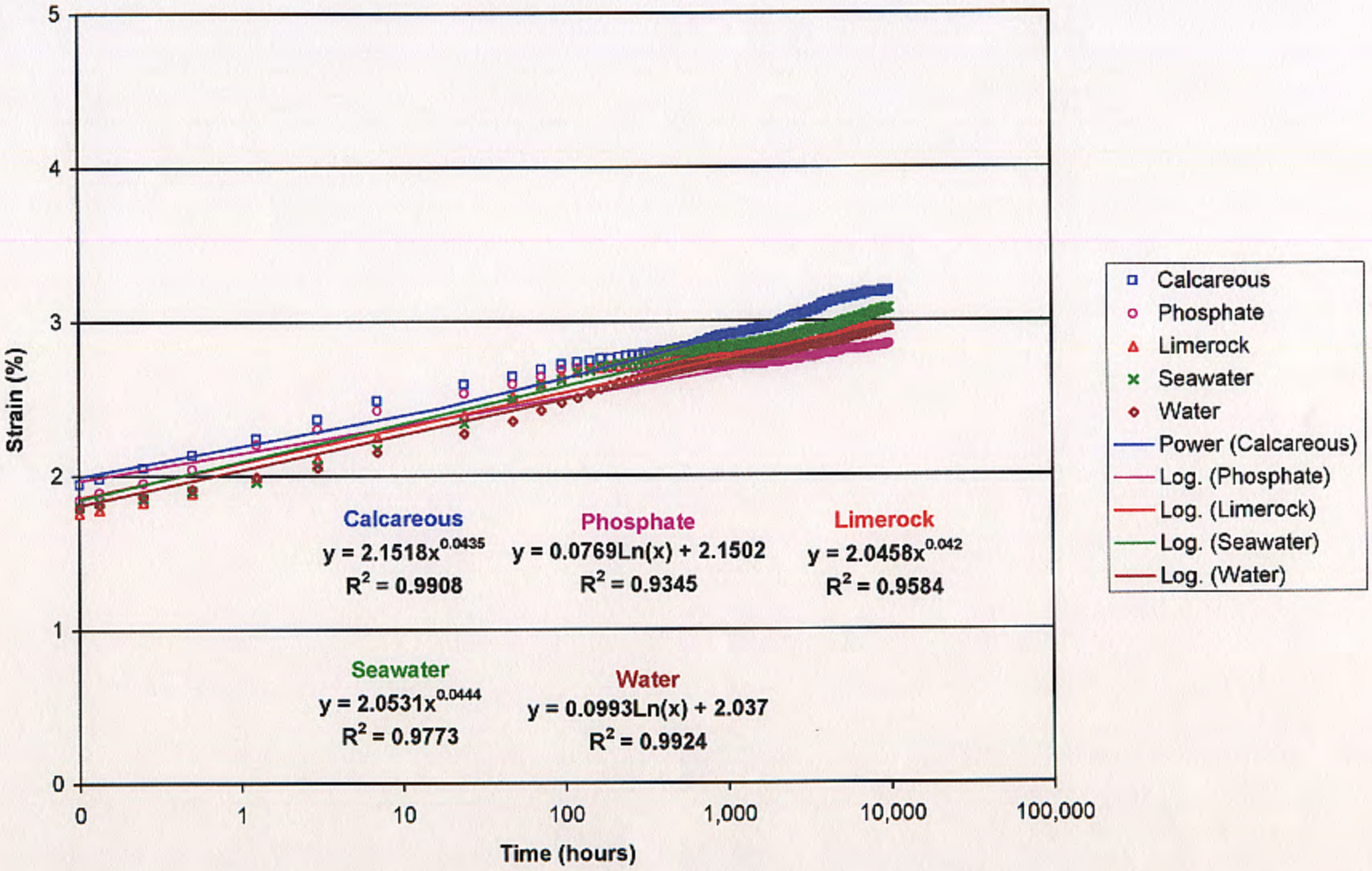

Fig. 6.35. Creep curves for PET geogrids, T = 30°C, Load level = 30% ultimate load - Specimen set I

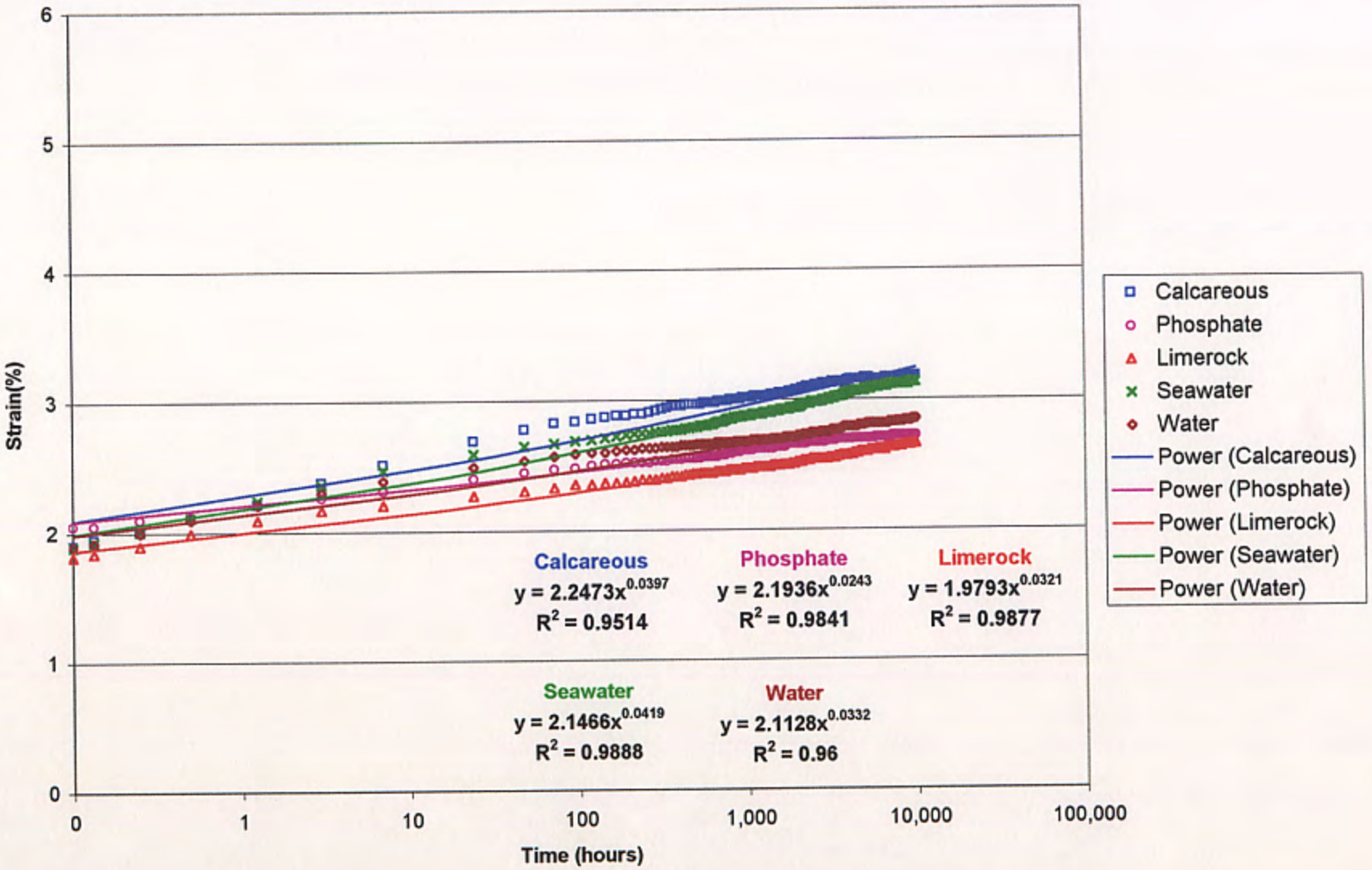

Fig. 6.36. Creep curves for PET geogrids, T = 30°C, Load level = 30% ultimate load - Specimen set II

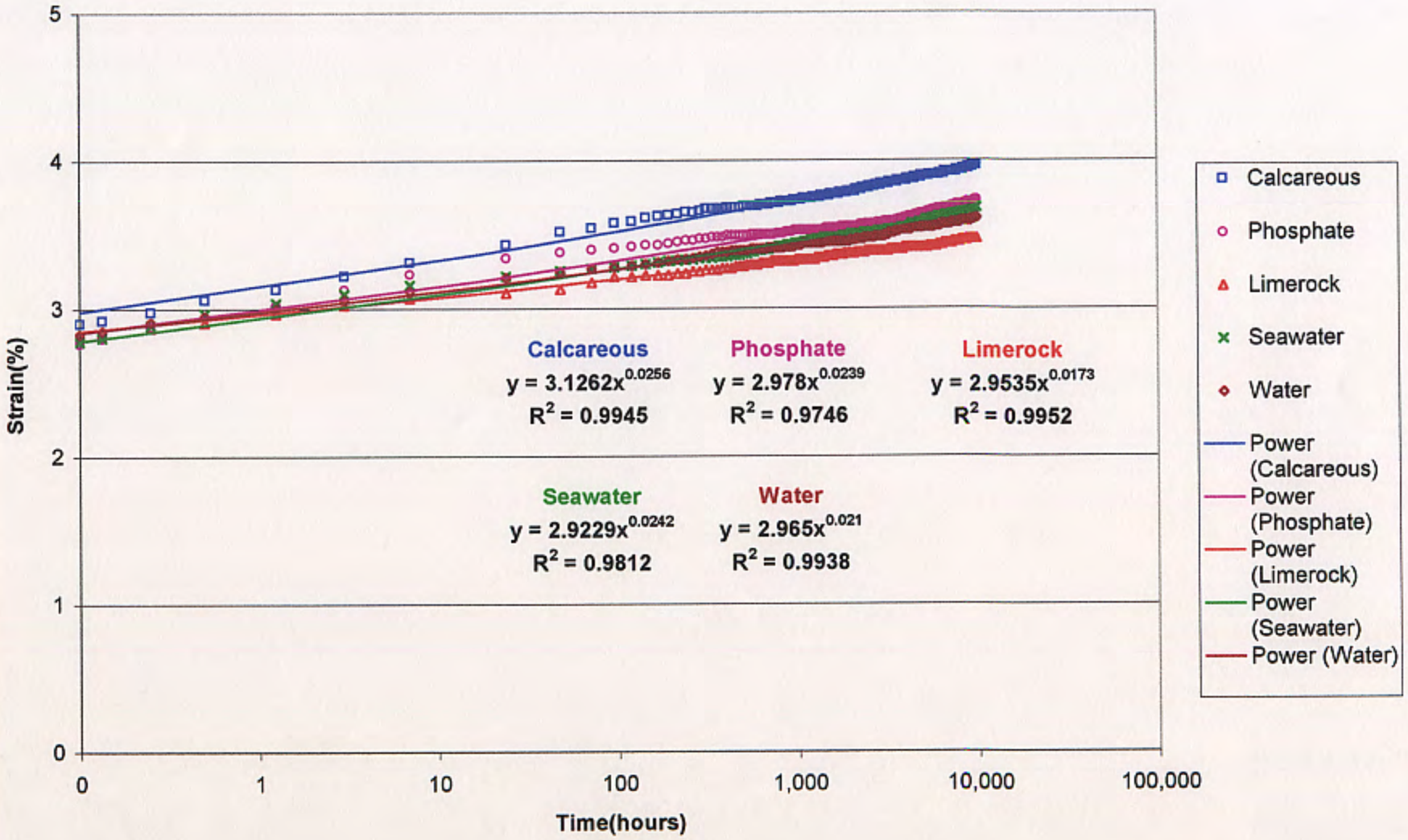

Fig. 6.37. Creep curves for PET geogrids, T = 30°C, Load level = 40% ultimate load - Specimen set I

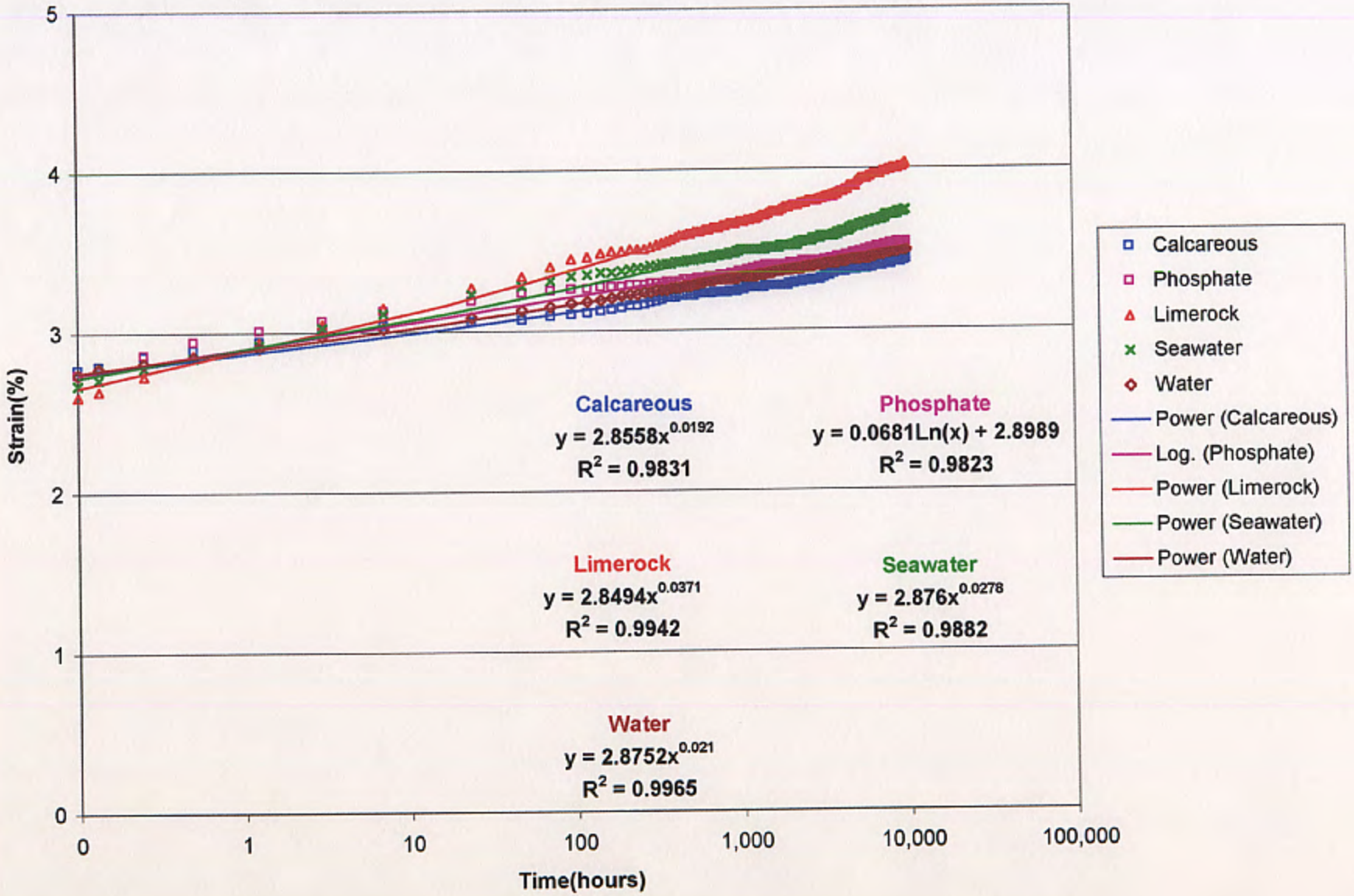

Fig. 6.38. Creep curves for PET geogrids, T = 30°C, Load level = 40% ultimate load - Specimen set II

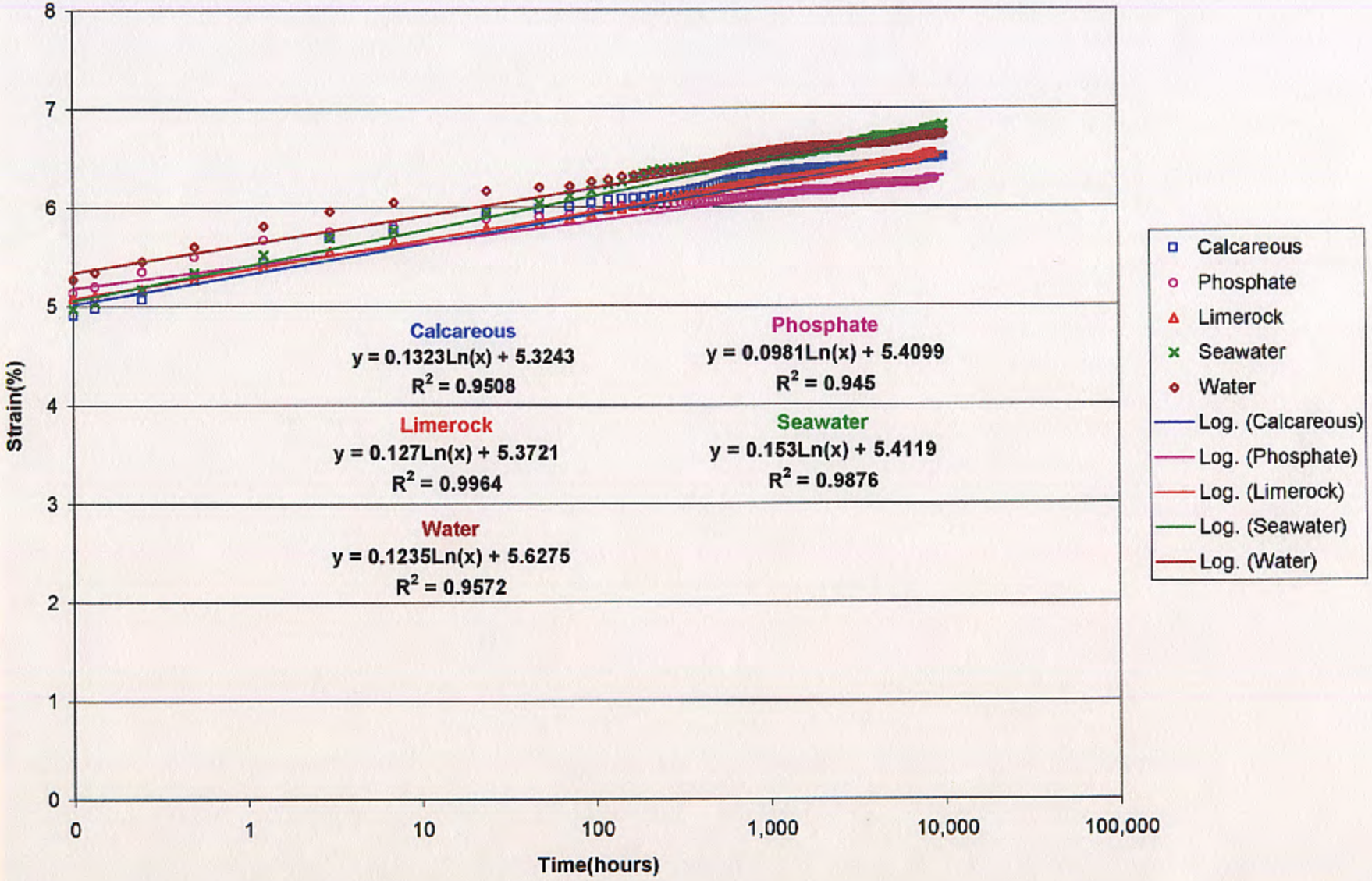

Fig. 6.39. Creep curves for PET geogrids, T = 30°C, Load level = 50% ultimate load - Specimen set I

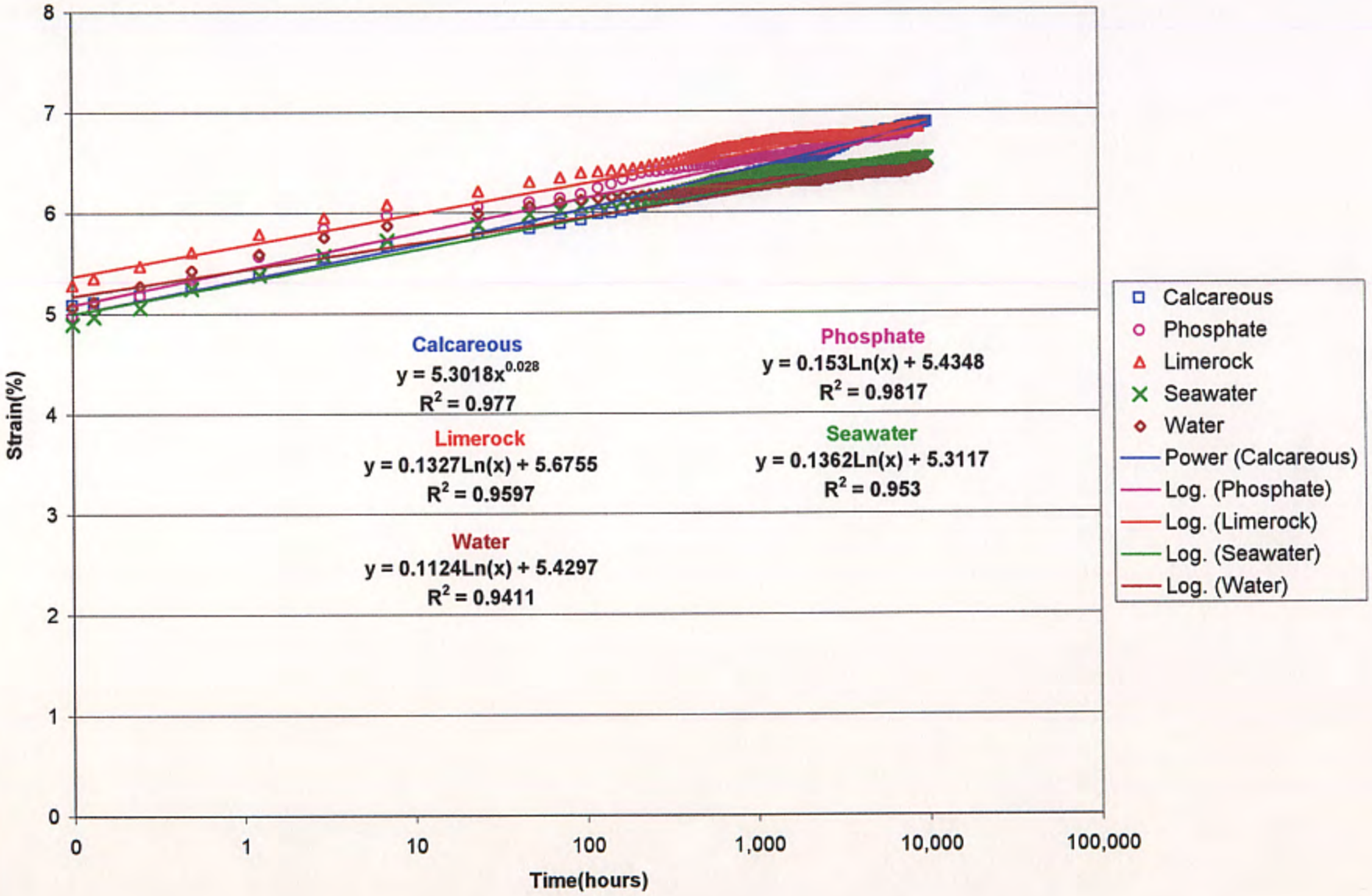

Fig. 6.40. Creep curves for PET geogrids, T = 30°C, Load level = 50% ultimate load - Specimen set II

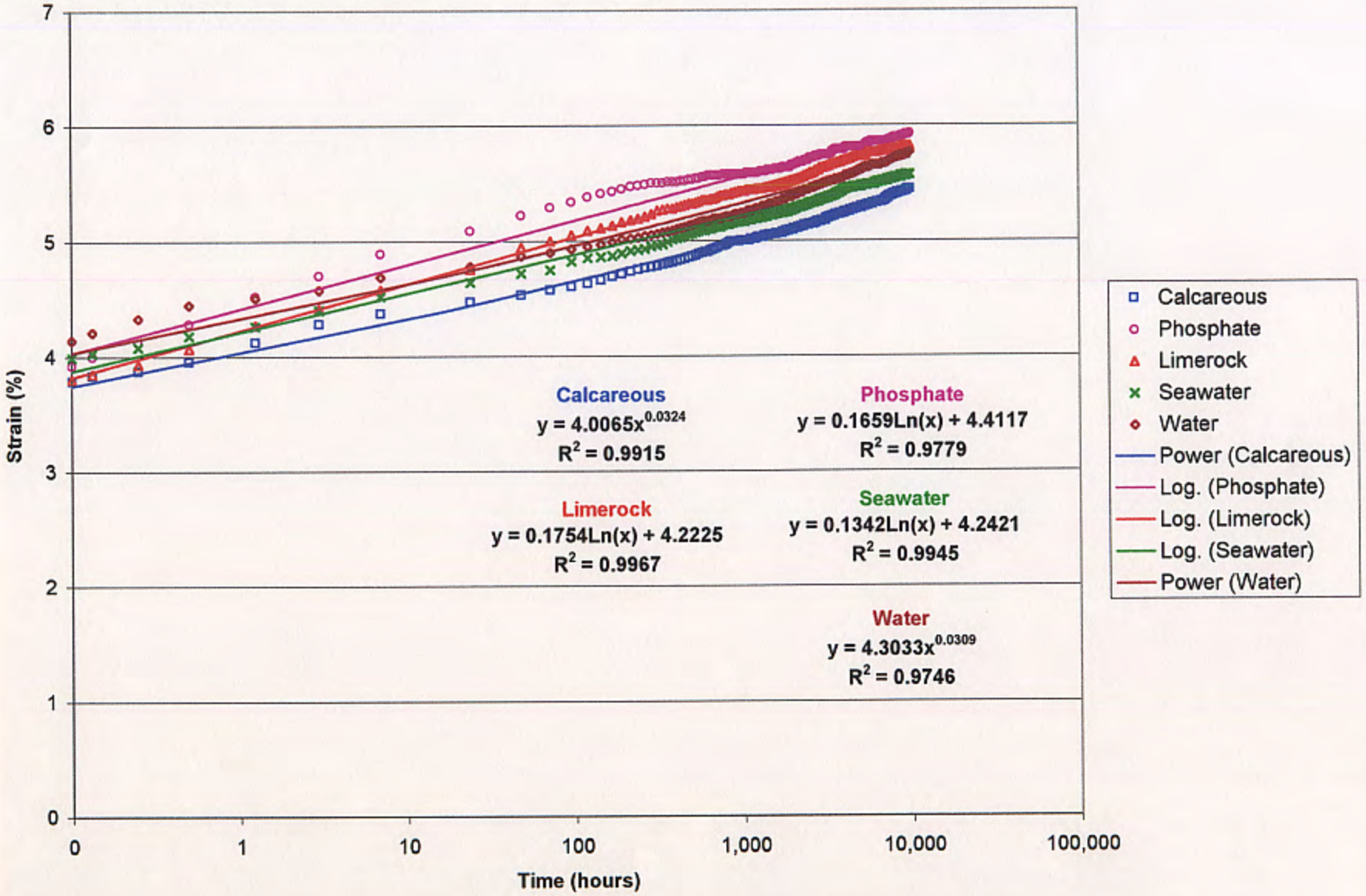

Fig. 6.41. Creep curves for PET geogrids, T = 45°C, Load level = 30% ultimate load - Specimen set I

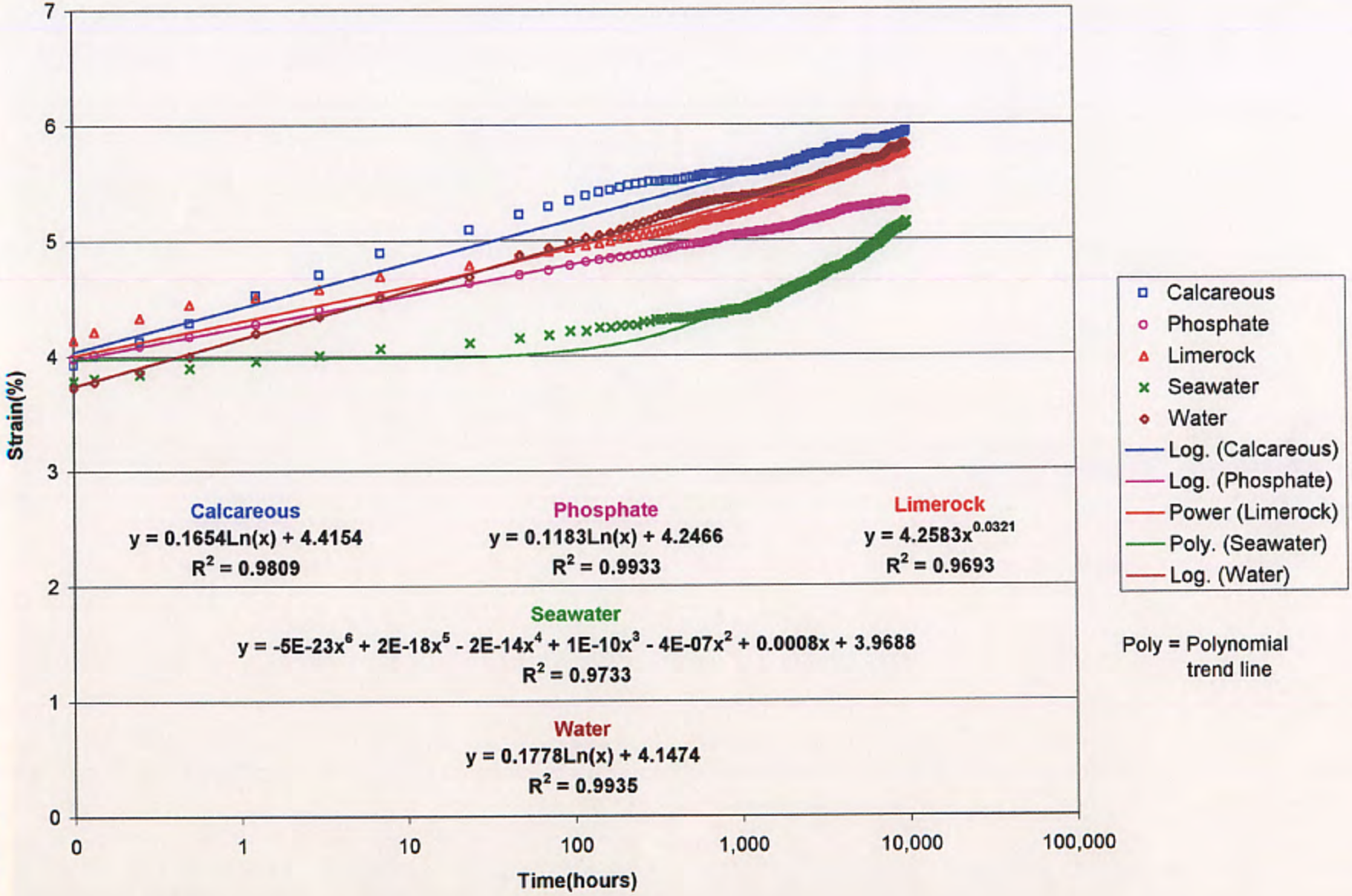

Fig. 6.42. Creep curves for PET geogrids, T = 45°C, Load level = 30% ultimate load - Specimen set II

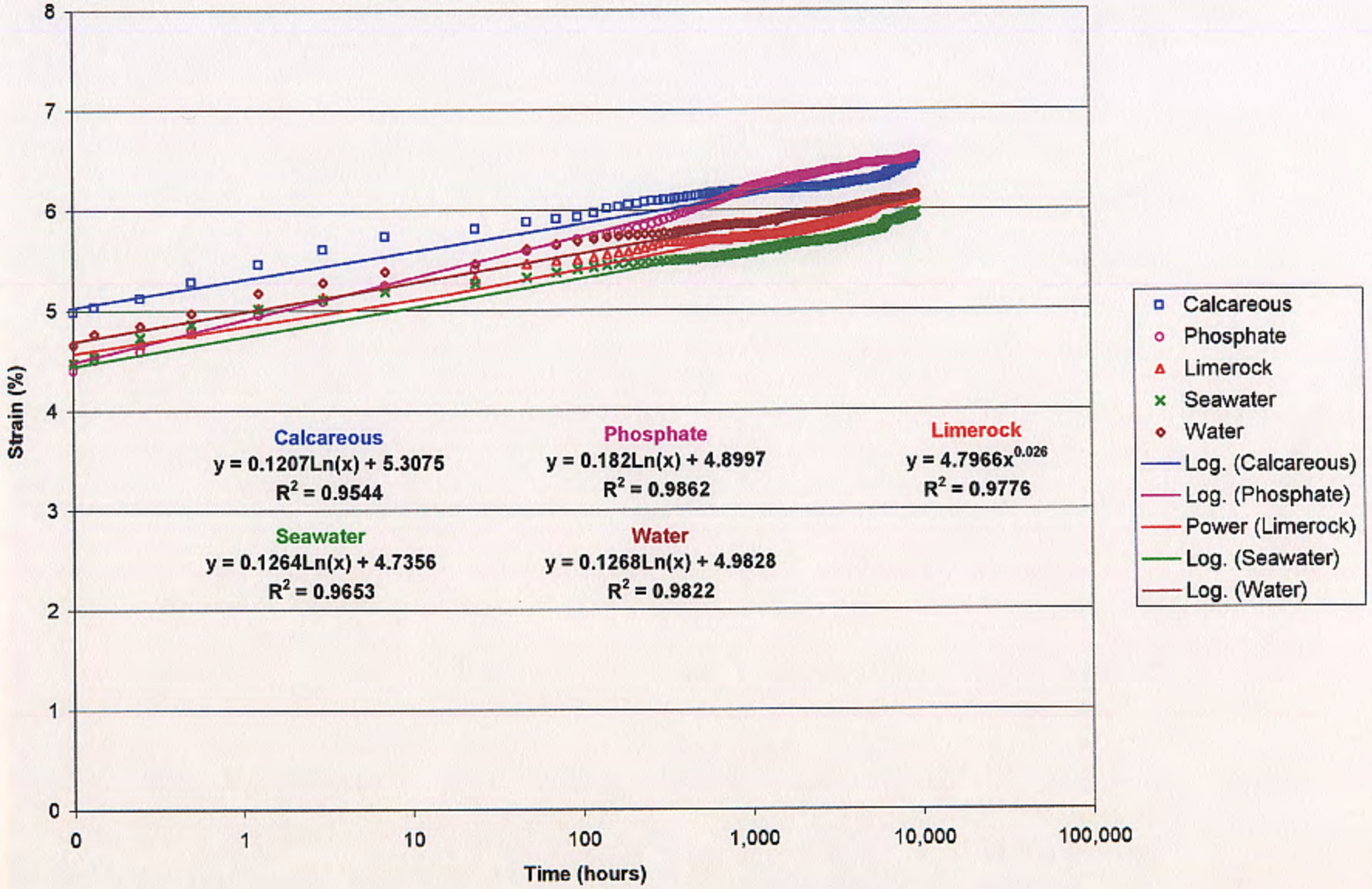

Fig. 6.43. Creep curves for PET geogrids, T = 45°C, Load level = 40% ultimate load - Specimen set I

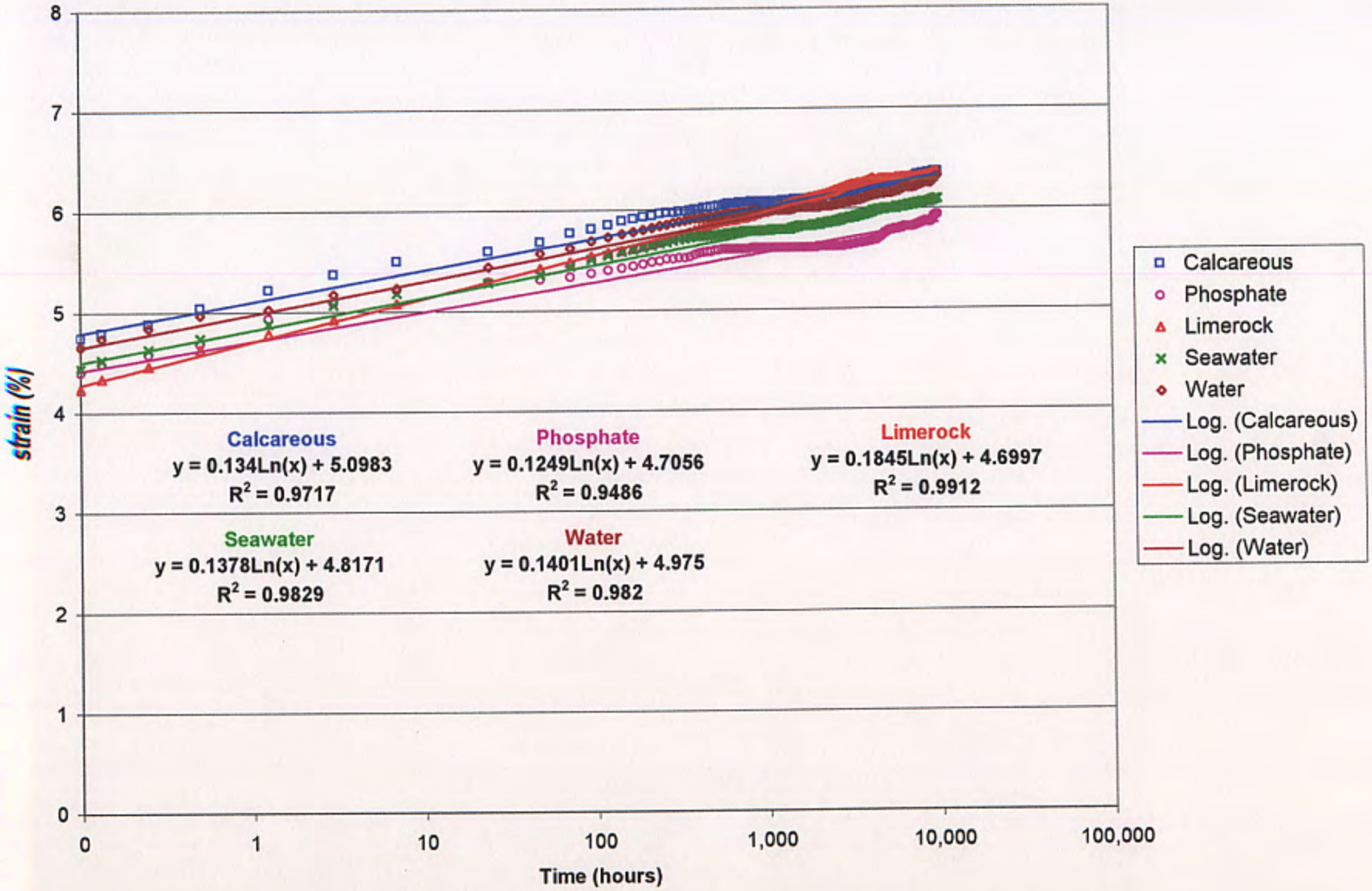

Fig. 6.44. Creep curves for PET geogrids, T = 45°C, Load level = 40% ultimate load - Specimen set II

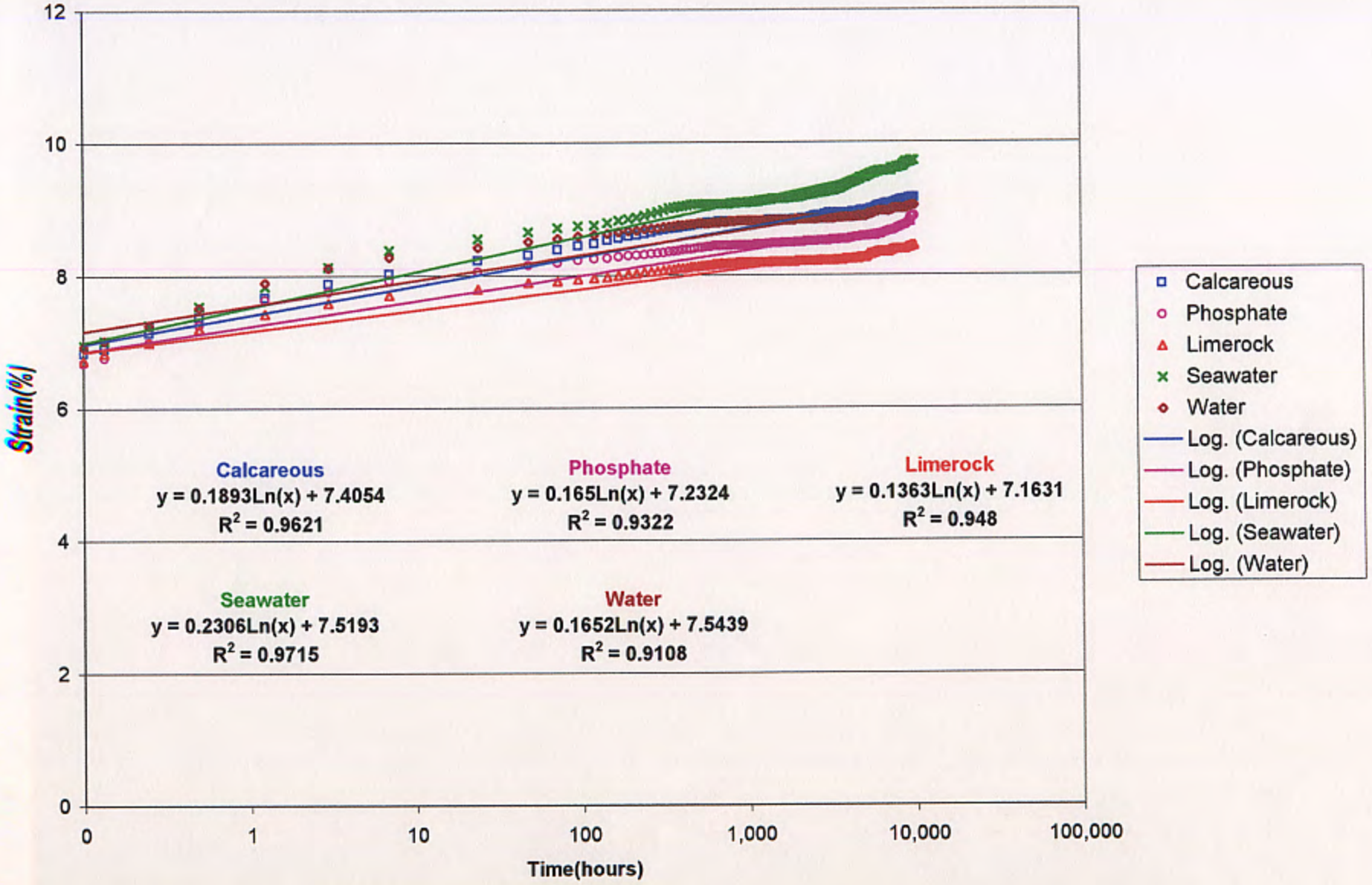

Fig. 6.45. Creep curves for PET geogrids, T = 45°C, Load level = 50% ultimate load - Specimen set I

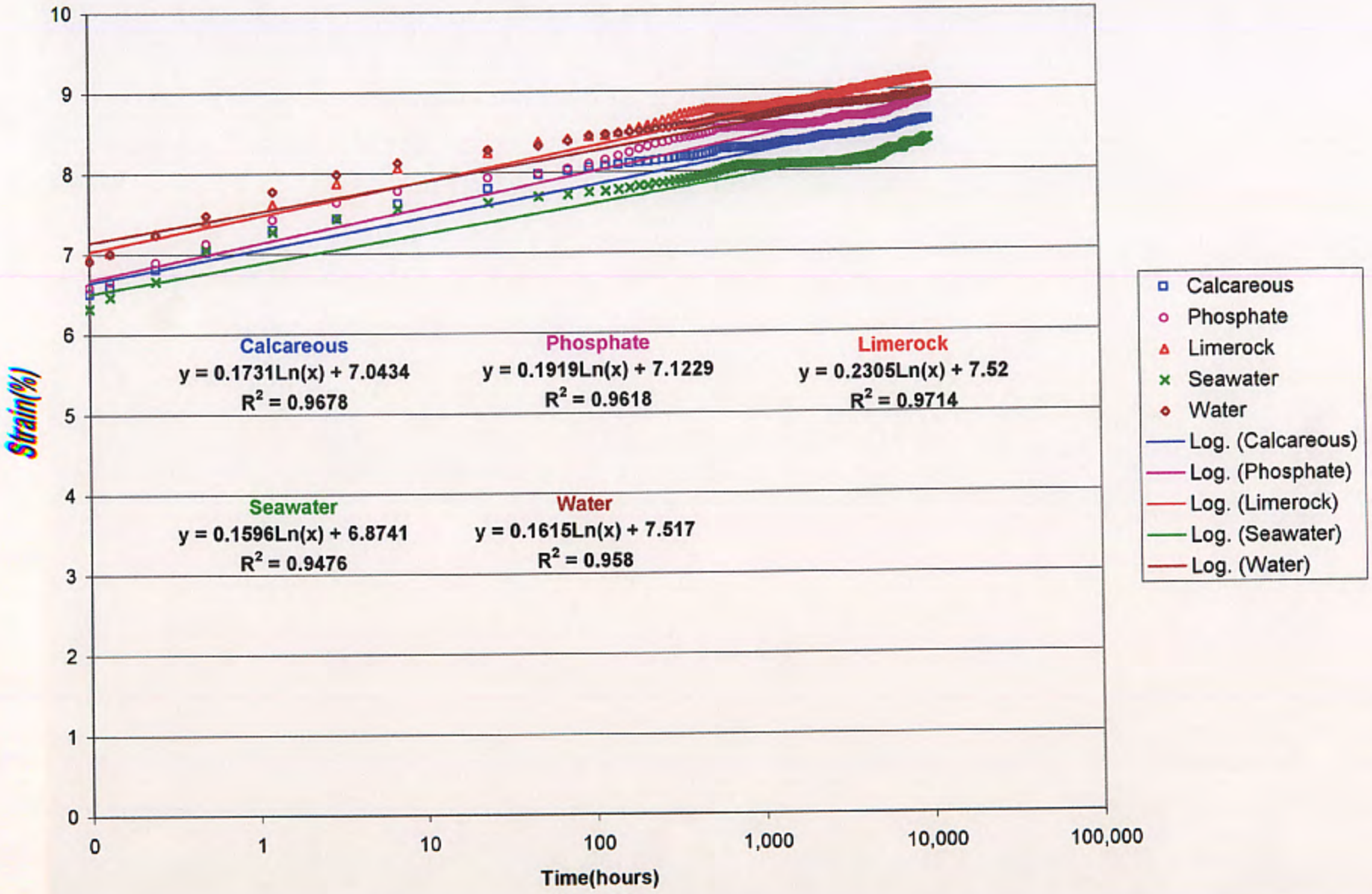

Fig. 6.46. Creep curves for PET geogrids, T = 45°C, Load level = 50% ultimate load - Specimen set II

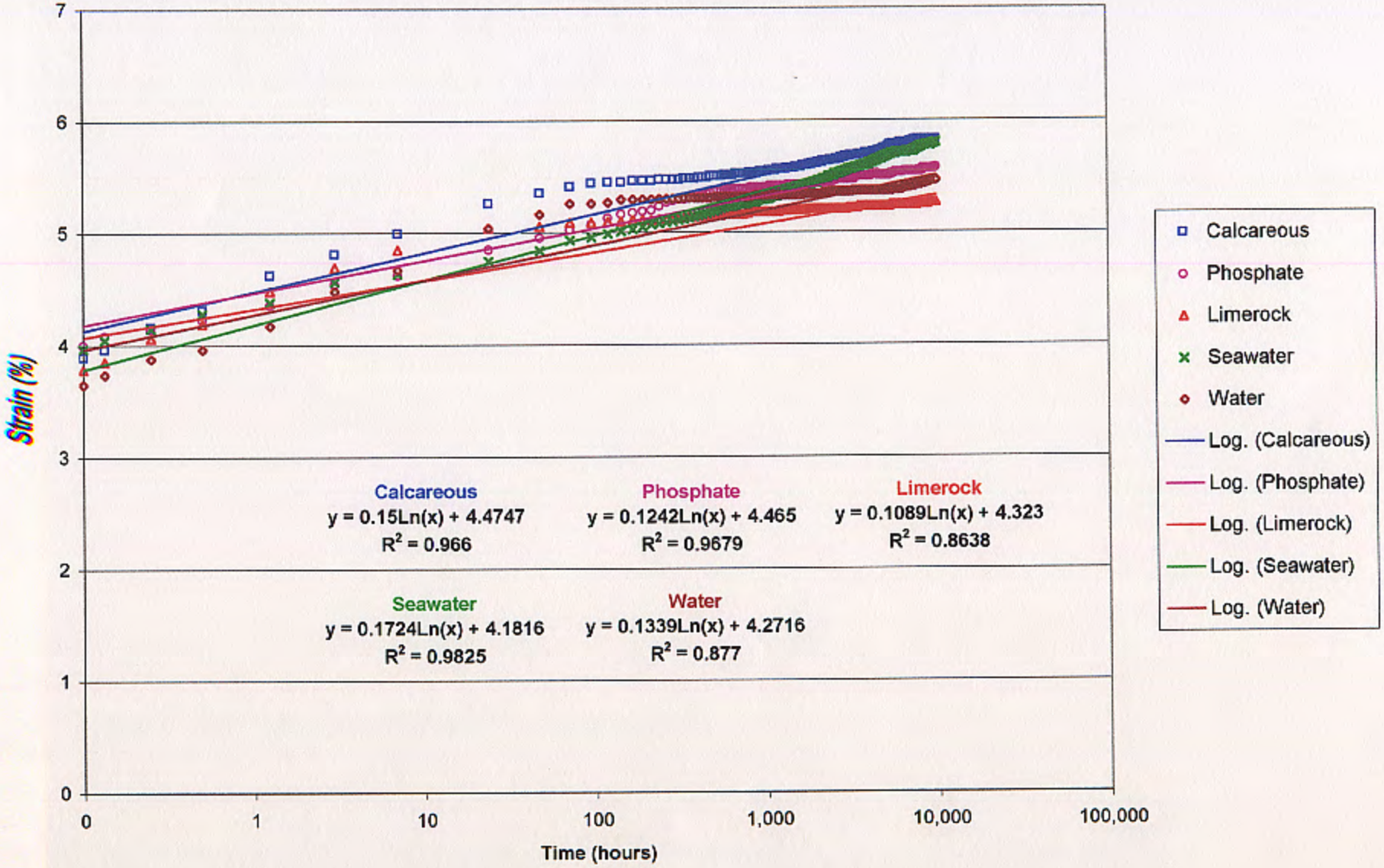

Fig. 6.47. Creep curves for PET geogrids, T = 55°C, Load level = 30% ultimate load - Specimen set I

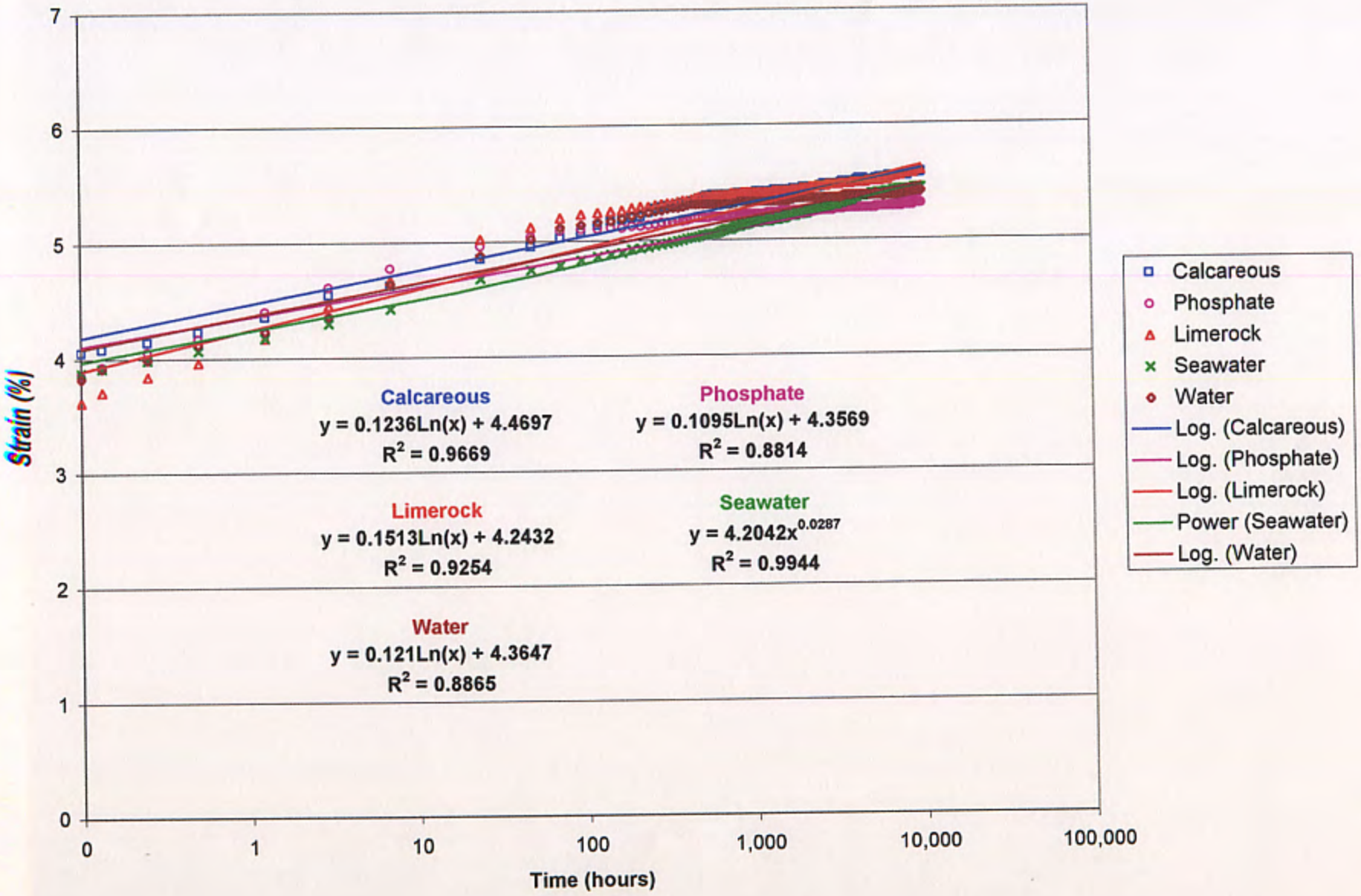

Fig. 6.48. Creep curves for PET geogrids, T = 55°C, Load level = 30% ultimate load - Specimen set II

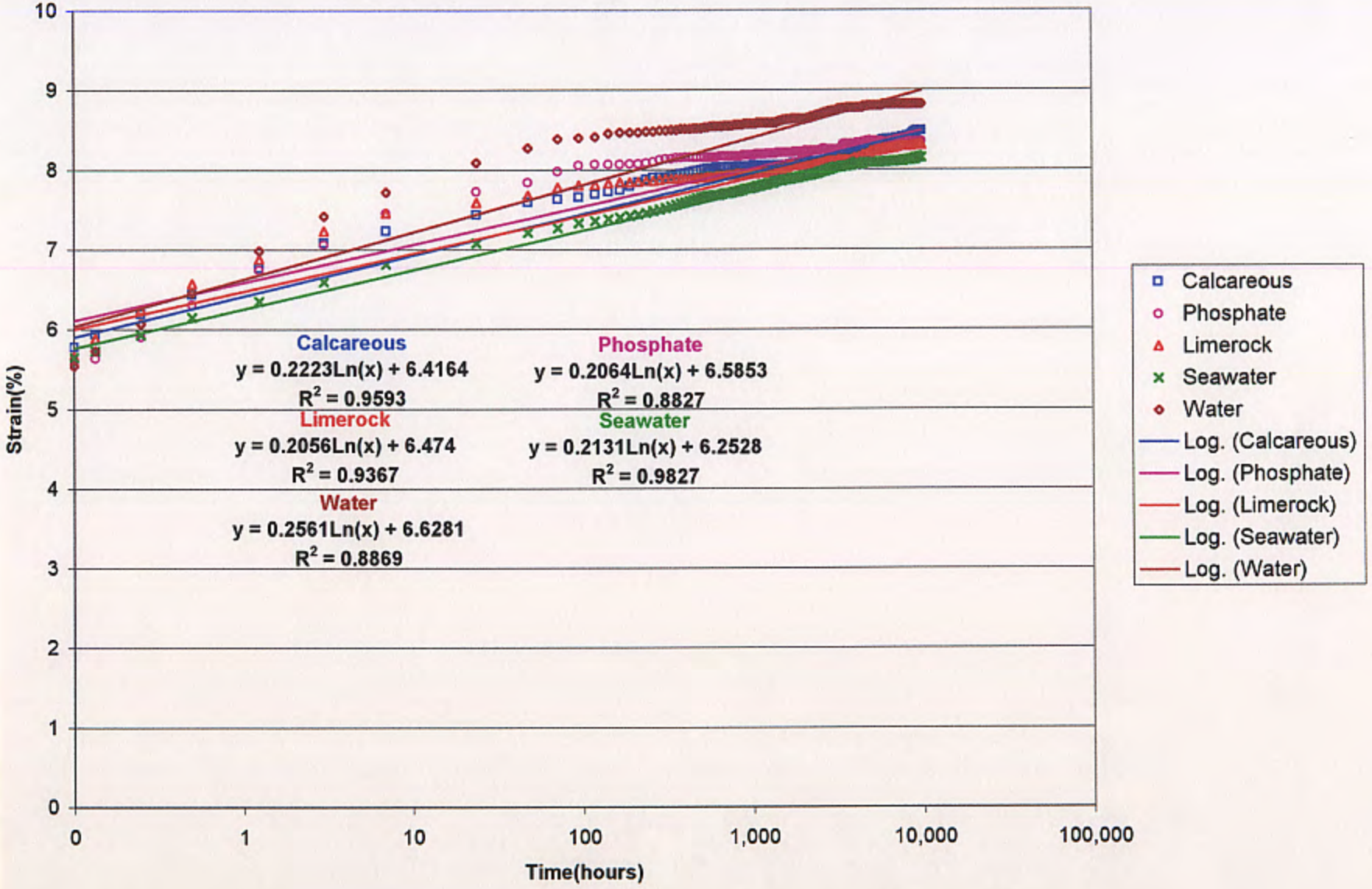

Fig. 6.49. Creep curves for PET geogrids, T = 55°C, Load level = 40% ultimate load - Specimen set I

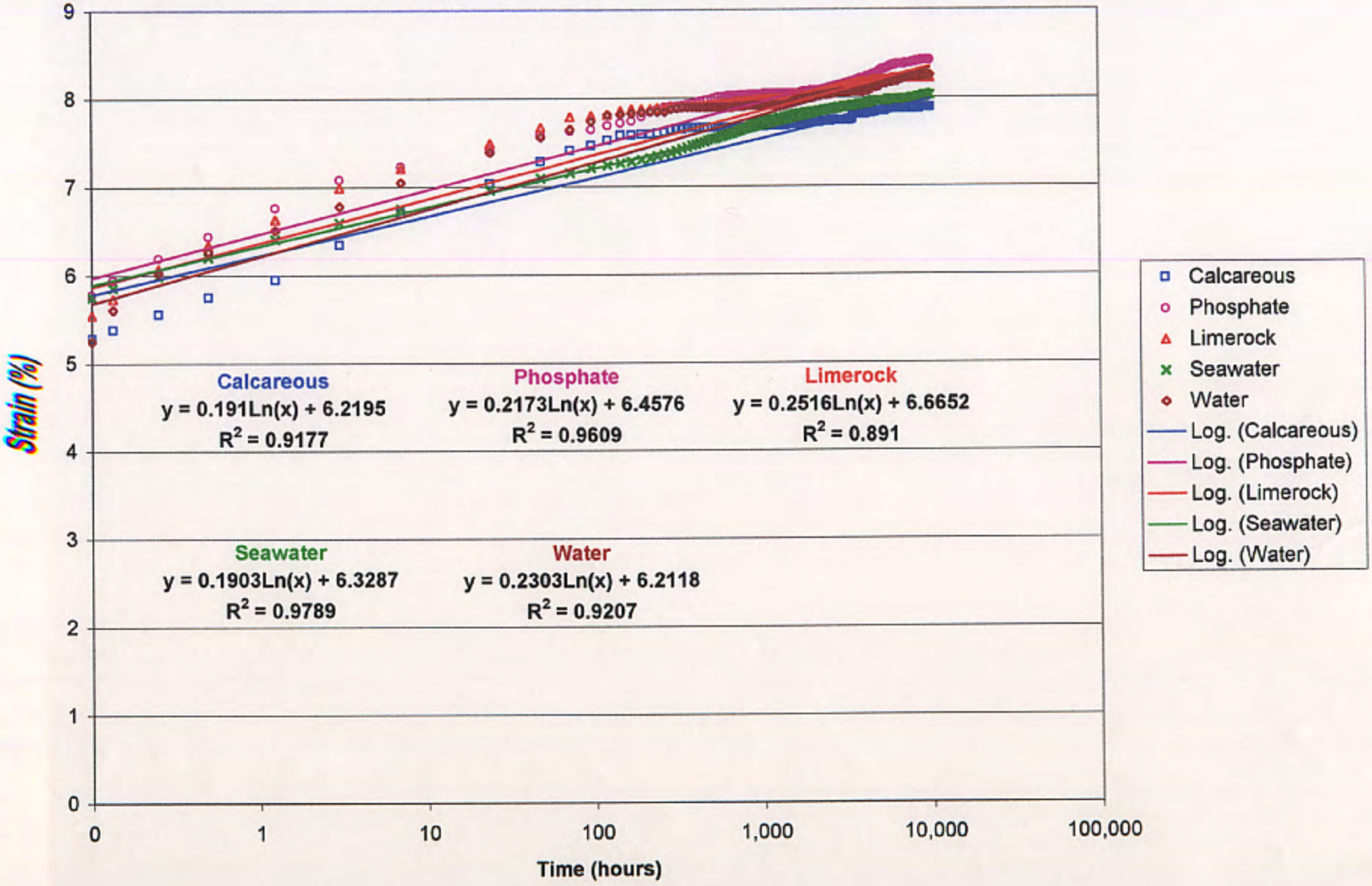

Fig. 6.50. Creep curves for PET geogrids, T = 55°C, Load level = 40% ultimate load - Specimen set II

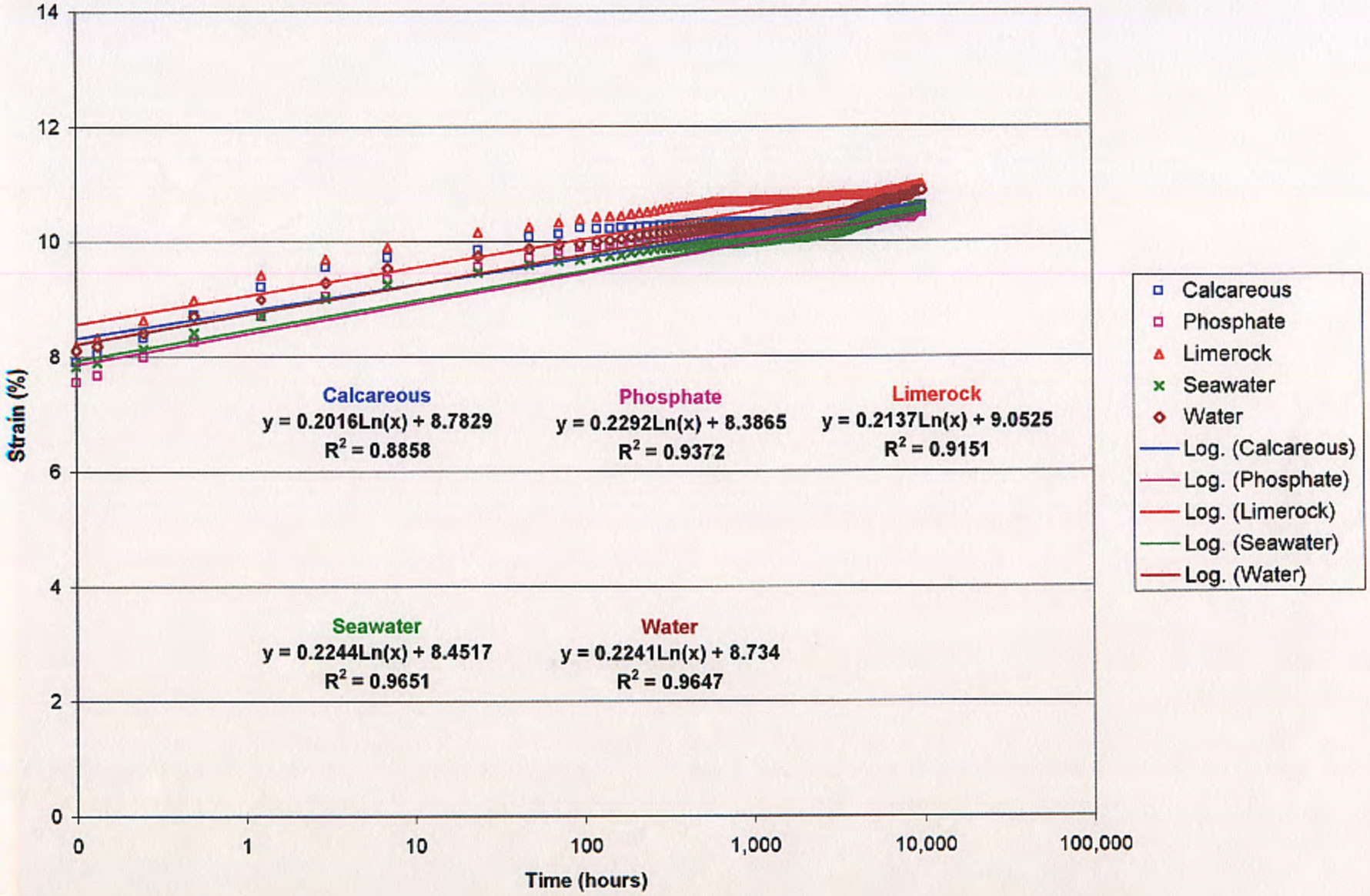

Fig. 6.51. Creep curves for PET geogrids, T = 55°C, Load level = 50% ultimate load - Specimen set I

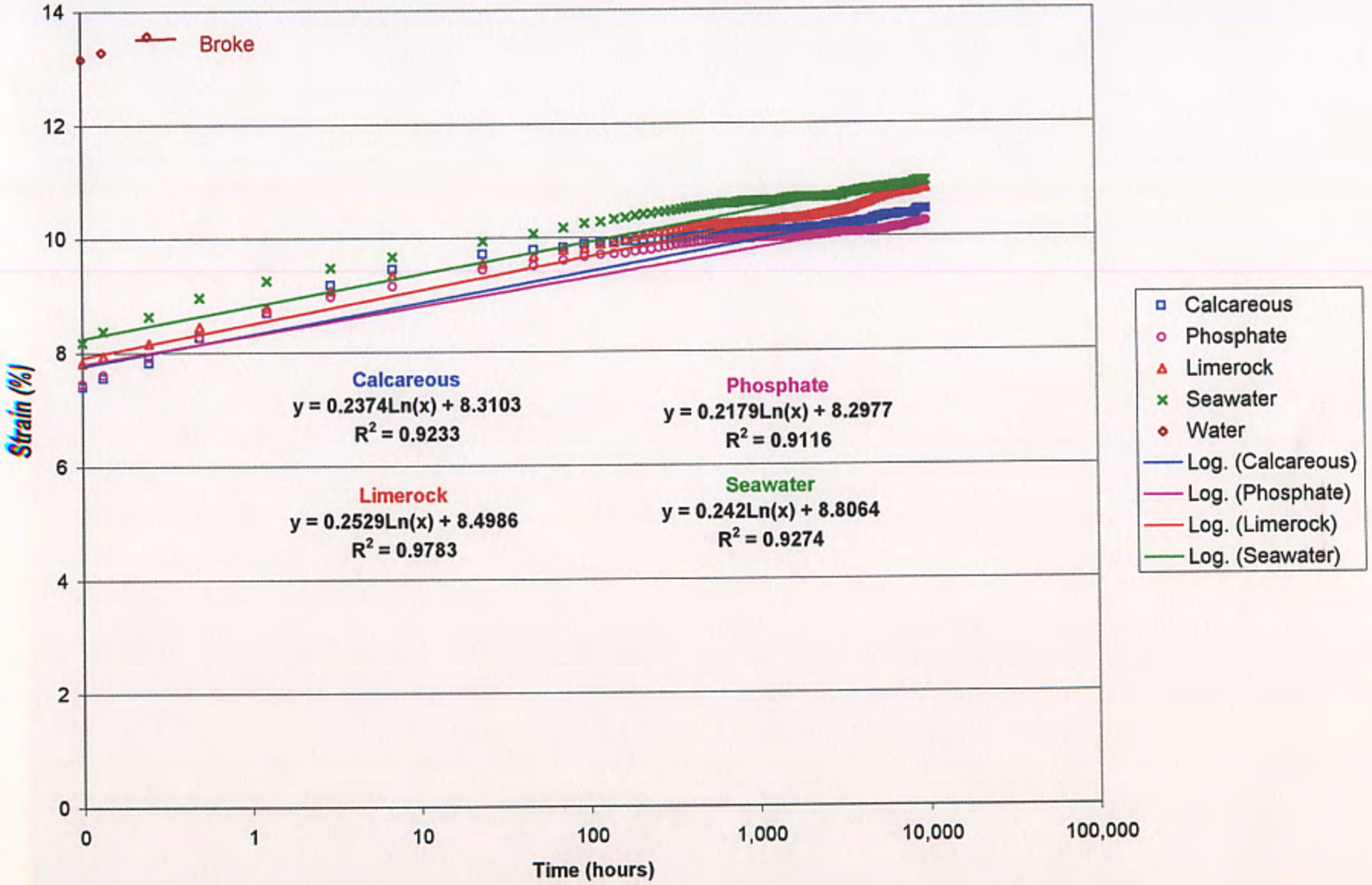

Fig. 6.52. Creep curves for PET geogrids, T = 55°C, Load level = 50% ultimate load - Specimen set II

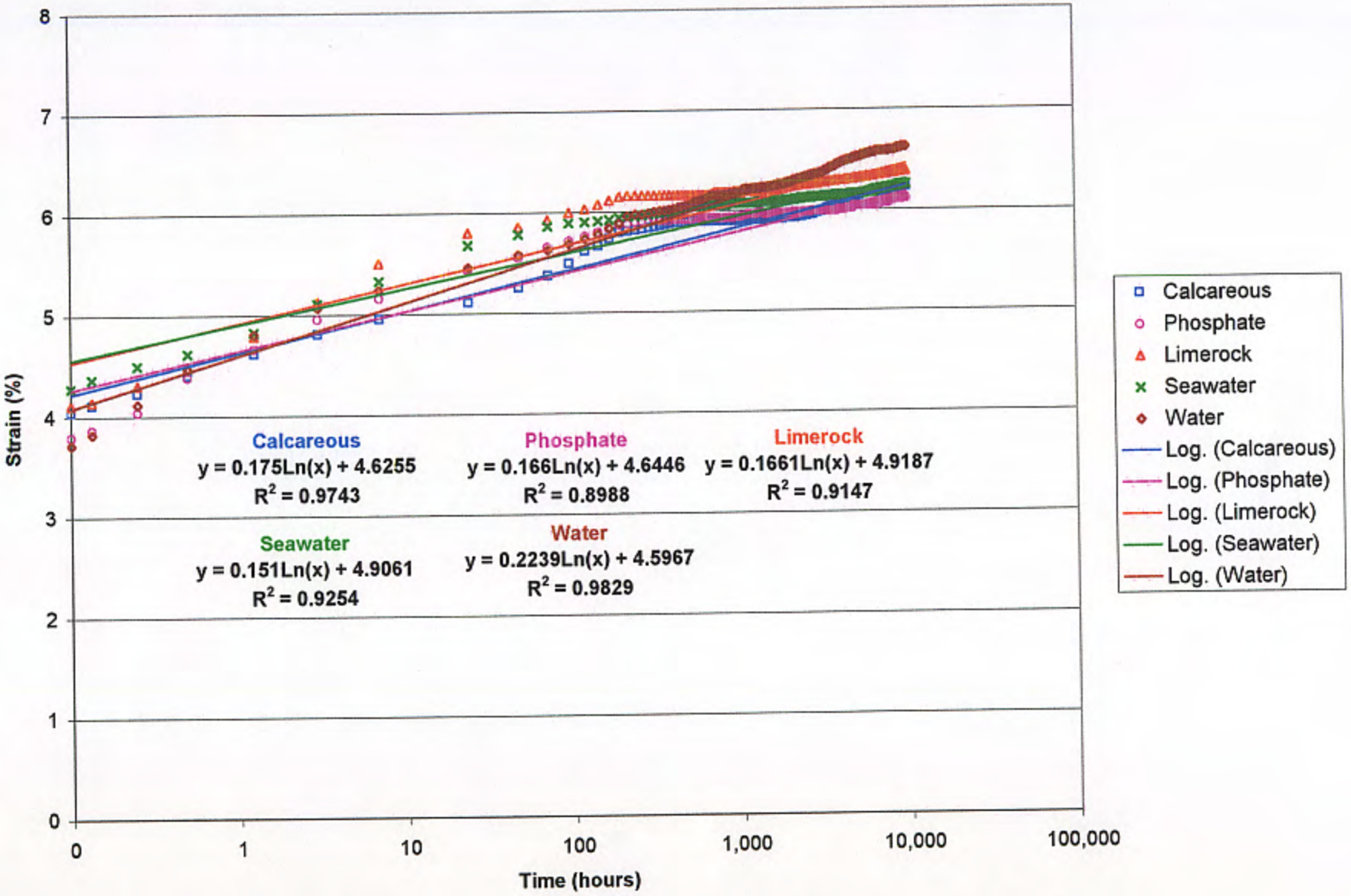

Fig. 6.53. Creep curves for PET geogrids, T = 65°C, Load level = 30% ultimate load - Specimen set I

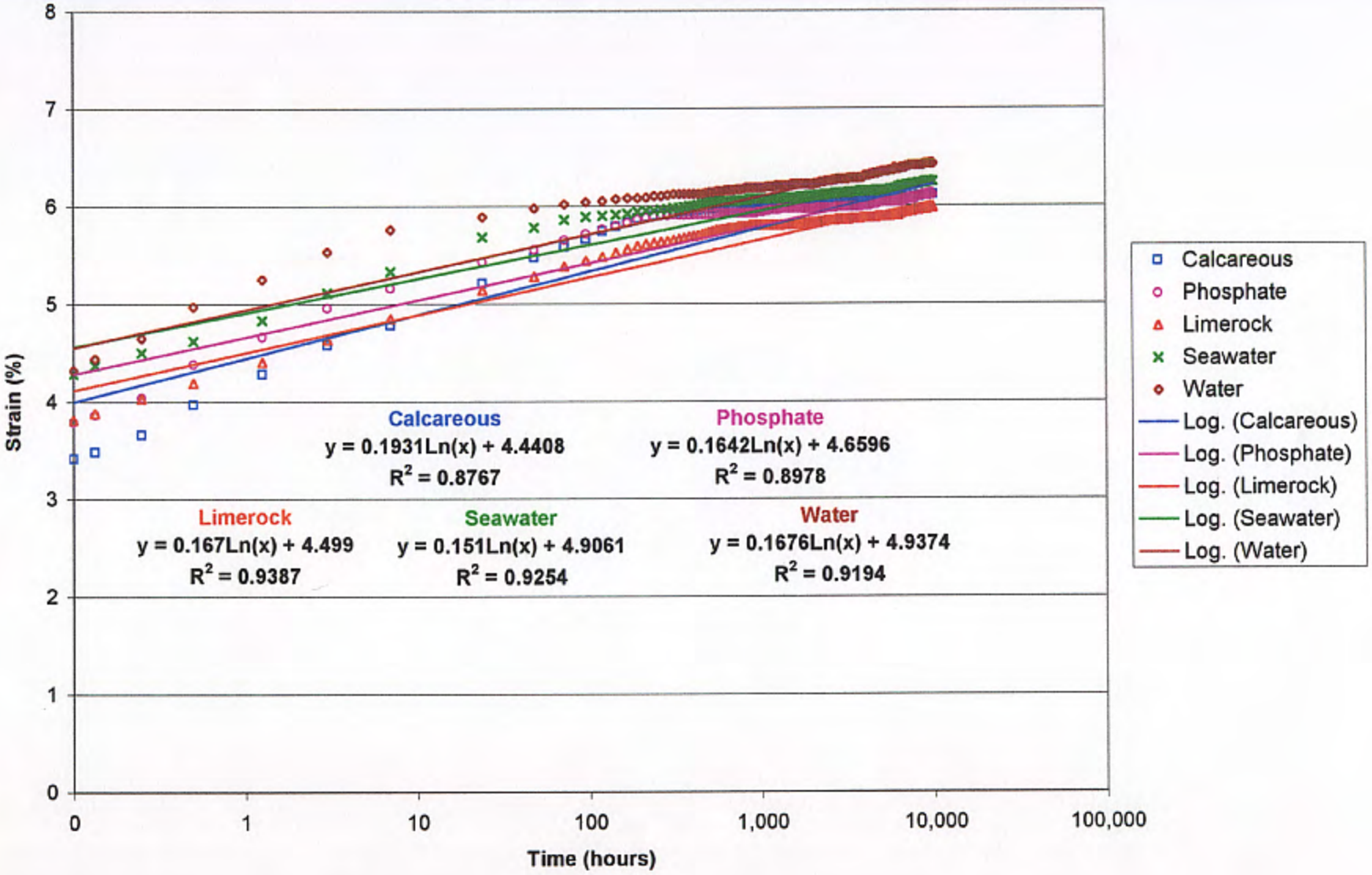

Fig. 6.54. Creep curves for PET geogrids, T = 65°C, Load level = 30% ultimate load - Specimen set II

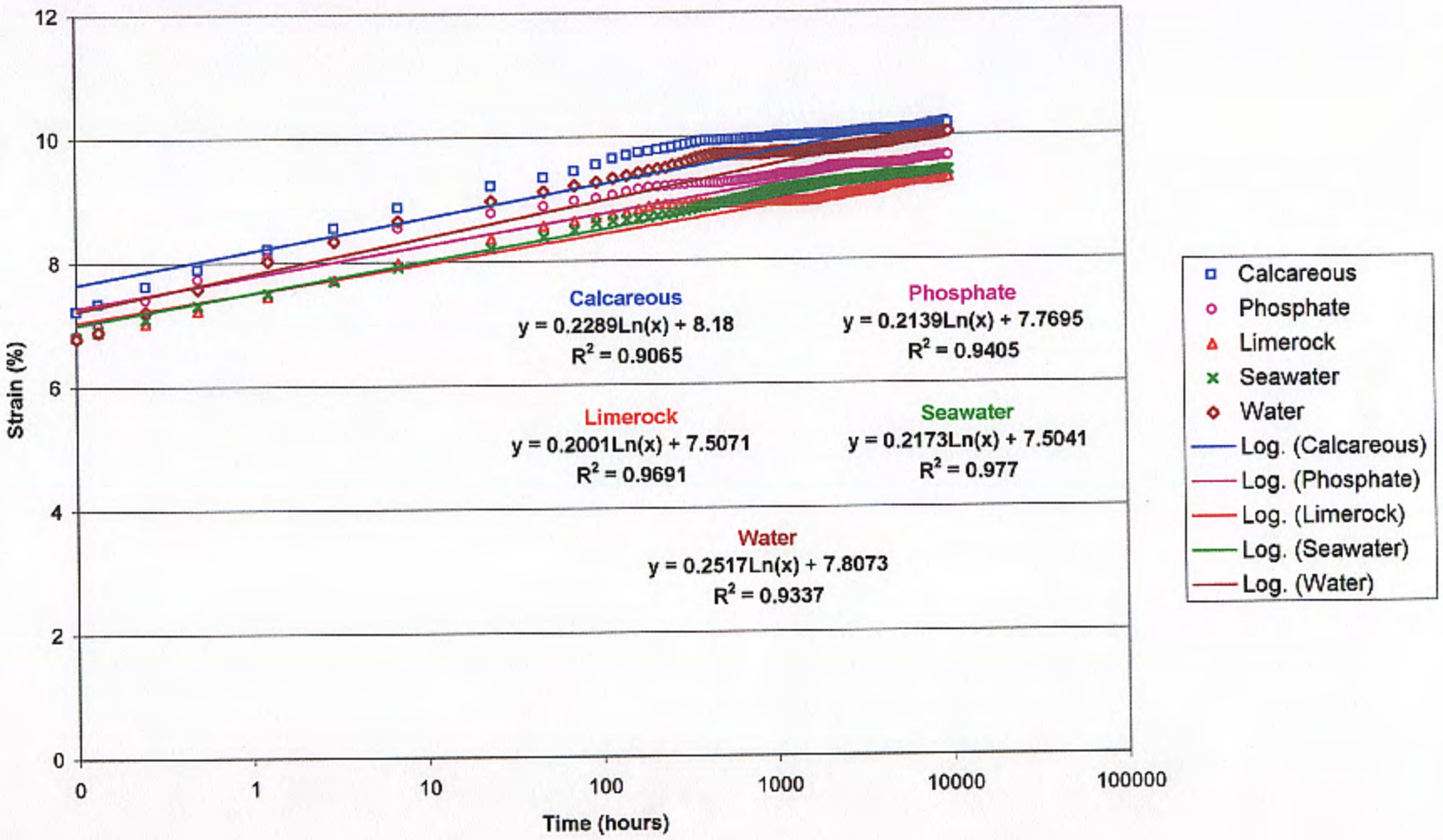

Fig. 6.55. Creep curves for PET geogrids, T = 65°C, Load level = 40% ultimate load - Specimen set I

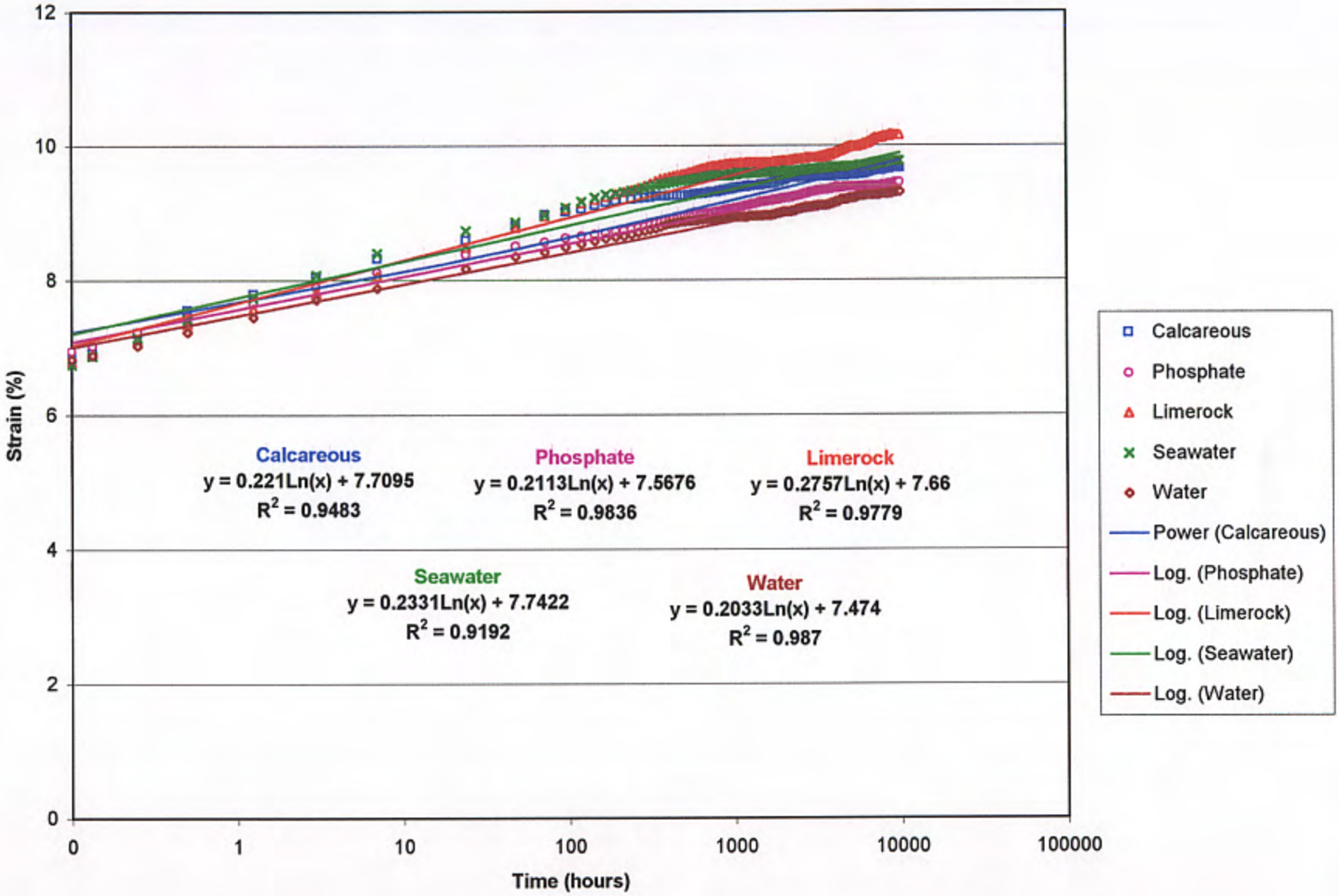

Fig. 6.56. Creep curves for PET geogrids, T = 65°C, Load level = 40% ultimate load - Specimen set II

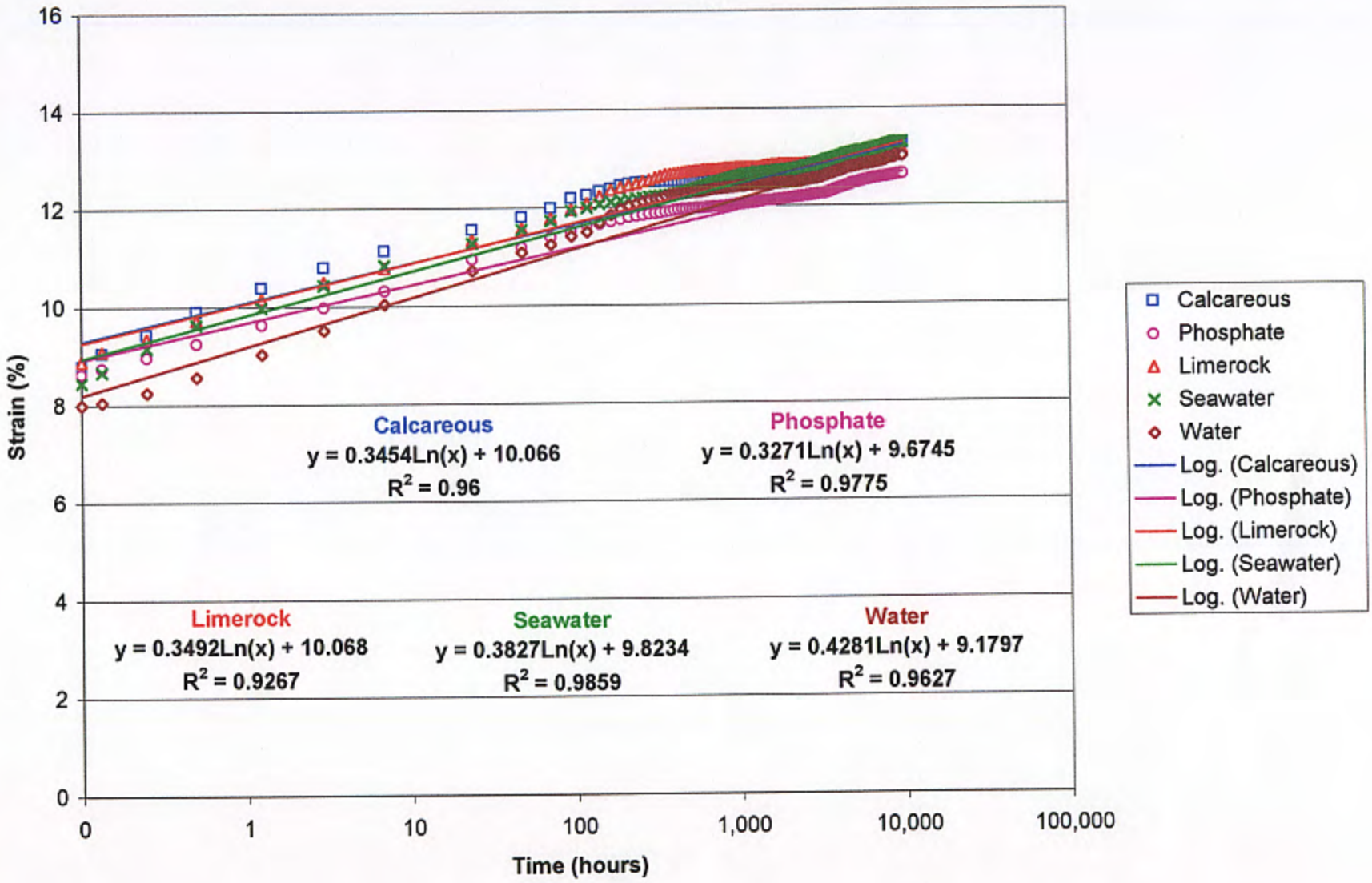

Fig. 6.57. Creep curves for PET geogrids, T = 65°C, Load level = 50% ultimate load - Specimen set I

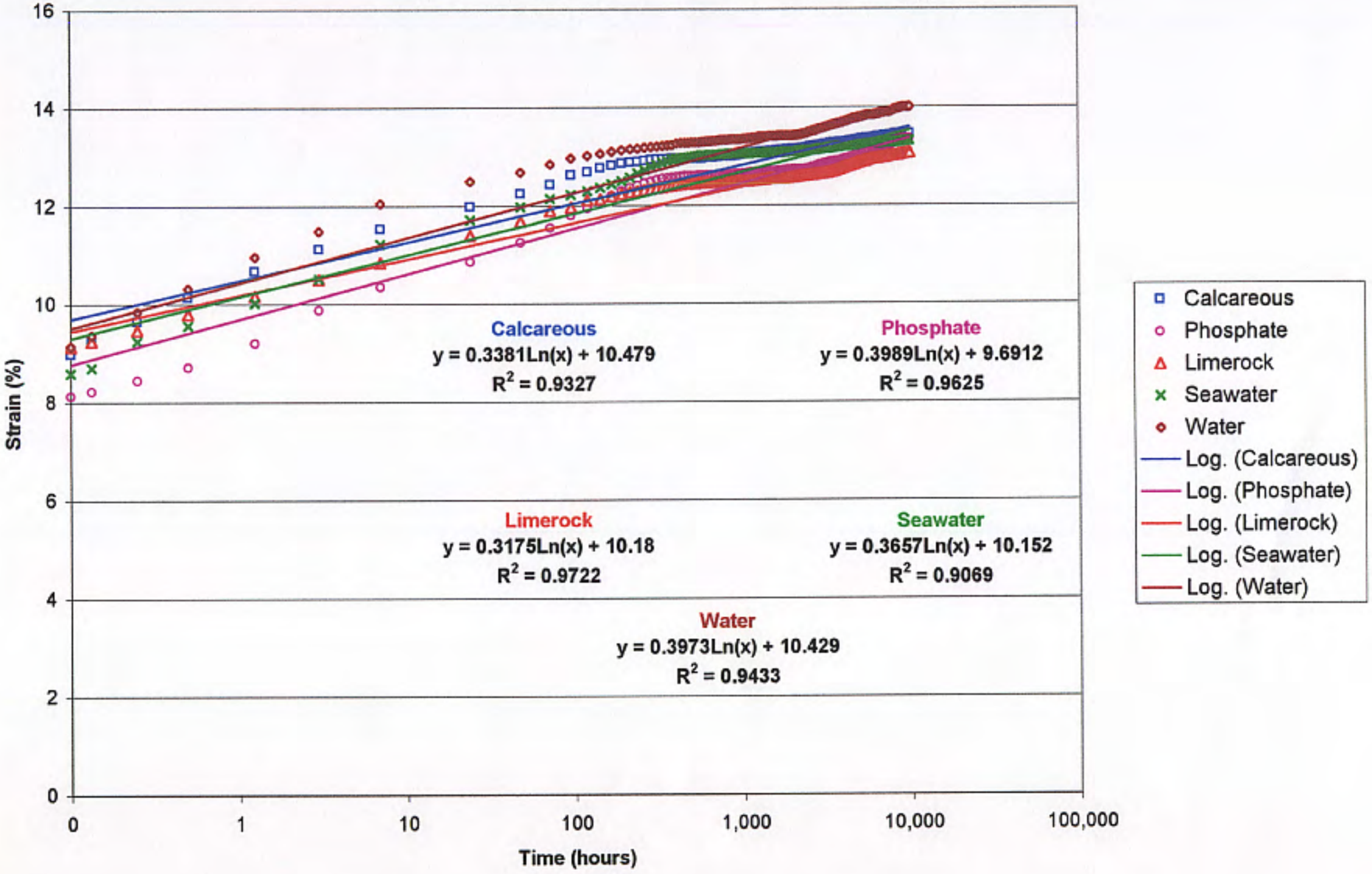

Fig. 6.58. Creep curves for PET geogrids, T = 65°C, Load level = 50% ultimate load - Specimen set II

CHAPTER 7

CREEP AND CREEP RUPTURE ANALYSIS

7.1 REGRESSION ANALYSIS

Regression analysis was carried out for the creep strain data obtained, and is included in Figs 6.11 to 6.58. Logarithmic trend lines and equations were selected for HDPE specimens with T = 30° C and Load levels = 30 and 40 (%) ultimate load, since they best fitted the creep strain data. For the rest of creep strain data for HDPE specimens, power trend lines gave the best results. For the PET specimens both power and logarithmic trends are used depending on each specific set of creep strain data. For the data for T= 45° C and Load level = 30 (%) - Specimen set II in seawater, a polynomial of the 6th order was the best option for the regression analysis.

From the plots of the creep strain data and the regression analysis, it can be seen that PET geogrids resist creep strain better than HDPE ones at similar temperatures and load levels. However, for both HDPE and PET specimens the increase in temperature

and load level have a strong effect on the creep strain behavior it is quite larger for HDPE specimens.

Tables 7.1 and 7.2 show the variations in creep strain for the different sets of data for HDPE specimens. It should be noticed that even though there is a large difference between the different solutions in some cases, it is not due to the exposure. For example in Figs. 6.19 and 6.20, which show creep strain for HDPE specimens at 45° C and Load level = 40 (%) ultimate load, the calcareous exposure data show the largest creep strain for specimen set I, and the lowest for specimen set II, indicating that variation in creep strain is mainly due to the differences between individual specimens.

Table 7.1 Creep strain (%) for HDPE Specimens 30° C and 45° C

Exposure (Temp / load level)	**30°C / 30%**	**30°C / 40%**	**30°C / 50%**	**45°C / 30%**	**45°C / 40%**	**45°C / 50%**
Initial Strain (%)	4.5 - 5	4.5 - 6	7.5 - 8	6 - 6.5	8.6 - 9.5	11 - 13.5
Final Strain (%)	8.5 - 9	11 - 11.5	17.5 - 20.5	10 - 11	16 - 19	34 -39

Table 7.2 Creep strain (%) for HDPE Specimens 55° C and 65° C

Exposure (Temp / load level)	**55°C / 30%**	**55°C / 40%**	**55°C / 50%**	**65°C / 30%**	**65°C / 40%**	**65°C / 50%**
Initial Strain (%)	6.3 - 7	9.5 - 10.5	14 - 16	8 - 9	11 - 13	19 - 26
Final Strain (%)	10.5 - 11.5	23 - 27	46 - 53	17 -19	28 - 33	46 - 56

From the results shown in Tables 7.1 and 7.2, it can be seen that the increase in temperature has a large influence on the amount of creep strain , and that specimens exposed to higher temperatures will be subjected to larger amounts of creep strain before

breaking than those exposed to lower temperatures. Also, the creep strain at breaking for the HDPE specimens was about 50% when exposed to 55° C or 65° C. The increase in load level also increases the amount of creep strain in the specimens, but the influence is not as large as that due to the temperature. However, the higher the temperature, the larger is the influence of the increase in load level .

Tables 7.3 and 7.4 show the variation in creep strain for the different sets of data for PET specimens. It should be noticed that the different solutions do not seem to influence the amount of creep strain .

Table 7.3 Creep strain (%) for PET Specimens 30° C and 45° C

Exposure (Temp / load level)	**30°C / 30%**	**30°C / 40%**	**30°C / 50%**	**45°C / 30%**	**45°C / 40%**	**45°C / 50%**
Initial Strain (%)	1.75 -2.1	2.6 - 2.9	4.9 - 5.3	3.8 - 4.2	4 - 5	6.3 - 7
Final Strain (%)	2.7 - 3.2	3.4 -4	6.3 - 6.9	5.2 - 5.9	5.6 -6.5	8.4 - 9.8

Table 7.4 Creep strain (%) for PET Specimens 55° C and 65° C

Exposure (Temp / load level)	**55°C / 30%**	**55°C / 40%**	**55°C / 50%**	**65°C / 30%**	**65°C / 40%**	**65°C / 50%**
Initial Strain (%)	3.6 - 4	5.2 - 5.8	7.8 - 8.2	3.4 - 4.3	6.7 -7.2	8.4 - 9
Final Strain (%)	5.3 - 5.9	7.9 - 8.8	10.2 - 11	6 - 6.6	9.2 - 10.2	13 - 14

From the results shown in Tables 7.3 and 7.4, it can be seen that the increase in temperature has a large influence on the amount of creep strain , but not as much as that encountered in HDPE specimens; for PET specimens the effects of temperature and load level are similar.

7.2 CREEP RUPTURE

The PET specimens did not experience creep rupture except for two specimens, and for those two cases the rupture can be attributed to either defects in the specimens or poor clamping. On the other hand, for the HDPE specimens, creep rupture was observed in all the specimens exposed to 50% of the ultimate load; and for the 55° C and 65° C temperatures, creep rupture occurred at 40% of the ultimate load. Tables 7.1 and 7.2 indicate that the specimens exposed to higher temperatures undergo larger deformations before creep rupture occurs. Tables 7.5 to 7.7 show the time of rupture for the HDPE geogrids.

Table 7.5 Creep rupture for HDPE specimens Load level = 50% ultimate load, T=30°C & 45°C

Exposure (Temp. / load level)	**30°C / 50%-set I**	**30°C / 50%-set II**	**45°C / 50%-set I**	**45°C / 50%-set II**
Solution	Time(hrs.) / Strain(%)	Time(hrs.) / Strain(%)	Time(hrs.) / Strain(%)	Time(hrs.) / Strain(%)
Calcareous	8520 / 19.1	7752 / 18.9	528 / 39.1	408 / 35.4
Phosphate	6768 / 18.1	8040 / 19.7	408 / 34.8	408 / 34.3
Limerock	3576 / 20.2	3696 / 17.5	480 / 38.7	480 / 37.4
Seawater	7584 / 19.5	6768 / 17.7	528 / 37	360 / 36.8

It can be observed in Table 7.5, that creep rupture occurred between 17.5 % and 20.2 % creep strain for the 30° C temperature and 50 % ultimate load, while for the 45° C temperature and 50% ultimate load the rupture occurred between 34.3 % and 39.1% creep strain . The rupture time for the 30° C temperature and 50 % ultimate load is

between 6,768 and 8,520 hours, except for the limerock exposure, while for the 45° C temperature and 50% ultimate load, the time to rupture varied from 360 to 528 hours. With these results it can be seen that the temperature has a strong effect on the percentage creep strain reached before creep rupture occurs and the time to creep rupture. The limerock exposure, at 30° C temperature and 50% ultimate load, reached creep rupture at only 3,576 to 3,696 hours. This can be attributed to non-uniform temperature exposure of the geogrid.

Table 7.6 Creep rupture for HDPE specimens Load level = 50% ultimate load, T=55°C & 65°C

Exposure (Temp. / load level)	**55°C / 50%-set I**	**55°C / 50%-set II**	**65°C / 50%-set I**	**65°C / 50%-set II**
Solution	Time(hrs.) / Strain(%)	Time(hrs.) / Strain(%)	Time(hrs.) / Strain(%)	Time(hrs.) / Strain(%)
Calcareous	120 / 46.2	48 / 52.5	5 / 46	7 / 55.9
Phosphate	120 / 51.2	120 / 50.3	5 / 51.3	7 / 54.7
Limerock	96 / 51.5	96 / 52.2	7 / 48.4	3 / 51.7
Seawater	144 / 51.2	72 / 50.9	5 / 55.1	5 / 50

For the 55° C and 65° C temperatures, the percentage of creep strain before creep rupture does not vary significantly suggesting that the creep strain limit for the material has been reached. The time to reach creep rupture was further reduced with the increment in temperature.

From Table 7.7, it can be seen that for the 55° C temperature and 40% ultimate load, the percentage of strain before creep rupture was between 23.3 and 27 %, while for the 65°C

temperature and 40% ultimate load it was between 29.6 and 32.7%, showing again that temperature affects the amount of creep strain reached before creep rupture.
Comparing Tables 7.6 and 7.7, it can be observed that the increase of load from 40% to 50% ultimate load also increases the creep strain before creep rupture.

It is clear from the results that the solution had no impact on the creep rupture, as the variabilities were principally from specimen to specimen. The only exception was limerock at 30° C temperature and 30% ultimate load. While this can be attributed to non-uniform distribution of temperature in the geogrid, which created regions, where the exposure temperature was higher than the 30° C required, not all the exposures indicated that to allow generalization.

Table 7.7 Creep rupture for HDPE specimens Load level = 40% ultimate load

Exposure (Temp. / load level)	**55°C / 40%-set I**	**55°C / 40%-set II**	**65°C / 40%-set I**	**65°C / 40%-set II**
Solution	Time(hrs.) / Strain(%)	Time(hrs.) / Strain(%)	Time(hrs.) / Strain(%)	Time(hrs.) / Strain(%)
Calcareous	4392 / 23.3	2256 / 27	168 / 29.6	168 / 32.7
Phosphate	3576 / 23.5	3144 / 23.3	96 / 31	120 / 31.6
Limerock	3168 / 24.1	3432 / 24.2	168 / 31.7	168 / 30.9
Seawater	2688 / 25.1	3192 / 23.6	240 / 29.9	240 / 30.2

CHAPTER 8

DURABILITY TESTING

8.1 MATERIAL PROPERTIES

8.1.1 GEOSYNTHETIC TEST SPECIMENS

The specimens used were the same as in the creep testing

8.1.2 ENVIRONMENTAL EXPOSURES

The environmental exposures used were the same as in the creep testing

8.2 TEST SETUP

8.2.1 INTRODUCTION

Twenty-seven tanks were fabricated at Florida Atlantic University (1997), to evaluate the durability of HDPE and PET geogrid specimens Fig. 8.1. Measurements included the ultimate load and load - strain curves . Different exposures and elevated temperatures were used to determine the long-term behavior of the geogrids and to simulate different exposure conditions, with soil water related to the soil conditions in Florida. The different variables are presented in the test procedures section (8.3).

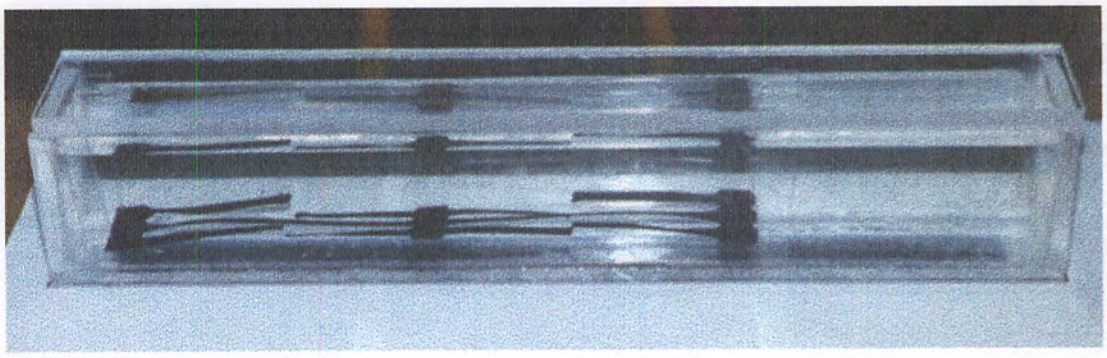

Figure 8.1 Durability tank

8.2.2 DURABILITY TANKS

The durability tanks contained the different solutions and soils, and twenty-four geogrid test specimens. The shop drawing is shown in Fig. 8.2,. The twenty-seven tanks were covered to avoid evaporation and placed in larger tanks. These were filled with

water just below the top edges of the small tanks to avoid mixing of the soil water with water from the large tanks. This created a bath to raise the temperatures of the durability tanks. To keep the tanks at the constant elevated temperatures of 35, 50 and 65°C, heaters and pumps were placed in the large tanks. The large tanks were also covered. See Figs. 8.3-8.8.

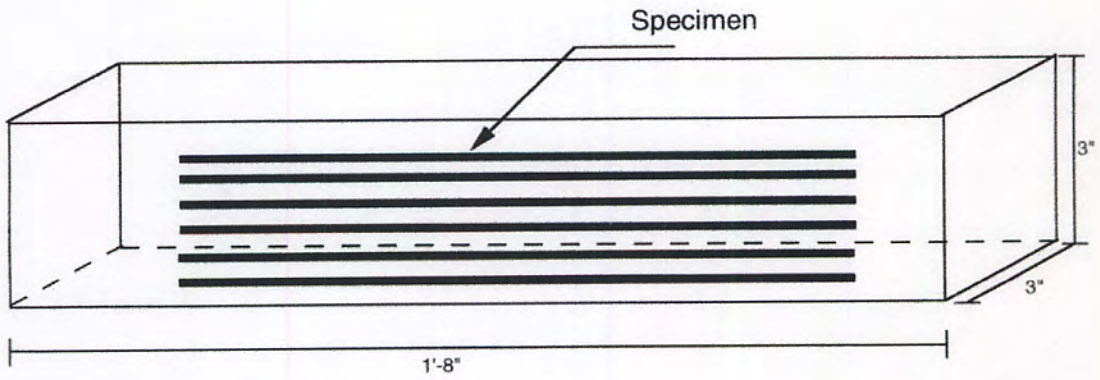

Figure 8.2 Durability tank shop drawing

Figure 8.3 Uncovered durability tanks

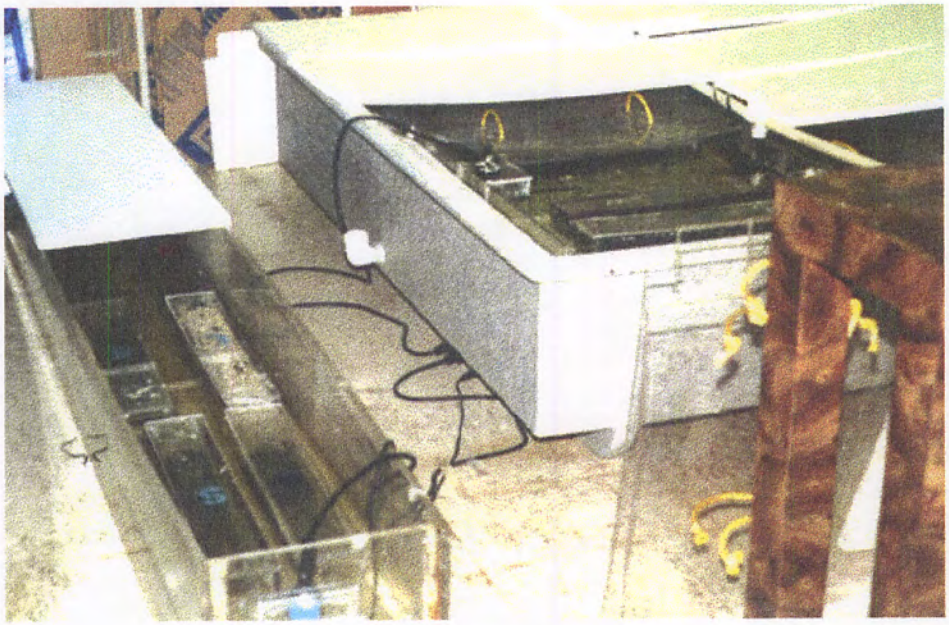

Figure 8.4 Durability tanks

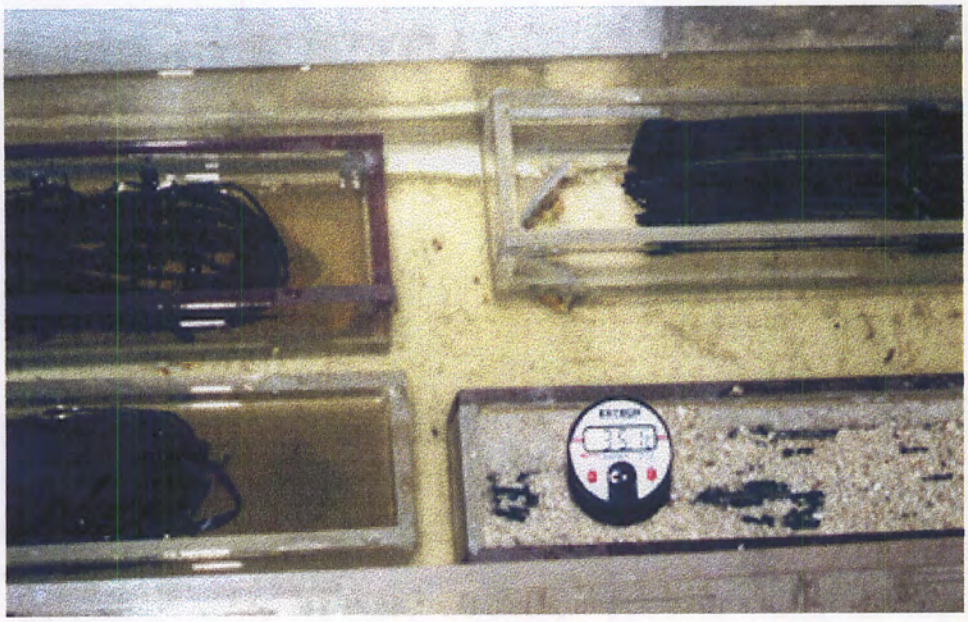

Figure 8.5 Temperature control, 35° C tank

Figure 8.6 Temperature control, 50° C tank

Figure 8.7 Temperature control, 65° C tank

Figure 8.8 pH control, Phosphate (pH = 4.5) tank

8.2.3 TENSION TESTING MACHINE

A Tinius Olsen DS-50 displacement controlled frame with a 1.33kN (300 lb.) load cell and a 6" RDP, LVDT were used to obtain the load-elongation curves. Fig. 8.9 shows the tension testing of a HDPE geogrid. Fig. 8.10 shows the PET tension testing.

8.2.4 CLAMPS (MODEL A AND B)

Two kinds of clamps were used to fasten the test specimens. The clamps were identical to the ones used for the creep and creep rupture testing.

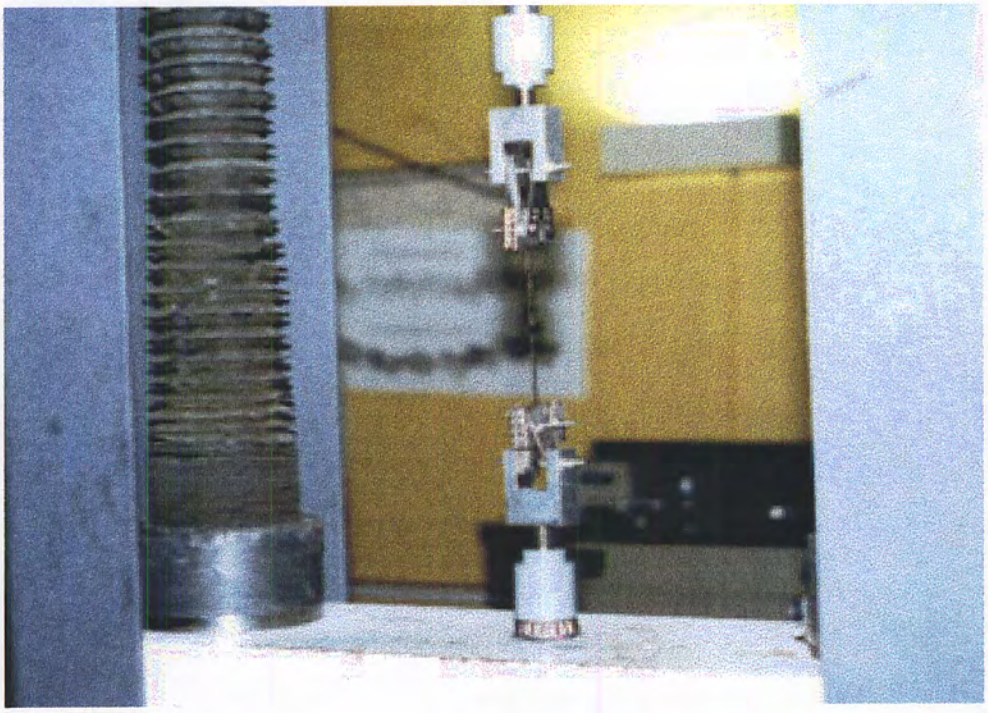

Figure 8.9 Tension testing of PET specimen

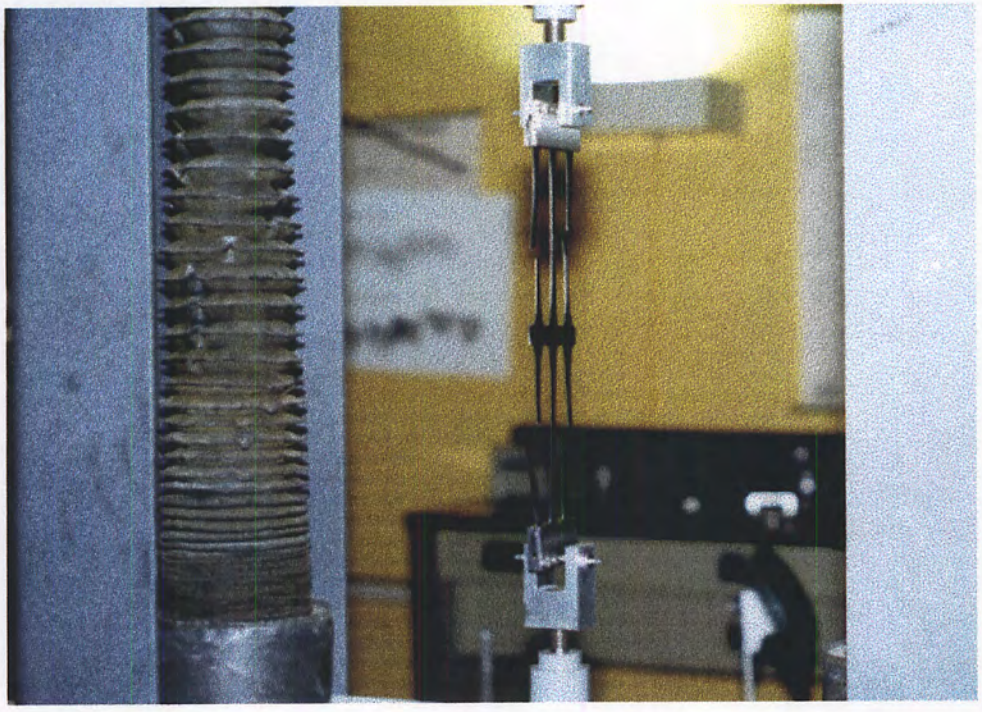

Figure 8.10 Tension testing of HDPE specimen

8.3 TEST PROCEDURES

8.3.1 INTRODUCTION

To simulate different exposure conditions, twenty seven tanks were fabricated with soil water related to the soil conditions in Florida.

The variables were as follows:

HDPE: 3 specimens x
3 temperatures x
4 solutions x
6 immersion periods

Total = 216 HDPE specimens

PET: 3 specimens x
3 temperatures x
5 solutions x
6 immersion periods

Total = 270 PET specimens

CONSOLIDATED TOTAL = 486 specimens

Temperatures:

95 °F (35°C)

122 °F (50°C)

149 °F (65 °C)

Solutions:

Phosphate (pH 4.5)

Calcareous (pH 9.0)

Sea water

water (only for PET specimens)

Limerock

Immersion periods:

30 days

60 days

90 days

120 days

365 days

417 days

8.3.2 TEST PREPARATION

8.3.2.1 Trimming the Geogrid Specimen

The geogrid specimen was cut to a width of 0.07 m (three ribs) for HDPE cutting the 2 outside ribs leaving only the middle one to sustain the loads and 0.03 m (single rib) for PET . For HDPE, the length was 0.34 m, and for PET 0.22 m.

8.3.2.2 Clamping the Test Specimen

The clamping procedures were similar to the ones described in section 6.3.2.2

8.3.3 PLACEMENT OF THE SOIL WATER SAMPLES AND TEST SPECIMEN

Prior to placement of the different soil water exposures, the durability tanks were thoroughly cleaned. The twenty-seven small durability tanks were placed inside the three large tanks, then different soil water exposures were set up in the small durability tanks. Once all the small tanks were filled with the soil water solutions and stabilized, the large tanks were filled up with water to a level 1 cm below the top edges of the small tanks, to avoid mixing of the water from the small tanks with that in the large ones. After the right levels were reached the heaters and pumps were connected. A period of at least 24 hours was used to stabilize the temperatures to follow ASTM standards D 5262 - 92 and

D 4595 -86. The test specimens were then placed in the small tanks, and both the small and large tanks covered.

8.3.4 TEMPERATURE, pH, AND WATER LEVEL CONTROL

The temperature was controlled daily to maintain the water soil at a temperature in the range of T ± 2° C to follow specifications in ASTM standards D 5262 - 92 and D 4595 -86, . The pH values were measured every three days, and adjusted when necessary by adding the corresponding material. Water was added to the large tanks when necessary, the tanks at 55 and 65 ° C had reservoir tanks to maintain constant water levels in the large tanks (Fig. 8.3). The water was kept above the levels of the specimens at all times.

8.3.5 GEOGRID SPECIMEN EXTRACTION AND CLEANING

Once the specified immersion period was reached, three specimens from each exposure and type were taken out the tanks. They were carefully rinsed in the water and dried immediately.

8.3.6 TENSION TESTING

A pretension force equal to 1.25% of the expected breaking force was applied in conformance with ASTM standards D 5262 - 92 and D 4595 -86. After the surcharge

was applied, the marking pen in the Tinius Olsen DS-50 machine was set in place and the LVDT set in the stating position. This was followed by the application of a constant displacement of 2 inches per minute, in accordance with GRI Test Method GG1-87.

8.4 TEST RESULTS

8.4.1 INTRODUCTION

The results are presented for durability tests on both HDPE and PET test specimens. The test parameters are listed in Section 8.3.1. The values of the three specimens tested for each condition were averaged, regression analysis carried out, and the Arrhenius curves plotted.

8.4.2 DURABILITY CURVES

The durability data shown in Tables 8.1 to 8.3 was obtained from the load-elongation curves presented in Appendix A. The plots for HDPE and PET are presented in Figures 8.11 to 8.19. It can be observed from the durability plots that the degradation in the HDPE specimens is very small; some of the durability plots even showed an increase in strength at the 65 °C temperature. This shows that the effect of environmental exposure on the HDPE geogrids is negligible. PET specimens showed some degradation, which seemed to be very similar for the different solutions, indicating hydrolysis as the main cause.

TABLE 8.1 Ultimate Strength (lb/rib) Control Values

High Desity Polyehtylene HDPE Geogrids				Polyester PET Geogrids	
	303			312	
	301			299	
	300			297	
	300			292	
	300			289	
	299			289	
	299			288	
	297			285	
	297			282	
	297			272	
	295			271	
	294			271	
	294			270	
	292			270	
	291			267	
	297			**284**	

TABLE 8.2 Ultimate strength (lb/rib) for HDPE geogrids

Period (hours)	720	1440	2160	2880	8760	10000
Calcareous 35°C	304	302	300	297	304	300
	301	301	298	292	290	296
	300	299	295	288	288	295
Average	**302**	**301**	**298**	**292**	**294**	**297**
Calcareous 50°C	305	303	302	293	287	301
	304	301	302	290	286	297
	301	300	300	287	285	294
Average	**303**	**301**	**301**	**290**	**286**	**297**
Calcareous 65°C	305	303	303	296	290	300
	302	302	299	293	280	296
	297	302	298	287	279	288
Average	**301**	**302**	**300**	**292**	**283**	**295**

TABLE 8.2. Cont. Ultimate strength (lb/rib) for HDPE geogrids

Phosphate 35°C	308	302	300	302	298	300
	306	302	298	294	291	293
	299	298	298	288	290	292
Average	**304**	**301**	**299**	**295**	**293**	**295**
Phosphate 50°C	302	302	303	297	295	294
	302	298	303	294	293	292
	301	297	297	290	288	292
Average	**302**	**299**	**301**	**294**	**292**	**293**
Phosphate 65°C	304	303	303	303	293	301
	297	302	303	296	289	294
	288	297	300	295	286	292
Average	**296**	**301**	**302**	**298**	**289**	**296**
Limerock 35°C	303	302	297	298	300	302
	300	299	291	294	299	296
	298	296	281	292	296	295
Average	**300**	**299**	**290**	**295**	**298**	**298**
Limerock 50°C	303	302	300	298	305	294
	299	300	297	294	305	292
	299	298	297	292	303	288
Average	**300**	**300**	**298**	**295**	**304**	**291**
Limerock 65°C	303	301	300	300	305	292
	300	300	297	297	296	290
	298	294	297	294	290	285
Average	**300**	**298**	**298**	**297**	**297**	**289**
	720	1440	2160	2880	8760	10000
Sea Water 35°C	302	300	301	302	306	300
	300	297	296	299	307	297
	297	296	292	294	306	292
Average	**300**	**298**	**296**	**298**	**306**	**296**
Sea Water 50°C	304	303	301	302	305	297
	303	300	300	296	306	293
	297	299	297	291	293	288
Average	**301**	**301**	**299**	**296**	**301**	**293**
Sea Water 65°C	304	302	302	297	304	298
	297	297	296	295	302	296
	296	291	294	294	300	293
Average	**299**	**297**	**297**	**295**	**302**	**296**

TABLE 8.3. Cont. Ultimate strength (lb/rib) for PET geogrids

Period (hours)	720	1440	2160	2880	8760	10000
Sea Water 35°C	305	286	286	288	305	288
	284	283	284	286	278	280
	265	279	279	273	267	273
Average	**285**	**283**	**283**	**282**	**283**	**280**
Sea Water 50°C	287	289	285	288	308	294
	282	276	282	282	288	292
	271	268	269	279	266	281
Average	**280**	**278**	**279**	**283**	**287**	**289**
Sea Water 65°C	282	277	276	273	283	275
	271	275	272	265	272	273
	256	266	258	263	260	251
Average	**270**	**273**	**269**	**267**	**272**	**266**
Water 35°C	288	279	282	287	290	304
	285	276	278	276	271	295
	257	273	272	270	266	280
Average	**277**	**276**	**277**	**278**	**276**	**293**
Water 50°C	291	299	279	286	272	278
	243	276	269	283	269	268
		267	264	271	252	255
Average	**267**	**281**	**271**	**280**	**264**	**267**
Water 65°C	305	275	279	275	269	249
	257	267	266	272	253	245
	240	265	251	267	238	240
Average	**267**	**269**	**265**	**271**	**253**	**245**

TABLE 8.3. Ultimate strength (lb/rib) for PET geogrids

Period (hours)	720	1440	2160	2880	8760	10000
Calcareous 35°C	278	286	286	298	304	306
	273	282	280	282	303	280
	261	280	268	251	267	263
Average	**271**	**283**	**278**	**277**	**291**	**283**
Calcareous 50°C	297	288	285	281	305	287
	259	269	281	277	277	258
	257	263	271	270	285	239
Average	**271**	**273**	**279**	**276**	**289**	**261**
Calcareous 65°C	292	295	286	274	268	267
	290	294	273	267	262	261
	249	282	259	258	256	261
Average	**277**	**290**	**273**	**266**	**262**	**263**
Phosphate 35°C	306	288	288	287	307	300
	305	282	281	279	304	270
	274	278	274	272	262	267
Average	**295**	**283**	**281**	**279**	**291**	**279**
Phosphate 50°C	308	276	281	269	275	277
	257	273	265	268	265	268
		264		262	242	269
Average	**283**	**271**	**273**	**266**	**261**	**271**
Phosphate 65°C	290	270	277	264	276	257
	258	263	267	258	247	243
	255	259	257	252	236	243
Average	**268**	**264**	**267**	**258**	**253**	**248**
Limerock 35°C	301	292	291	286	285	289
	290	283	288	284	271	282
	284	274	282	274	268	
Average	**292**	**283**	**287**	**281**	**275**	**286**
Limerock 50°C	295	282	282	275	294	307
	281	268	281	270	283	264
	280	266	277	266	266	233
Average	**285**	**272**	**280**	**270**	**281**	**268**
Limerock 65°C	298	279	273	273	276	270
	267	271	267	267	270	239
	249	264	256	259	264	220
Average	**271**	**271**	**265**	**266**	**270**	**243**

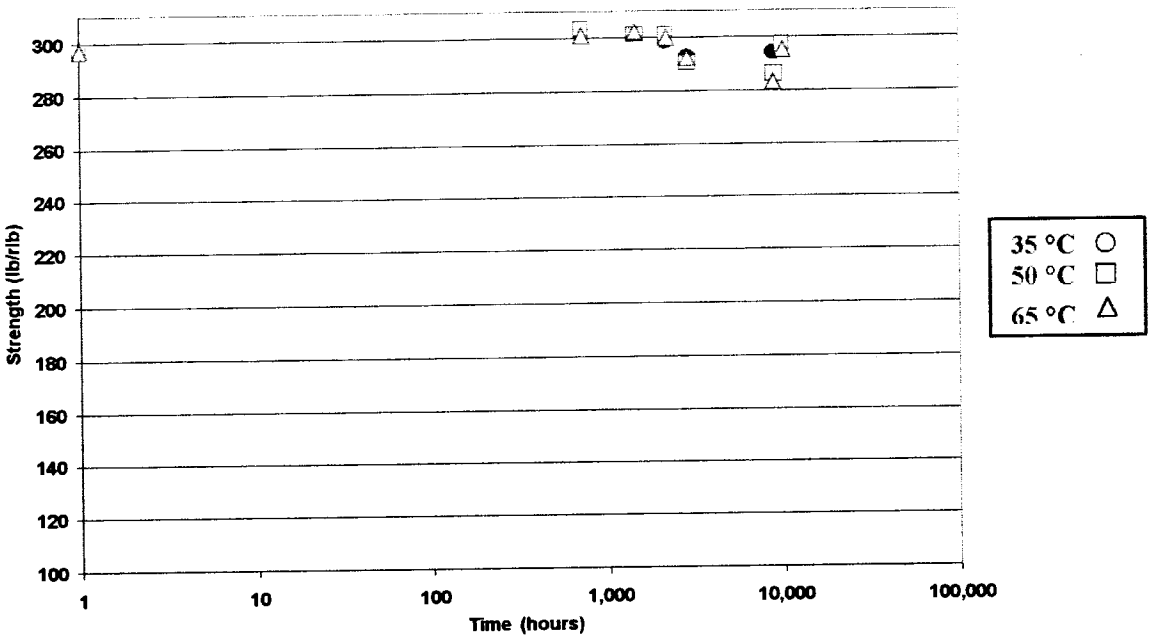

Figure 8.11 Durability plots for HDPE geogrids in calcareous solution

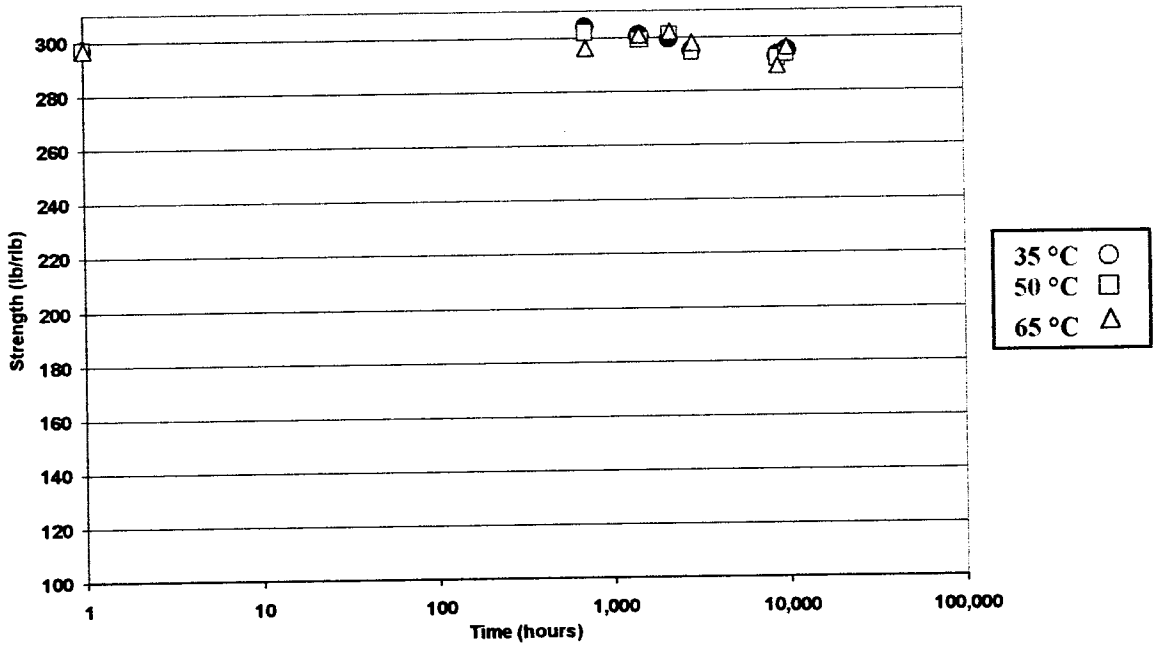

Figure 8.12 Durability plots for HDPE geogrids in phosphate solution

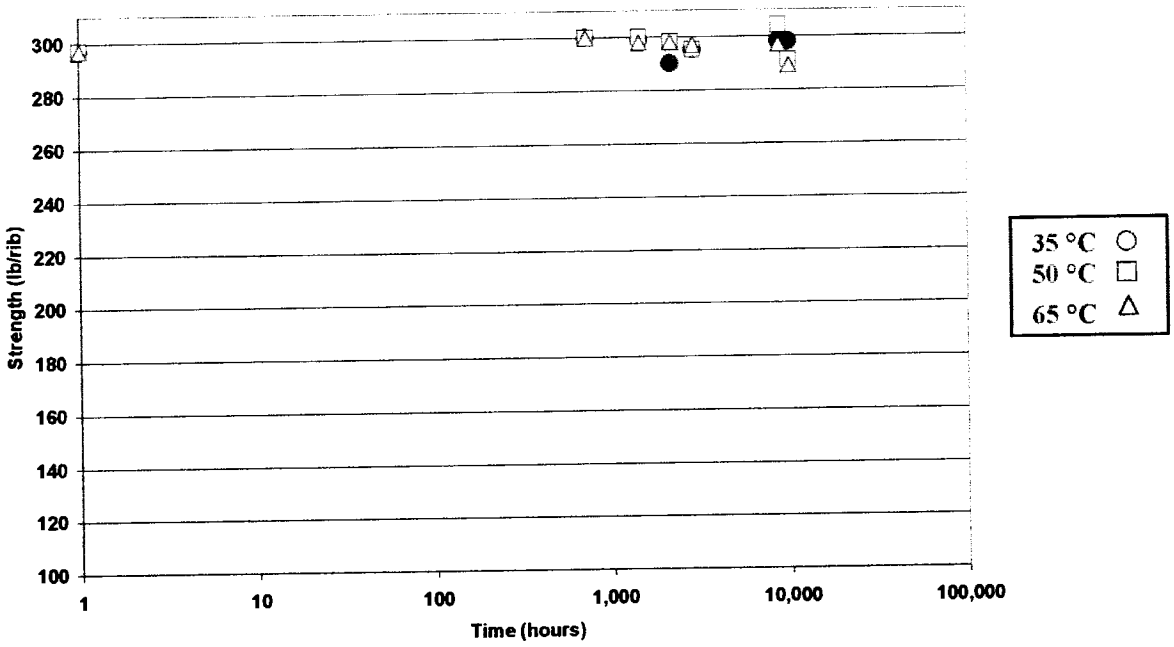

Figure 8.13 Durability plots for HDPE geogrids in limerock

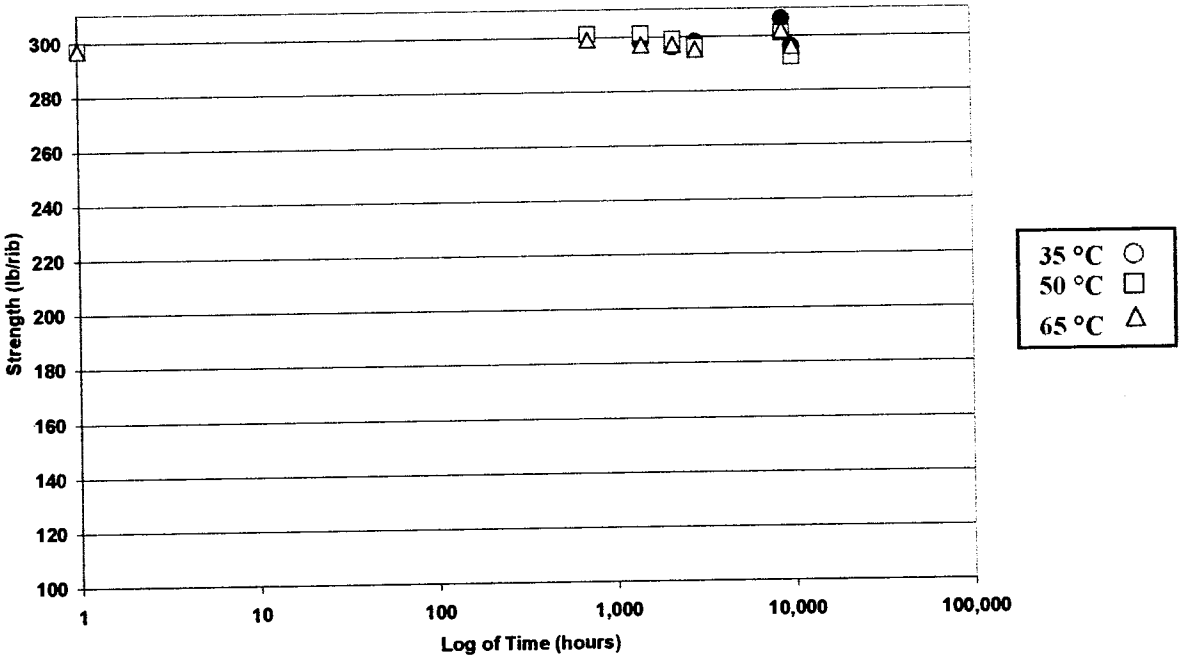

Figure 8.14 Durability plots for HDPE geogrids in seawater

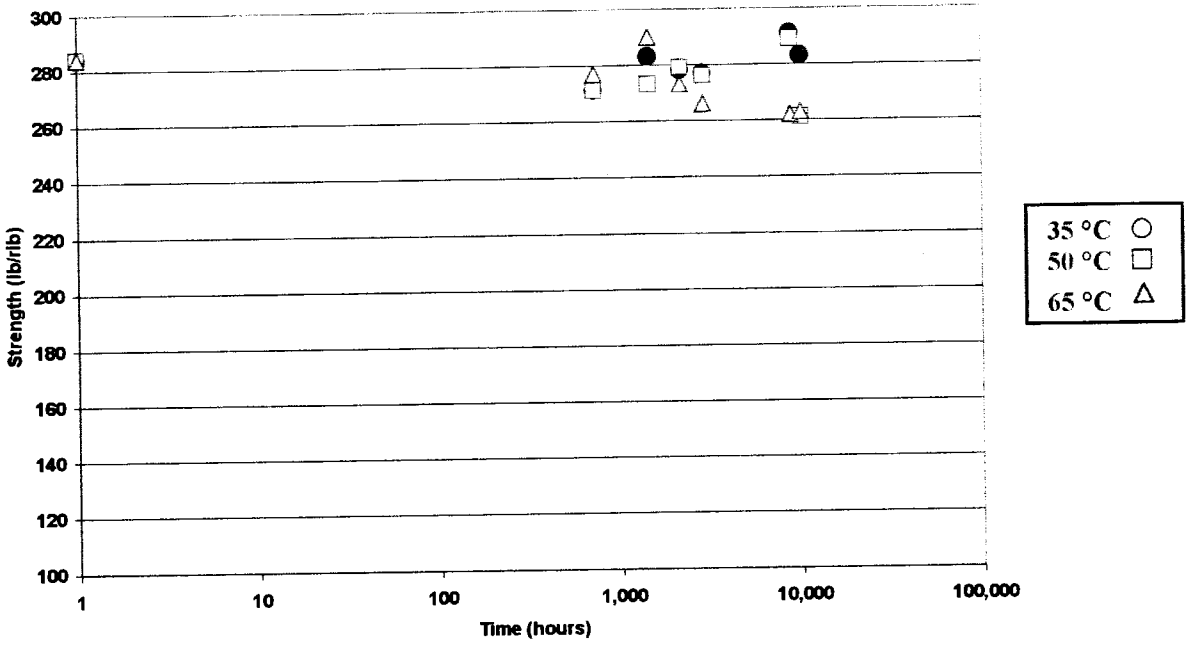

Figure 8.15 Durability plots for PET geogrids in calcareous solution

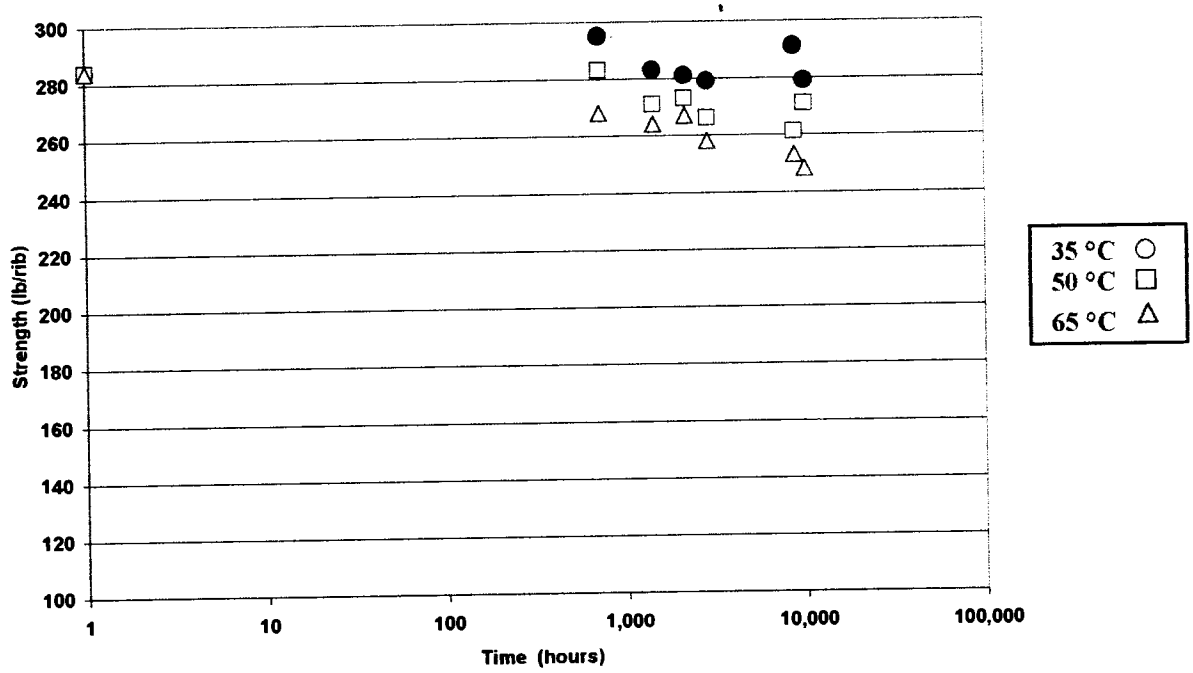

Figure 8.16 Durability plots for PET geogrids in phosphate solution

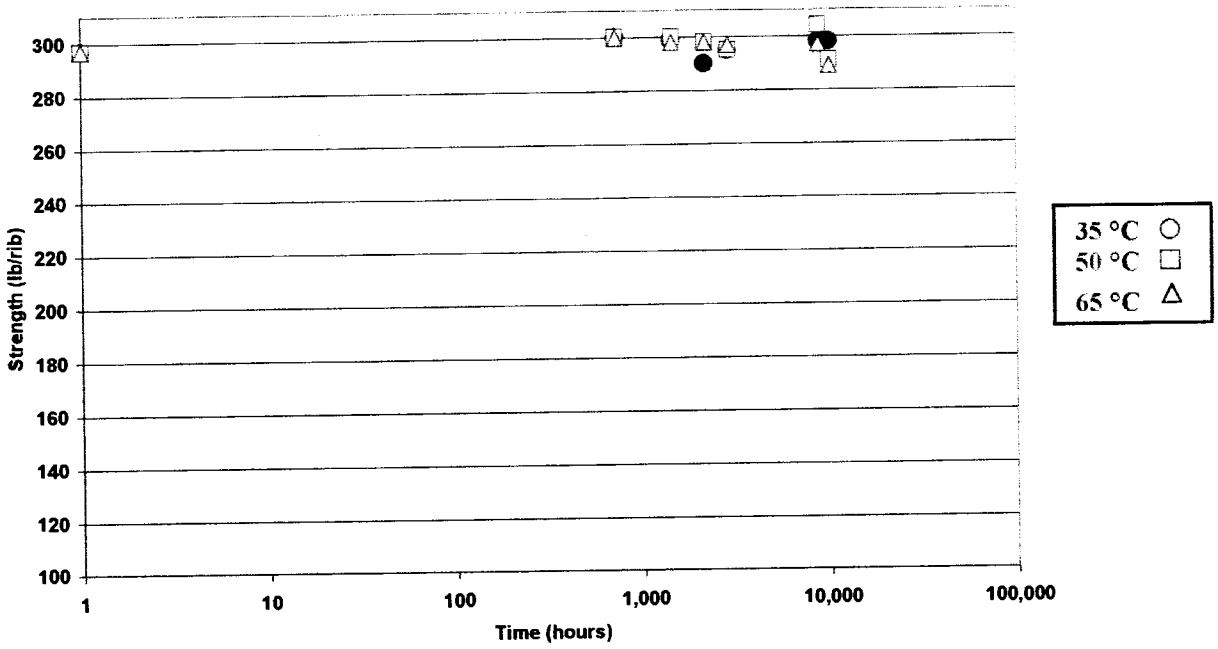

Figure 8.17 Durability plots for PET geogrids in limerock

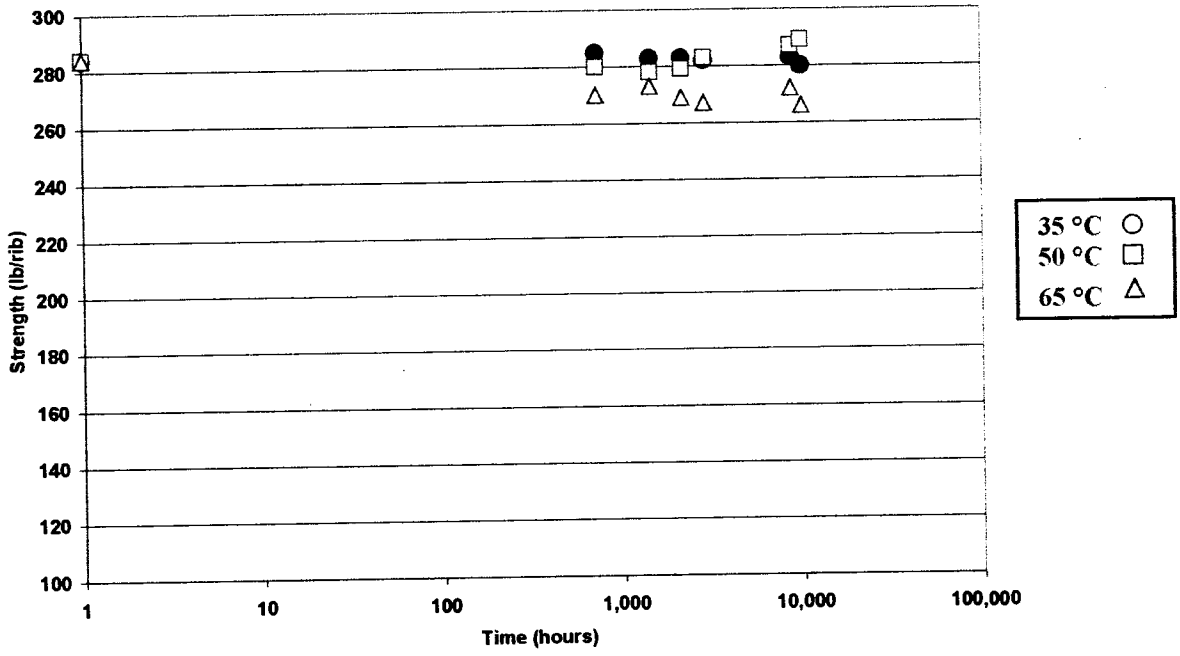

Figure 8.18 Durability plots for PET geogrids in seawater

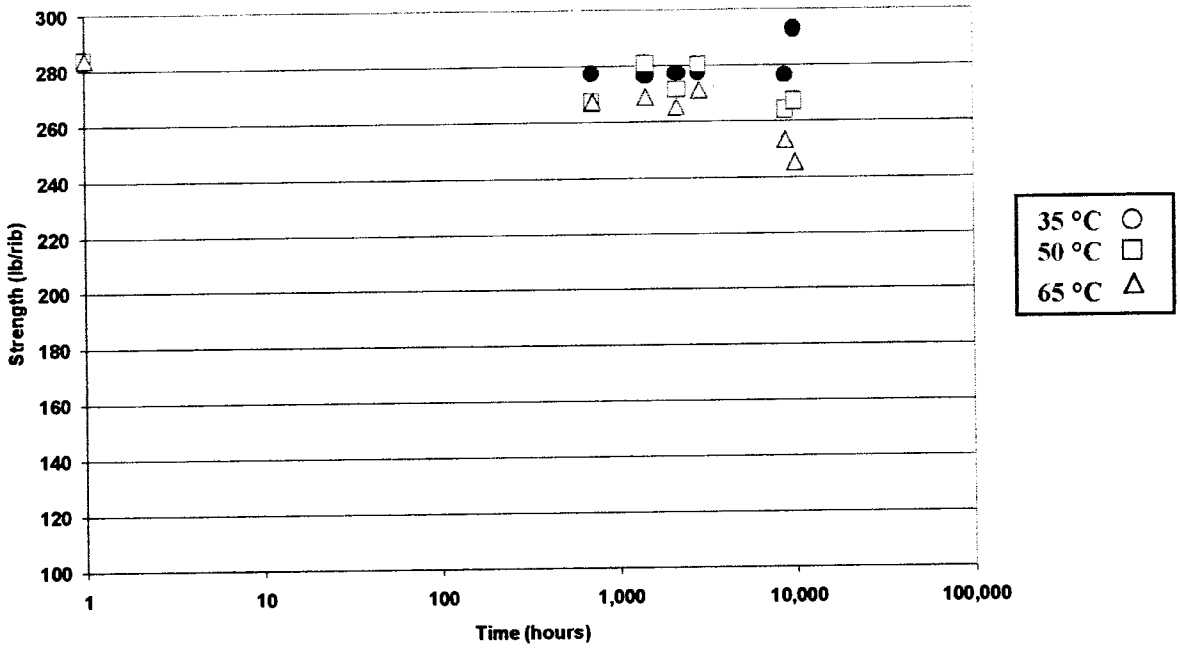

Figure 8.19 Durability plots for PET geogrids in water

CHAPTER 9

DURABILITY ANALYSIS

9.1 REGRESSION ANALYSIS

Regression analysis was carried out for the durability data obtained, to plot the durability curves presented in Figs. 9.1 -9.9. Exponential trend lines and equations were selected since they best fitted the durability data. It can be observed that the degradation in the HDPE specimens is very small as in the case of durability plots; some of the durability curves (e.g. seawater) even showed an increase in strength at the 65 °C temperature. This shows that the effect of environmental exposure on the HDPE geogrids is negligible. PET specimens showed some degradation, which seemed to be very similar for the different solutions, indicating hydrolysis as the main cause.

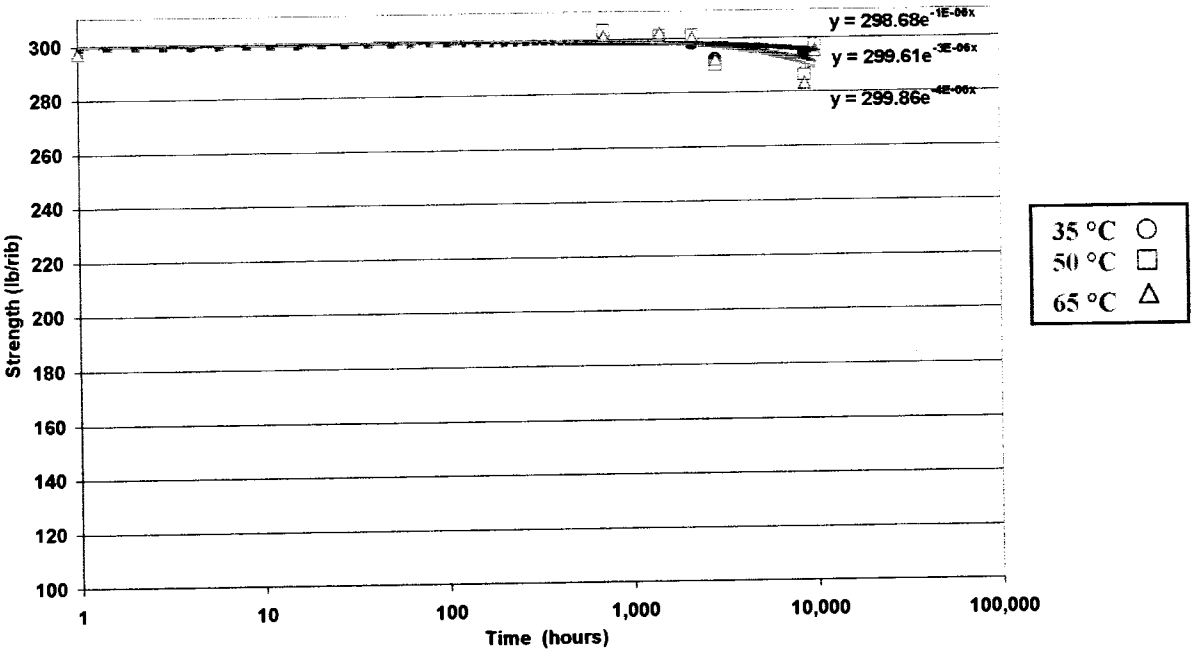

Figure 9.1 Durability curves for HDPE geogrids in calcareous solution

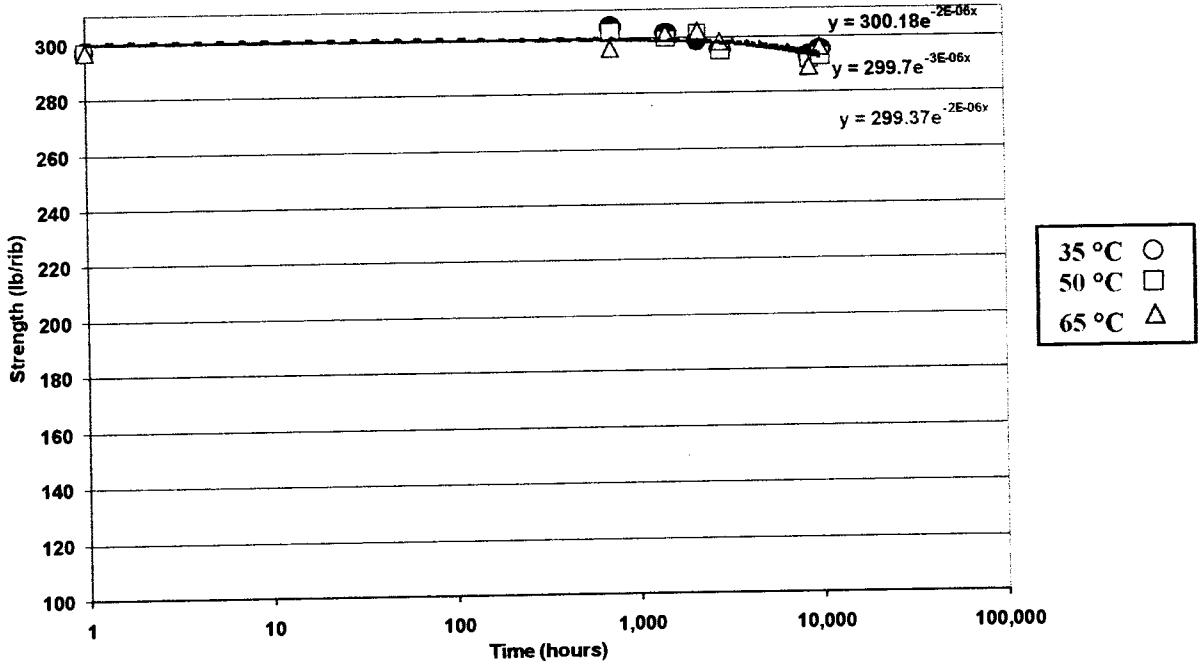

Figure 9.2 Durability curves for HDPE geogrids in phosphate solution

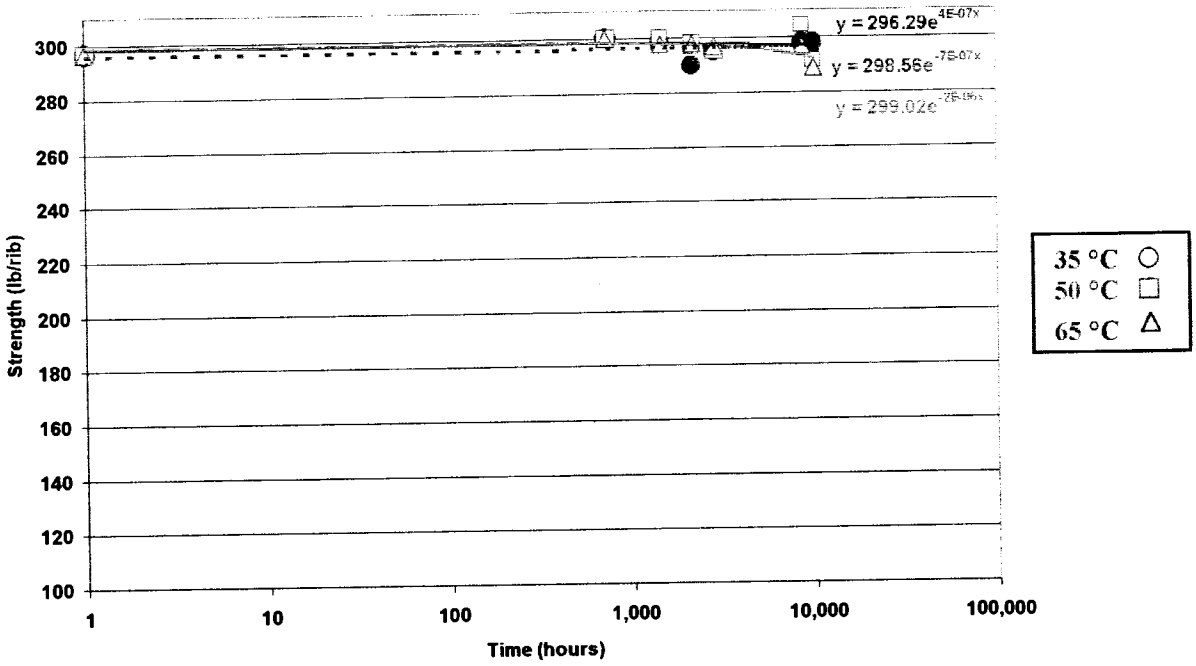

Figure 9.3 Durability curves for HDPE geogrids in limerock

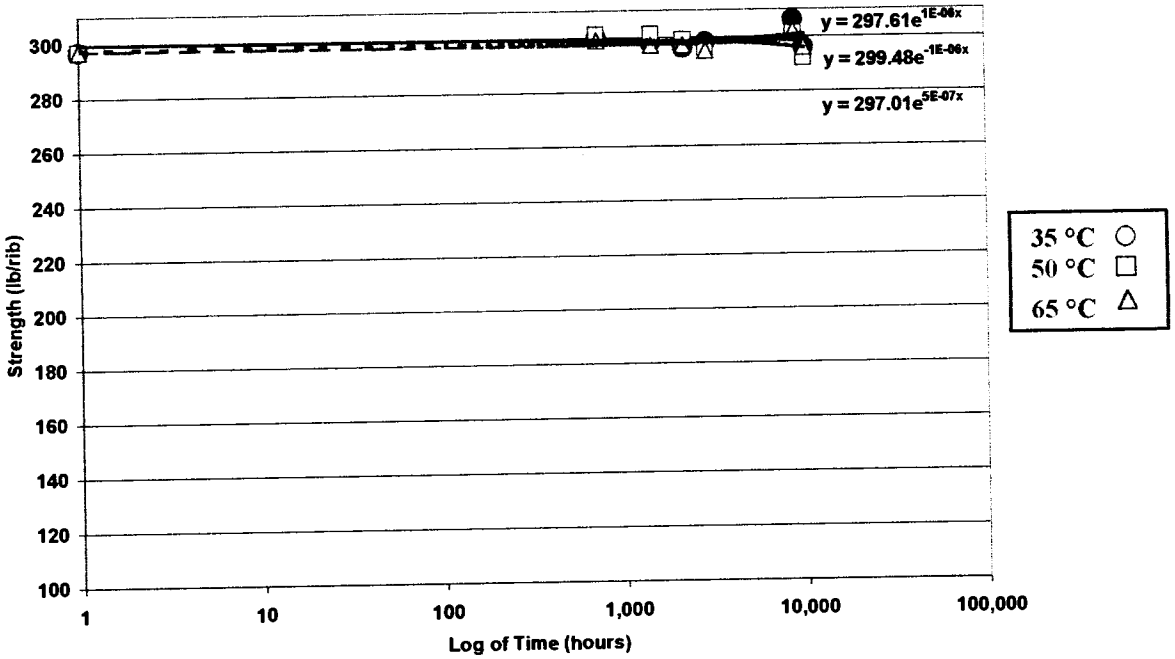

Figure 9.4 Durability curves for HDPE geogrids in seawater

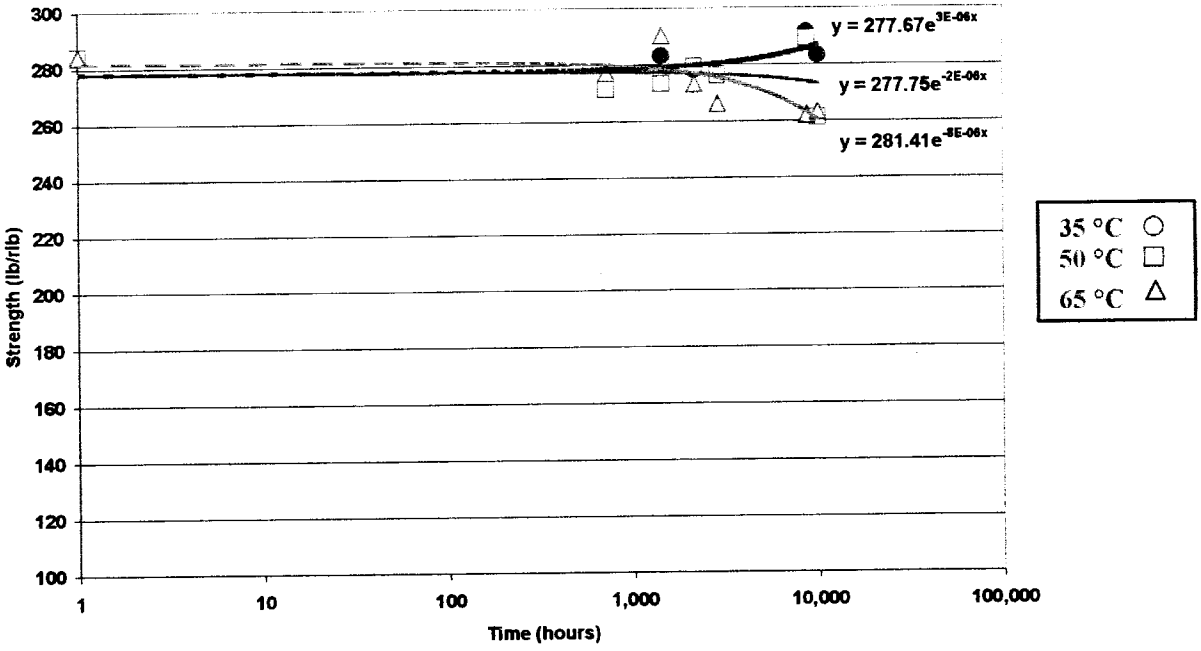

Figure 9.5 Durability curves for PET geogrids in calcareous solution

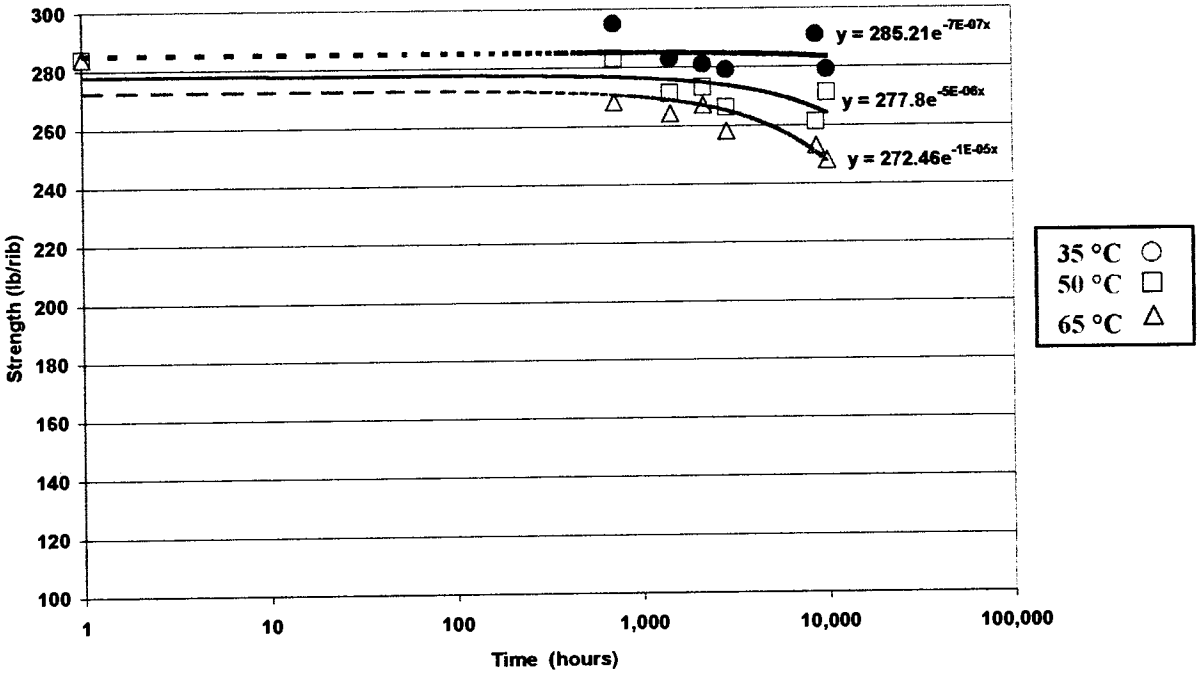

Figure 9.6 Durability curves for PET geogrids in phosphate solution

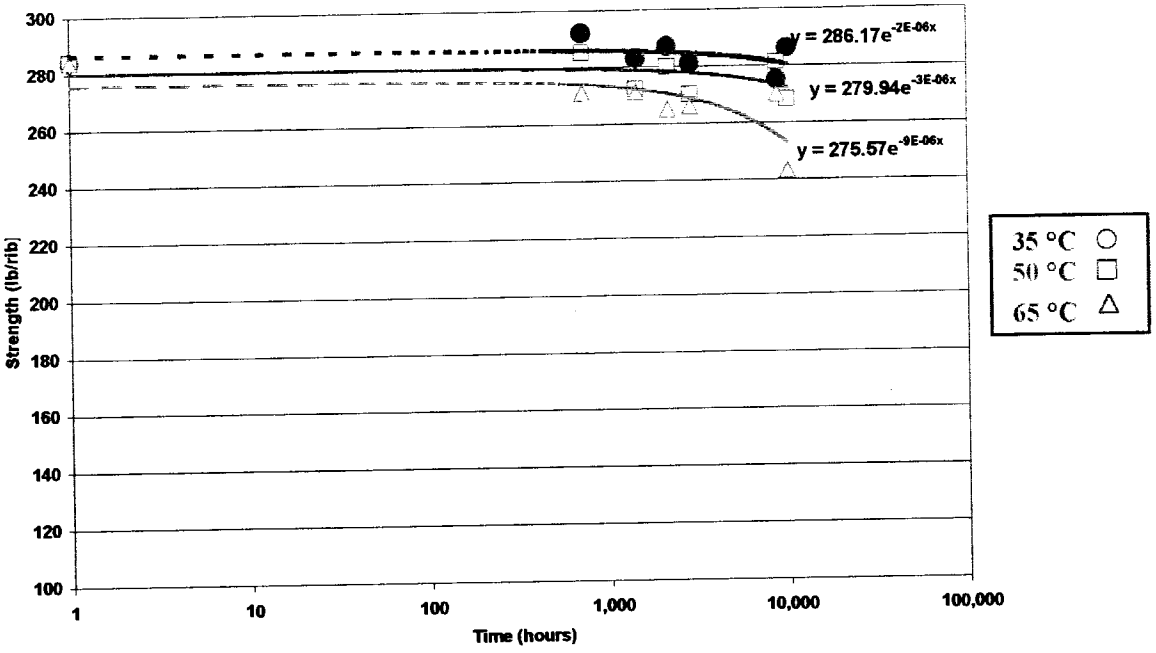

Figure 9.7 Durability curves for PET geogrids in limerock

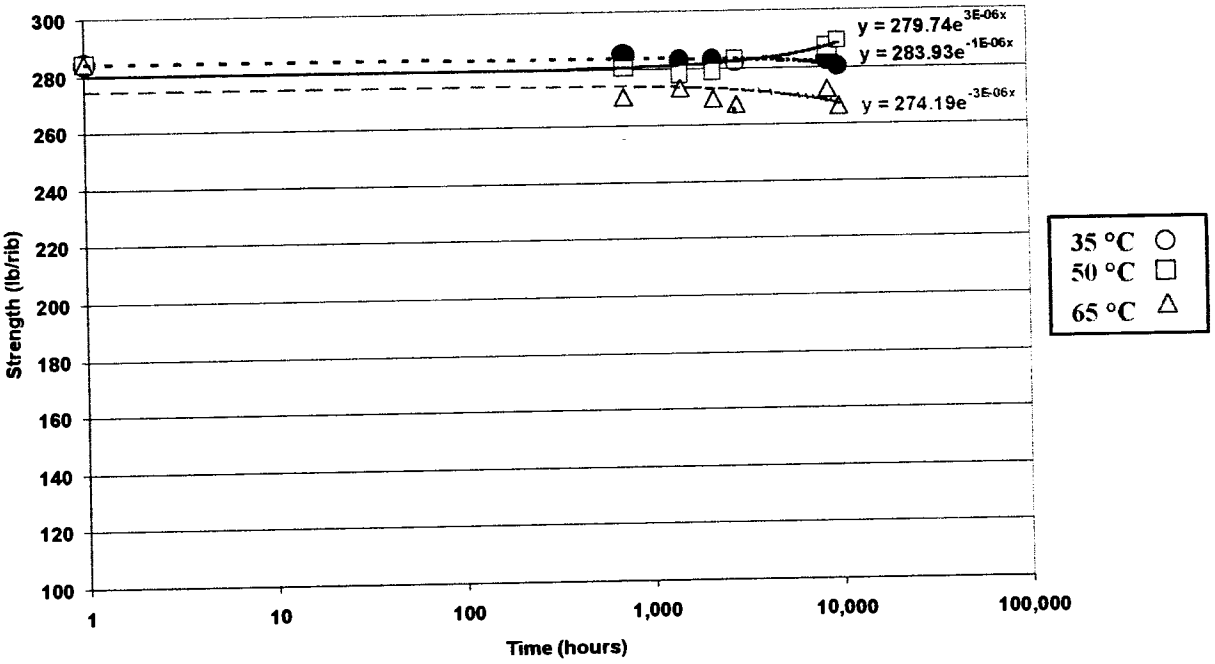

Figure 9.8 Durability curves for PET geogrids in seawater

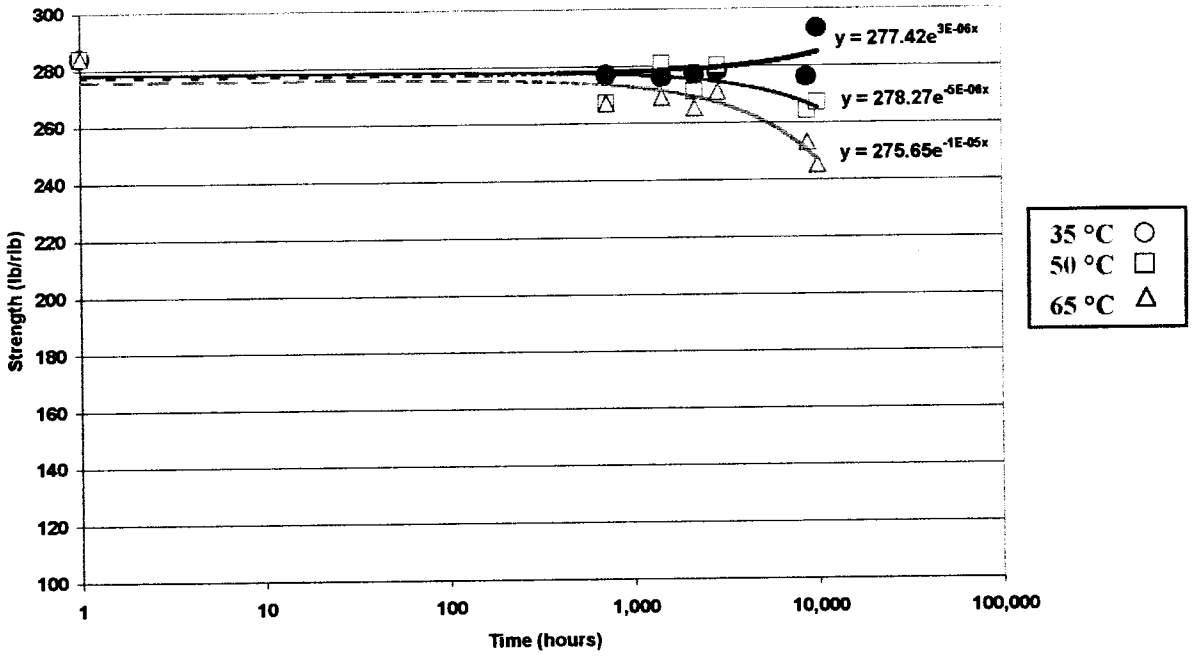

Figure 9.9 Durability curves for PET geogrids in water

9.2 ARRHENIUS MODELING

The arrhenius method was applied to find the expected time to a specific property retain in the specimen, figs. 9.10 to 9.19 show the property retained for the different exposures. It can be observed that HDPE specimens basically retain the whole property, while for PET specimens there is some small loss of strength mainly for the 65° C exposure. It can be notice that there is a large variability from specimen to specimen for the PET geogrids. This variability is greater than the differences due to the different exposures.

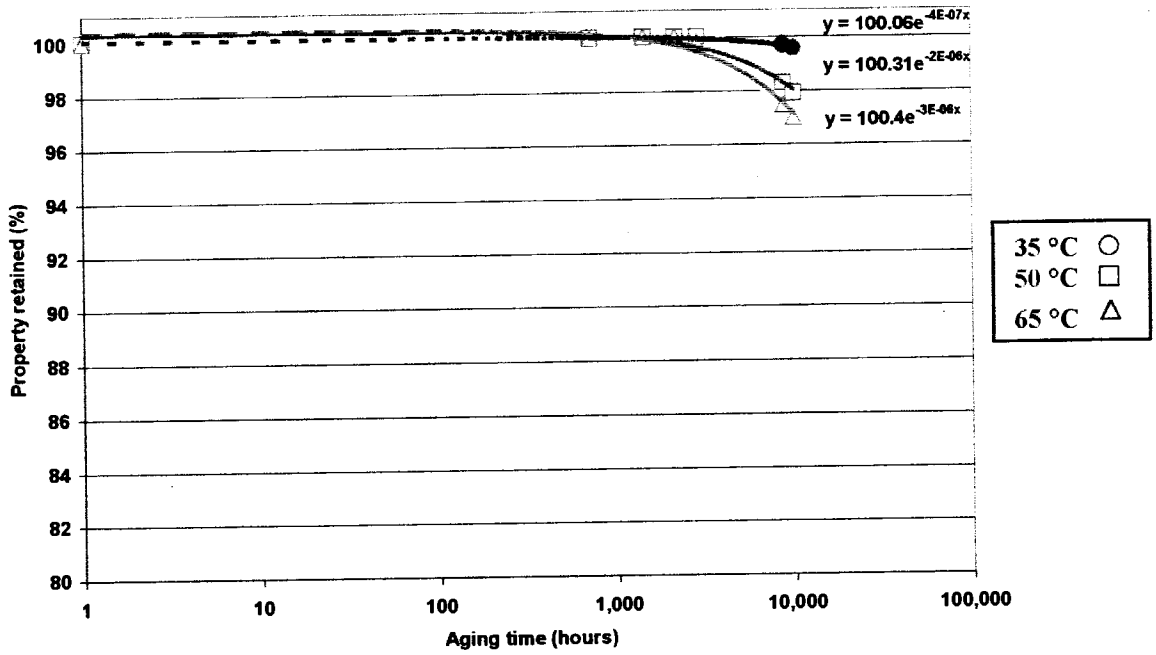

Figure 9.10 Property retained curves for HDPE geogrids in calcareous solution

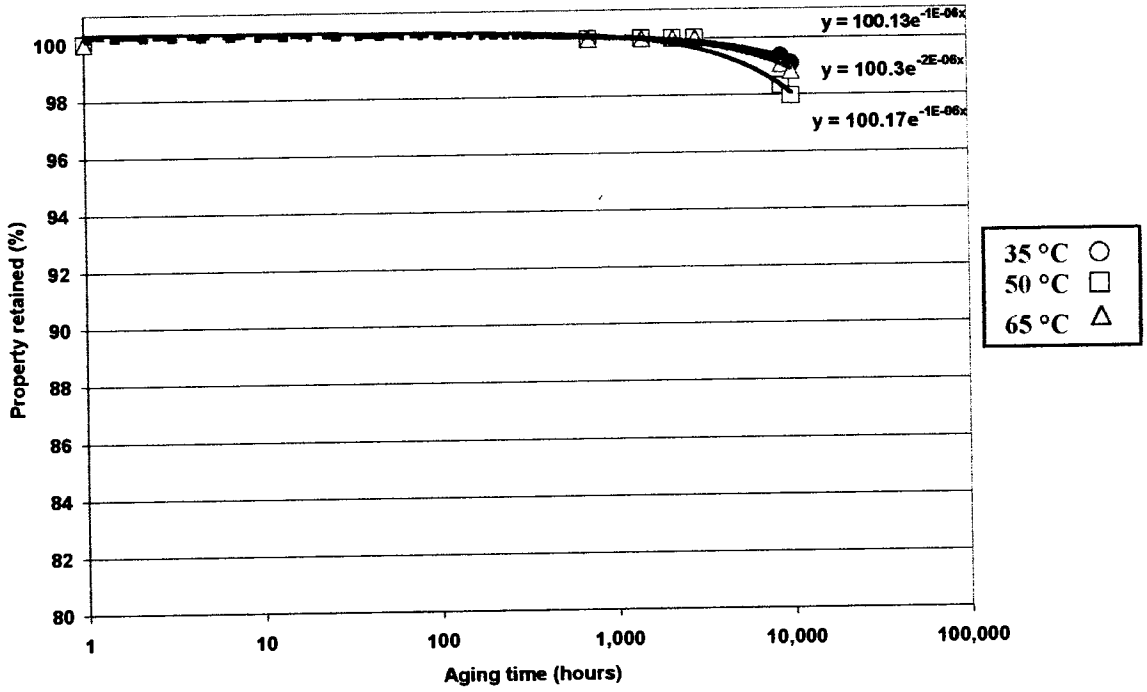

Figure 9.11 Property retained curves for HDPE geogrids in phosphate solution

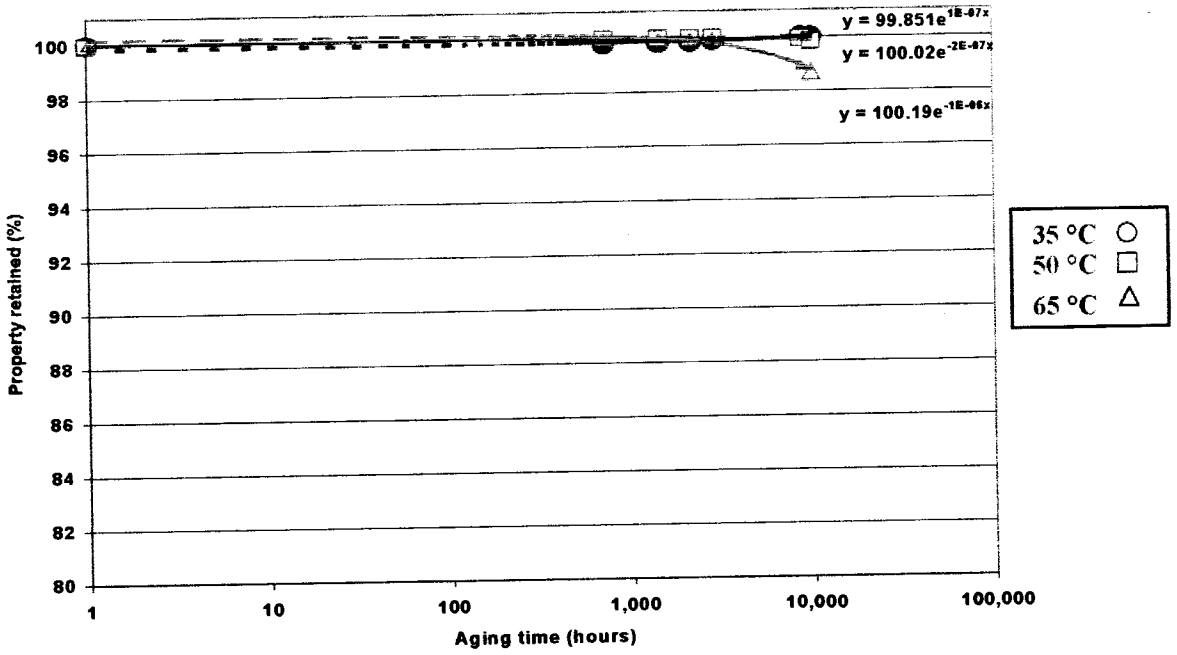

Figure 9.12 Property retained curves for HDPE geogrids in limerock

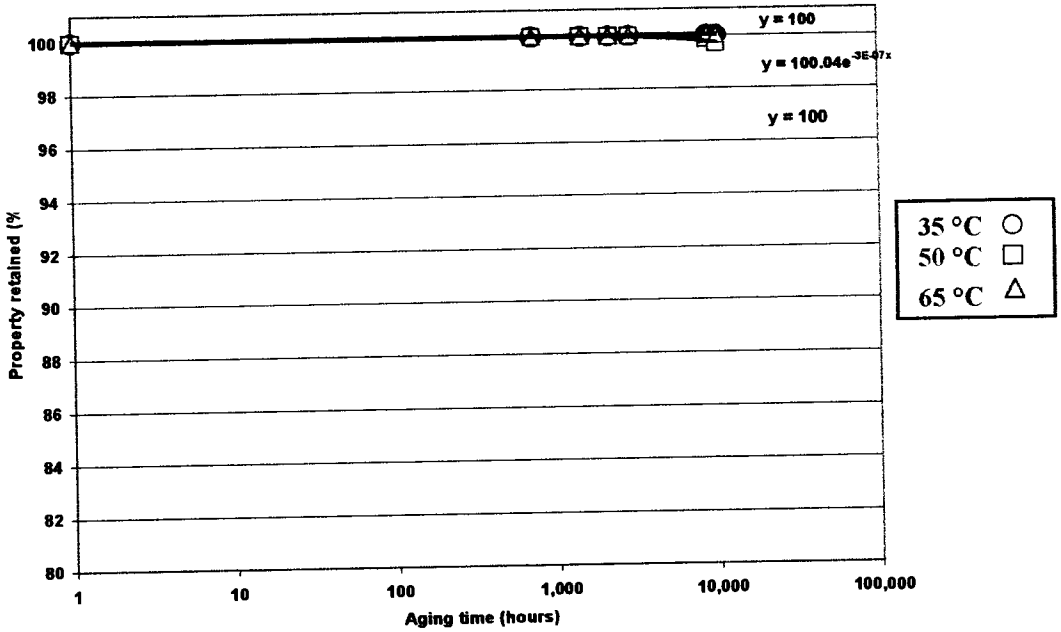

Figure 9.13 Property retained curves for HDPE geogrids in seawater

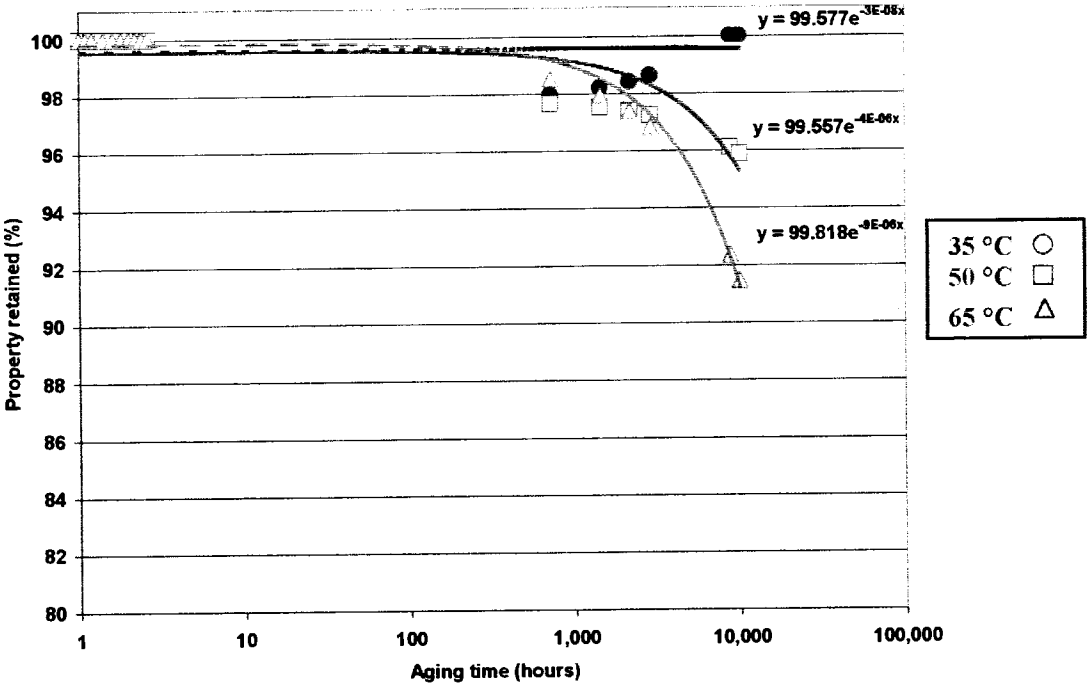

Figure 9.14 Property retained curves for PET geogrids in calcareous solution

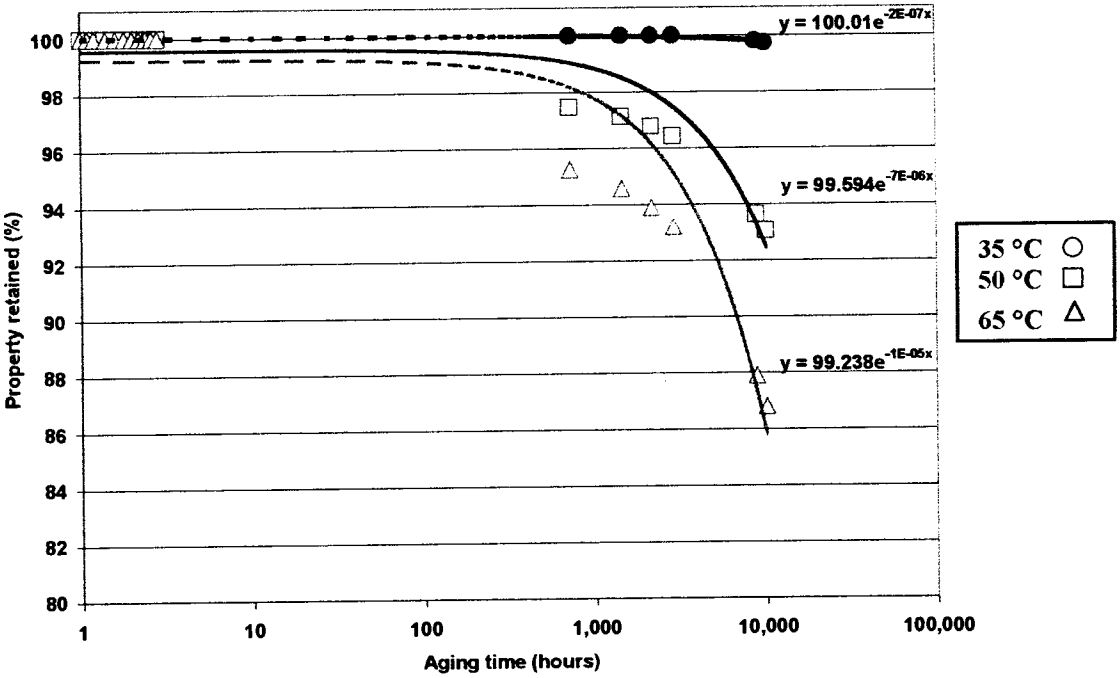

Figure 9.15 Property retained curves for PET geogrids in phosphate solution

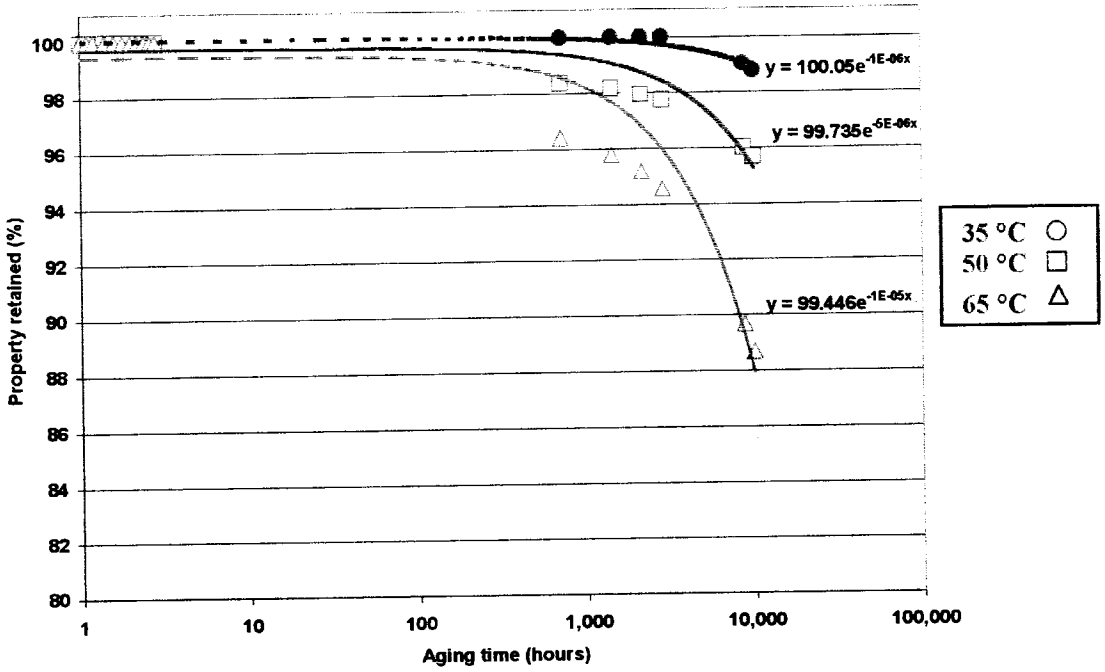

Figure 9.16 Property retained curves for PET geogrids in limerock

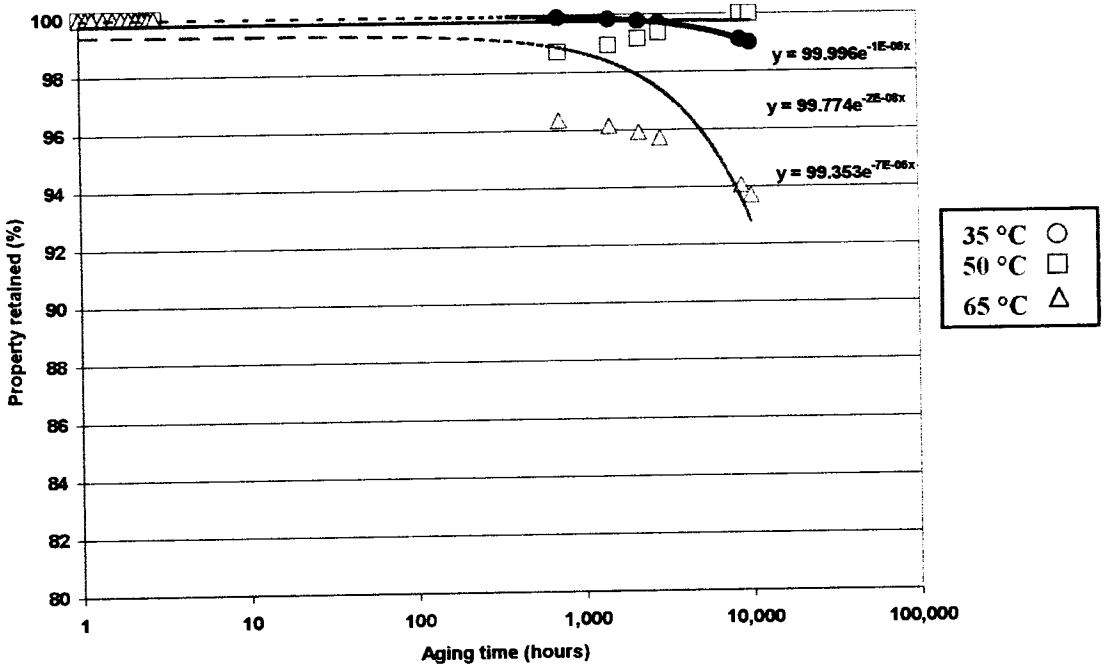

Figure 9.17 Property retained curves for PET geogrids in seawater

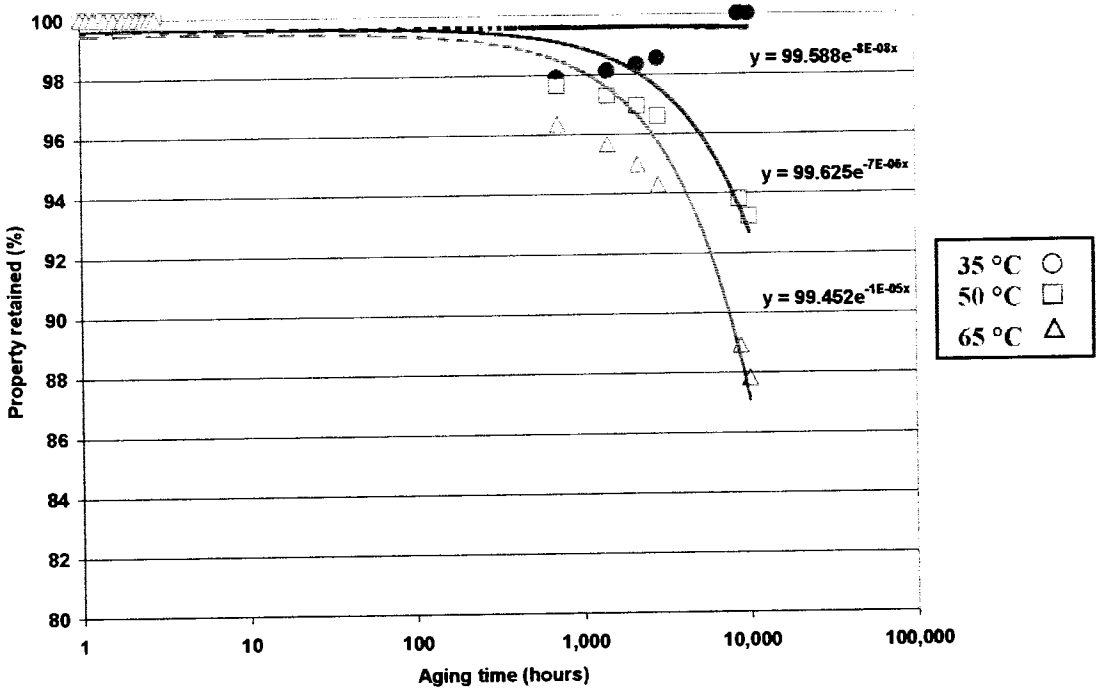

Figure 9.18 Property retained curves for PET geogrids in water

To improve the regression analysis for PET specimens, ten fictitious points were added for the first 3 hours assuming 100% property retained which is reasonable for a long-term time frame of 10,000 hours.

The property retained curves were obtained by using the equations obtained in the regression analysis for the durability curves. The value of the time was substituted in the equation to find the amount of degradation in the specimen.

Example:

For the calcareous solution at 35° C, the equation shown in fig. 9.1 is as follows:

$$y = 298.68e\text{-}1E\text{-}06x \quad (9.1)$$

where

y = strength (lb./rib)

x = time in (hours)

this equation was put into Table 8.1 in column 2.

Table 9.1 Property retained (%) for HDPE geogrids in calcareous solution

Temperature	35°C	50°C	65°C
Time	Strength lb./rib		
720	298	299	299
1440	298	298	298
2160	298	298	297
2880	298	297	296
8760	296	292	290
10000	296	291	288
Time	Property Retained (%)		
1	100.0	100.0	100.0
720	100.0	100.0	100.0
1440	100.0	100:0	100.0
2160	100.0	100.0	100.0
2880	100.0	100.0	99.8
8760	99.7	98.3	97.5
10000	99.6	97.9	97.0

The tables for the other exposures were obtained in a similar way. The property retained curves were obtained from the results given in the lower part of Table 9.1. The next step for plotting the Arrhenius curves was to tabulate the reaction rate vs. the inverse of the temperature in degrees Kelvin ranging from 65° C to 35° C . In Column 2 of Table 9.2 gives the reaction rate, which is the inverse of the time at which the corresponding

property retained, is reached. This is obtained from the equations for in the property retained curves.

Example

For the calcareous solution at 35° C, the equation shown in Fig. 9.10 is as follows:

$$y = 100.06e\text{-}4E\text{-}07x \qquad (9.2)$$

where

y = property retained (%)

x = aging time (hours)

Substituting for y gives

$$x = \ln(y/100.06)/(-4E\text{-}7) \qquad (9.3)$$

This is the equation used to obtain the values for column 2 in Table 9.2. For HDPE geogrids, only 99% property retained was used since this is the largest degradation encountered in the time of exposure (10,000 hours). As it observed in Table 9.1, the results are only for the calcareous and phosphate exposures because the limerock exposure at 35°C and 50°C did not reach 99% property retained, and for the seawater exposure the 99% property retained was not reached for any of the three temperatures. For the PET specimens the 99, 97 and 95% property retained values are presented in Tables 9.3 to 9.5.

Table 9.2 Reaction Rate (1/t) vs 1/Temperature for 99% life property for HDPE geogrids

1/Temperature (K)	1/ Aging time (Reaction rate)
	Calcareous
0.00296	0.000213639
0.00310	0.000152143
0.00325	

Table 9.3 Reaction Rate (1/t) vs 1/Temperature for 99% life property for PET geogrids

1/Temperature (K)	1/ Aging time (1/t) (Reaction rate)				
	Calcareous	Phosphate	Limerock	Seawater	Water
0.00296	0.001093736	0.004164662	0.002224727	0.001966671	0.002195262
0.00310	0.00071295	0.001170163	0.000675966		0.001112296
0.00325					

Table 9.4 Reaction Rate (1/t) vs 1/Temperature for 97% life property for PET geogrids

1/Temperature (K)	1/ Aging time (1/t) (Reaction rate)				
	Calcareous	Phosphate	Limerock	Seawater	Water
0.00296	0.000314273	0.000438404	0.000401545	0.000292054	0.000400575
0.00310	0.000153732	0.000265243	0.000179819		0.000262151
0.00325					

Table 9.5 Reaction Rate (1/t) vs 1/Temperature for 95% life property for PET geogrids

1/Temperature (K)	1/ Aging time (1/t) (Reaction rate)				
	Calcareous	Phosphate	Limerock	Seawater	Water
0.00296	0.000181922	0.000229126	0.000218637	0.000156242	0.000218349
0.00310		0.000148226	0.000102797		0.000147256
0.00325					

For HDPE we see that only the calcareous solution is tabulated this is because 99% of property retained was not reach in any of the other solutions. For PET specimens, the blank cells in tables 9.3 to 9.5 mean that the value of 1/t is smaller than 0.0001 or that the time to reach a specific property retained is more than 10,000 hours. This makes the Arrhenius modeling inaccurate, for this reason it is not possible to include those values in the calculations.

The Arrhenius curves are presented in Figs. 9.19 to 9.22. In Fig. 9.19 only the curve for HDPE geogrids subjected to calcareous exposure is presented for 99% property retained since is the only one with enough data due to the small degradation of HDPE.

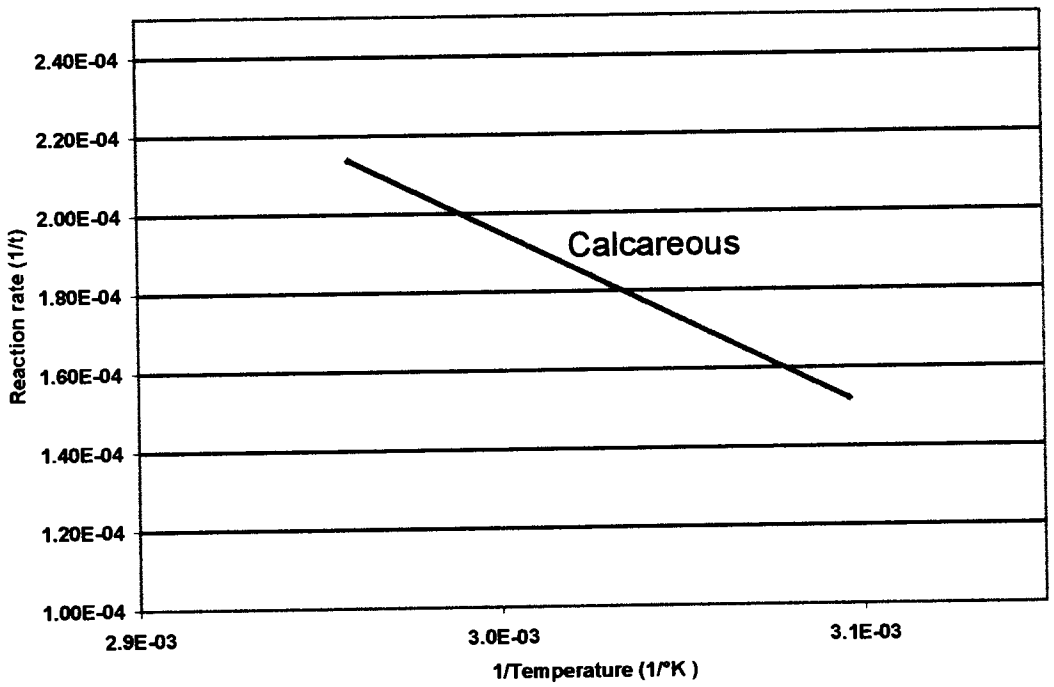

Fig. 9.19 Arrhenius curves for 99% of property retained for HDPE geogrids

In Fig. 9.20 the Arrhenius curves are presented for PET geogrids in all the exposures, except seawater, for which the 50° C exposure showed an increase in property retained and the 35° C exposure did not reach 99% of property retained in 10,000 hours. The same was the case for the curves for 97% of property retained. Also, for the calcareous exposure at 50° C the property retained did not reach 95%. All the Arrhenius curves were plotted using only the data for 55° C and 65° C temperatures, since for 35° C the degradation was minimal in all cases and did not even reach the 99% property retained.

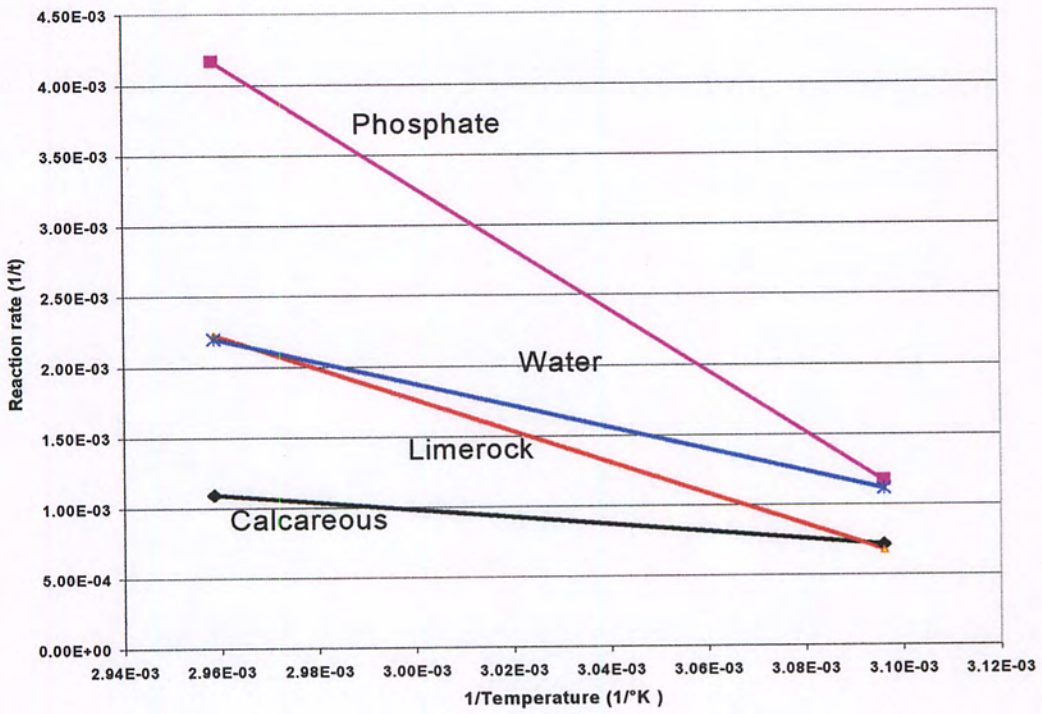

Fig. 9.20 Arrhenius curves for 99% of property retained for PET geogrids

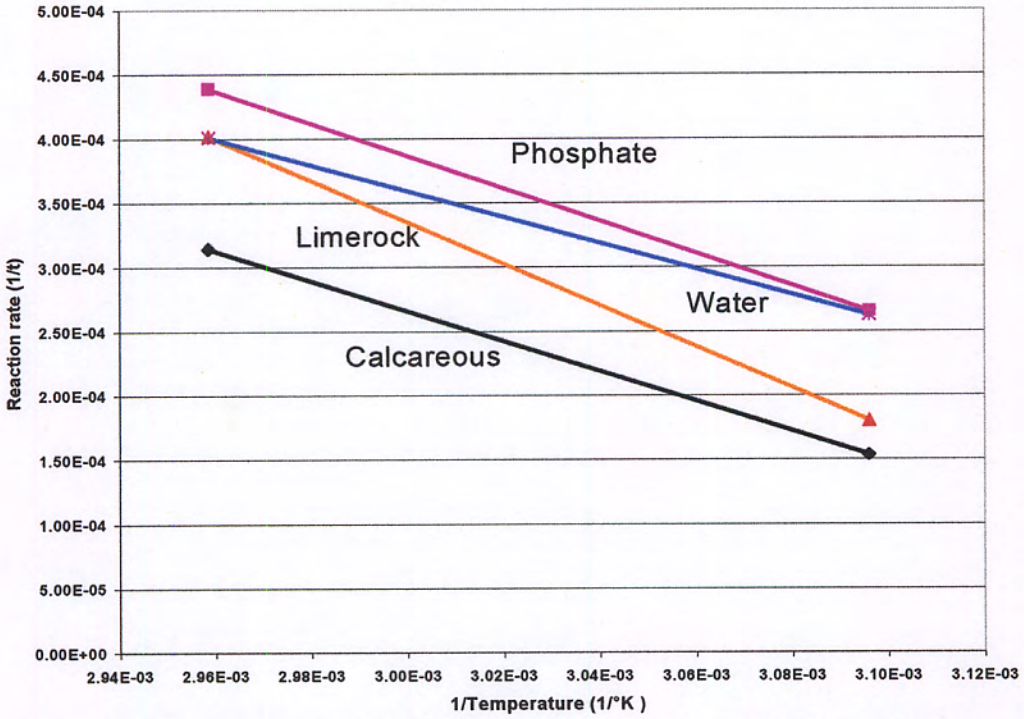

Fig. 9.21 Arrhenius curves for 99% of property retained for PET geogrids

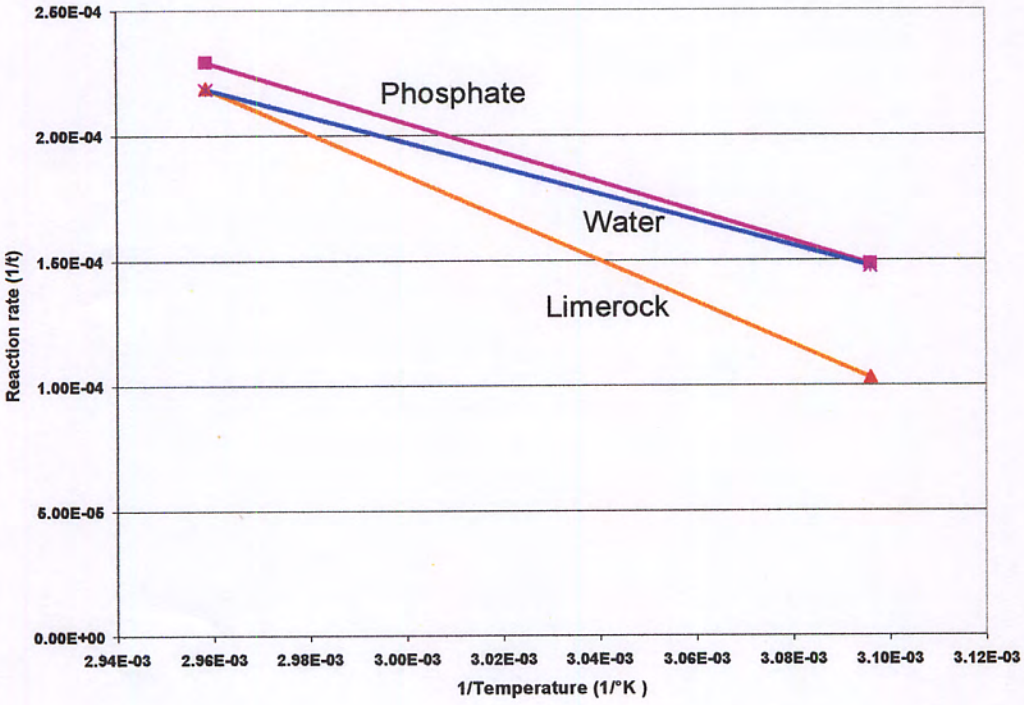

Fig. 9.22 Arrhenius curves for 99% of property retained for PET geogrids

Equation 9.4 gives the Arrhenius equation [Koerner, 1998]:

$$\frac{r_{T\text{-test}}}{r_{T\text{-site}}} = e^{-Eact/R[1/T\text{-test} - 1/T\text{-site}]} \qquad (9.4)$$

Where:

Eact/R = slope of Arrhenius plot,

T-test = incubated (high) temperature, in °K,

T-site = site-specific (lower) temperature, in °K,

r = reaction time,

Eact = effective activation energy, J/mole, and

R= universal gas constant, 8.314 J/mole

Eqn. 9.4 can also be written as follows:

$$\ln(r_{T\text{-test}} / r_{T\text{-site}}) = (Eact/R)(1/T\text{-test}-1/T\text{-site}) \qquad (9.5)$$

or

$$\frac{Eact}{R} = \frac{\ln(1/t1) - \ln(1/t2)}{(1/T1) - (1/T2)} \qquad (9.6)$$

Where:

t = time, hour,

T = temperature, °K

In Table 9.6 the first two columns show the calculated values required to obtain E_{act}/R . Column 3 gives the values of [1/T-test - 1/ T-site]. Column 4 gives the calculated values of the entire left term of the Arrhenius equation. Column 5 shows the time predicted for a specific property retained for the HDPE specimens. As indicated before only the calcareous exposure testing give enough data to predict the property retained.

Table 9.6 Calculation of time to reach 99% of property retained for HDPE geogrids at 20° C.

$\ln(1/t_1)-\ln(1/t_2)$	(1/T1) - (1/T2	$\frac{1}{\text{(T-test)}} - \frac{1}{\text{(T-site)}}$	$e^{-Eact/R[1/T\text{-test} - 1/T\text{-site}]}$	$r20°C = \frac{r_{T\text{-test}}}{e^{-Eact/R[1/T\text{-test} - 1/T\text{-site}]}}$
Calcareous				(YEARS)
0.339469433	-0.00014	-0.000454389	0.325405824	**1.6**

The same procedure was used for the PET specimens, for these specimens only the seawater did not provide enough data for 99 and 97% property retained. The same was the case for seawater and calcareous solution for the 95% property retained.

Table 9.7 Calculation of time to reach 99% of property retained for PET geogrids at 20° C.

$\ln(1/t_1)-\ln(1/t_2)$	(1/T1) - (1/T2)	$\frac{1}{\text{(T-test)}} - \frac{1}{\text{(T-site)}}$	$e^{-Eact/R[1/T\text{-test} - 1/T\text{-site}]}$	$r20°C = \frac{r_{T\text{-test}}}{e^{-Eact/R[1/T\text{-test} - 1/T\text{-site}]}}$
Calcareous				(YEARS)
0.427943721	-0.00014	-0.000454389	0.242857251	**0.4**
Phosphate				
1.269491881	-0.00014	-0.000454389	0.015019259	**1.8**
Limerock				
1.191246347	-0.00014	-0.000454389	0.019455006	**2.6**
Water				
0.679874618	-0.00014	-0.000454389	0.105561764	**0.5**

Table 9.8 Calculation of time to reach 97% of property retained for PET geogrids at 20° C.

$\ln(1/t_1)-\ln(1/t_2)$	(1/T1) - (1/T2)	$\frac{1}{\text{(T-test)}} - \frac{1}{\text{(T-site)}}$	$e^{-Eact/R[1/T\text{-test} - 1/T\text{-site}]}$	$r20°C = \frac{r_{T\text{-test}}}{e^{-Eact/R[1/T\text{-test} - 1/T\text{-site}]}}$
				(YEARS)
Calcareous				
0.715052553	-0.00014	-0.000454389	0.093968245	**3.9**
Phosphate				
0.502495621	-0.00014	-0.000454389	0.189790005	**1.4**
Limerock				
0.803367263	-0.00014	-0.000454389	0.07016751	**4.1**
Water				
0.42397907	-0.00014	-0.000454389	0.246062506	**1.2**

Table 9.9 Calculation of time to reach 95% of property retained for PET geogrids at 20° C

$\ln(1/t_1)-\ln(1/t_2)$	(1/T1) - (1/T2)	$\frac{1}{\text{(T-test)}} - \frac{1}{\text{(T-site)}}$	$e^{-Eact/R[1/T\text{-test} - 1/T\text{-site}]}$	$r20°C = \frac{r_{T\text{-test}}}{e^{-Eact/R[1/T\text{-test} - 1/T\text{-site}]}}$
				(YEARS)
Phosphate				
0.435530573	-0.00014	-0.000454389	0.236839534	**2.1**
Limerock				
0.754661738	-0.00014	-0.000454389	0.082431093	**6.3**
Water				
0.393922112	-0.00014	-0.000454389	0.27177893	**1.9**

Results that were possible to obtain seem adequate, except for phosphate exposure, for which the 97% degradation seemed to occur before the 99%. This is because the property retained curve for 65° C crosses basically the 99 and 97% of property retained simultaneously.

CHAPTER 10

DISCUSSION

10.1. INTRODUCTION

The ultimate load capacity of a geogrid, used as reinforcement in the reinforced soil structure, is mainly determined by the material properties, the geometry of the specimen, and the configuration of the test apparatus. The test specimen parameters are the geometry of the specimen, such as in-plane or out-of-plane transverse elements, orientation, tensile strength, extendibility, and creep behavior. For the pullout testing, the test soil parameters comprise the particle size, shape, gradation, relative density, dilatancy, and water content, for creep, creep rupture, durability and degradation the testing soil-water parameters include pH, composition of the different exposures, type of soil, load level and temperature. The test apparatuses of interest are based on the loading systems, the sample dimensions, exposure material containment, and the boundary conditions.

10.2 GENERAL TESTING METHODS

The design of a reinforced retaining wall with polymeric geogrids, or geotextiles, requires an appropriate testing procedure to evaluate the stress-strain properties of the reinforcement embedded in the soil and its long-term pullout performance.

For pullout there are two major testing methods: (1) displacement-rate controlled, and (2) load controlled. In the displacement rate controlled test (DCT), the test specimen is subjected to a constant pullout displacement rate, and the applied pullout load is recorded. This test procedure provides the interface parameters related to the short-term pullout performance, such as peak and residual pullout resistance, interface stiffness modulus, and front end displacement. In the load-controlled test (LCT), pullout loads are applied incrementally and maintained constant during the testing time. The strains along the geogrid specimen are measured, and the data interpretation yields time-dependent response parameters related to the long-term pullout performance. The pullout testing in this investigation is load-controlled.

For creep and creep rupture, the test procedure consists of the application of a constant load at a constant temperature for a specified time interval. There are two possible variations in the size of the specimen: i) the wide-width strip and ii) the single rib. These two methods are for tensile testing for durability. Creep testing is normally

carried out for unexposed specimens. In this study different exposures were used together with various temperatures.

For durability, there are two tensile strength methods, i) the wide-width strip method "ASTM D 4595-86" and ii) the Geogrid Rib Tensile Strength "GRI GG1-87" method.

In the wide-width strip method, the width of the specimen is greater than the length of the specimen; this is to avoid contraction effects. [ASTM D 4595-86].

In the Geogrid Rib Tensile Strength method (single rib), only one rib was tested, although the specimens were cut to three ribs and exposed to the solutions. Then at the time of testing, the two side ribs were cut, so that only the central rib was tested. This was done to avoid the contraction effects.

10.3 ANALYSIS PROCEDURES

There are many factors attributed to the pullout resistance of geogrid in the soil, such as i) the geometry and material properties of the test specimen (geogrid dimension, tensile strength, stiffness, creep and geometric shape), ii) the type and mechanical properties of soil (shear strength, relative density and confining pressure *etc.*), and iii) test procedures (loading system, boundary conditions and testing apparatus). A general

functional expression for the pullout resistance was proposed by Jewell *et al.* (1984) as follows:

$$P = 2LW\sigma_n' f_b \tan\phi \tag{10.1}$$

where

$$f_b = \alpha_b\left(\frac{\tan\delta}{\tan\phi}\right) + \alpha_b\left(\frac{B}{S}\right)\frac{1}{2\tan\phi}\left(\frac{\sigma_b'}{\sigma_n'}\right) \tag{10.2}$$

B thickness of bearing members

L embedment length

P pullout load

S spacing between bearing members

W embedment width

α_b fraction of geogrid width over which the bearing surface extends

α_s fraction of geosynthetic surface area that is solid

δ friction angle between soil and geosynthetic surface

ϕ friction angle of soil

σ_b' effective bearing stress between soil and geogrid

σ_n' normal effective stress between soil and geosynthetic

This approach forms the basis of the recommendations for the calculation of pullout resistance advocated by the US Federal Highways (1990).

Christopher *et al.* (1990) developed another general relationship for the pullout resistance per unit width of reinforcement as follows:

$$P = 2LW\sigma_n^{/}F^{*}\alpha \tag{10.3}$$

W embedment width

where $F^{*}\alpha$ is an interaction factor that describes the interface bond. For a geogrid specimen, $F^{*}\alpha$ is equivalent to the term of $f_s tan\phi$. The value of $F^{*}\alpha$ is dependent on the type of geogrid, the magnitude of the confining pressure, and the relative displacement between geogrid and soil.

The pullout resistance can also be expressed as a dimensionless coefficient of sliding:

$$f = \frac{\tan\delta}{\tan\phi} = \frac{\tau}{\sigma_n^{/}\tan\phi} = \frac{P_{max}}{2LW(\sigma_n^{/}\tan\phi + c)} \tag{10.4}$$

so

$$P_{max} = 2LW(\sigma_n^{/}\tan\phi + c)f \tag{10.5}$$

For cohesionless sand, $c = 0$, therefore,

$$P_{max} = 2LW(\sigma_n^{/}\tan\phi)f \tag{10.6}$$

f coefficient of frictional interaction

P_{max} maximum pullout capacity of the reinforcement embedded in the soil

The coefficient, *f*, is the ratio of the shear force developed along the interface of the soil and reinforcement to the shear strength of the soil. It is a critical value in the calculation of the bond length of the geogrid reinforcement.

FHWA (Federal Highway Administration, 1985) has provided the estimated field values for the coefficient of sliding for geogrids in specific granular backfills:

Table 10.1 Estimated field values for the coefficient of sliding for geogrids

f	geogrid open area (%)
0.5	80% or more
0.7	51% - 70% or more
0.6	50% or less

From the test results, the value of the sliding coefficient is about 1.02-1.12 for sand and limerock. This is much higher than the values given by FHWA (Geogrid UX16000SB has an open area of 60%). This can be explained by the values recommended by the FHWA accounting for capacity reduction factors in Load Resistance Factor Design (LRFD).

For creep and creep rupture test data; regression analysis was carried out with logarithmic, power and polynomial trend lines, and equations formulated for the sets of data. The findings showed that HDPE is greatly affected by the increase in temperature

and load levels, with temperature being very significant. For the PET specimens, the amount of creep is not as large and the temperature and the load level increases seem to have similar effects on the specimens. Creep rupture occurred only for the HDPE specimens. All the specimens exposed to load levels of 50% ultimate load broke. Even specimens exposed to 40% of the ultimate load, with 55 and 65° C exposures, also broke. This can be attributed to defects in the specimens or poor clamping.

For durability testing, the Arrhenius method was used; Equation 10.7 gives the Arrhenius equation [Koerner, 1998]:

$$\frac{r_{T\text{-test}}}{r_{T\text{-site}}} = e^{-Eact/R[1/T\text{-test} - 1/T\text{-site}]} \qquad (10.7)$$

where

Eact/R = slope of Arrhenius plot,

T-test = incubated (high) temperature, in °K,

T-site = site-specific (lower) temperature, in °K,

r = reaction time,

Eact = effective activation energy, J/mole, and

R= universal gas constant, 8.314 J/mole

Eqn. 9.7 can also be written as follows:

$$\ln(r_{T\text{-test}}/ r_{T\text{-site}}) = (Eact/R)(1/T\text{-test}-1/Tsite) \qquad (10.8)$$

or

$$\frac{Eact}{R} = \frac{\ln(1/t1) - \ln(1/t2)}{(1/T1) - (1/T2)} \qquad (10.9)$$

where: t = time, hour, and, T = temperature, °K

The term E_{act}/R was obtained using the slopes of the Arrhenius plots, with these values, the site specific times for property retained at specified temperatures can be determined by using Eqn. 10.7, the time required for a specimen to reach a specified amount of degradation, was quantified as property retained or remaining % tensile strength of the specimen.

From the results obtained, it can be seen that the HDPE specimens retained most of their strength; the Arrhenius method could be used only for the calcareous exposure, since none of the other exposures led to the 99% property retained state, except the 65° C exposure. For PET geogrids in all the exposures, except seawater for which the 50° C exposure showed an increase in property retained and the 35° C exposure, the specimens did not reach 99% of property retained in 10,000 hours. The same was the case for the curves for 97% of property retained. Also, for the calcareous exposure at 50° C, the property retained did not reach 95%. All the Arrhenius curves were plotted using only the data for 55° C and 65° C temperatures, since for 35° C, the

degradation was minimal in all cases and did not even reach the 99% property retained value.

10.4 PRACTICAL DESIGN APPLICATIONS

For the reinforced earth design, the sliding coefficient is very dependent on the type of geogrid, the spacing of layers, and the length of the reinforcement. In the reinforced soil slope design (Figs 10.1 and 10.2), the bond length required is critical to mobilize the allowable design strength. Both the sliding coefficient and the bond length required are based on the data from the pullout testing.

The ultimate pullout load must be less than or equal to the allowable long-term pullout design load. The safety factor of 1.5 (FHWA, 1991) is applied to the bond length in the design. For reinforced soil slope and embankment applications, the strains are not the controlling factor but the bond length. These types of structures can tolerate a larger deformation and more movement. The geogrid PET is a very good choice for these applications because of low cost and easy handling and high resistance to creep and creep rupture.

In reinforced earth wall design, the deformation and displacement control is very important for the structure performance. The limiting strain becomes the critical design factor. For design applications, greater density of reinforcement is highly recommended

for both geogrids HDPE and PET, and it is important to evaluate and verify the resistance factors for creep, durability, and construction damage.

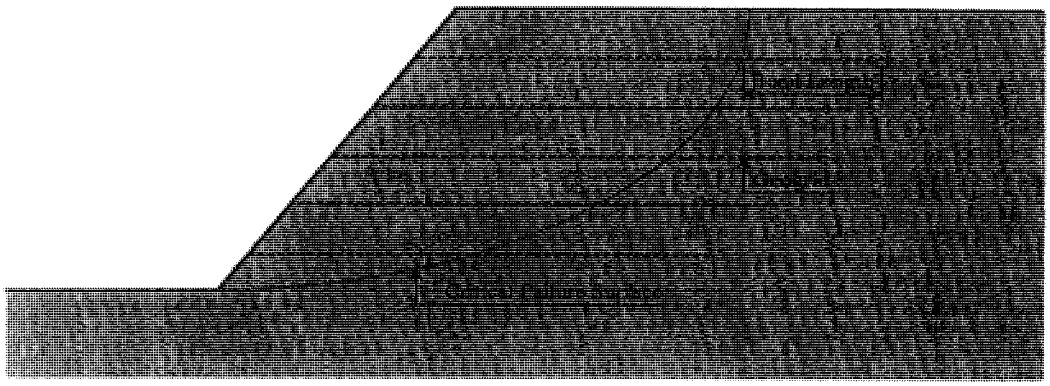

Fig. 10.1 Design controlled by bond length

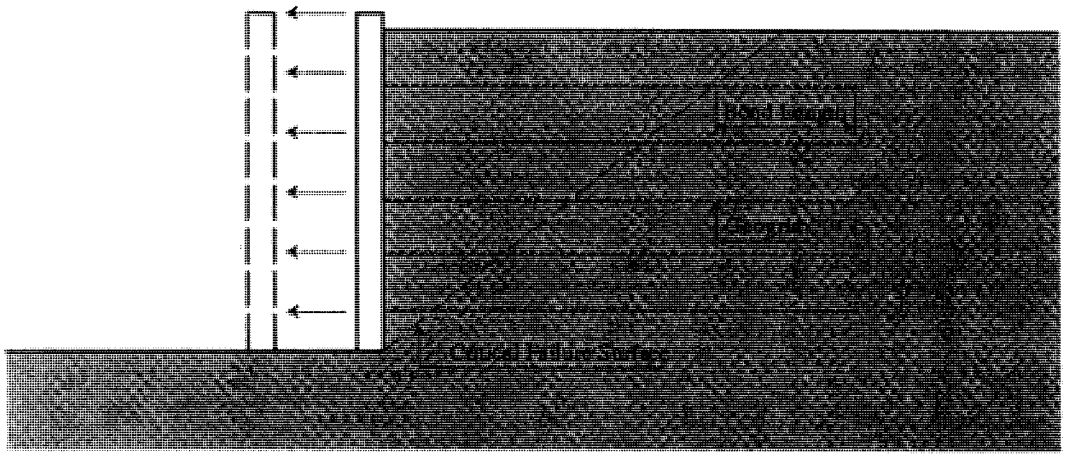

Fig. 10.2 Design controlled by deformation

CHAPTER 11

CONCLUSIONS

11.1 PULLOUT

11.1.1 INTRODUCTION

In this section, some interpretations are made to obtain soil-geogrid interaction factors for engineering design. A comprehensive comparison is presented to evaluate the working performance of the two kinds of geogrids, HDPE and PET. The analysis is mainly for the pullout resistance capacity under different testing conditions, sand (saturated and unsaturated), limerock (saturated and unsaturated).

11.1.2 ELASTICITY OF GEOGRIDS HDPE AND PET

The HDPE geogrid is made of stiff low-creep-sensitivity polymers. It has a relatively higher modulus of elasticity compared to the PET geogrid. This is the reason why under the same pullout load, the same soil, and the same testing condition, the HDPE geogrid experiences a smaller strain at all the four gage locations. The PET geogrid, on the other hand, displays a very uniform deformation capacity. The pullout transfers evenly to the rear part. During the pullout process, the movement of the test specimen was very smooth and gentle, while the pullout characteristic pattern of the HDPE geogrid demonstrated some degree of discontinuity and suddenness. This is attributed to its high stiffness and specific profile.

11.1.3 EFFECTIVENESS OF SOIL GRADATION ON GEOGRIDS

The pullout resistance developed between geogrid specimen and soil is composed of two parts; one is the frictional force at the two surfaces between geogrid specimen and soil, the other the bearing force at the transverse ribs. The geometric difference in the geometry of the geogrids HDPE and PET resulted in difference in performance based on the embedding soil. For the PET geogrid, the open area is relatively small, with not much protruding contour in geometry; the pullout resistance derived from interface friction provides the larger resistance compared to bearing. In contradistinction, for the HDPE geogrid, the bearing resistance component takes most of the pullout load.

Under unsaturated working conditions, the geogrid HDPE has a sliding coefficient of 1.05 in coarser soil with good gradation, compared to 1.02 for the finer sand specimen. In contrast for the PET geogrid, the sliding coefficient in coarser soil condition was 1.08, but for the finer soil condition, the sliding coefficient increased to 1.12.

Based on the tests and theoretical analysis, the PET geogrid has better pullout resistance performance than the HDPE geogrid, when used in fine sand (sliding coefficient is 1.12 under unsaturated working condition). Since fine sand can provide more contact surface, a larger friction resistance is mobilized. On the other hand, for the HDPE geogrid, a coarser sand with good gradation is the better choice (sliding coefficient is 1.05 under unsaturated working condition).

11.1.4 SATURATED AND UNSATURATED CONDITIONS

The effect of water on the pullout can be divided into two major categories. One is the reduction of effective stress, the other the effect of lubrication. The reduction will depend on the water level above the reinforcement. The pore water pressure can be excessive for fine granular soils with low permeability. However, the lubrication effect is very complicated, it depends on a variety of factors, such as the geogrid type, geogrid geometry, and confining pressure. The experimental results are the most effective to determine the reduction factor by comparison of the sliding coefficients.

For a PET geogrid in limerock, the sliding coefficient was 1.08 under the unsaturated testing condition, and 0.669 under the saturated condition. This gives a 38.1% reduction due to the wetting effect. Similarly, the sliding coefficient for test specimen PET in sand was 1.12 in the unsaturated condition, and 0.688 under saturated condition. From the test results, it can be inferred that the wetting condition causes a 38.6% decrease in the resistance.

For the test specimen HDPE in limerock, the sliding coefficient was 1.05 in the unsaturated condition and 0.758 under the saturated condition. The decrease is only 27.8%. In sand, the sliding coefficient was 1.02 under the unsaturated condition, and 0.729 under the saturated condition, with a 28.5% reduction.

For fine sand with good gradation, a reduction of about 43% was observed by Chua et al. in the pullout tests performed in the University of New Mexico (1993). As for the test in clay, a reduction of about 19% was observed. (Chua et al, 1993) pointed out that the optimum moisture content for this clay was about 20.4% which might explain the small reduction in resistance.

From the test results, it can be inferred that the saturated condition has more impact on fine sand than coarser sand; the reduction in the sliding coefficient is larger for the PET geogrid than the HDPE geogrid. This is because the friction resistance is subjected to a greater loss due to saturation, and the bearing resistance is marginal.

11.1.5 COMPARISON BETWEEN PULLOUT TEST AND FINITE ELEMENT ANALYSIS

Fig 11.1 shows that the results from the experimental investigation and the finite element analysis, for the unsaturated soil test condition, are in good agreement. The strains at the front end were about eight times higher than those at the rear end. This shows that the friction developed between the reinforcing element and the soil, and the bearing, can very effectively prevent the pullout force from transmitting. Both HDPE and PET are very good materials for geogrid soil reinforcement. However, there is an identified need to analytically predict the pullout strength for saturated soil conditions.

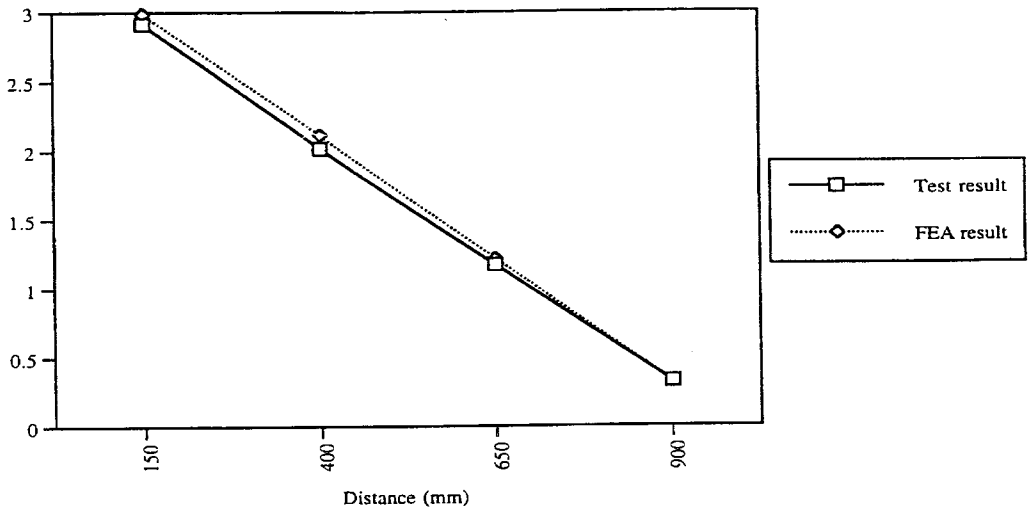

Figure 11.1 Observed and calculated strain distributions for a HDPE geogrid in sand under unsaturated condition

11.2 CREEP AND CREEP RUPTURE

11.2.1 INTRODUCTION

A comprehensive comparison was made to evaluate the creep and creep rupture behavior of the two kinds of geogrids, HDPE and PET, including the effect of the different exposures. Regression analysis was carried out to process the data.

11.2.2 DATA DISTRIBUTION

In the creep plots, considerable variability of the data was encountered. This can be attributed to the testing of single rib specimens. The need to test more specimens for each condition has been identified. In the present research, it was not possible to test more than two specimens for each solution due to a large number of variables.

11.2.3 CREEP AND CREEP RUPTURE CURVES

Regression analysis helped to eliminate the variability and provide the equations to identify the creep strain at any given time. It can be observed that temperature and load have a strong effect on the creep behavior of HDPE geogrids. There is a large difference in creep strains between the HDPE geogrids exposed to 30 °C and the ones exposed to 65 °C, under the same load levels. Also, specimens exposed to higher temperatures showed a larger amount of creep strain before breaking, than those exposed to lower

temperatures. Higher the temperature, the greater was the influence of increasing the load level. For PET specimens, the influence of temperature and load level is similar.

It is clear that HDPE geogrids undergo larger creep strain than PET geogrids. The different exposures do not play an important role in the rate of creep strain. It can be observed that there are larger variabilities from specimen to specimen, than from different solutions.

Creep rupture occurred in all the HDPE specimens exposed to 50% of the ultimate load. For the specimens exposed to 40% of the ultimate load, creep rupture occurred for specimens exposed to 55° C and 65° C temperatures. From the results, it was found that specimens exposed to similar loading, but higher temperatures, underwent larger deformations before creep rupture occurred, and the time to failure is reduced. Also, an increase of the load level produced an increase in the amount of creep strain reached before creep rupture occurred.

For the 55° C and 65° C temperatures, the percentage of creep strain before creep rupture did not vary significantly, indicating that the creep strain limit for the material has been reached. The time to reach creep rupture was further reduced with the increment in temperature.

The PET specimens did not experience creep rupture except for two specimens; for these two cases, the rupture can be attributed to either defects in the specimens or defective clamping.

11.3 DURABILITY AND DEGRADATION

11.3.1 INTRODUCTION

A comprehensive comparison is presented to evaluate the working performance of the two kinds of geogrids, HDPE and PET, and the effect of the different exposures on the geogrids. Analysis was carried out to improve the data by regression analysis and the Arrhenius method applied to predict the life of the specimens.

11.3.2 DATA DISTRIBUTION

In the durability plots, a large variability of the data was encountered, this is attributed to the testing of single rib specimens. The need to test more specimens for each condition has been identified. In the present research, it was not possible to test more than three specimens for each solution due to a large number of variables. The variability in the specimens is greater in the PET geogrids. This is because of the fabrication process and characteristics of the material. This is also because the PET geogrid is produced with bundled fibers, which are not always distributed evenly, and individual fibers can break at different times. For the seawater exposure, a considerable increase, instead of a decrease in strength, was observed, which can only be attributed to having specimens with a higher number of fibers in those particular specimens.

11.3.3 DURABILITY CURVES

The regression analysis helped to eliminate the variability and provide the equations to be used to find the property retained. In these curves it can be seen that the effect of degradation in HDPE geogrids is negligible for up to 10,000 hours for seawater and limerock, for the calcareous (pH 9.0), and phosphate (pH 4.5) exposures, a negligible degradation was observed at 10,000 hours with the maximum degradation of 3% for the calcareous solution and 1.2% for 65° C and 2.1% for 50° C in the phosphate solutions. For 35° C, the degradation was less than 1% in any exposure. These results indicate excellent performance of HDPE geogrids in the solutions to which they were exposed.

The PET geogrids showed a small degradation, mainly for the 65 °C. The variation in degradation between the different solutions was minimal indicating hydrolysis as the main cause. The maximum degradation was 13.3% for the Phosphate solution at 65° C, but the maximum at 35° C for the limerock exposure was only 1.2%. This indicates that hydrolysis is the main cause, since the amounts of degradation do not vary uniformly in the different exposures, and hydrolysis is accelerated by elevated temperatures.

11.3.4 ARRHENIUS MODELING

The Arrhenius method is not precise for small degradations; for the HDPE specimens, the Arrhenius method for 99% property retained, or 1% degradation, could be applied only to the calcareous exposure, since it was the only exposure with 65° C and the 55° C, that crossed the 99% property retained, as none of the exposures at 35° C crossed the 99% property retained. The results show that it will take 1.6 years for a 1% degradation at 20° C.

For the PET specimens, for 99% property retained the Arrhenius method could be applied to all the exposures except seawater, for which the 55° C curve did not cross the 99% property retained. For 97%, the same applied, and for 95%, the calcareous exposure at 50° C, also, did not reach 1% degradation. For HDPE, none of the 35° C curves crossed the 99% property retained or 1% degradation.

REFERENCES

AASHTO D 5397-53: Standard Method for Evaluation of Stress Crack Resistance of Polyolefin Geomembranes Using Notched Constant Tensile Load Test, American Association of State and Highway Transportation Officials, Washington, DC.

Aklonis, J. J. and Macknight, W. J., " Introduction to Polymer Viscoelasticity", John Wiley and Sons, New York, 1983, pp. 47-50.

Allen, T. M., "Determination of Long-Term Strength of Geosynthetics: A State-of-the-Art Review", Proc., Geosynthetics '91 Conference, Atlanta, 1991, pp. 351-379.

Allen, T. M., J. R. Bell, and T. S. Vinson, "Properties of Geotextiles in Cold Regions Applications," Transportation Research Report No. 83-6, Oregon State University, 1983.

Allen, T. M. and Elias V., " Overview and Status Report for FHWA HP & R National Pooled Fund Study", Durability Of geosynthetics For High way Applications", Earth Engineering and Sciences, Inc. , 1995

ASTM Standard D2837

ASTM D 2990-93a: "Standard Test Methods for Tensile, Compressive, and Flexural Creep and Creep-Rupture of Plastics", 1993.

Bailey II, J. S., "New Jersey DOT Accepts Value Engineering Replacement of High-Strength Geotextile with Geogrid System for Embankment Stabilization", Proc., Symposium on Mechanically Stabilized Backfill Walls, 1995, Transportation Research Board, Washington, DC., 1995.

Barrows, R. and Machan, G., "Reinforcement of a Failed Embankment Over Slough Mud", Proc., Geosynthetics '91 Conference, Atlanta, GA, 1991, pp. 839-848.

Bathurst, R. J., "Instrumentation of Geogrid-Reinforced Soil Walls", Transportation Research Record 1277, Washington, DC., 1991, pp. 102-111.

Bathurst, R.J. and Raymond, G.P., " Geogrid Reinforcement of Ballasted Track", Transportation Research Record 1153.

Billiard, J. W. and Wu, J. T. H., "Load Test of a Large-Scale Geotextile-Reinforced Retaining Wall", Proc., Geosynthetics '91 Conference, Atlanta, GA, 1991, pp. 537-548.

Bonaparte, R. and Berg R. R., "Long-term Allowable Tension for Geosynthetic Reinforcement", Proc., Geosynthetics '87, Vol. 1, New Orleans, LA, February 1987, pp. 181-192.

Bright, D. G., "The Environmental Stress Cracking of Polymers Used in Geosynthetic Products", Proc., Geosynthetics '93 Conference, Vancouver, Canada, 1993, pp. 925-934.

Bright, D.G. " Procedures and Test Standards For Evaluating The Properties of Geosynthetics", Industrial Fabrics Association International Geotextile Division.

Bright, D.G. and Wrigley, N. E., " The Manufacture of Homogeneous Geogrids", Geosynthetic Resins, Formulations and Manufacturing, 1994, pp. 189-197.

Bright D.G. "Problems with Current Methodology in Using the Arrhenius Equation to Predict the long-term Behaviour of Polymeric Materials in Geotechnical Environment", American Society for Testing and Manufacturing, Philadelphia, pp. 236-147.

Bush, D.I., "Variation of Long-Term Design Strength of Geosynthetics in Temperature up to 40°C", Proc. IV Int. Conf. on Geotextiles, Geomembranes and Related Products, 1992, pp. 673-676, The Hague, The Netherlands, 1990.

Cassady L. and Bright D.G. " Durability of Geosynthetics Exposed to Nine Years of Natural Weathering", Geosynthetics'95, pp. 841.

Cassady P.E. and Thomas R.W. " An introduction to polymer science for geosynthetic applications 1-6", pp. 6-36.

Cazzuffi D., Ghinelli A.: "European Experimental Approach to the Tensile Creep Behavior of High-Strength Geosynthetics", Geosynthetics '97 Conference Proceedings, Long Beach, 1997, pp.253-266.

Cazzuffi S. and Corbet S.: "Compressive Creep Test and Inclined Plane Friction Test for Geosynthetics in Landfills", Sardina, 1995, pp.477-491.

Chang, D. T., Chen, T. C., and Su, K. H., "Utilization of Geotextile-REinforced Retaining Wall for Stabilizing Weathered Mudstone Slope", Proc., Geosynthetics '91 Conference, Atlanta, GA, 1991, pp. 739-753.

Cheng S.C. and Christopher B., " A Probabilistic Review of Geotextile Reinforced Slope Design ", Geosynthetics '91 Conference Atlanta, USA, pp. 455-468.

Chourey-Curtis V.E. and Butchko S.T., "Structural Geogrids Used to Stabilize soil Venner Covers", Geosynthetics '91 Conference Atlanta, USA, pp. 125-143.

Chua, K. M., Aspar, W., and De La Rocha, A., "Simulating Failures of Geosynthetics-Reinforced Earth Structures Under Saturated Conditions", Geosynthetics '93, Vancouver, Canada, 1993, pp. 417-430.

Cowell, M. J. and Sprague, C. J., "Comparison of Pull-Out Performance of Geogrids and Geotextiles", Proc., Geosynthetics '93, Vancouver, Canada, 1993, pp. 579-592.

Daniel E. H.: " The Effect of Compressive Creep on the Structural Integrity and Drainage Capacity of Landfill Lining Systems", Master of Science Thesis, Florida Atlantic University, Advisor: Reddy, D.V., December 1995.

Den Hoedt: "Creep Relaxation of Geotextile Fabrics", Geotextiles and Geomembranes, No 4, 1986, pp. 83-92.

Elias, V., "Durability/Corrosion of Soil Reinforcement Structures", FHWA/RD-89/186. Federal Highway Administration, Washington, DC. 1990

Environment Protection Agency: "How to Meet Requirements for Hazardous Waste Landfill Design, Construction and Closure", Pollution Technology Review, 1990, No. 185, pp. 113.

Farrag, K., "Evaluation of the Effect of Moisture Content on the Interface Properties of Geosynthetics", Proc., Geosynthetics '95 Conference, Nashville, TN, 1995.

Farrag, K., Acar, Y. B., and Juran, I., "Pull-Out Resistance of Geogrid Reinforcements" Geotextiles and Geomembranes, Vol. 12, 1993, pp. 133-159.

Fishman, K. L. and Desai, C. S., "esponse of a Geogrid Earth Reinforced Retaining Wall With Full Height Precast Concrete Facing", Proc., Geosynthetics '91 Conference, Atlanta, GA, 1992, pp. 691-700.

Geosynthetic Research Institute (GRI) GM-5: "Notched Constant Tensile Load (NLTL) Test for Polyolefin Resins or Geomembranes", 1992, pp. 70-79.

Giroud, J. P., Arman, A., and Bell, J. R., "Geotextiles in geotechnical engineering practice and research", Report of ISSMFE Technical Committee, Geo-text, Geomember, 2, 1985, 179-242.

GRI test Method GG3 "Creep Behavior and Long Term Design Load of Geogrids", Geosynthetic Research Institute, Drexel University.

Hass R., " Test Program Results and Development Of Design Guidelines", Waterloo, Ontario, Canada .

Hess T.G. and Adams T.M. " Retaining Stucture Selection AT the project Level ". Transportation Research Board 77th Annual Meeting January 11-15, 1998 Washington D.C.

ICI: "Durability of Polyester, Polyaramid and Polyethylene Materials in Soil Reinforcement Applications", Report to British Standart Technical Committee CBS/56, 1986.

Jailloux, J. M. and Segrestin, "Present State of Knowledge of Long-Term Behavior of Materials Used as Soil Reinforcements", International Geotechnical Symposium on Theory and Practice of Earth reinforcement, 1988, Japan, pp. 105-110

Jarrett P.M. " Load Test On Geogrid Reinforced Gravel Fills Constructed on Peat Subgrades ", Third International conference on Geotextiles, 1986, Vienna, Austria

Jones C. J. F. P., "Design and Construction of Reinforced Soil Structures", SERC/Netlon Symposium on Polymer Grid Reinforcement in Civil Engineering, London, 1984.

Jones, M. and Ingold, T. S., "Durability of Polyolefinic Soil Reinforcements", Proc. 8th European Congress on Corrosion, Vol. 1, 1985, pp. 9-1 to 9-7.

Juran, I., Farrag, K., and Richmond, "Short and Long Term Performance of Polyolefin Geogrids", Proc. Geosynthetics '91 Conf., Atlanta, GA, pp. 387-599.

Keller, R. G., "Experiences with Mechanically Stabilized Structures and Native Soil Backfill", Proc., Symposium on Mechanically Stabilized Backfill Walls, Preprint No. 950752, Transportation Research Board, Washington, DC., 1995.

Kemp, S., Martin, J. S., and Stadler, A. T., "The Design and Construction of Geogrid-Reinforced Retaining Walls at the South Carolina Port Authority's Wando Terminal", Proc., Geosynthetics '93 Conference, Vancouver, Canada, 1993, pp. 153-166.

Koerner R. M., "Designing with Geosynthetics", 4th Edition, Prentice Hall, Inc., Englewood Cliffs, N.J., 1998.

Koerner, R. M. et al., "Stress Strain Time Behavior of Geotextiles in Uniaxial Tension", Proc., Symposium on Geotextiles, ASCE, Portland, 1980, pp. 31-52.

McGown, A., K. Z. Andrews, and M. H. Kabir, "Load-Extension Testing of Geotextiles Confine In-Soil", Proc., Second International Conference on Geotextiles, Las Vegas, NV, Vol. III, 1982, pp. 793-798.

Merry S.M., Bray J. D.: "Temperature Dependent Multi-Axial Creep Response of HDPE Geomembrances", '97 Conference Proceedings, Long Beach, 1997, pp. 163-177.

Min, Y., "Creep and Pullout Behavior of Geogrid Embedded in Sand Subjected to Sustained and Cyclic Loads", Proc. Geosynthetics International, Nashville, TN, 1995, pp. 1125-1198.

Montanelli F. and Rimoldi P.: "Long Term Performance of GCL and Drainage Composite Systems", Proceedings Sardina 95, Fifth International Landfill Symposium, 1995, pp. 359-368.

Moreno, O. A., King, J. L., and MacDonald, R. A., "From a Contractor's Viewpoint: Construction Technicalities of a Tiered Modular Block Wall -- The Fiesta, Texas Case", Proc., Geosynthetics '93 Conference, Vancouver, Canada, 1993, pp. 167-187.

Peggs, I. D. and Kanninen, M. F., "HDPE Geosynthetics: Premature Failures and Their Prediction", Proc. Geosynthetics International, Vol. 2, No. 1, 1995, pp. 327-339.

Popelar, C. H., " Acomparison of the Rate Process Method and the Bidirectional Shifting Method", Thirteenth Plastic Fuel Gas Pipe Symposim, San Antonio, TX, 1993, pp. 140-151.

" Renforced Earth Walls Section 528 , District Materials", " DAVID MIRO".

Raju D. M. and Fannin R. J., "Large Scale Pullout Testing of Geosynthetics", A thesis submitted in partial fulfillment of the M. A. Sc. Degree at the University of British Columbia, 1991.

Ramos, H. R., McDaniel, G. T., and Maher, S. A., "Geogrids Strengthen Foundation for Mechanically Stabilized Earth Retaining Wall -- A Case Study", Proc., Geosynthetics '93 Conference, Vancouver, Canada, 1993, pp. 365-377.

Sandri, D., Martin, J. S., Vann, C. W., Ferrer, M., and Zeppenfeldt, I., "Installation Damage Testing of Four Polyester Geogrids in Three Soil Types", Proc., Geosynthetics '93 Conference, Vancouver, Canada, 1993, pp. 743-455.

Schneider, H. and Groh M. " An Analysis of Durability Problems of Geotextiles", Proceedings Geosynthetics 19987 Conference, New Orleans, pp 434-441

Shelton W.S. and Bright D.G. "Using the Arrehenius Equation and Rate Expressions to Predict the Long TErm Behavior Of Geosynthetic Polymers", Geosynthetics '93 - Vancouver, Canada - 229, pp. 789-802.

Sing A., and Mitchell J.K.: "General Stress-Strain-Time Function for Soils", Journal of the soil Mechanic and Foundation, ASCE, 94 (SMI), 1994, pp. 21-46.

Smith, T. E., Brandon, T. L., Imad, L. A., Lacina, B. A., Bhutta, S. A., and Hoffman, S. E., "Laboratory Behavior of Geogrid and Geotextile Reinforced Flexible Pavements", Technical Report, Virginia Polytechnic Institute and State University, Blacksburg, VA, February 1995, pp. 148.

Stein E.G., Knight D.P., Vollmer S.C. and Larkin P.E. "Geosynthetics Solve Three Distinct Pronblems in Wetlands Construction on Maryland State Highway Administration route 100". Transportation Research Board 77th Annual Meeting January 11-15, 1998 Washington D.C.

Tensar Technical Note: PT 13.0, "High Density Polyethylene Resin Characteristics Which Affect Performance of Products Bearing High Sustained Loads in Soil Reinforcement Application", October 1987.

Thielen D.L. and J.G. Collin "Geogrid Reinfocement For Surficial Stability of Slopes", Geosynthetics '93 - Vancouver, Canada - 229

US Department of Transportation Report: FHWA-RD-89-186, "Durability/Corrosion of Soil Reinforced Structures", December 1990.

Van Zanten, R. V., "Designing with Geosynthetics in Civil Engineering", John Wiley and Sons, 1986.

Wharton, G., Harper, W. J., and Witt, C. M., "Geogrid and Geotextile Reinforced Foundation for Major Refinery Processing Unit", Proc., Geosynthetics '93 Conference, Vancouver, Canada, 1993, pp. 339-353.

Wrigley, N. E., "Durability and Long Term Performance of Tensar Polymer Grids for Soil Reinforcement", Materials Science and Technology, Vol. 3, 1987.

Yarger, T. L. and Barnes, R. S., "Montana Department of Transportation's Introduction to Geogrid Use for Steepened Embankment Design", Proc., Geosynthetics '91 Conference, Atlanta, GA, 1991, pp. 311-326.

Yovanish D.J. and Berry S.W. "Design and Construction of an 18 Foot High Geogrid Stayed Concrete Block Wall A Case History", Geosynthetics '91 Conference Atlanta, USA

APPENDIX A

LOAD - ELONGATION CURVES

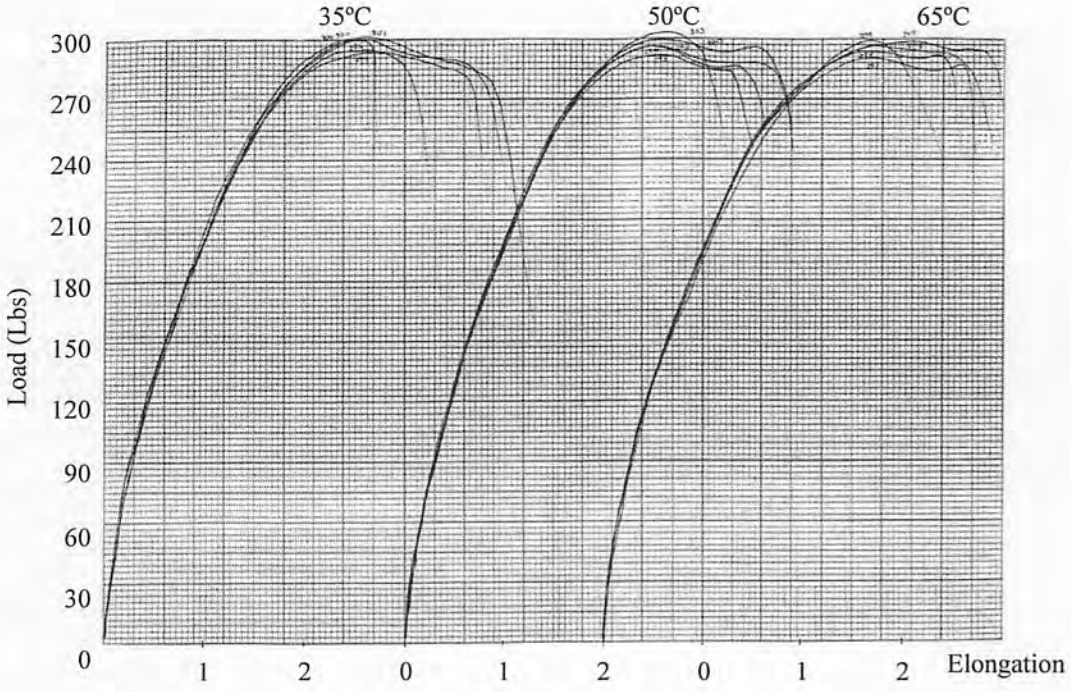

Fig. A.1 Load – Elongation curves for HDPE specimens, Control Values

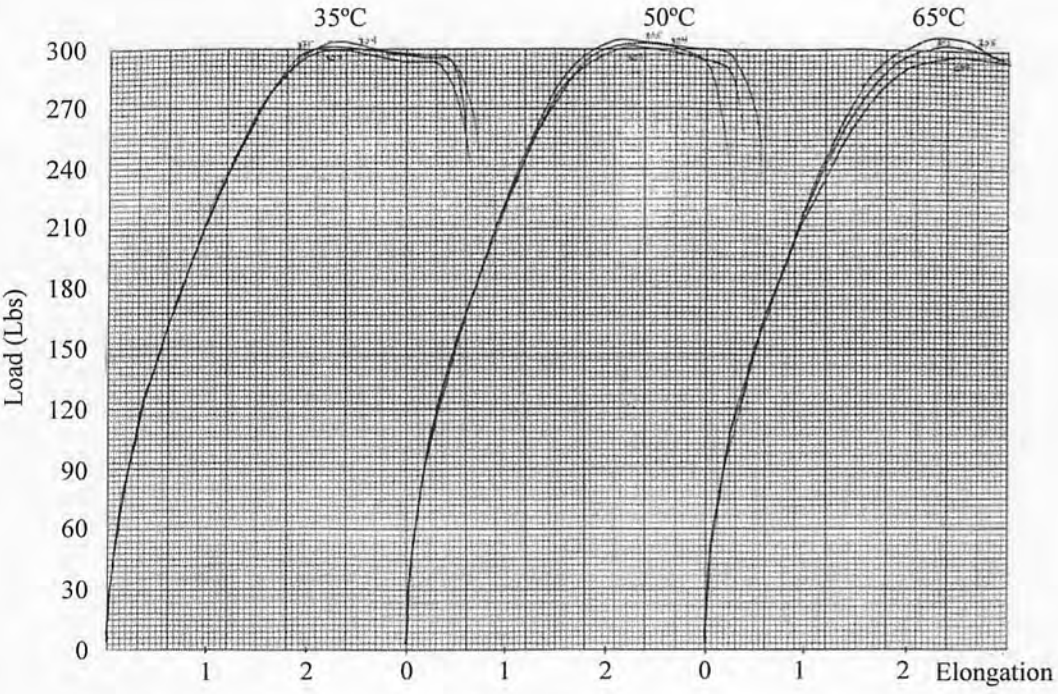

Fig. A.2 Load – Elongation curves for HDPE specimens, 30 days, Calcareous exposure

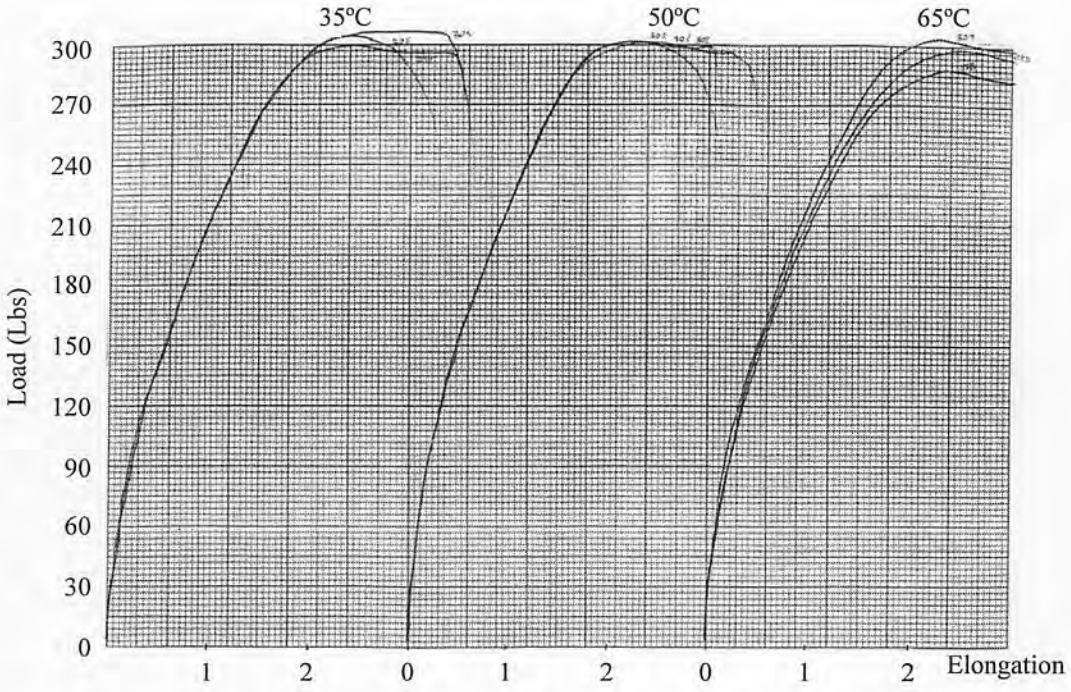

Fig. A.3 Load – Elongation curves for HDPE specimens, 30 days, Phosphate exposure

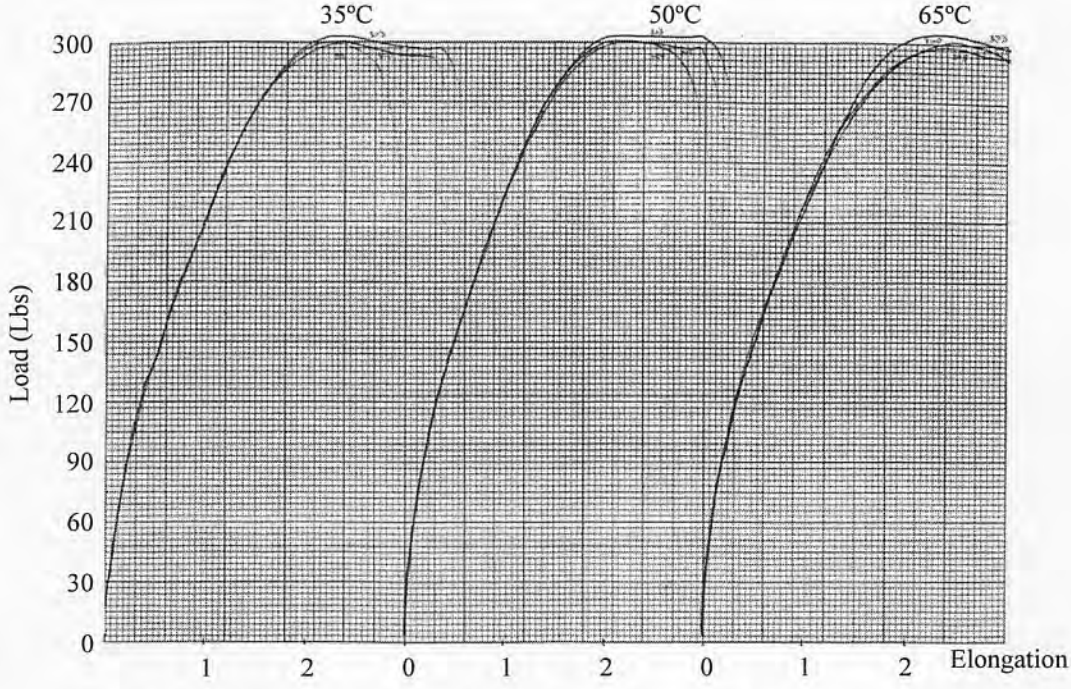

Fig. A.4 Load – Elongation curves for HDPE specimens, 30 days, Limerock exposure

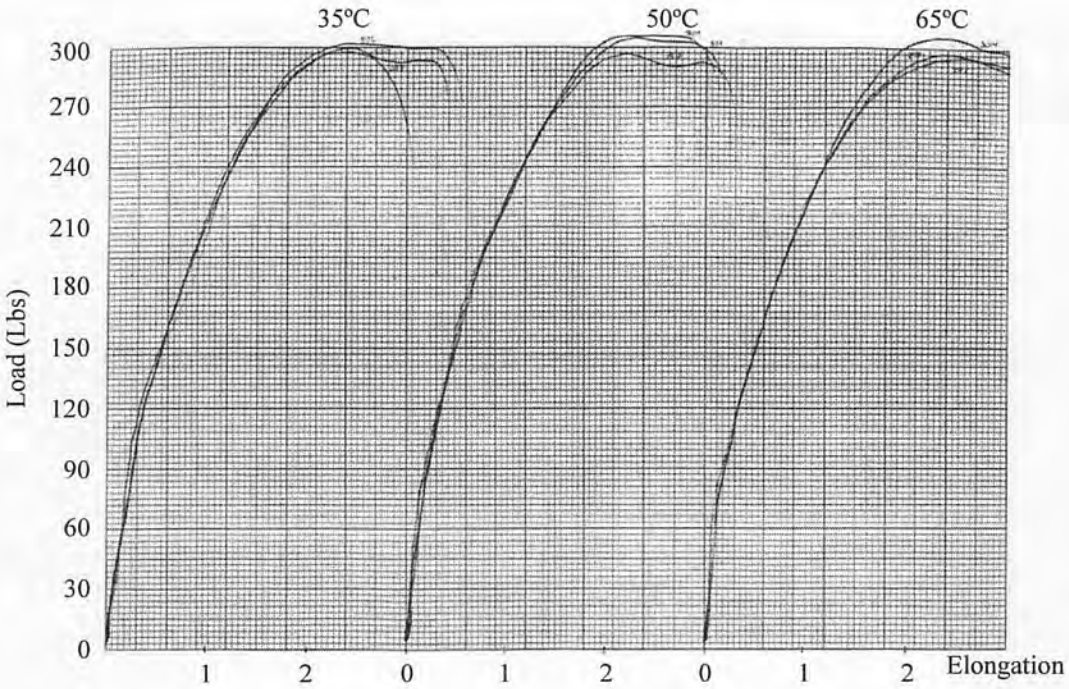

Fig. A.5 Load – Elongation curves for HDPE specimens, 30 days, Seawater exposure

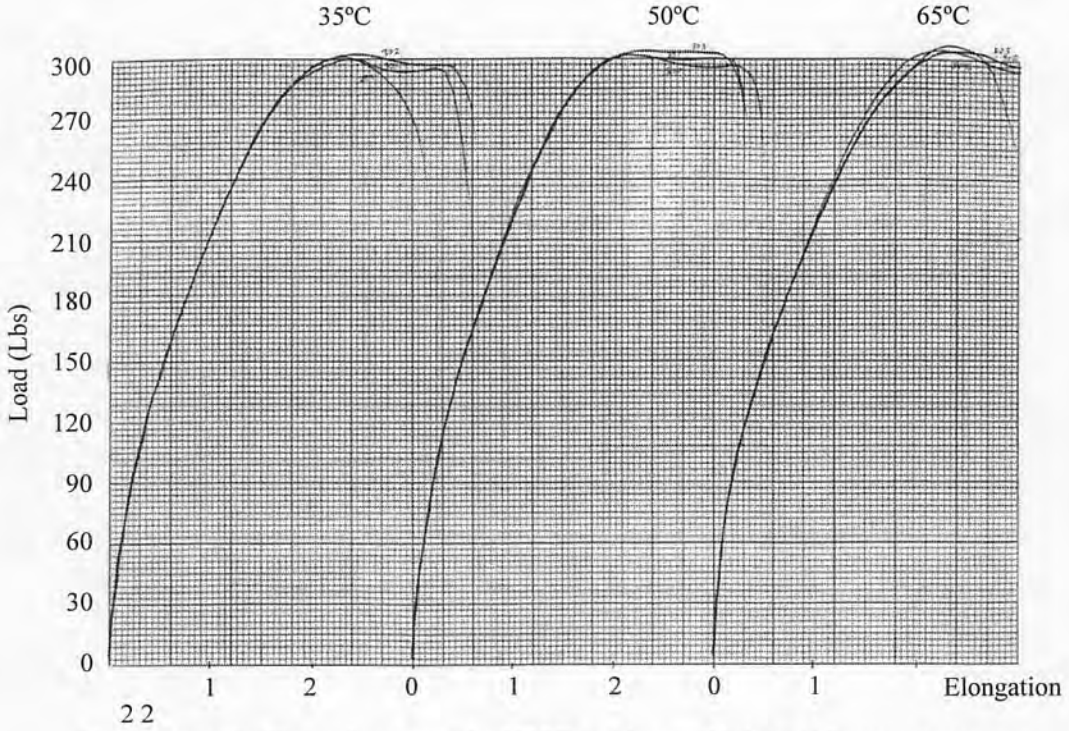

Fig. A.6 Load – Elongation curves for HDPE specimens, 60 days, Calcareous exposure

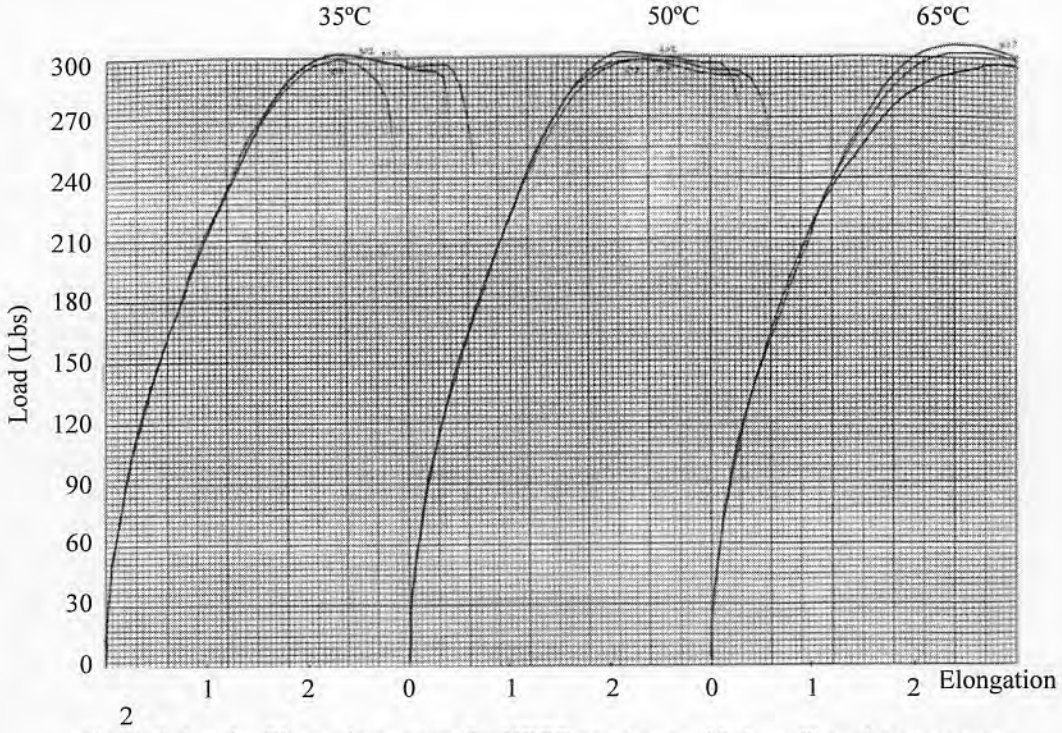

Fig. A.7 Load – Elongation curves for HDPE specimens, 60 days, Phosphate exposure

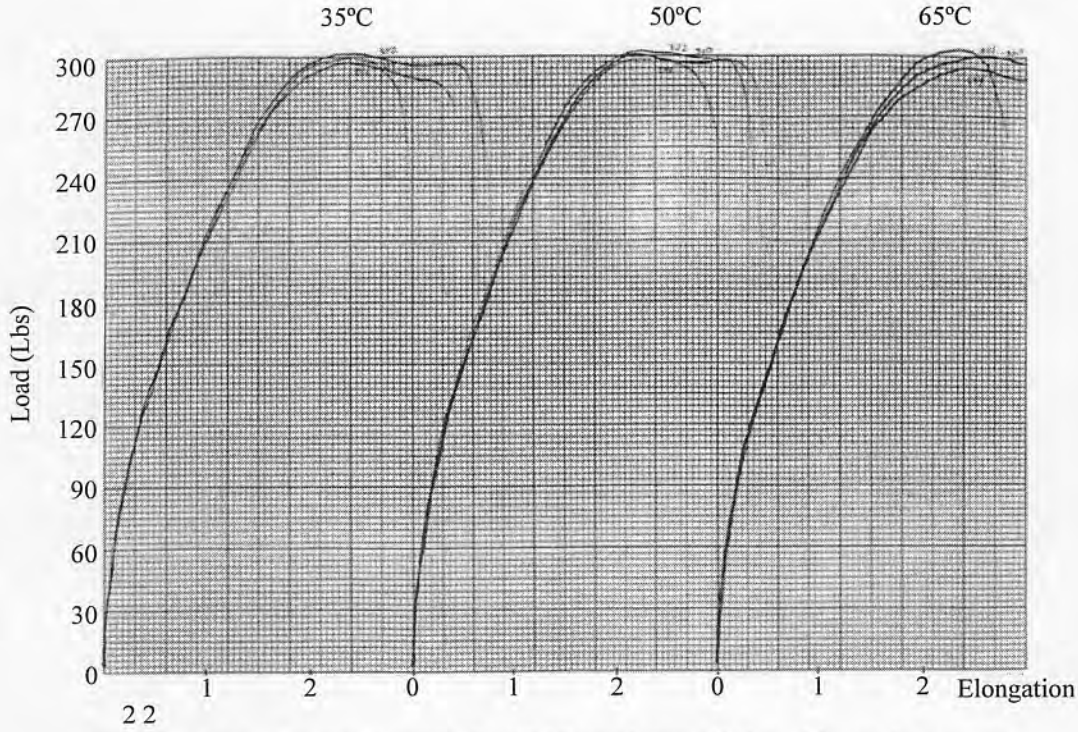

Fig. A.8 Load – Elongation curves for HDPE specimens, 60 days, Limerock exposure

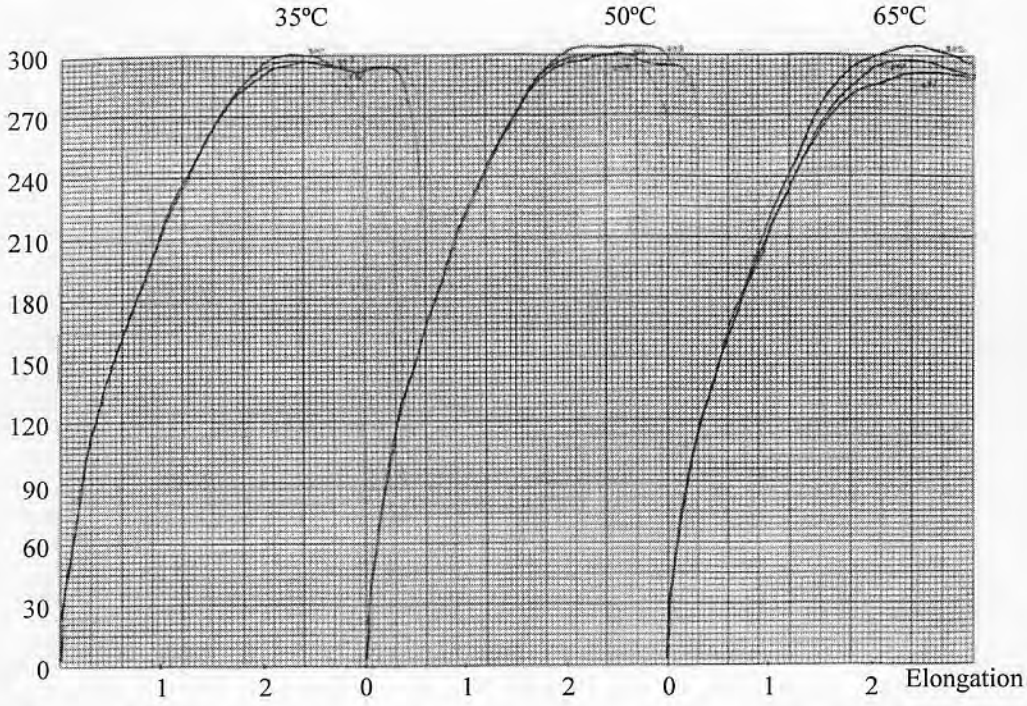

Fig. A.9 Load – Elongation curves for HDPE specimens, 60 days, Seawater exposure

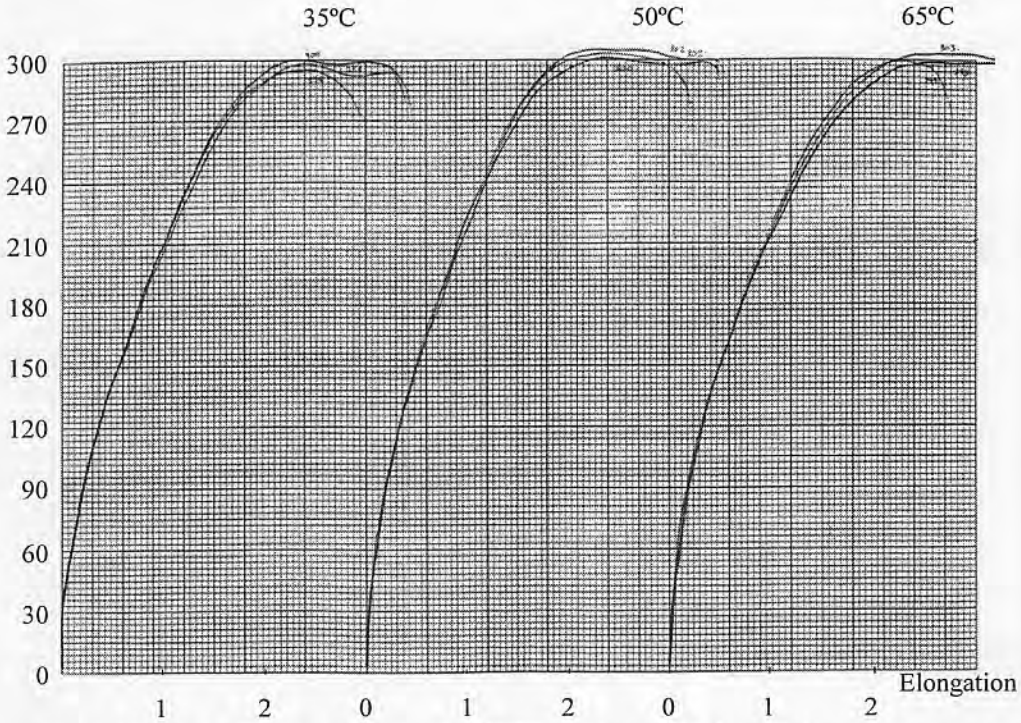

Fig. A.10 Load – Elongation curves for HDPE specimens, 90 days, Calcareous exposure

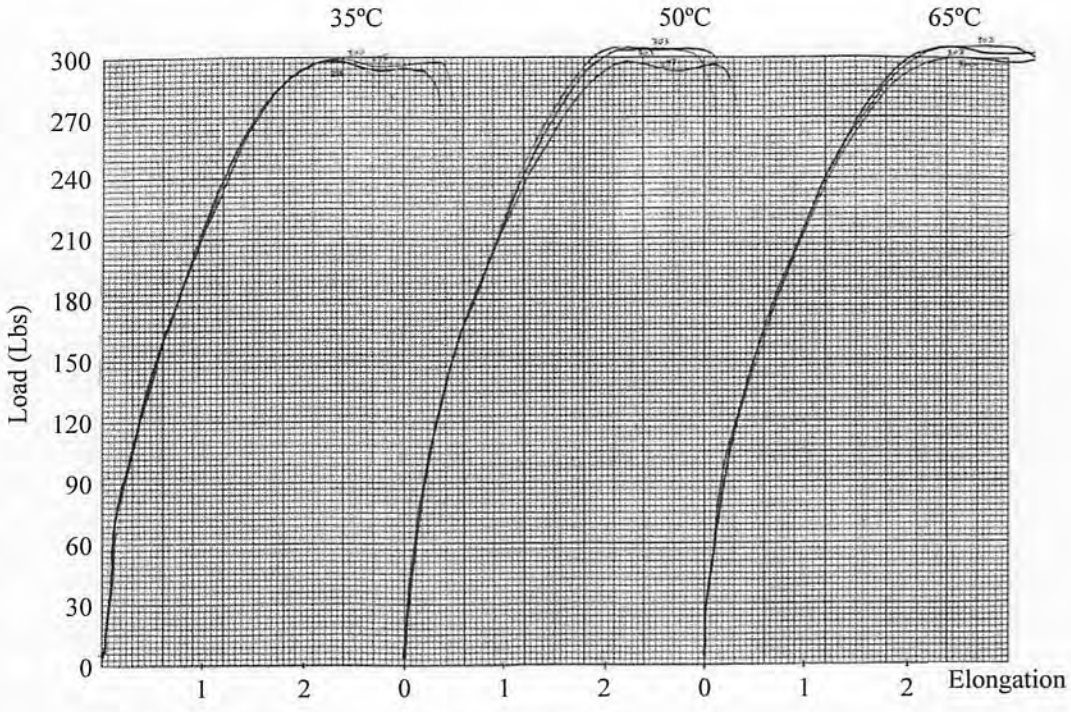

Fig. A.11 Load – Elongation curves for HDPE specimens, 90 days, Phosphate exposure

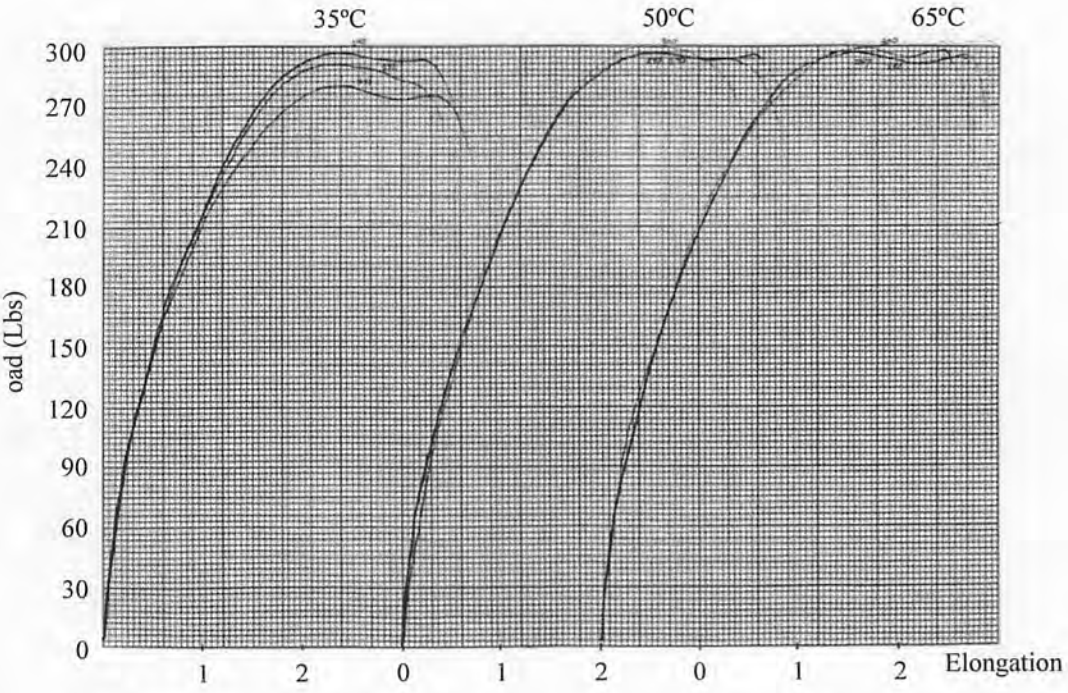

Fig. A.12 Load – Elongation curves for HDPE specimens, 90 days, Limerok exposure

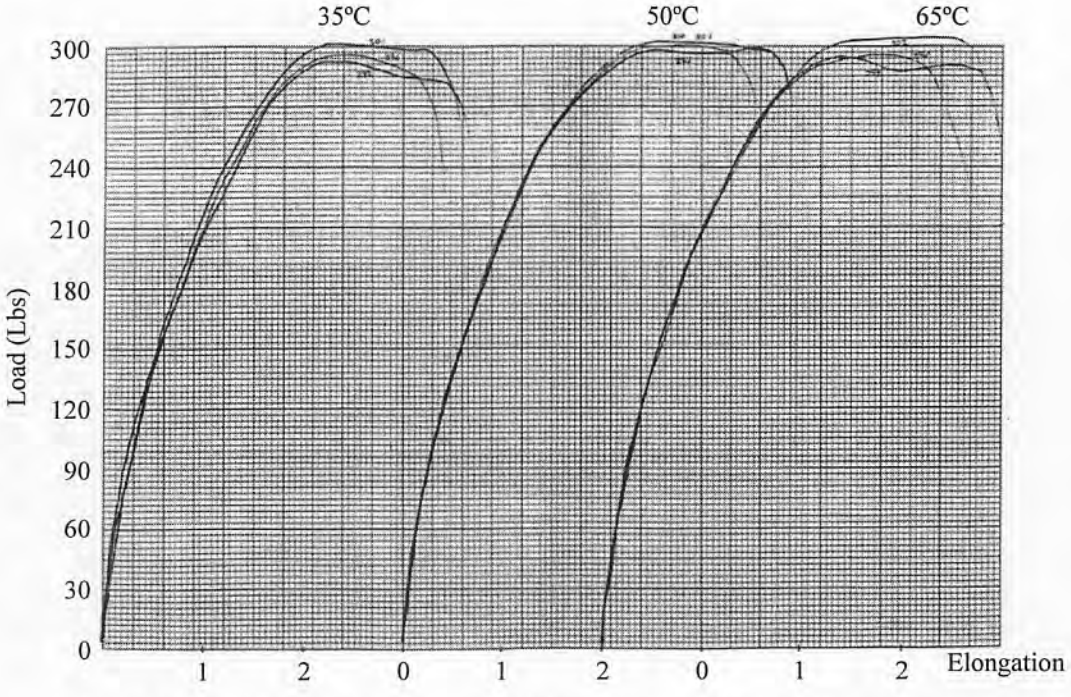

Fig. A.13 Load – Elongation curves for HDPE specimens, 90 days, Seawater exposure

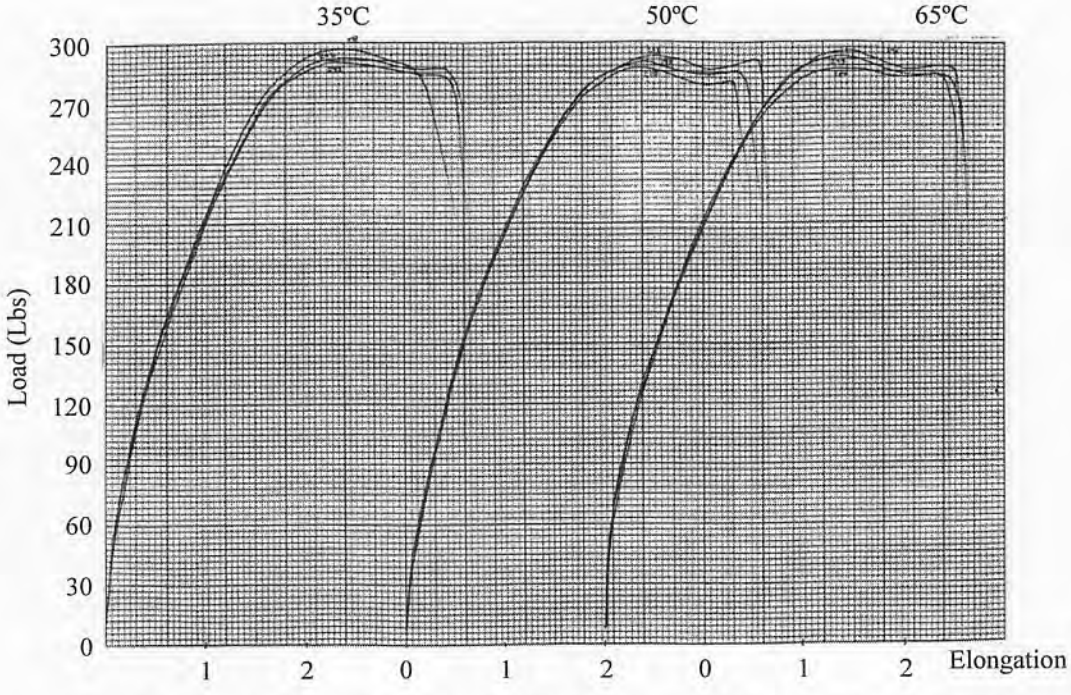

Fig. A.14 Load – Elongation curves for HDPE specimens, 120 days, Calcareous exposure.

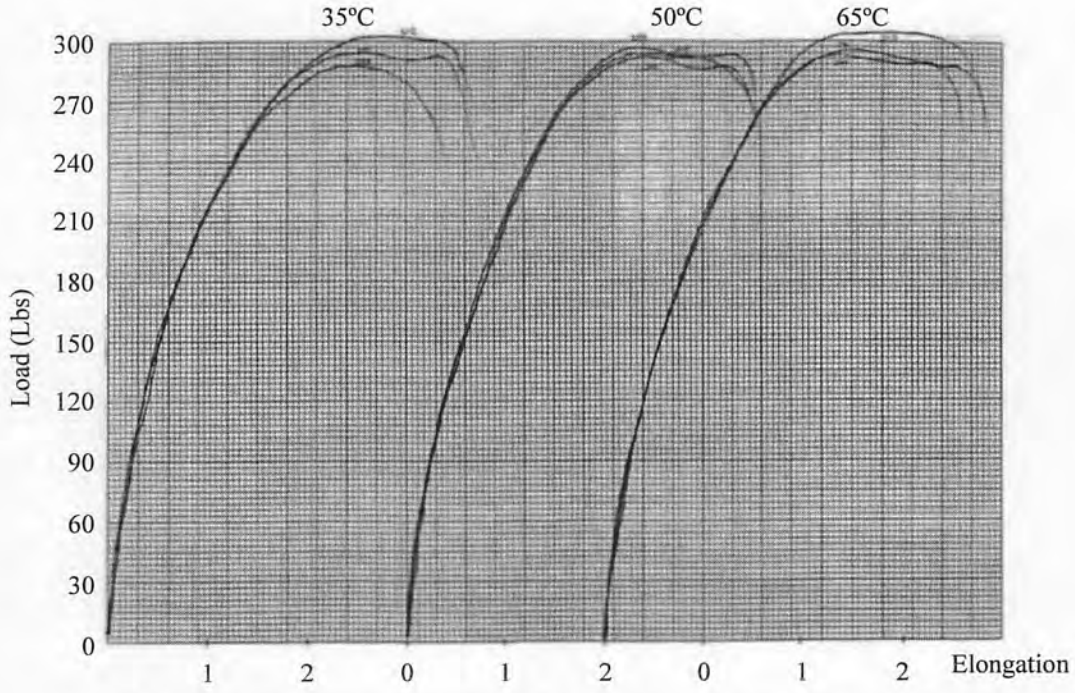

Fig. A.15 Load – Elongation curves for HDPE specimens, 120 days, Phosphate exposure

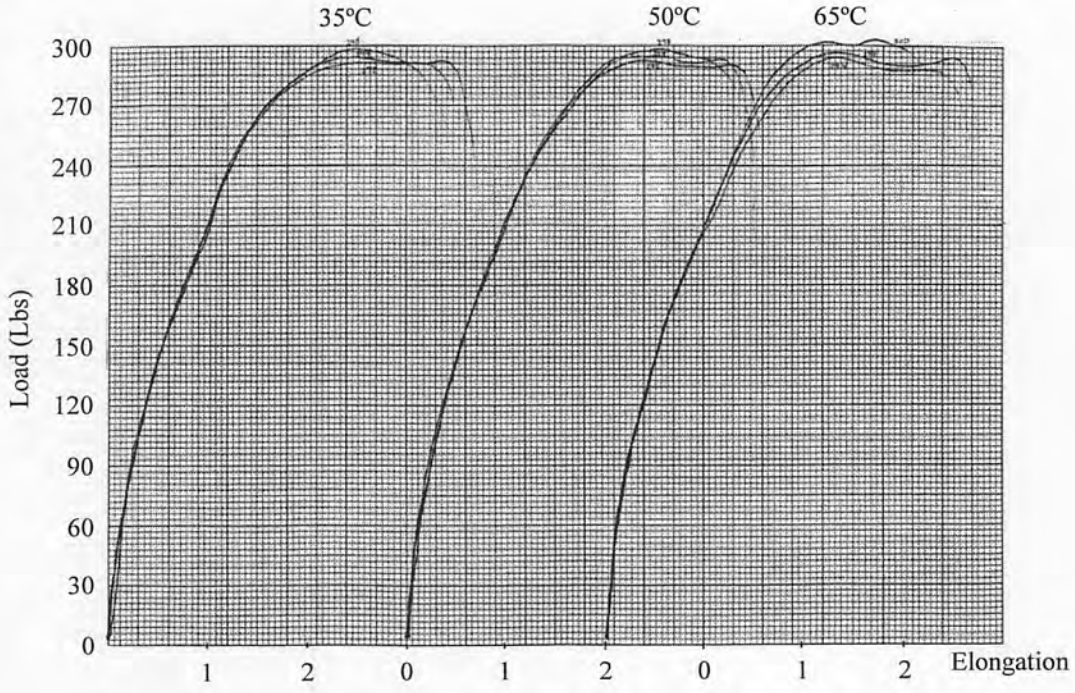

Fig. A.16 Load – Elongation curves for HDPE specimens, 120 days Limerock exposure.

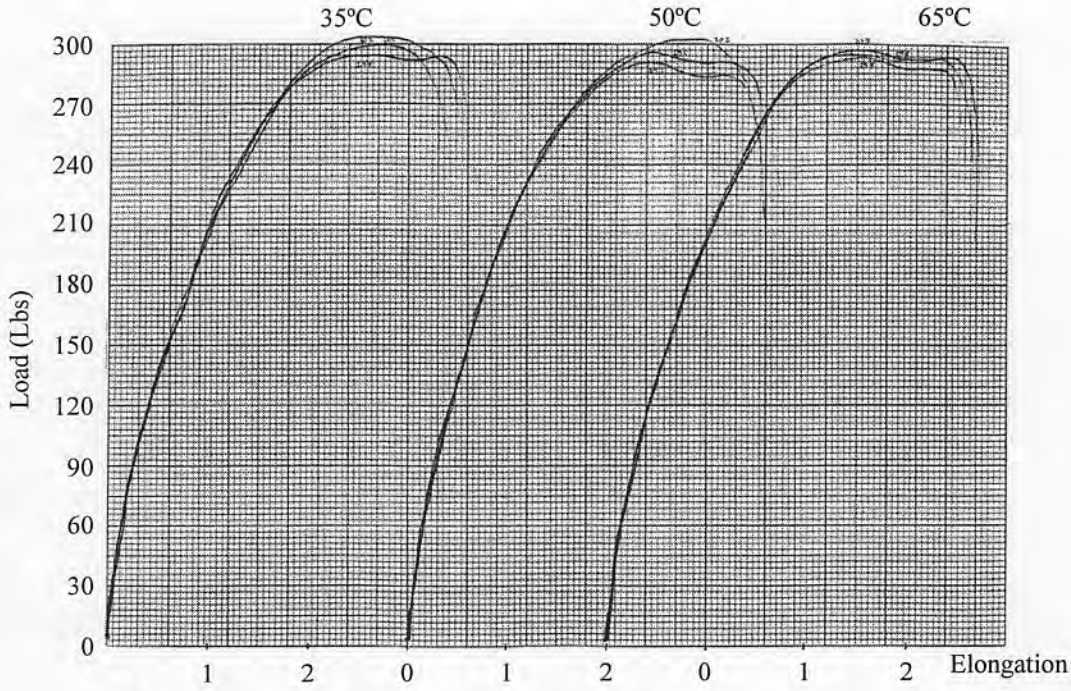

Fig. A.17 Load – Elongation curves for HDPE specimens, 120 days, Seawater exposure

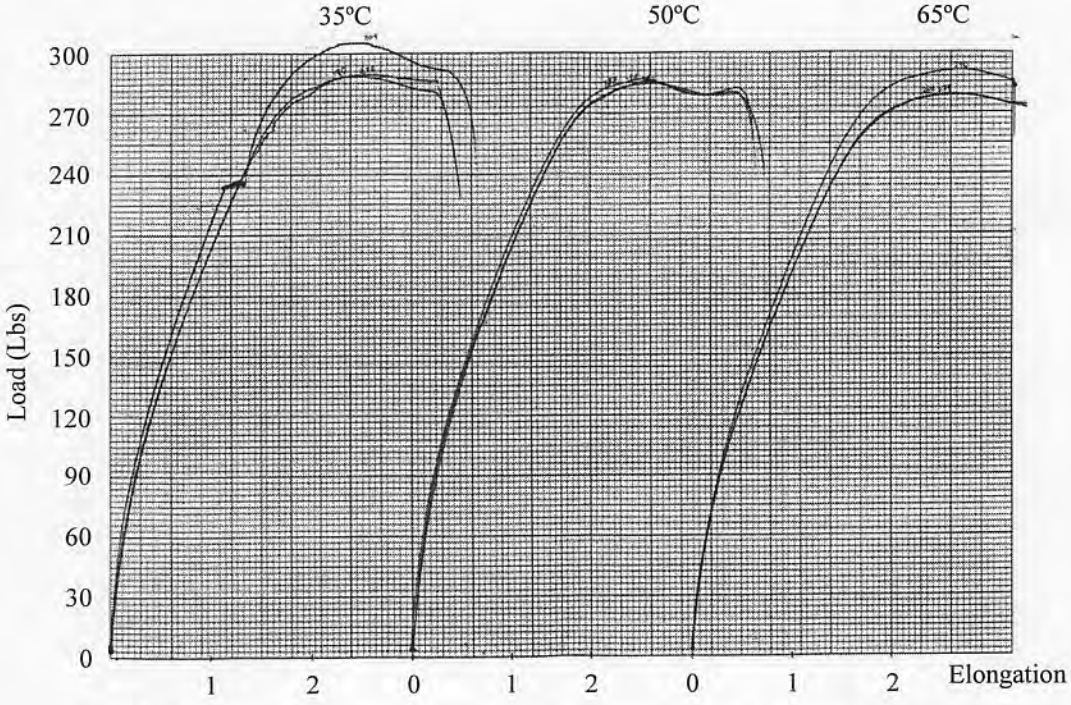

Fig. A.18 Load – Elongation curves for HDPE specimens, 365 days, Calcareous exposure

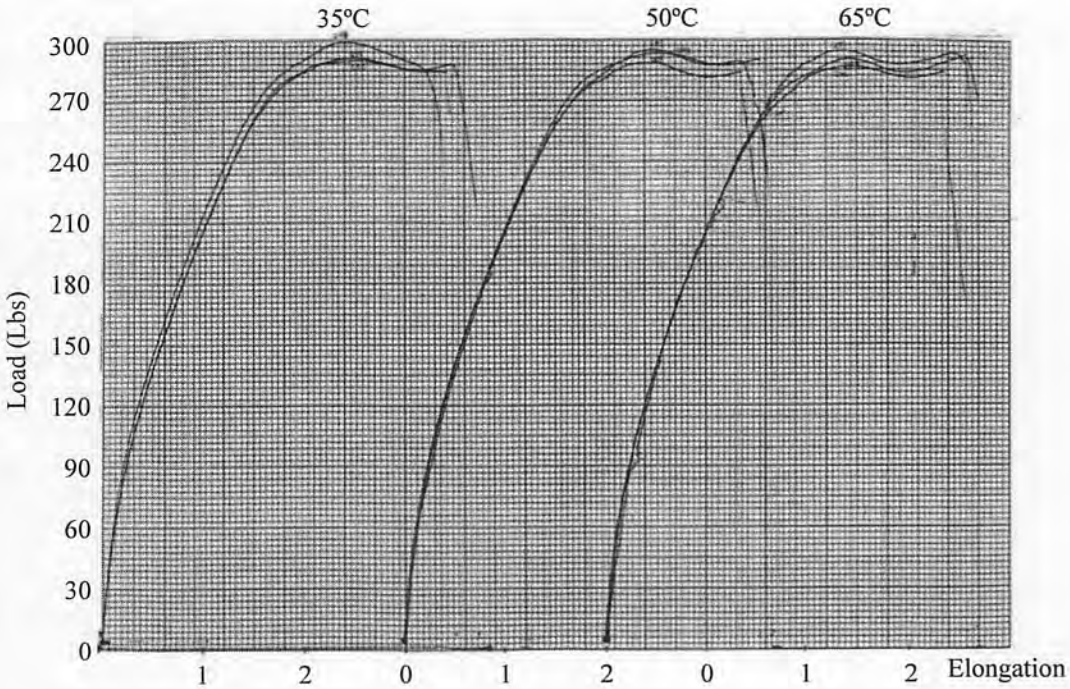

Fig. A.19 Load – Elongation curves for HDPE specimens, 365 days, Phosphate exposure

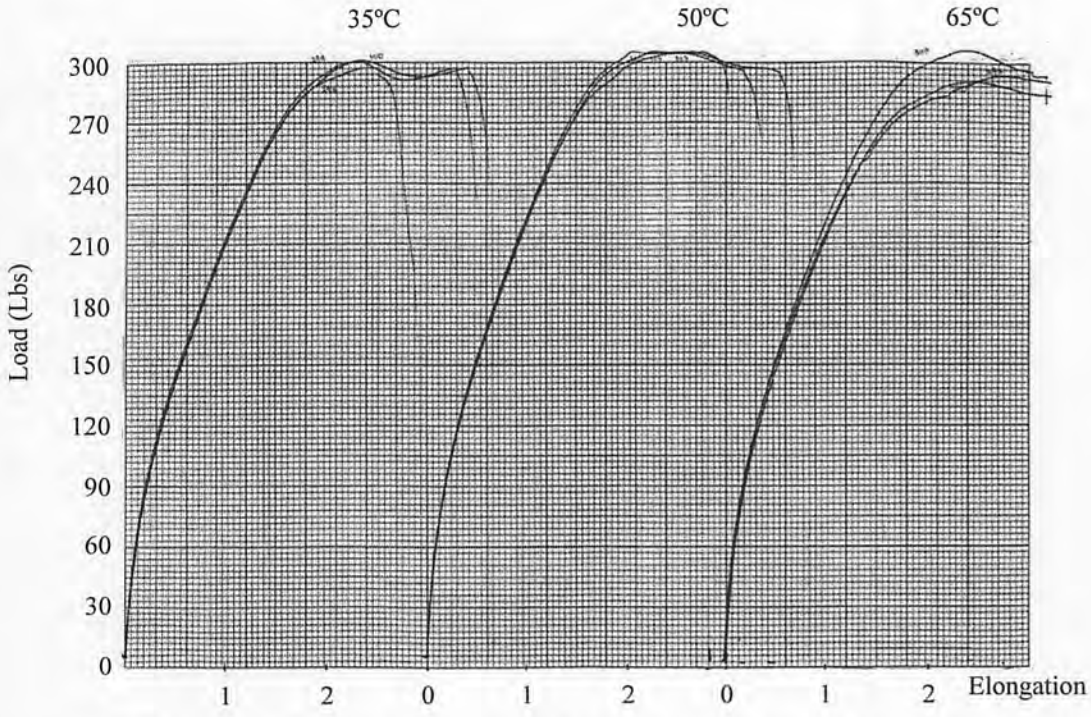

Fig. A.20 Load – Elongation curves for HDPE specimens, 365 days, Limerock exposure

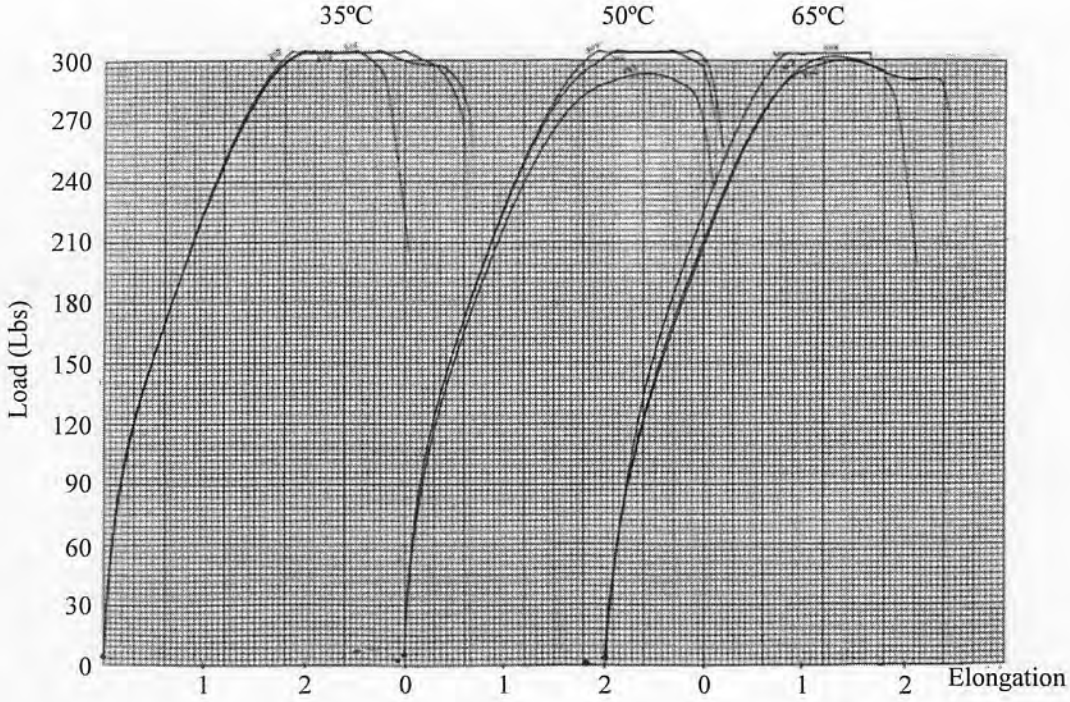

Fig. A.21 Load – Elongation curves for HDPE specimens, 365 days, Seawater exposure

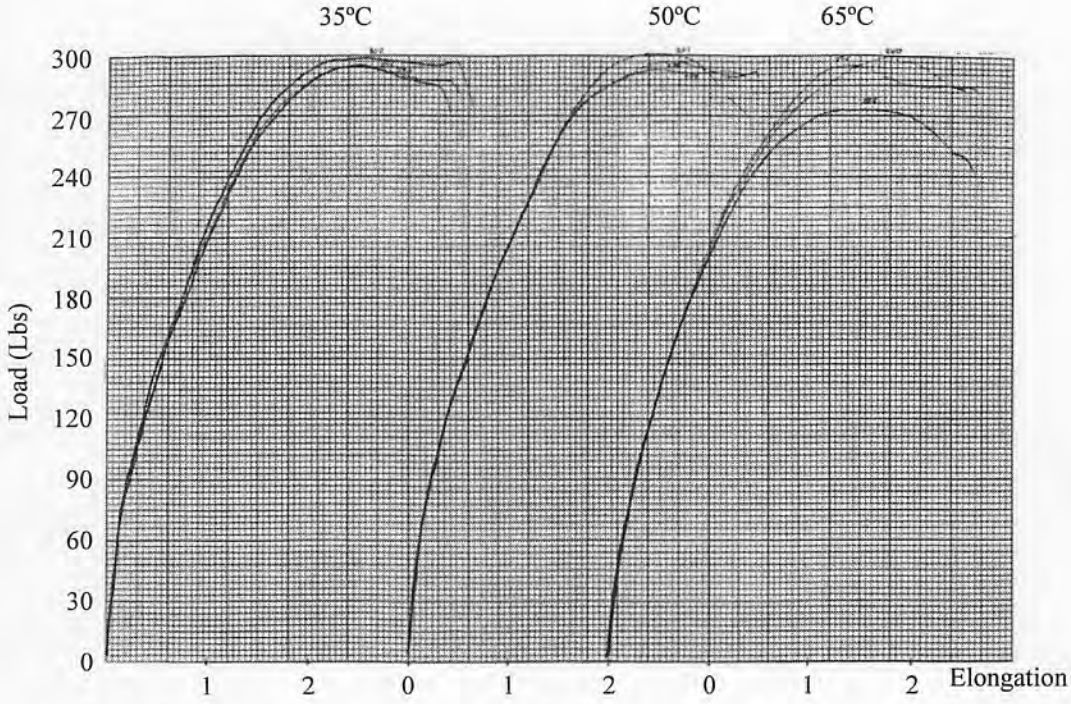

Fig. A.22 Load – Elongation curves for HDPE specimens, 417 days, Phosphate exposure

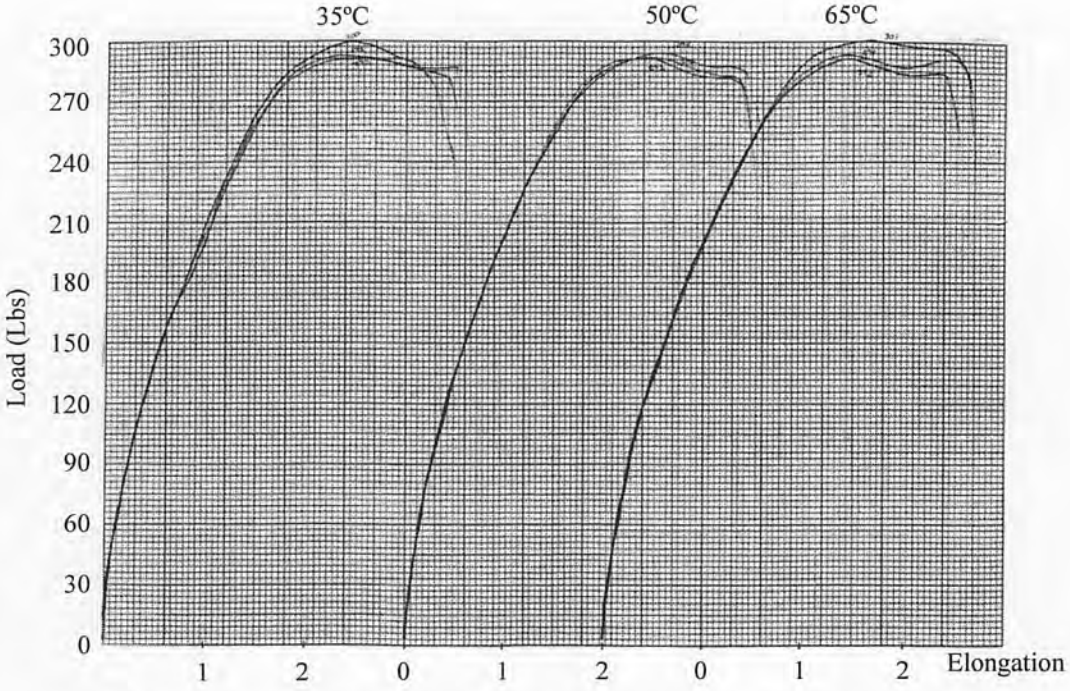

Fig. A.23 Load – Elongation curves for HDPE specimens, 417 days, Phosphate exposure

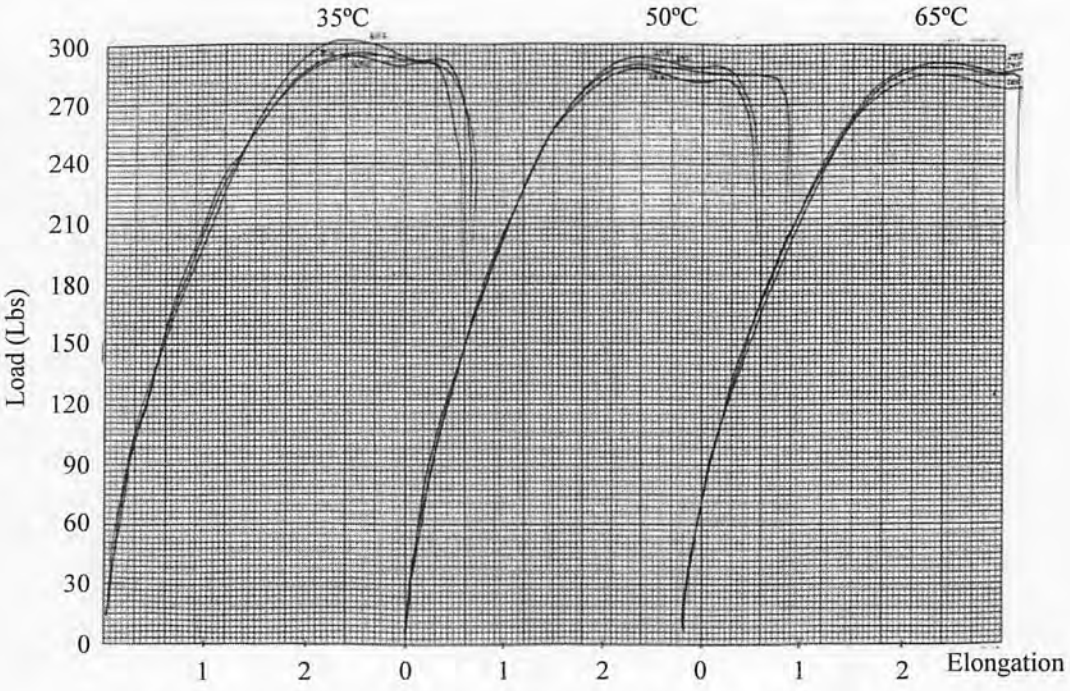

Fig. A.24 Load – Elongation curves for HDPE specimens, 417 days, Limerock exposure

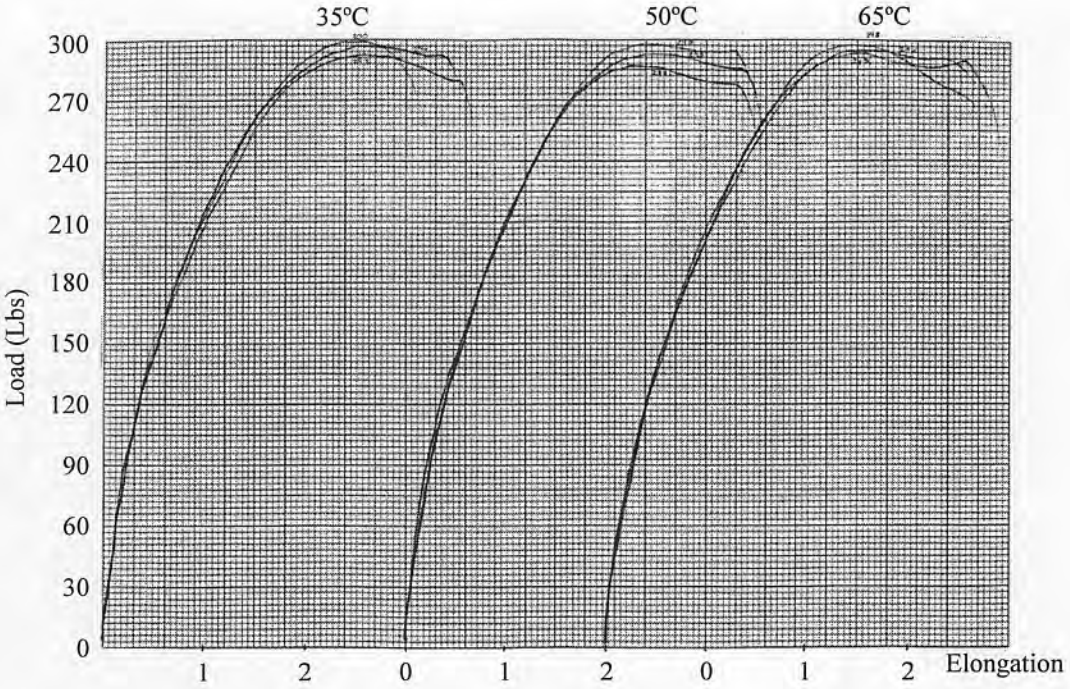

Fig. A.25 Load – Elongation curves for HDPE specimens, 417 days, Seawater exposure

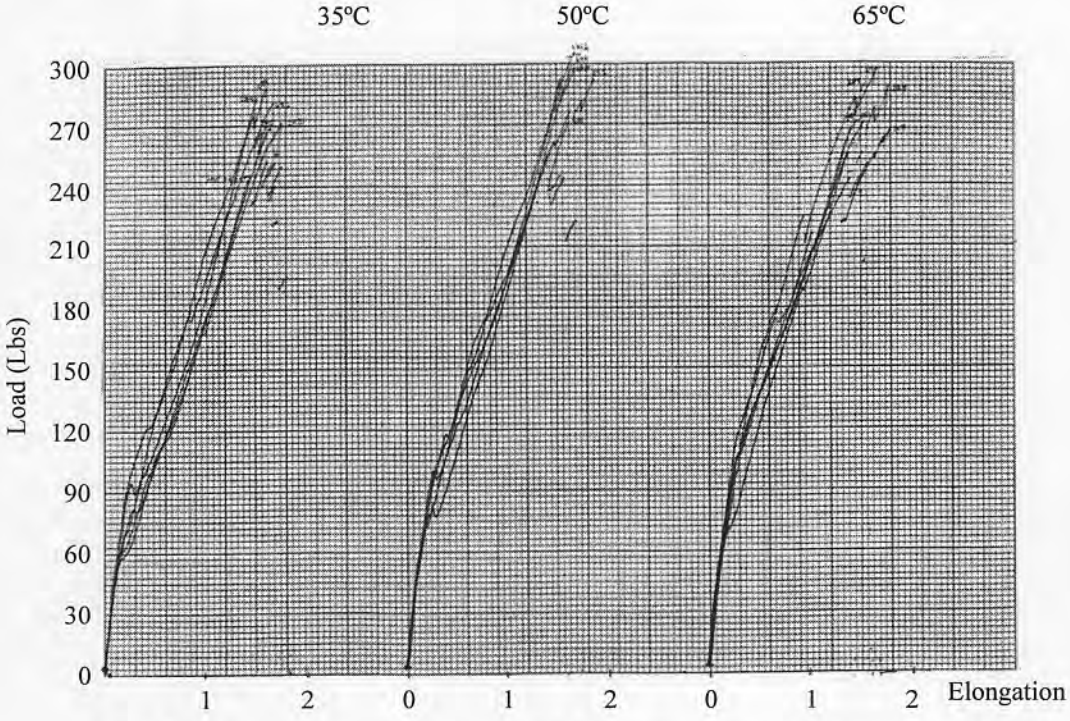

Fig. A.26 Load – Elongation curves for PET specimens, Control Values

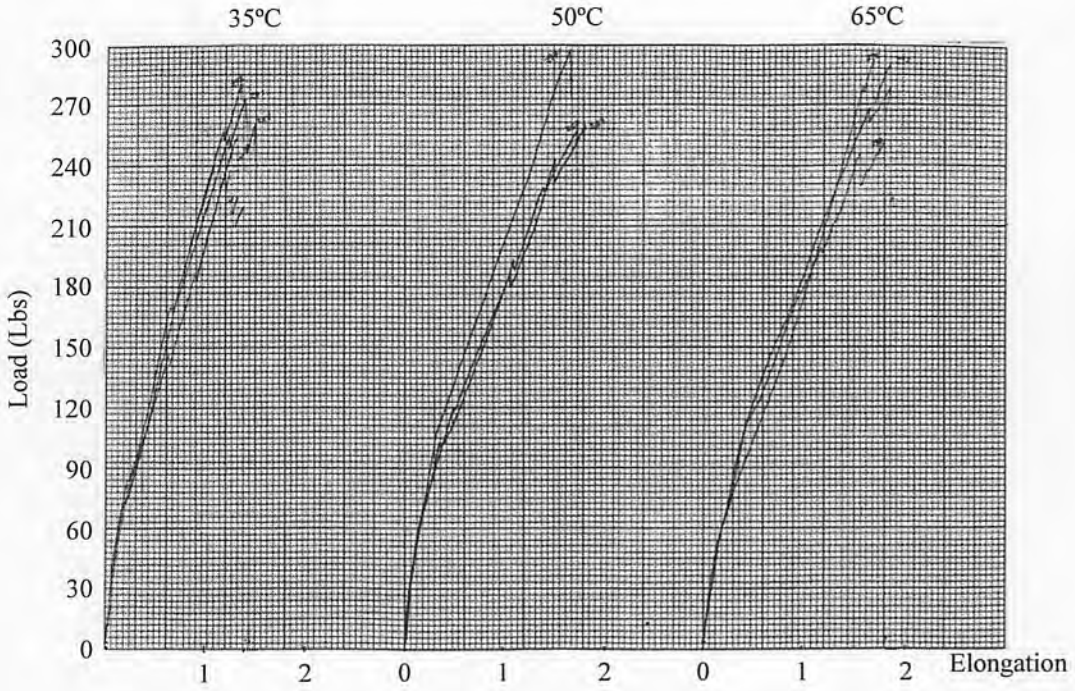

Fig. A.27 Load – Elongation curves for PET specimens, 30 days, Calcareous exposure

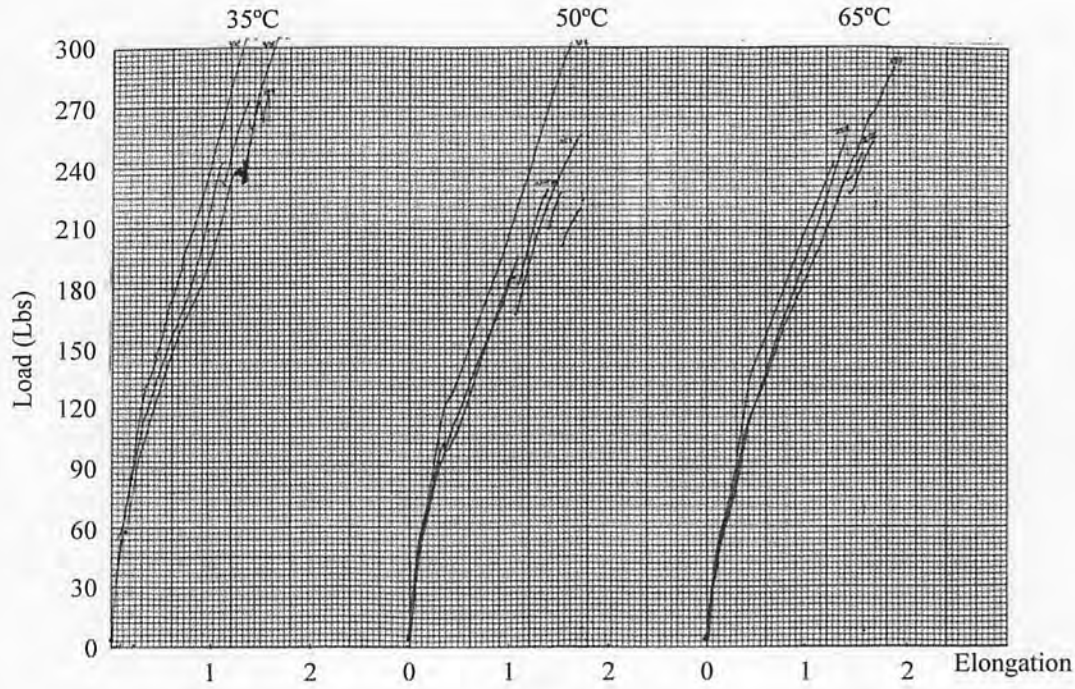

Fig. A.28 Load – Elongation curves for HDPE specimens, 30 days, Phosphate exposure

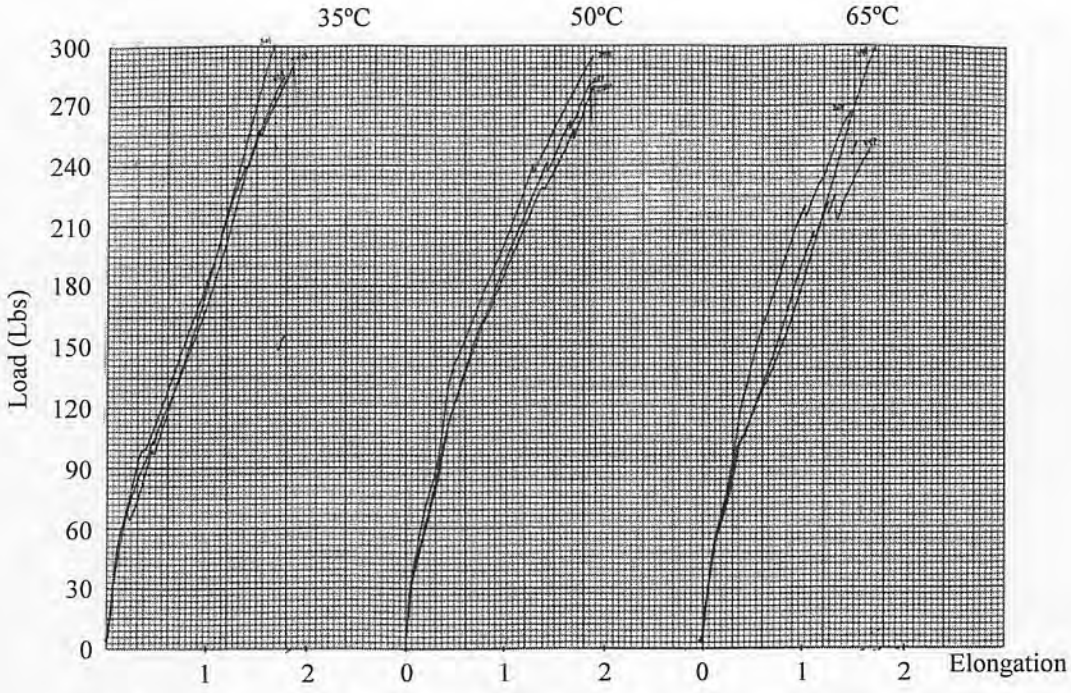

Fig. A.29 Load – Elongation curves for PET specimens, 30 days, Limerock exposure

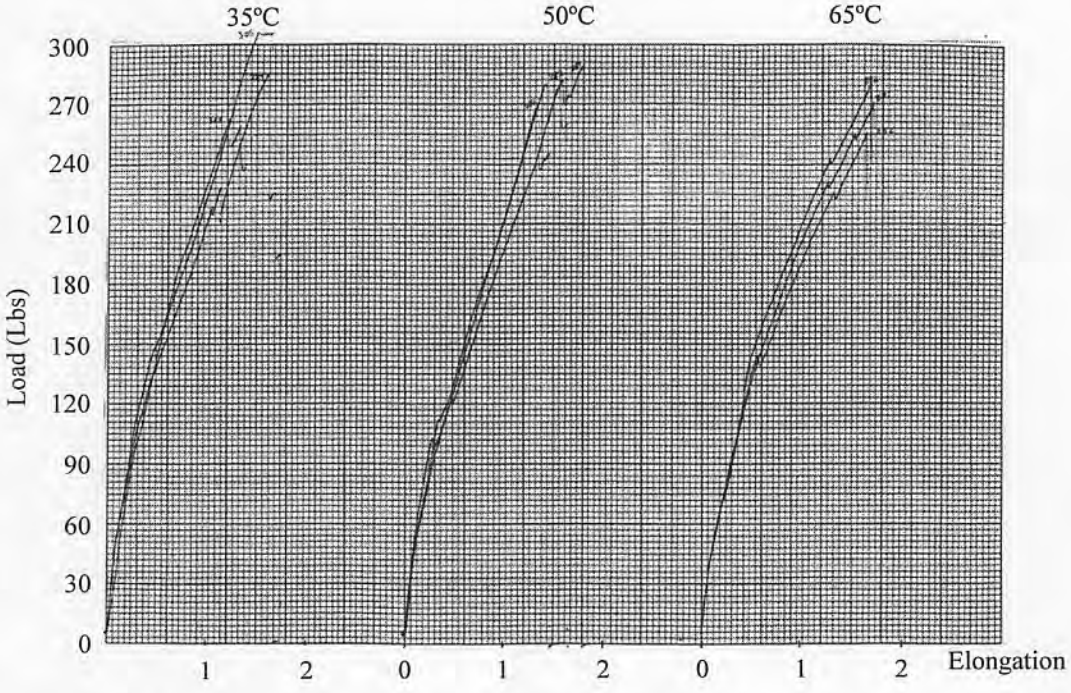

Fig. A.30 Load – Elongation curves for PET specimens, 30 days, Seawater exposure

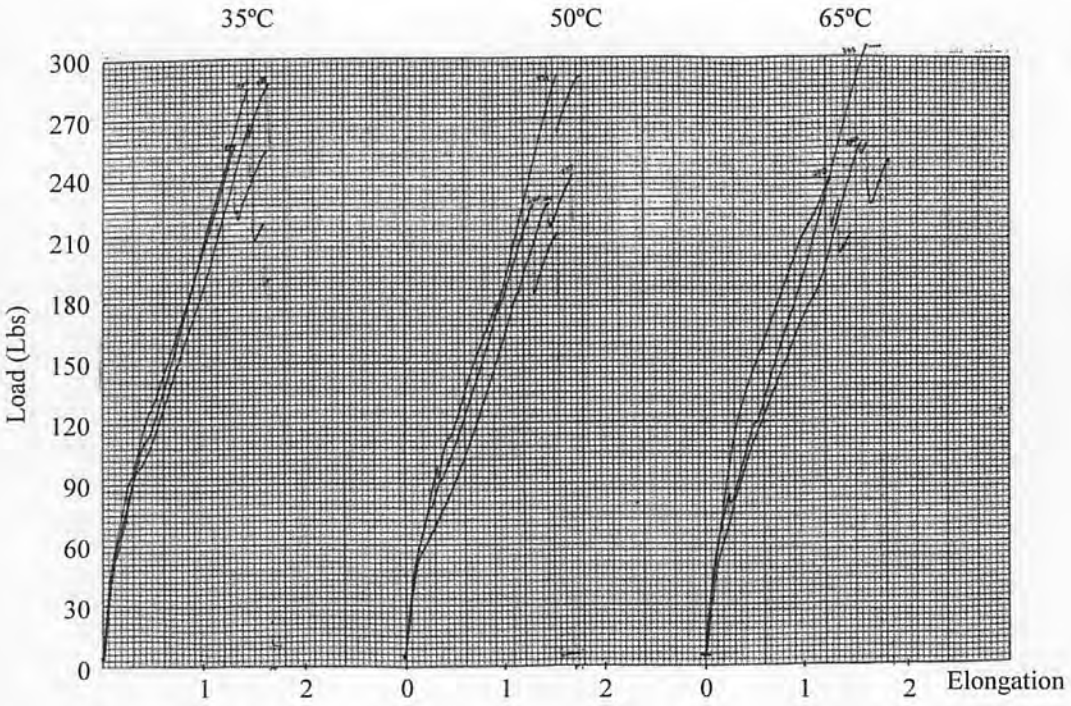

Fig. A.31 Load – Elongation curves for PET specimens, 30 days, Water exposure

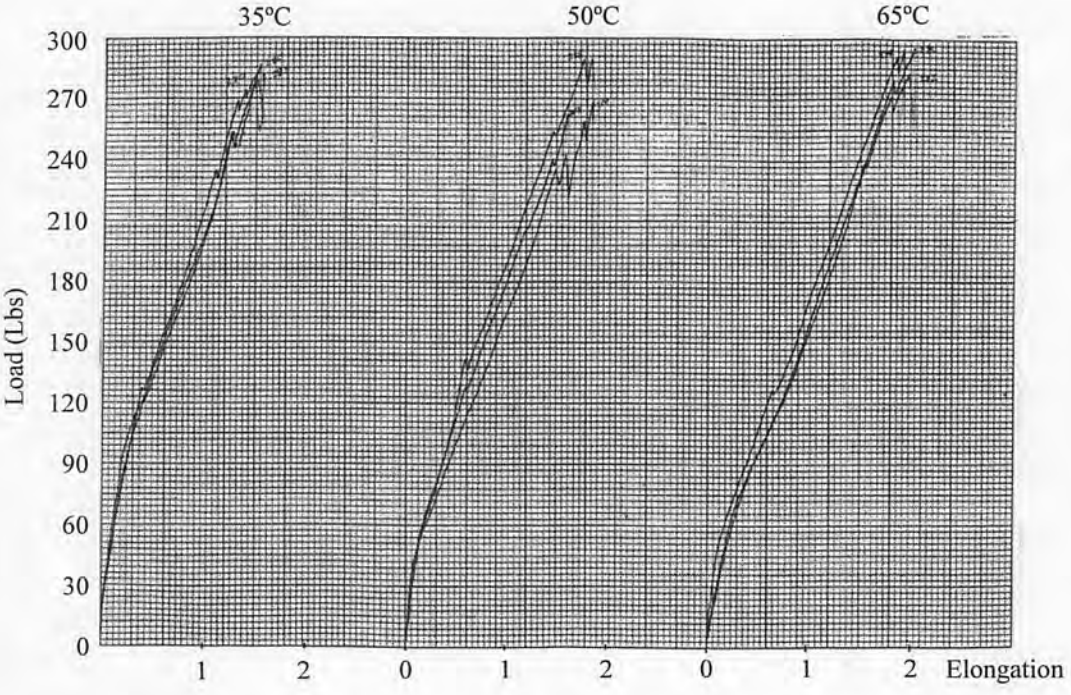

Fig. A.32 Load – Elongation curves for PET specimens, 60 days, Calcareous exposure

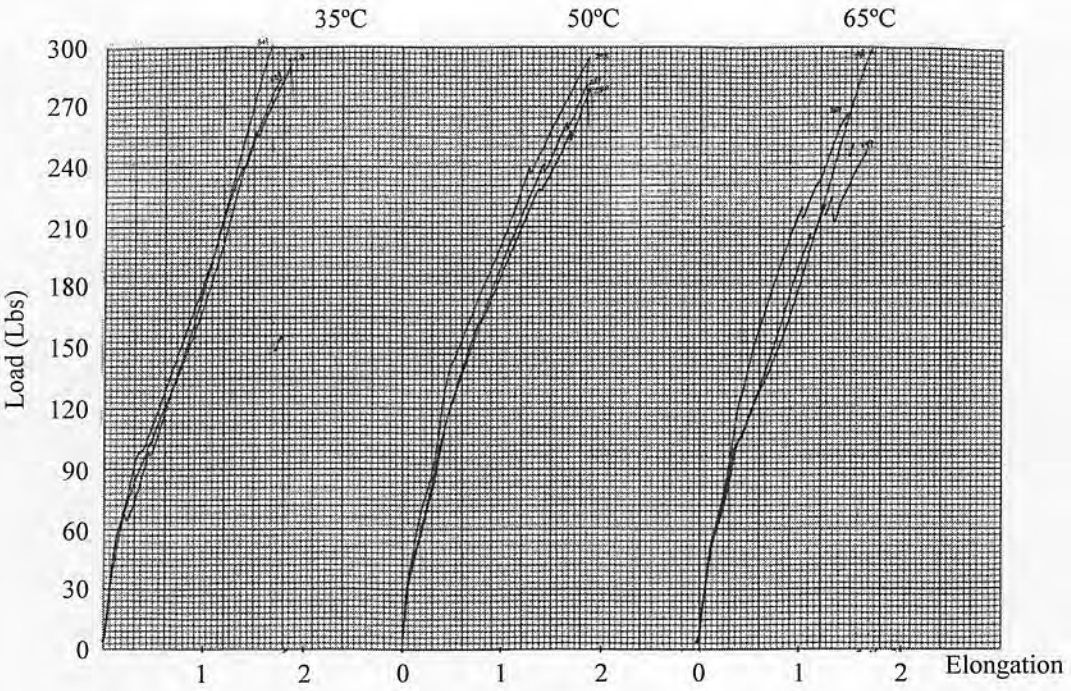

Fig. A33 Load – Elongation curves for PET specimens, 60 days, Phosphate exposure

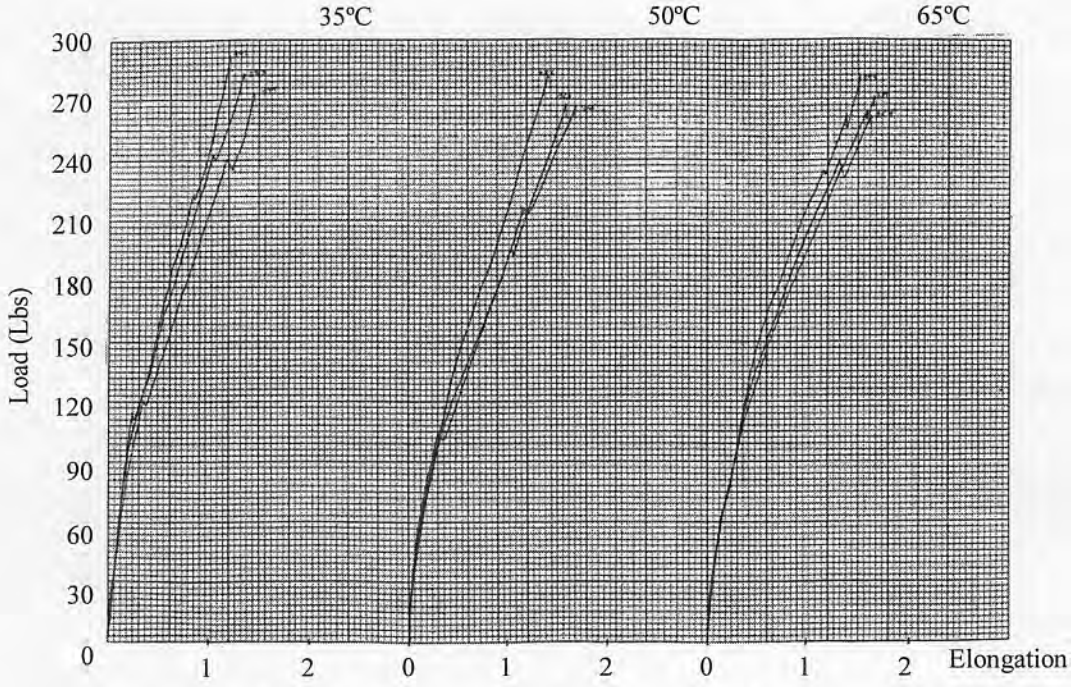

Fig. A34 Load – Elongation curves for PET specimens, 60 days, Limerock exposure

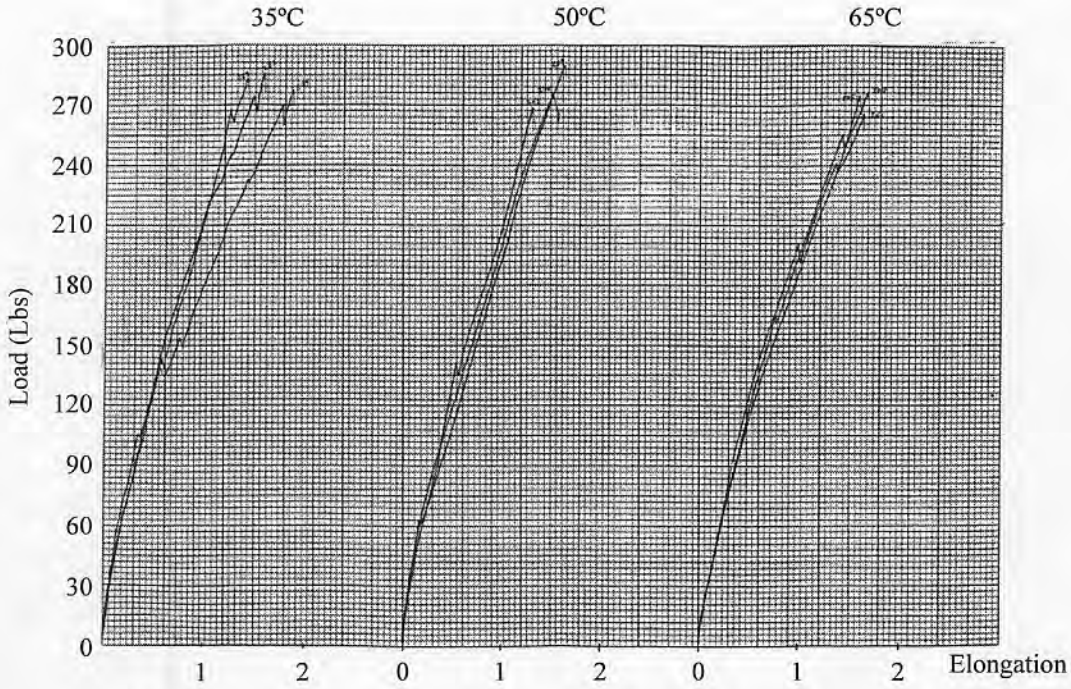

Fig. A.35 Load – Elongation curves for PET specimens, 60 days, Seawater exposure

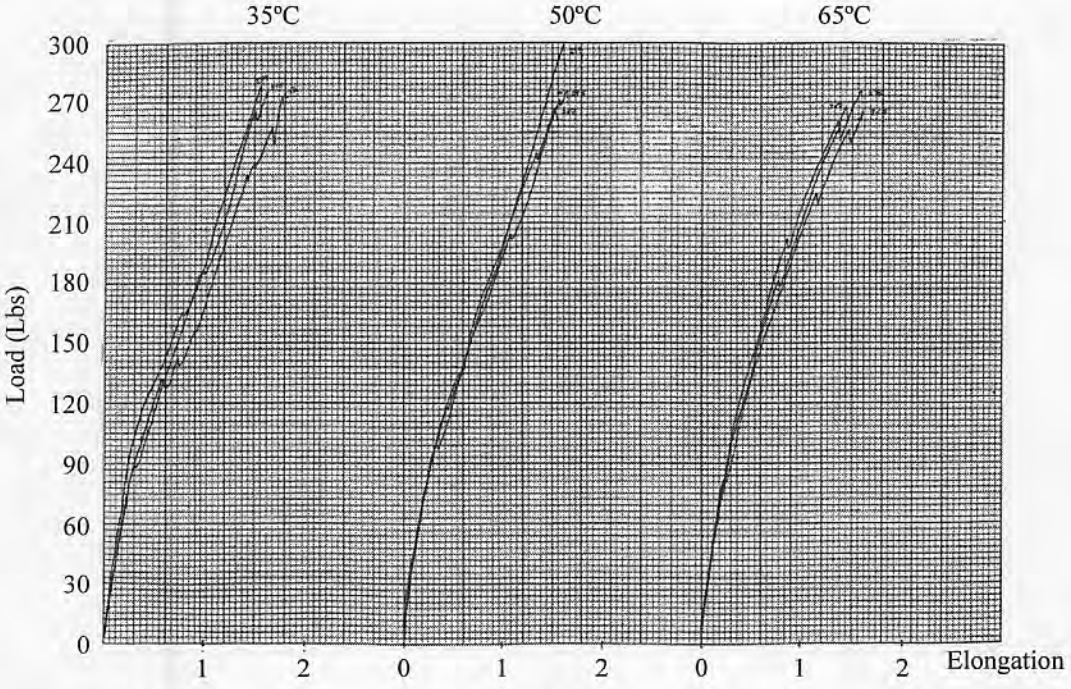

Fig. A.36 Load – Elongation curves for HDPE specimens, 60 days, Water exposure

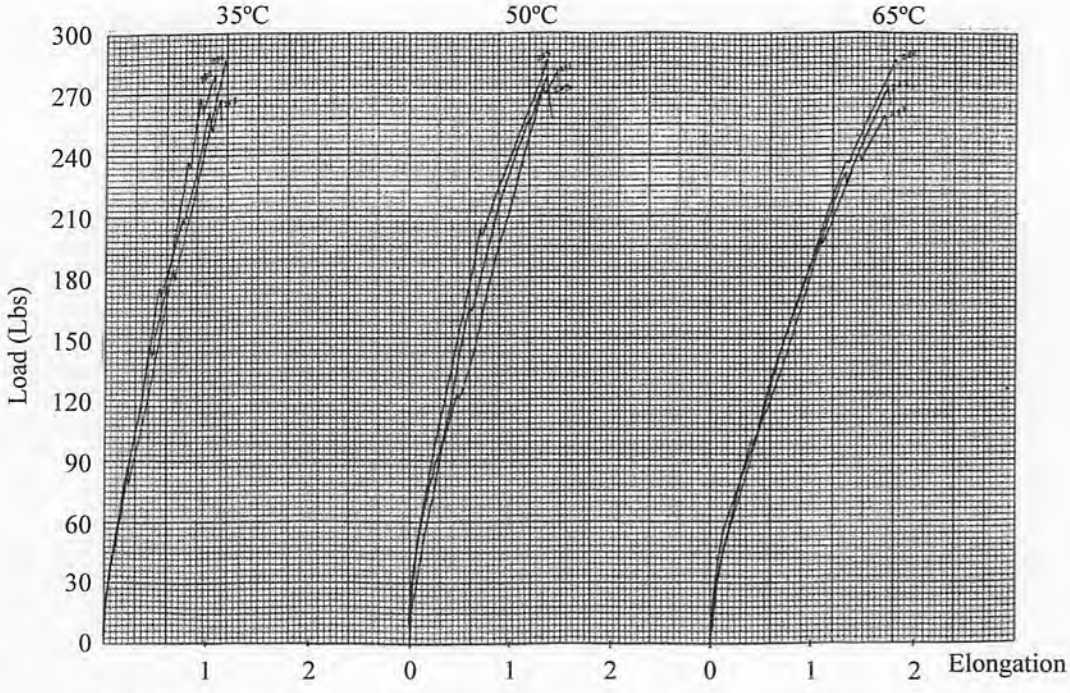

Fig. A.37 Load – Elongation curves for PET specimens, 90 days, Calcareous exposure

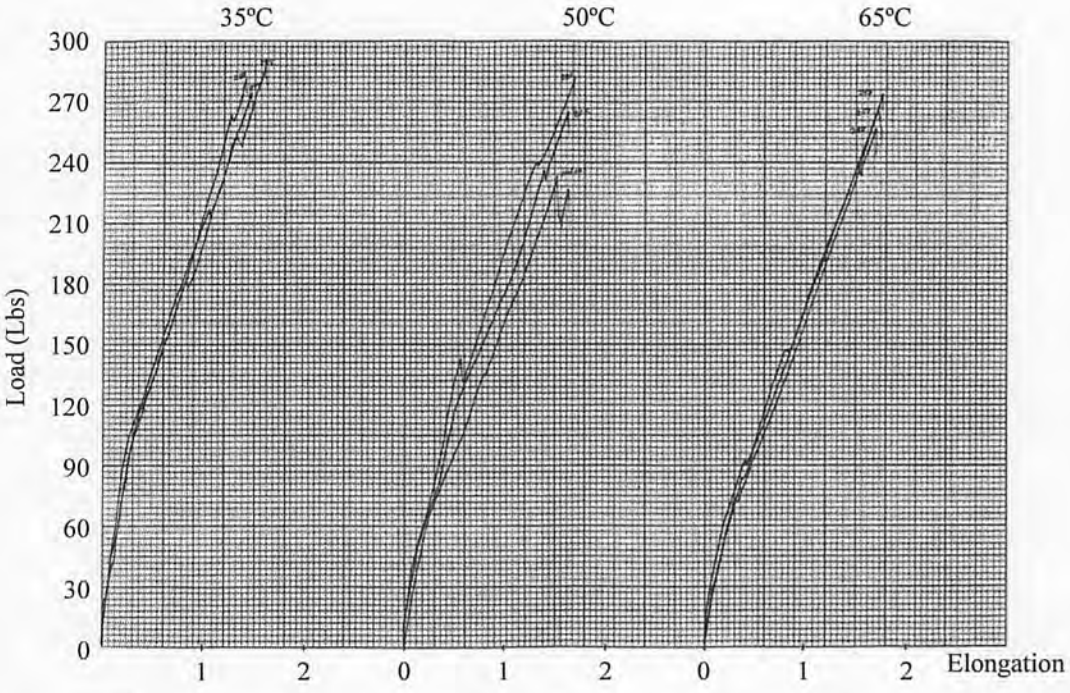

Fig. A.38 Load – Elongation curves for PET specimens, 90 days, Phosphate exposure

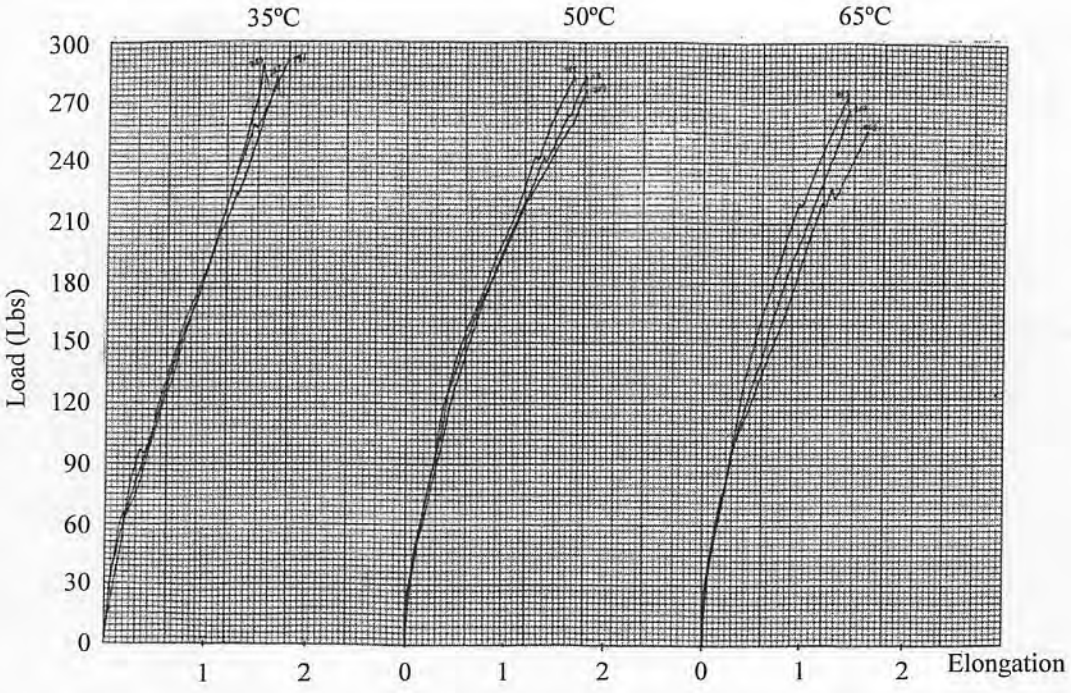

Fig. A.39 Load – Elongation curves for PET specimens, 90 days Limerock exposure

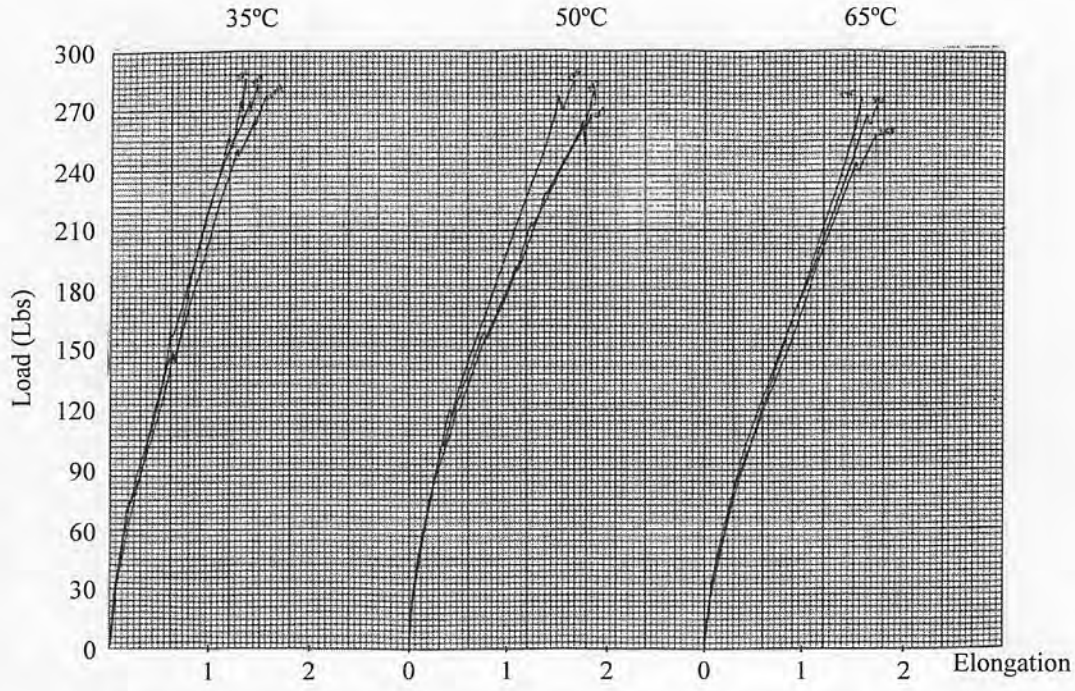

Fig. A.40 Load – Elongation curves for PET specimens, 90 days, Seawater exposure

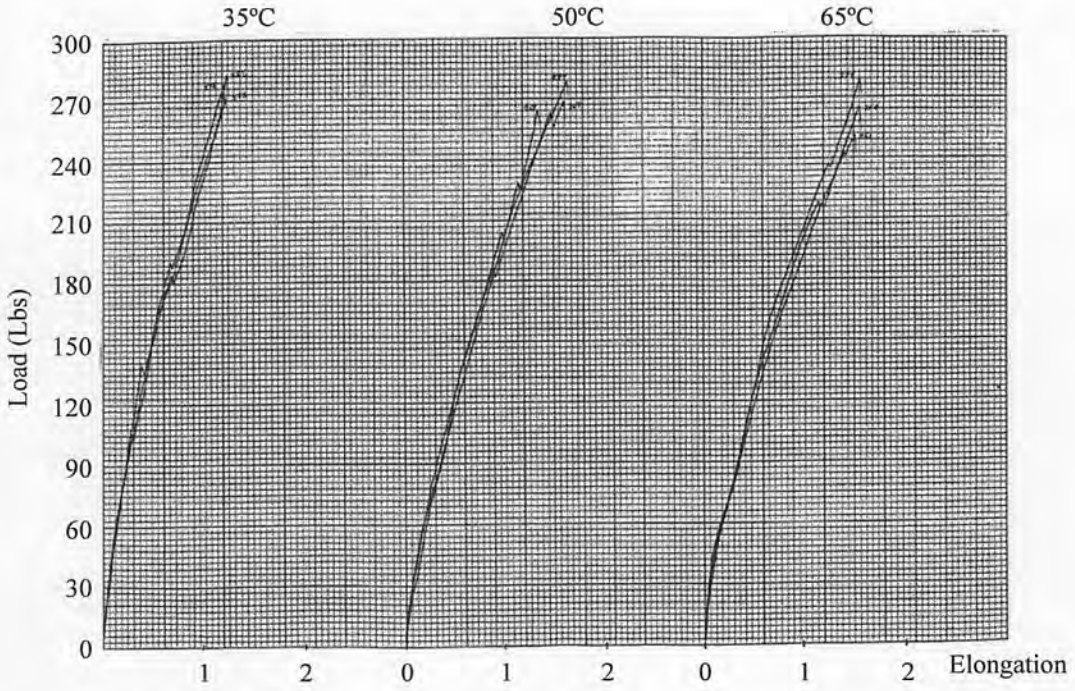

Fig. A.41 Load – Elongation curves for PET specimens, 90 days, Water exposure

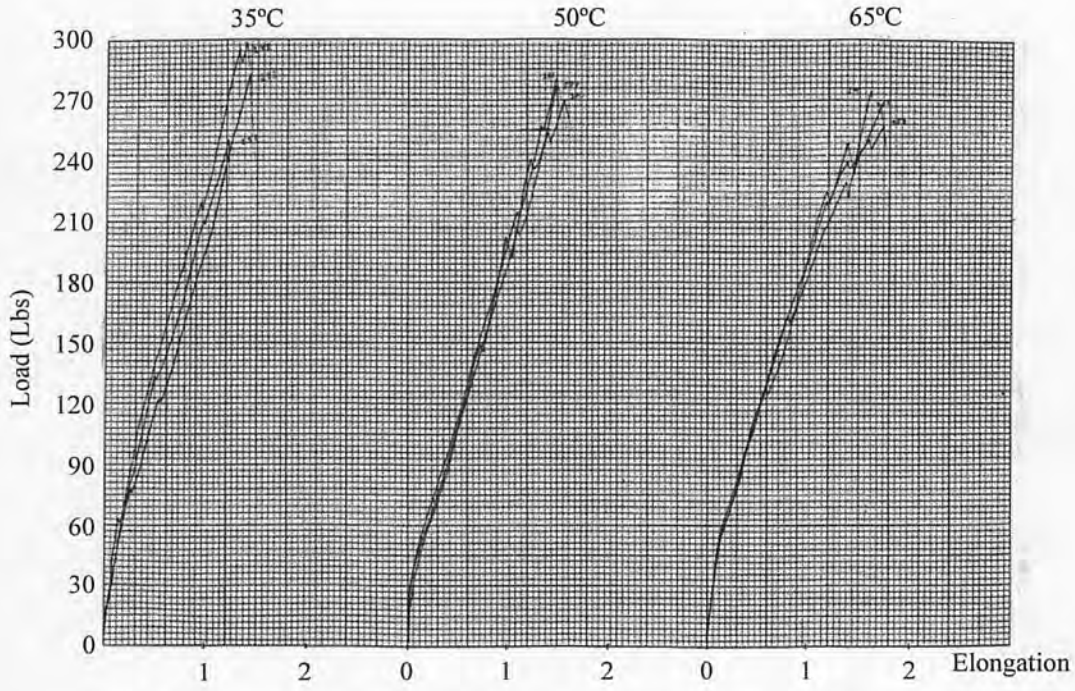

Fig. A.42 Load – Elongation curves for PET specimens, 180 days, Calcareous exposure

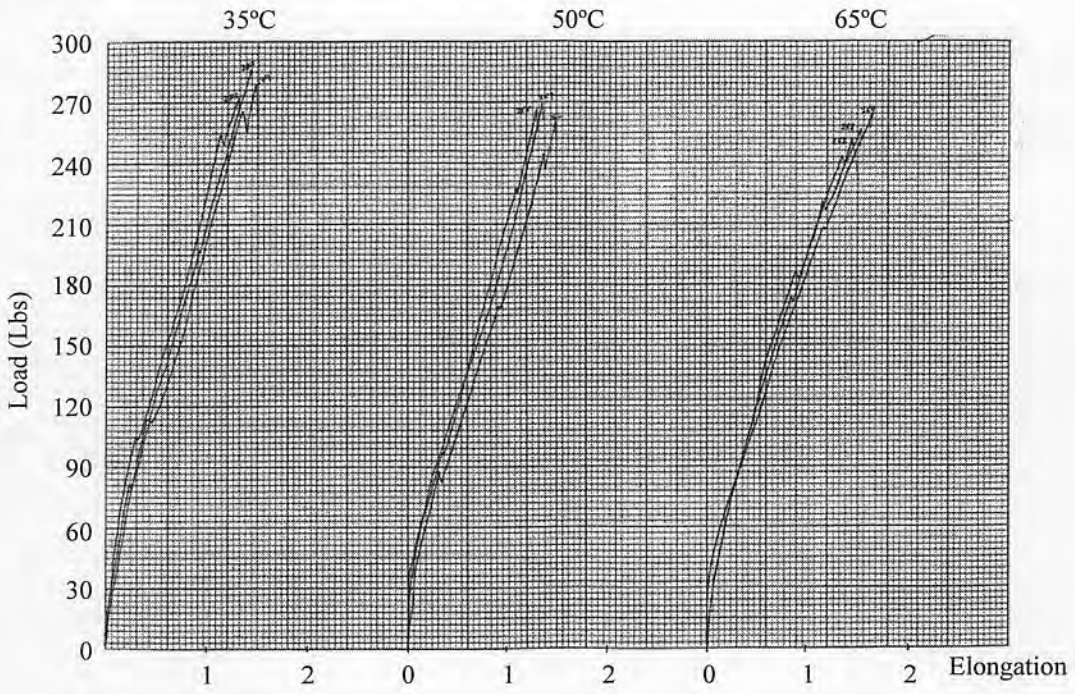

Fig. A.43 Load – Elongation curves for PET specimens, 180 days, Phosphate exposure

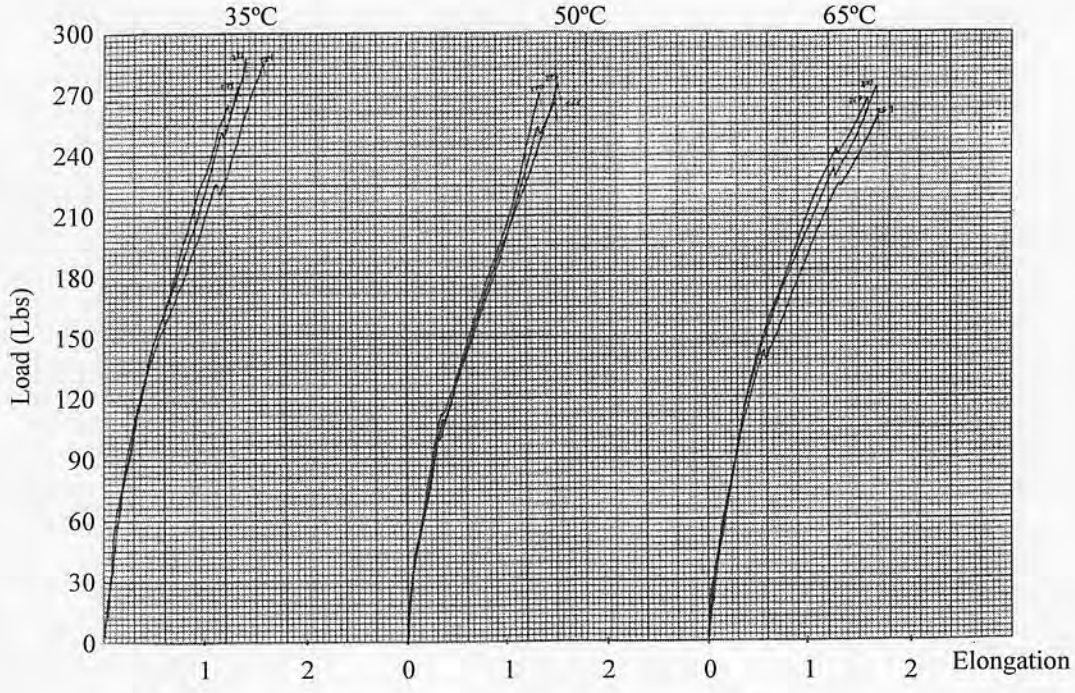

Fig. A.44 Load – Elongation curves for PET specimens, 180 days Limerock exposure

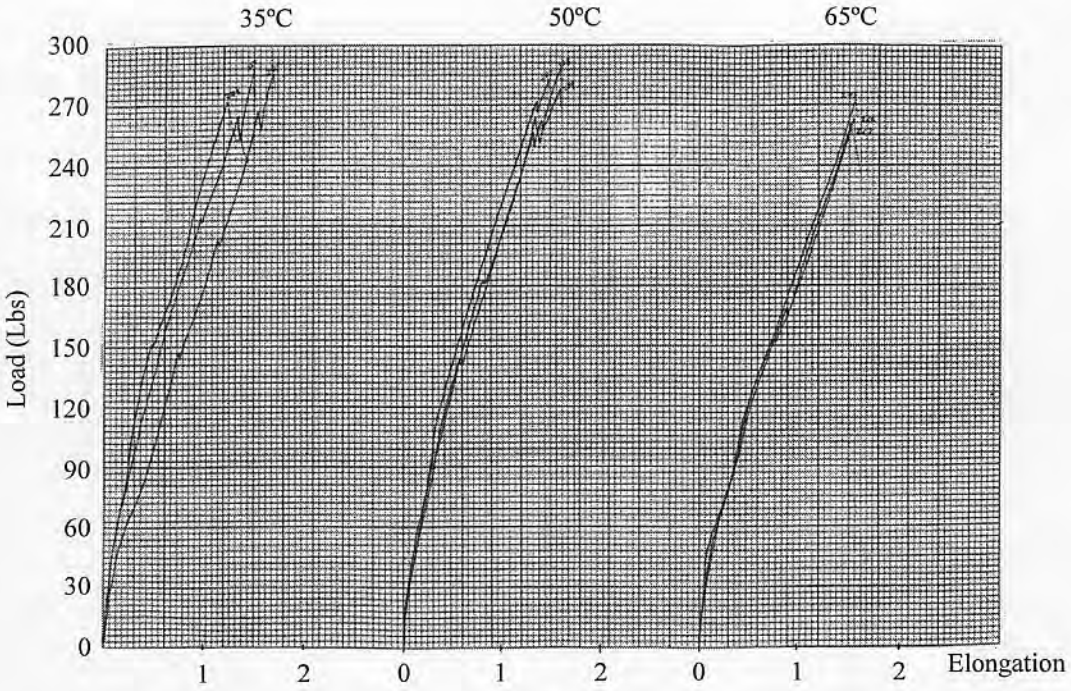

Fig. A.45 Load – Elongation curves for PET specimens, 180 days, Seawater exposure

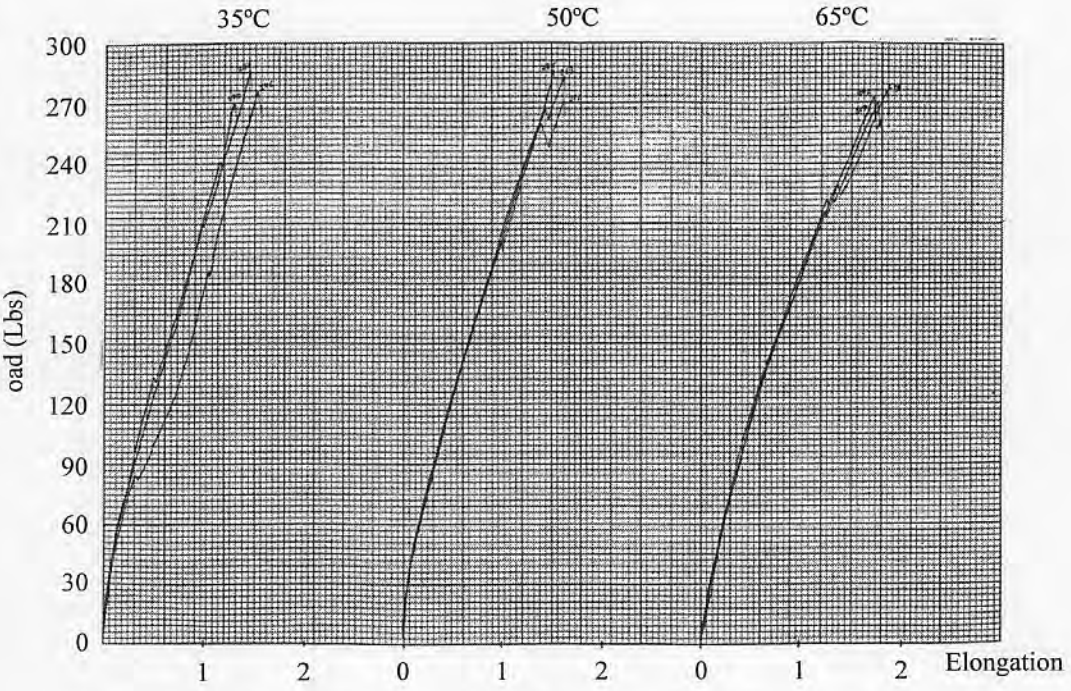

Fig. A46 Load – Elongation curves for PET specimens, 180 days, Water exposure

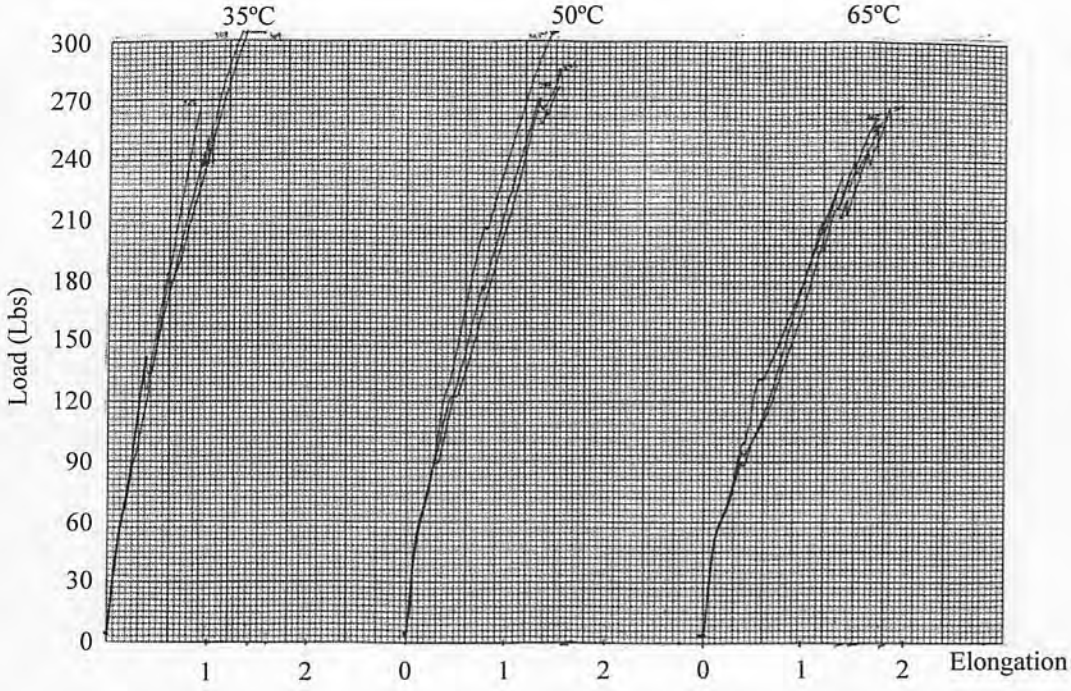

Fig. A.47 Load – Elongation curves for PET specimens, 365 days, Calcareous exposure

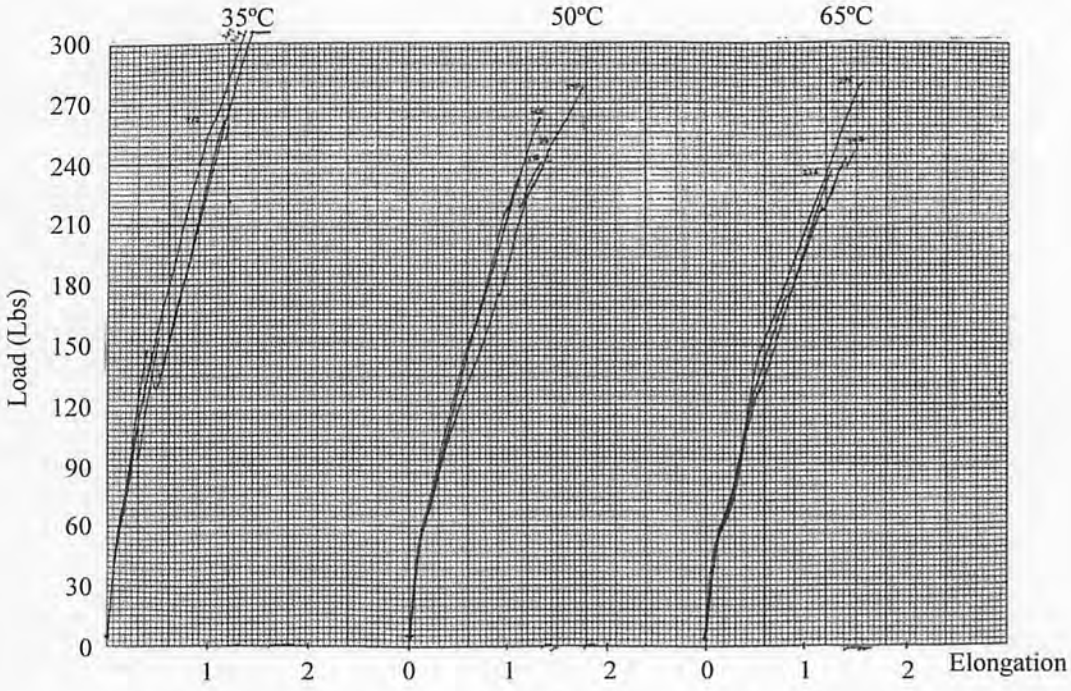

Fig. A.48 Load – Elongation curves for PET specimens, 365 days, Phosphate exposure

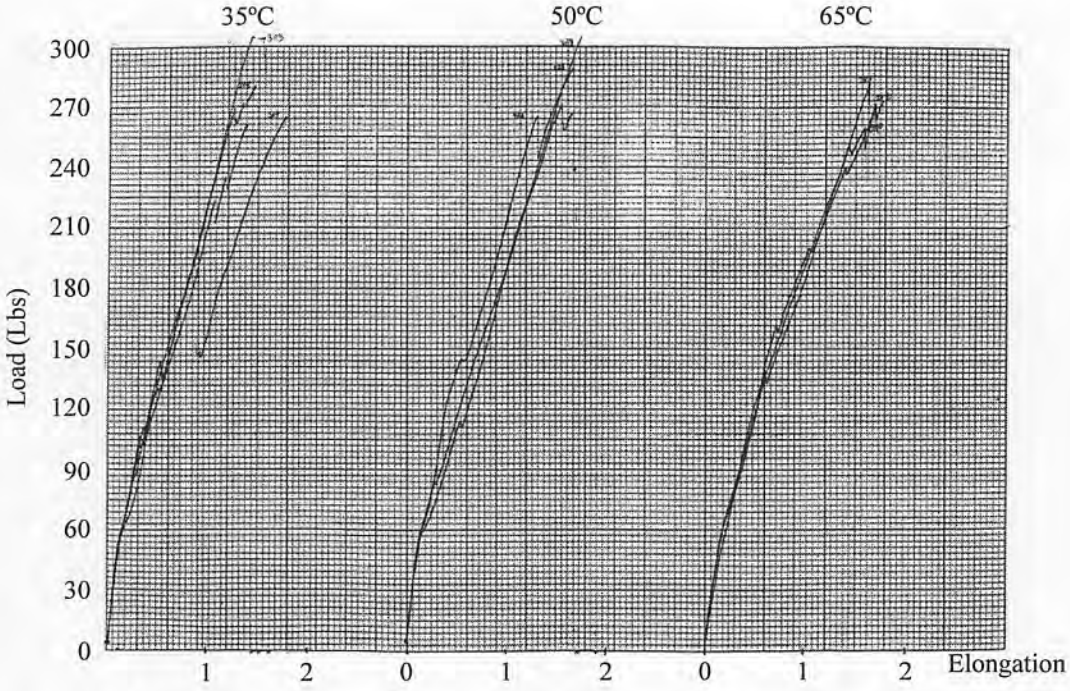

Fig. A.49 Load – Elongation curves for PET specimens, 365 days, Seawater exposure

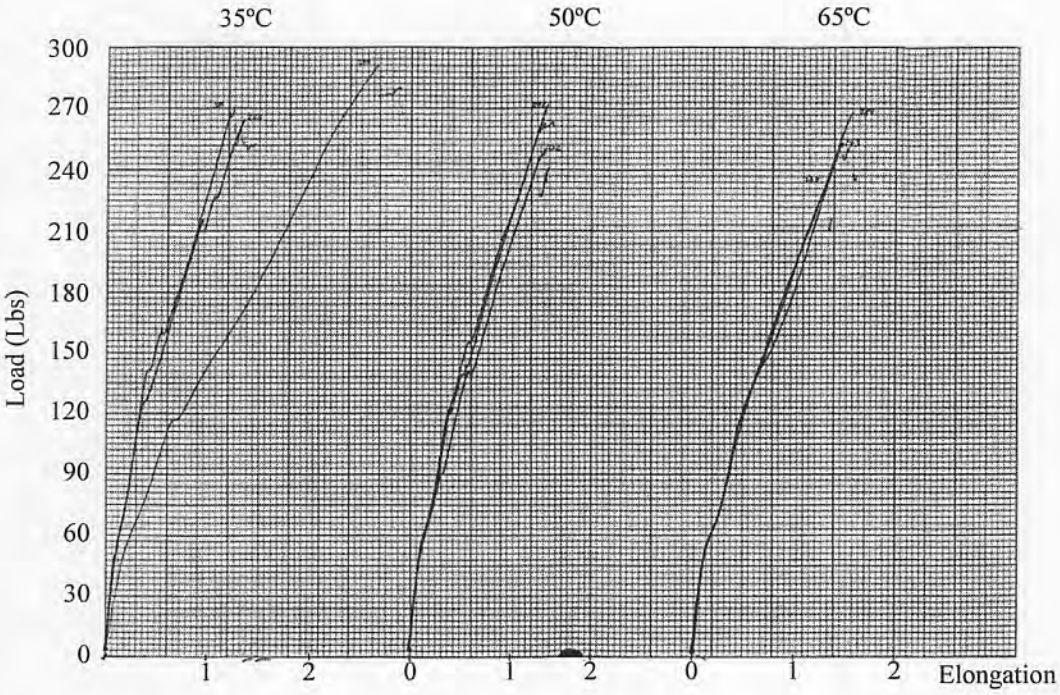

Fig. A.50 Load – Elongation curves for PET specimens, 365 days, Water exposure

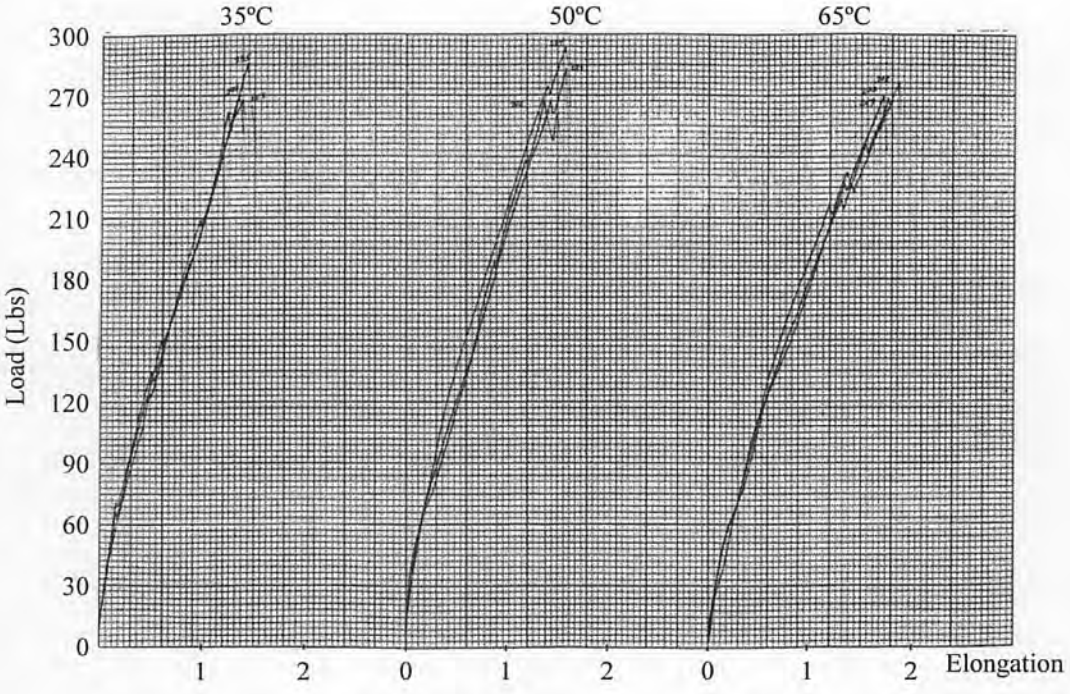

Fig. A.51 Load – Elongation curves for PET specimens, 365 days, Limerock exposure

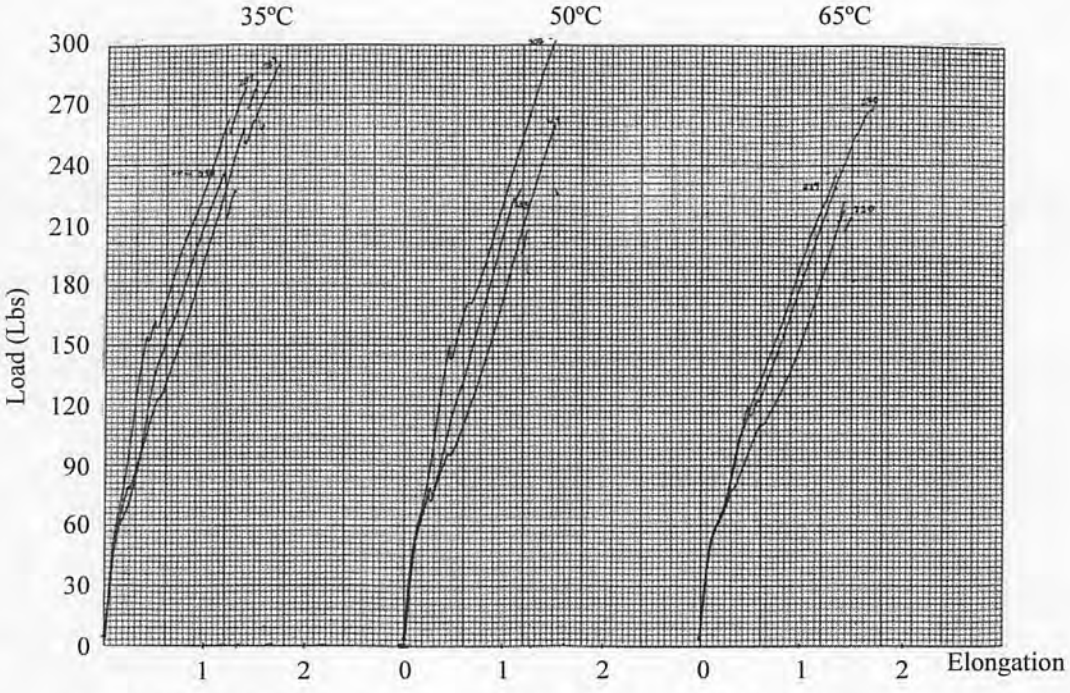

Fig. A.52 Load – Elongation curves for PET specimens, 417 days, Limerock exposure

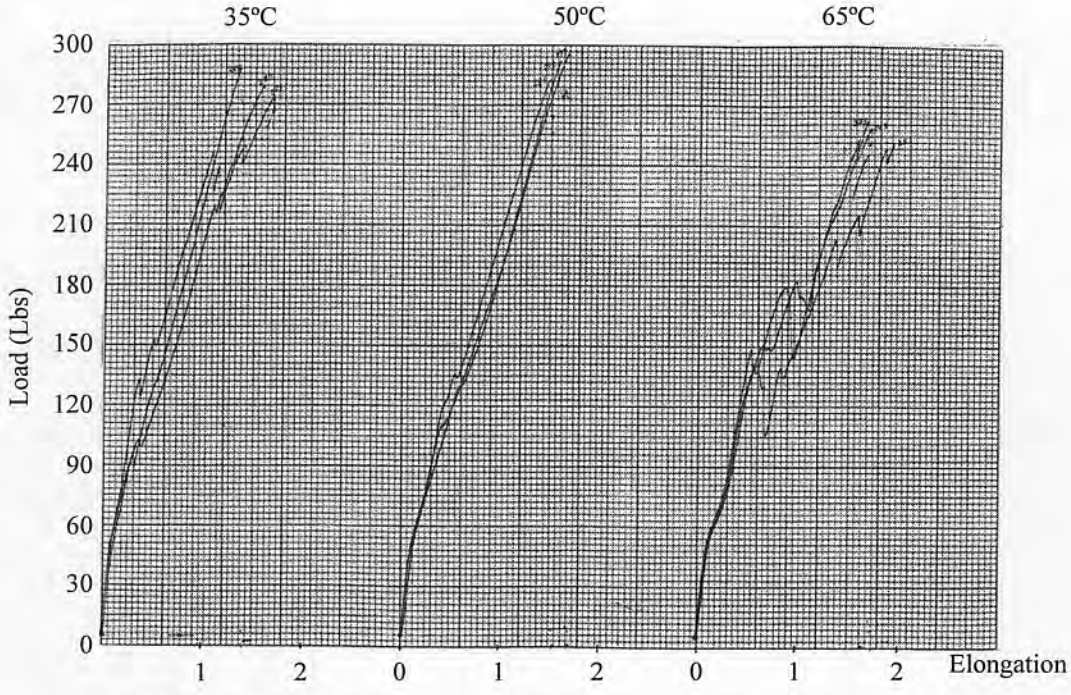

Fig. A.53 Load – Elongation curves for PET specimens, 417 days, Seawater exposure

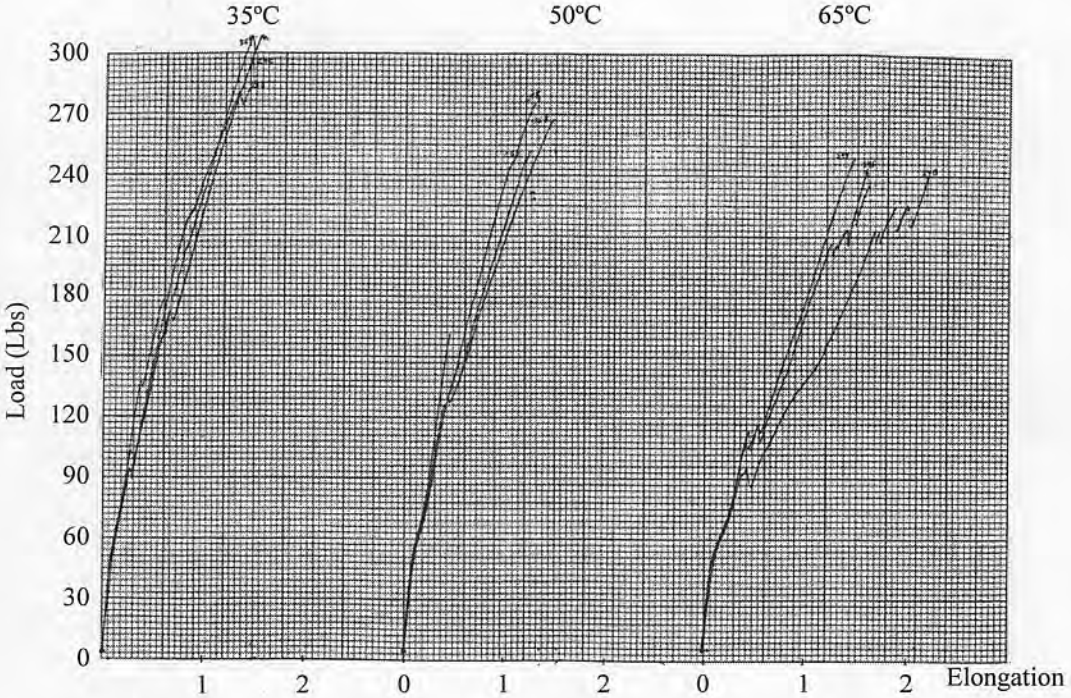

Fig. A.54 Load – Elongation curves for PET specimens, 417 days, Water exposure

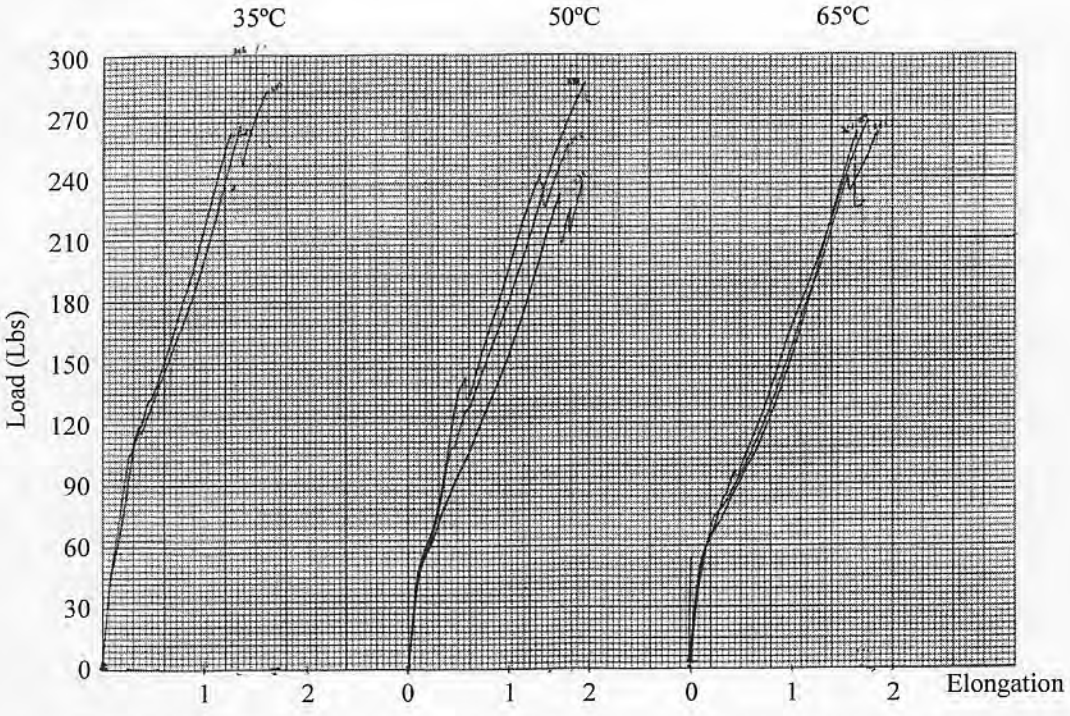

Fig. A.55 Load – Elongation curves for PET specimens, 417 days, Calcareous exposure

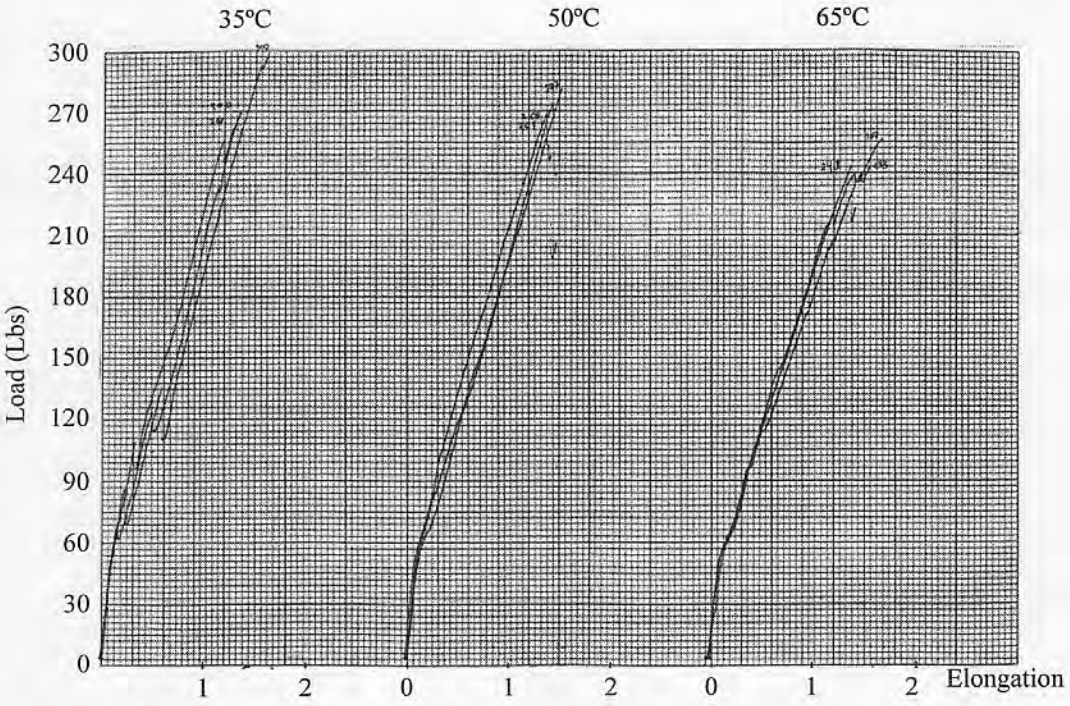

Fig. A.56 Load – Elongation curves for PET specimens, 417 days, Phosphate exposure